UNIVERSITY OF SOUTHAMPTON

Studies on Active Site Mutants of Human Non-Pancreatic Secreted Phospholipase A$_2$

By
Suzanne H. Edwards BSc (Hons.)

A thesis submitted for the degree of Doctor of Philosophy

Division of Biochemistry and Molecular Biology

September 2001

Studies of Active Site Mutants of Human Non-pancreatic Secreted Phospholipase A$_2$

By Suzanne H. Edwards

Phospholipase A$_2$ (PLA$_2$) is an enzyme that catalyses the hydrolysis of phospholipids at the sn-2 fatty-acyl bond, liberating free fatty acids and lysophospholipids. As many as eleven different forms of the enzyme have been characterised, including both secreted and cytosolic, calcium dependent and independent varieties. These PLA$_2$s are involved in a range of physiological processes including phospholipid digestion, signal transduction and host defence, and have been isolated from a diverse range of organisms and cells.

This thesis is concerned with the human non-pancreatic secreted form of PLA$_2$ (hnpsPLA$_2$), which is secreted by a variety of cells including platelets, macrophages and smooth muscle cells. HnpsPLA$_2$ is a 14 kDa, calcium-dependent extracellular enzyme believed to be an acute phase protein, with an important antimicrobial role. It is the binding of this enzyme to the phospholipid interface that is crucial in the physiological regulation of the enzyme. In order to study interfacial binding in the absence of catalysis, structurally intact but inactive mutants were required. The production of the mutants H48Q, H48N and H48A appeared to be the obvious strategy based on previous work on other secreted phospholipases A$_2$ from bovine pancreas and bee venom. However, the mutant H48Q unexpectedly retained significant (~4%) catalytic activity that was contrary to all previous work in the field.

In this thesis it is established that the high residual activity of the H48Q mutant is genuine, not due to contamination, and can be seen under a variety of assay conditions. The crystallisation of the H48Q mutant to a resolution of 1.5 Å allowed a comparison with the corresponding wild-type enzyme (N1A) that was also crystallised. This comparison revealed that all the important features of the catalytic machinery were in place and the two structures were virtually superimposable. In particular, the catalytic calcium ion occupied an identical position in the active site of the two proteins and the two catalytic water molecules were clearly resolved in the H48Q mutant. A 'two-water mechanism' in which the second water molecule at the active site hydrogen bonds to the glutamine could explain the residual activity of the H48Q.

A second active site mutant (H48N) showed minimal activity and was used to study the interfacial binding properties of the enzyme. The results highlighted the use of this mutant in interfacial binding assays and confirmed the high affinity of this enzyme for anionic interfaces. The third active site mutant, H48A, was completely inactive. However, this mutant could not be expressed in significant amounts and was not further investigated.

Acknowledgements

This thesis is dedicated
to the memory of Colin

Contents

List of Figures

Chapter Three – The H48Q Mutant of HnpsPLA$_2$

Chapter Four - The H48A and H48N Mutants of HnpsPLA$_2$

Chapter Five - Crystallographic Studies of N1A and H48Q HnpsPLA$_2$

List of Tables

Abbreviations

BPI	Bactericidal/Permeability Increasing Protein
BSA	Bovine Serum Albumin
cAMP	Cyclic Adenosine Monophosphate
CHO	Chinese Hamster Ovary Cells
cPLA$_2$	Cytosolic Phospholipase A$_2$
DAUDA	11(5-dimethylaminonapthalenesulphonylamino) undecanoic acid
DOPC	Dioleoyl phosphatidylcholine
DOPG	Dioleoyl phosphatidylglycerol
DOPM	Dioleoyl phosphatidylmethanol
EDTA	Ethylenediaminetetraacetic acid
ESI-MS	Electrospray Ionisation Mass Spectrometry
E. coli	Escherichia coli
FABP	Fatty Acid Binding Protein
FPLC	Fast Protein Liquid Chromatography
HnpsPLA$_2$	Human Non-pancreatic Secreted Phospholipase A$_2$
HSPG	Heparan Sulphate Proteoglycan
IBS	Interfacial Binding Surface
iPLA$_2$	Calcium Independent Phospholipase A$_2$
IPTG	Isopropyl-β-thiogalactopyranoside
kDa	Kilo Dalton
MAPK	Mitogen-Activated Protein Kinase
M. luteus	Micrococcus luteus
MLV	Multilamellar vesicles
MW	Molecular Weight
nn-sPLA$_2$	Naja naja secreted phospholipase A$_2$
PAF	Platelet-Activating Factor
pBPB	para-Bromophenacyl Bromide
PCR	Polymerase Chain Reaction
PC	Phosphatidylcholine
PG	Phosphatidylglycerol
POPG	1-oleoyl, 2-palmitoyl phosphatidylglycerol
pp-sPLA$_2$	Porcine pancreatic secreted phospholipase A$_2$
PS	Phosphatidylserine
PLA$_1$	Phospholipase A$_1$
PLA$_2$	Phospholipase A$_2$
PLC	Phospholipase C
PLD	Phospholipase D
PMSF	Phenylmethylsulphonyl Fluoride
RP-HPLC	Reverse Phase High Pressure Liquid Chromatography
sPLA$_2$	Secreted Phospholipase A$_2$
S. aureus	Staphylococcus aureus
SUV	Small Unilamellar Vesicle
TFA	Trifluoroacetic Acid
WT	Wild Type

Standard one and three letter codes for amino acids are used. Secreted phospholipase A$_2$ residues are numbered according to the sequence alignment of these enzymes with the porcine pancreatic enzyme.

Chapter One - Introduction

1.1 Phospholipases and Phospholipids.

Phospholipids represent the major type of lipid found in biological membranes. Phospholipids derived from glycerol – phosphoglycerides – consist of a glycerol backbone with two fatty acids esterified at the sn-1 and sn-2 positions, a phosphate group and an alcohol head group, such as choline or ethanolamine. Phospholipases are a family of enzymes that catalyse the hydrolysis of phospholipids. There are four classes of phospholipase, each of which cleave phospholipids at a different site. Phospholipases A_1 and A_2 (PLA$_1$ and PLA$_2$) hydrolyse the sn-1 and sn-2 ester bonds respectively to release long chain fatty acids. Phospholipase C (PLC) cleaves at the sn-3 bond releasing the phosphorylated head group and diacylglycerol, while phospholipase D (PLD) removes only the head group generating phosphatidic acid. The generalised structure of a phospholipid is shown in figure 1.1, and the sites of action of the four types of phospholipase are indicated.

1.2 Phospholipase A_2.

The phospholipases that are the focus of this thesis, and which have been extensively studied are PLA$_2$s. PLA$_2$s are found in a variety of cellular and extracellular locations, and are involved in a range of physiological processes including phospholipid digestion, signal transduction and host defence [1-4]. PLA$_2$s have a broad specificity for substrate, with different groups of the enzyme showing a preference for particular head groups. Most of the PLA$_2$s are relatively insensitive to fatty acyl chain length, with a notable exception being the enzyme from group IV, which is specific for arachidonic acid [5,6]. PLA$_2$s cleave phospholipids at the sn-2 position, liberating free fatty acids and lysophospholipids.
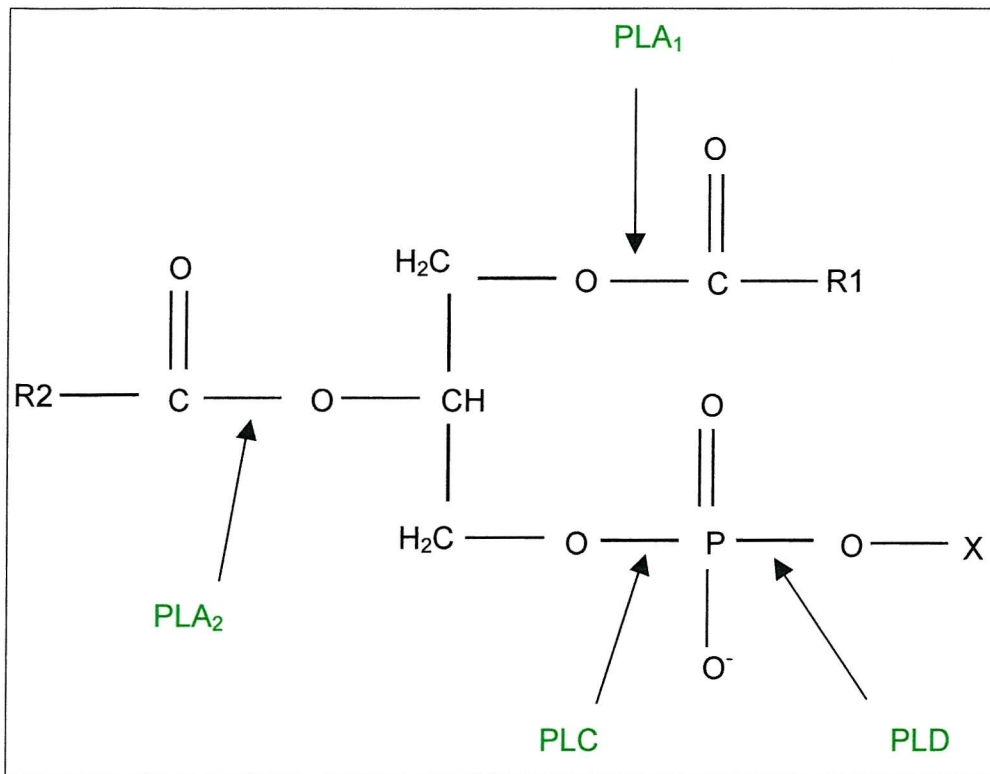
Figure 1.1 Sites of Action of the Phospholipases.

A typical glycerol-based phospholipid is shown. R1 and R2 represent fatty acids, X represents the alcohol head group. Arrows indicate the site of hydrolysis by the phospholipase specified.

A generalised reaction scheme is shown in figure 1.2. Both of the hydrolysis products may act as second messengers, or undergo metabolism to form pro-inflammatory factors thereby implicating PLA_2 in the pathogenesis of many inflammatory disease states [7-9]. For example, arachidonic acid is the precursor for production of eicosanoid mediators, and similarly, lysophospholipids are precursors in the biosynthesis of platelet activating factor (PAF). As many as eleven different groups of PLA_2 have been identified to date, and the following section indicates their main characteristics.
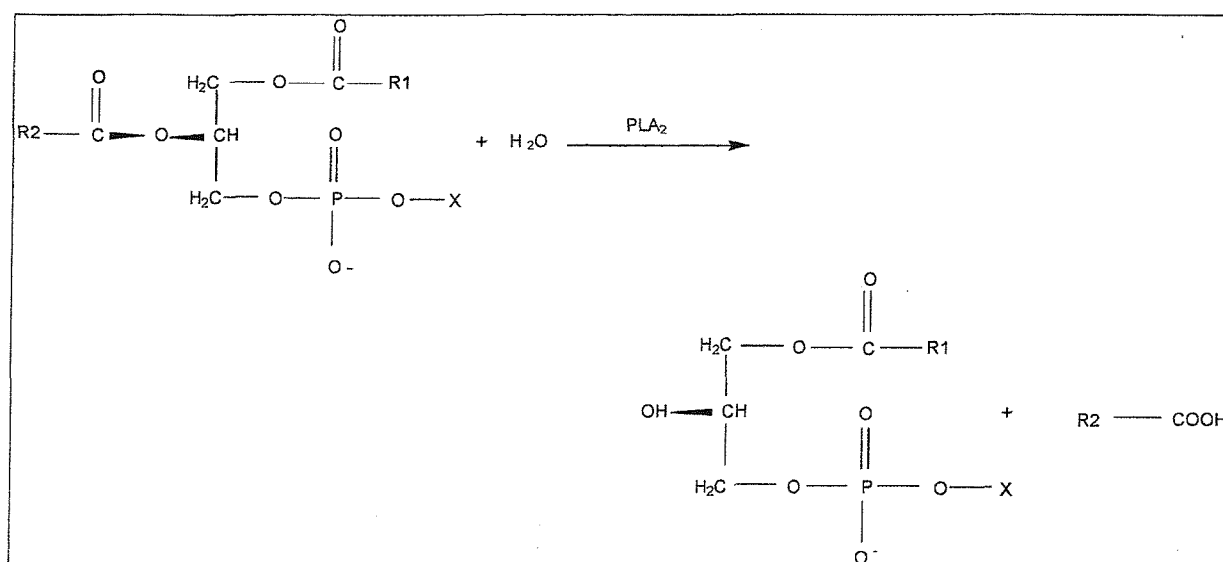
Figure 1.2. Phospholipid Hydrolysis by PLA$_2$

The hydrolysis of phospholipid by PLA$_2$ is shown, with the resulting lysophospholipid and fatty acid products. R1 and R2 represent fatty acid chains, X represents the head group.

1.3. Characteristics of the Different Groups of PLA$_2$s.

1.3.1 PLA$_2$s from Groups I – III.

The PLA$_2$s classified into groups I, II and III are small, secreted PLA$_2$s (sPLA$_2$) which contain multiple disulphide bonds and require mM Ca^{2+} for catalytic activity. Originally isolated from various snake venoms, sPLA$_2$s were also discovered in the pancreatic juice of pigs, cattle and other species including man. These enzymes were classified as either group I or group II sPLA$_2$s according to the positioning of their disulphide bonds and the presence of loops or extensions novel to each group. Non-pancreatic mammalian sPLA$_2$s were later added to group II, and the discovery of a unique sPLA$_2$ isolated from bee venom resulted in the addition of a third group of classification.

4

The group I enzymes were originally isolated from pancreatic juice and the venom of snakes from the *Elapidae* and *Hydrophidae* families [10]. These enzymes are secreted, with a mass of approximately 14 kDa, and a mM Ca^{2+} requirement for activity. They all contain seven disulphide bonds, and catalysis proceeds via a conserved His-Asp pair [11]. In addition, these PLA_2s have an extra segment not found in the group II enzymes, which is called the pancreatic or elapid loop as it was first identified in the group I enzymes [11]. The group I PLA_2 in pancreatic tissue exists as an inactive proenzyme - the propeptide is cleaved by trypsin to yield an active enzyme, the main role of which is digestion of phospholipids in food [12]. In fact, the pancreatic enzyme has a diverse tissue distribution – it is expressed in lung, kidney, spleen, ovary and prostate tissue – and therefore has been implicated in physiological roles other than just phospholipid digestion, including cell proliferation and migration, and in acute lung injury [1]. It has been proposed that cell surface receptors for some $sPLA_2$s, including the pancreatic enzyme, may be implicated in some of the effects of these enzymes on cell function. This is a controversial area, and the full physiological significance of receptor-mediated $sPLA_2$ activity is not clear, but has recently been reviewed [13,14].

$sPLA_2$s from group II were initially identified from snakes in the *Crotalidae* and *Viperidae* classes, while the mammalian form was isolated from cells, tissues and inflamed sites in the 1980s. The group II enzymes have high sequence and structural homology to the group I PLA_2s, and are distinguished from them by the position of one of their disulphide bonds [12,15]. The group II enzymes have been further classified into groups IIA – IIF, indicating the diversity of this group of PLA_2s [1]. The human non-pancreatic secreted PLA_2 from group IIA is the subject of this thesis, and a more detailed description of this enzyme will be given later on.

The $sPLA_2$ originally classified as a group III enzyme was isolated from honeybee venom, but it is now known that group III $sPLA_2$s can be found in

venom from lizards and scorpions, as well as from humans [1]. These sPLA$_2$s are similar in their size and Ca^{2+} requirement to groups I and II, but only contain five disulphide bonds. Although catalysis proceeds in a similar manner to that of groups I and II, they are quite different structurally - sequence homology is only ~ 29 % [14]. The areas of homology with other 14 kDa PLA$_2$s are limited to the catalytic His/Asp pair, the calcium binding loop and some cysteine residues [16]. This type of PLA$_2$ is the main allergen and immunogen in bee venom, with the catalytic activity being a major feature of the allergenicity of this enzyme. That catalysis is important for the immune response elicited by individuals exposed to this allergen was deduced by experiments, which showed that the catalytically inactive H34Q mutant was less able to induce antibody responses in mice as compared to the active, wild type enzyme [16].

1.3.2 Group IV PLA$_2$.

Group IV PLA$_2$s are considerably larger (85 kDa) cytosolic PLA$_2$s (cPLA$_2$), which were first isolated from platelets and macrophages [17]. These enzymes are specific for phospholipids with arachidonic acid at the sn-2 position and as arachidonate can be metabolised to form inflammatory lipid mediators e.g. eicosanoids, cPLA$_2$ has an important role in controlling and maintaining levels of this precursor [6]. These enzymes have no homology with any of the other PLA$_2$s, and their sub µM Ca^{2+} requirement is needed to bind cPLA$_2$ to the membrane or phospholipid vesicle, rather than being involved in catalysis itself. cPLA$_2$ has a calcium lipid-binding domain (CaLB domain) at the N-terminal, which is required for this Ca^{2+}-dependent translocation of the enzyme to the membrane [18].

A serine residue (Ser-228), which is part of a sequence similar to the lipase consensus sequence (GXSXG) was found by mutation studies to be involved in catalysis, along with Asp 549 and these residues are located along with two Arg

residues in a deep cleft in the protein [19]. The catalytic mechanism of cPLA$_2$ is proposed to involve a serine-acyl intermediate, and it is notable that in this class of PLA$_2$ a histidine residue is not involved in catalysis [20].

cPLA$_2$ can be activated by phosphorylation on Ser residues, and the increased cPLA$_2$ activity in stimulated cells has been attributed to phosphorylation on Ser-505 by mitogen-activated protein kinase (MAPK) [21]. A further phosphorylation site has been found at Ser-727, but a kinase other than MAPK is responsible for phosphorylating this residue [21]. cPLA$_2$s have multiple enzymatic ability, showing lysophospholipase and transacylase activity in addition to PLA$_2$ activity. The transacylase activity suggests that an acyl-enzyme intermediate is formed in the cPLA$_2$ reaction, and lysophospholipase activity would provide an efficient mechanism to control the accumulation of potentially harmful lysophospholipids [22].

1.3.3 Group V PLA$_2$.

A recently identified form of secreted PLA$_2$ was isolated from human, rat and mouse tissues, with high expression in the heart and placenta [13,23]. These enzymes were designated to a new group of PLA$_2$, group V, as although they are small (14 kDa), and share the same catalytic machinery as the group I and II enzymes, they have only six disulphides. They also lack the elapid loop and carboxyl extension found in groups I and II respectively. The group V enzymes have been shown to hydrolyse phosphatidylcholine vesicles and outer membranes of mammalian cells much more efficiently than the group II enzymes [13,24]. The affinity of the human group V enzyme for phosphatidyl choline (PC) interfaces was shown to be > 50 times greater than the group IB and IIA human sPLA$_2$s. This is thought to be due in part to the position of one of the four tryptophan residues (Trp-31) found in this PLA$_2$. This surface-exposed tryptophan is believed to anchor the enzyme to the PC interface [25,26]. These

PLA$_2$s were also found to be synthesised by inflammatory cells such as macrophages, and from these findings, it has been postulated that group V PLA$_2$ triggers eicosanoid production from inflammatory cells [27].

Some early work implicated the group IIA enzyme in the inflammatory response. It is now considered likely that this is attributable to the as then unrecognised group V enzyme.

1.3.4 PLA$_2$s from Groups VI, VII and VIII – Calcium Independent PLA$_2$s (iPLA$_2$).

Group VI PLA$_2$s are one of the few classes of this enzyme that are calcium-independent (iPLA$_2$s). The first iPLA$_2$ to be identified was isolated from P388D$_1$ macrophages, and it was later found to be a species variant of another iPLA$_2$ that was discovered in Chinese Hamster Ovary (CHO) cells [28,29]. This 85-88 kDa enzyme has a unique 752 amino acid sequence containing a lipase consensus sequence and eight ankyrin repeats, which may be important for self-aggregation or interaction with other proteins [30]. The lack of any consensus sequences for post-translational modifications such as phosphorylation is consistent with the possibility that group VI iPLA$_2$ functions to remodel membranes, to introduce arachidonic acid at the sn-2 position to allow subsequent release by cPLA$_2$ [31,32].

Platelet activating factor (PAF) is a phospholipid mediator that is synthesised by a number of stimulated inflammatory cells, including macrophages and eosinophils. Its structure is that of PC, with the fatty acyl chain at sn-2 being replaced with an acetyl group (figure 1.3). As well as platelets, PAF activates cells such as neutrophils, macrophages and polymorphonuclear leukocytes (PMN). PAF acetylhydrolase (PAF-AH) is the enzyme responsible for the degradation of PAF and this enzyme has been found to be a member of the PLA$_2$

family. Both plasma and intracellular forms of the enzyme have been isolated, and although they do not share any sequence homology, they are both calcium independent and contain a common active site serine residue, and have been classified as group VII and VIII PLA$_2$s.

The group VII PLA$_2$ was identified in human plasma. Its amino acid sequence is unique apart from the lipase consensus sequence GXSXG at serine 273 [33]. This serine is thought to be involved in catalysis, as the serine in the same position in lipases acts as a nucleophile in the active site. In addition, the activity of this PAF-AH can be inhibited by the serine esterase inhibitor diisopropyl fluorophosphate (DFP) [34]. This 45 kDa PLA$_2$ enzyme was shown to have activity on phospholipids containing a shortened chain at the *sn*-2 position i.e. oxidised phospholipids. Its profound lack of activity on phospholipids with a long chain at the sn-2 position explains how this enzyme can circulate without hydrolysing the lipids in blood cell membranes etc [35].
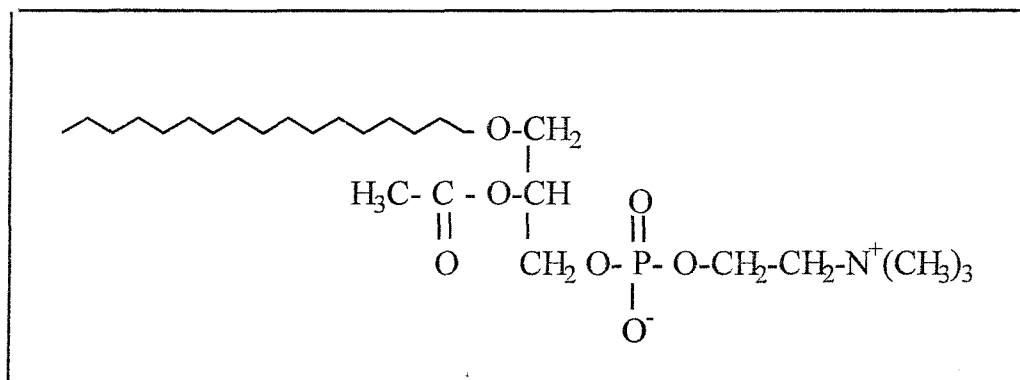
Figure 1.3 The Structure of Platelet-Activating Factor (PAF).

It has been found that ~ 4 % of the Japanese population are deficient in group VII PLA$_2$ activity, and that the prevalence of the deficiency of the PAF-AH is highest

in asthmatics. A point mutation, V279F, has been shown to be responsible for this inactivity, and clinical studies are in progress to try and better define the relationship between this PLA_2 and asthma in the Japanese population [36,37].

The intracellular PAF-AH classified as a group VIII PLA_2 was first isolated from bovine brain [38]. It was shown to be a ~ 100,000 Da heterotrimeric enzyme consisting of 3 subunits of 45, 30 and 29 kDa respectively, of which the latter subunit was found to be active [38]. This PAF-AH can hydrolyse oxidised PC, although this phospholipid was only half as effective as a substrate as PAF. No activity towards PC or PE containing two long fatty acyl chains could be detected [38]. The activity of bovine brain PAF-AH was inhibited by the alkylating agent *para*-bromopenacyl bromide (*p*BPB), which targets histidine residues in the active site of PLA_2s, as well as DFP (see above) [34,38-40]. These results indicated the presence of both a histidine and serine at the active site of this class of enzymes.

1.3.5 Group IX PLA_2s.

The PLA_2s from the marine snail and human spleen (groups IX and X respectively) are the most recently classified PLA_2s. The group IX PLA_2 was isolated from the marine snail *Conus magnus*, which is a predatory snail that preys on fish and molluscs [41]. The PLA_2 isolated (conodipine-M) has a molecular weight of 13.6 kDa and a structure that consists of two polypeptide chains connected by one or more disulphides. These enzymes are calcium dependent, but require much lower concentrations than other calcium-dependant $sPLA_2$s, and accordingly have been shown to lack the conserved Ca^{2+} binding residues. Venom from cone snails is often very complex, consisting of up to 100 components, and this is the first example of one such component being shown to have enzymatic activity [41].

1.3.6 Group X PLA$_2$.

The PLA$_2$ classified as group X was identified in 1997, when it was isolated from human foetal lung. It has since been found in the spleen, thymus and peripheral blood leukocytes, and was shown to be actively secreted. It has a molecular weight of 13.6 kDa, 16 cysteine residues and a carboxyl extension, and also has a long prepropeptide. This PLA$_2$ is more acidic than any other group of sPLA$_2$, and has a pI of ~ 5.3 [42]. It was assigned to a new group, as although it shares homology with the sPLA$_2$s in groups I and II, it also contains the disulphide bonds between cysteines 11-77 and 50-137, which are features of group I and II enzymes respectively [42]. Group X PLA$_2$ was shown to release arachidonic acid from PC much more efficiently than human sPLA$_2$s from groups IB, IIA, IID and V, and its expression in immunity-related tissues suggests some involvement in inflammatory responses [43].

1.3.7 Group XI PLA$_2$.

Novel PLA$_2$s, which contain seven unique disulphide bonds, have been identified in plants including rice and elm. These enzymes have been shown to have PLA$_2$ activity, but their lack of similarity to other PLA$_2$ groups has led to their being assigned to a new group of PLA$_2$s – group XI [1].

1.3.8 PLA$_2$ Classification.

The PLA$_2$s have recently been divided into two groups: those utilising a catalytic histidine, and those that use a serine for catalysis [1]. Tables 1.1 and 1.2 detail the main characteristics of these two groups of PLA$_2$. It is presumed that those enzymes in table 1.1 are extracellular and require mM Ca^{2+} for catalytic activity,

11

while the PLA_2s in table 1.2 are larger enzymes that do not contain disulphide bonds, and do not require calcium for catalytic activity.

1.4 Characteristics of Human Non-pancreatic Secreted PLA_2 ($HnpsPLA_2$).

Human non-pancreatic secreted PLA_2 is a group IIA enzyme, and is the subject of this thesis. $HnpsPLA_2$ was first identified from the synovial fluid of patients suffering from rheumatoid arthritis [44,45], and has since been found in a variety of cells, including platelets, macrophages, spleen, smooth muscle and placenta [7]. It is widely believed that human $sPLA_2$ has a role in inflammation and host defence. The constitutive expression of the enzyme in tissues such as thymus, tonsil, spleen etc., which are all involved in inflammatory responses lends weight to this theory, as does the fact that $sPLA_2$ in the small intestine is concentrated in the Paneth cells, which are actively involved in antimicrobial action in this part of the body.

Expression of $sPLA_2$ can be induced by a number of factors including interleukins 1α and β (IL-1α, IL-1β), and tumour necrosis factor α (TNF-α), which cause elevated transcription and secretion of $sPLA_2$. Interleukin 6 (IL-6) also has an effect on $sPLA_2$ expression, consistent with the IL-6 responsive elements which are found in the $sPLA_2$ gene promoter. The reverse effect on expression is seen with a number of suppressers of $sPLA_2$, of which the most notable are the anti-inflammatory glucocorticoids [4].

$HnpsPLA_2$ is an example of an enzyme, which, before it can catalyse the hydrolysis of phospholipid substrate must first bind to its substrate interface. This phenomenon is termed interfacial binding, and is discussed in more detail later.

Group		Sources	Size (kDa)	Di-S (no.)	Unique Di-S	C-term Extension (no. of residues	Molecular Characteristics
I	A	Cobra/krait venom	13-15	7	11-77	/	
	B	Mammalian pancreas	13-15	7	11-77	/	5 residue pancreatic/elapid loop, propeptide
II	A	Human synovial fluid/platelets, rattlesnake venom	13-15	7	50-137	7	
	B	Gaboon viper venom	13-15	6	50-137	6	Lacks disulphide at C61-C94
	C	Rat/mouse testes	15	8	50-137, 86-92	7	
	D	Human/mouse spleen/pancreas	14-15	7	50-137	7	
	E	Human/mouse brain/heart/uterus	14-15	7	50-137	7	
	F	Mouse testes/embryo	16-17	7	50-137	30	Extra cysteine in C-terminal extension
III		Bee, lizard, scorpion, human	15-18	5	N/A	N/A	Human form (55 kDa) has novel C- and N-terminal domains
V		Mammalian heart/lung/macrophage	14	6	/	/	
IX		Marine snail venom	14	6	N/A	N/A	
X		Human spleen/thymus/leukocyte	14	8	11-77, 50-137	8	
XI	A	Green rice shoots	12.4	6	N/A	N/A	
	B	Green rice shoots	12.9	6	N/A	N/A	

Table 1.1 Characteristics of Secreted PLA$_2$s using a Histidine Residue for Catalysis.

13

Group		Alternative name	Sources	Size (kDa)	Ca^{2+} require-ment/role	Molecular Characteristics
IV	A	cPLA$_2$ α	Human U937 cells/platelets, rat kidney, RAW 264.7	85	< µM Membrane translocation	C2 domain, α/β-hydrolase, phosphorylation
	B	cPLA$_2$ β	Human liver/pancreas/brain/ heart	114	< µM Membrane translocation	C2 domain, α/β-hydrolase
	C	cPLA$_2$ γ	Human heart/skeletal muscle	64	/	Prenylated. α/β-hydrolase
VI	A-1	iPLA$_2$ – A	P388D$_1$ macrophages, CHO cells	84-85	N/A	8 ankyrin repeats
	A-2	iPLA$_2$ – B	Human B-lymphocytes	88-90	N/A	7 ankyrin repeats
	B	iPLA$_2$ - γ/2	Human heart/skeletal muscle	88	N/A	Membrane-bound
VII	A	PAF-AH	Mammalian plasma	45	N/A	Secreted, α/β-hydrolase, Ser/His/Asp triad
	B	PAF-AH (II)	Human/bovine liver/kidney	40	N/A	Myristoylated, Ser/His/Asp triad
VIII	A	PAF-AH Ib α$_1$ (subunit of trimer)	Human brain	26	N/A	G-protein fold, Ser/His/Asp triad, dimeric
	B	PAF-AH Ib α$_2$ (subunit of trimer)	Human brain	26	N/A	G-protein fold, Ser/His/Asp triad, dimeric, active as hetero- or homodimer

Table 1.2 Characteristics of PLA$_2$s Using a Serine Residue for Catalysis.

14

Group IIA sPLA$_2$ is a highly cationic protein containing ten arginine and thirteen lysine residues, and has an isoelectric point (pI) in excess of 10.5. This excess of positive charge is probably linked to the antimicrobial properties of the enzyme, which are discussed later. In addition, the enzyme has a considerable preference for anionic interfaces resulting from the presence of anionic phospholipids or other anionic ligands. In contrast, hnpsPLA$_2$ has a very low affinity for zwitterionic interfaces as seen in the outer leaflet of the plasma membrane, where PC and sphingomyelin are the predominant phospholipids [5]. Thus, the normal, healthy mammalian cell membrane is protected from the hydrolysing activity of this extracellular enzyme. That this membrane preference is due to the presence of anionic charge rather than anionic phospholipid can be demonstrated by the fact that the presence of the anionic ligand cholesterol sulphate, which is not a substrate, dramatically enhances the ability of the enzyme to hydrolyse a PC interface [4,6].

Group IIA sPLA$_2$ is found in particularly high concentrations in platelets, and activation of platelets *in vivo* leads to increased levels of PLA$_2$ in the blood. It is notable that these raised levels of the enzyme quickly return to normal, which is due to the association of sPLA$_2$ with heparan sulphate proteoglycans (HSPG) on the surface of the cell [47]. The affinity of sPLA$_2$ for heparin and HSPG is a unique feature of this group of PLA$_2$, and it is thought that sPLA$_2$ that is bound to HSPG cannot exhibit hydrolytic activity, as a major contribution to heparin binding is a group of cationic residues at the N-terminal which are also required for substrate binding [48,49]. HnpsPLA$_2$ is thought to preferentially associate with the glypican family of HSPG, which are attached to the cell surface via glycosyl phosphatidyl inositol (GPI) [50]. These GPI - anchored glypicans are found in caveolae, which are micro domains on the cell membrane capable of endocytosing molecules and sending them to precise locations within the cell. It is believed that via this mechanism, hnpsPLA$_2$ can be internalised and directed to the perinuclear compartments, where it is close to the cyclooxygenase-2 (COX-2)

enzyme, which is pivotal in the production of prostaglandins from arachidonic acid [50].

1.5 The Physiological and Pathological Roles of HnpsPLA$_2$.

1.5.1. Inflammation.

Human non-pancreatic secreted PLA$_2$ is distributed in a variety of tissues including platelets, spleen, placenta, macrophages and smooth muscle. This enzyme accumulates to very high levels in inflamed tissues, and plasma of patients with rheumatoid arthritis, septic shock, Crohns disease and ulcerative colitis. High concentrations are also found in tears, bronchoalveolar fluid, and seminal and peritoneal fluids [13]. In some disease states e.g. arthritis, Crohns disease, the levels of circulating hnpsPLA$_2$ are a direct reflection of the severity of the disease [7].

When this PLA$_2$ isoform was first isolated from the synovial fluid of arthritic patients [44,45], it was believed to be a key enzyme in inflammation, due to its ability to release arachidonic acid, a precursor in the inflammatory cytokine pathway, from phospholipids. But although hnpsPLA$_2$ can catalyse the release of arachidonic acid from phospholipids, it is not specific for this fatty acid, and as an extracellular enzyme, it was thought that it was unlikely to be the regulator of this key step in inflammation. When the group IV cytosolic form of the enzyme was identified (cPLA$_2$), it provided an enzyme that was both intracellular and arachidonic acid specific (section 1.3.2) [6,17]. Subsequent studies using gene knockout mice (i.e. those lacking the cPLA$_2$ gene) proved that it was this class of PLA$_2$ that was primarily responsible for arachidonic acid release. This left the precise role of secreted PLA$_2$ in inflammation unclear [51,52].

Some of the most convincing evidence that $sPLA_2$ was not the major enzyme in inflammation came from studies on mice. Some inbred mice strains have a natural frameshift mutation in their $sPLA_2$ gene, which causes production of a non-functional enzyme [53]. The phenotype of these $sPLA_2$ deficient mice is similar to that of $sPLA_2$ expressing mice, both in normal physiological terms and in response to an inflammatory challenge. So either another $sPLA_2$ type can compensate for the lack of type IIA $sPLA_2$, or this enzyme does not have a key role in inflammation. Transgenic mice that overexpressed the gene for $sPLA_2$ were also studied, and in terms of inflammation, these mice showed no overt change in their inflammatory response either [54]. The effect of $hnpsPLA_2$ in a number of inflammatory situations was also explored using a number of different animal models, and injecting $hnpsPLA_2$ at different sites and stages of inflammation [7]. In general, it was hard to elucidate an exact role for human $sPLA_2$ in inflammation, but it is now generally accepted that $hnpsPLA_2$ can only be inflammatory in the presence of some pre-existing inflammatory condition, and that the presence of human $sPLA_2$ alone was not sufficient to provoke an inflammatory response.

The present thinking is that a primary function of human non-pancreatic secreted PLA_2 is that of an acute phase protein, which has a role in the removal of damaged/apoptotic cells, and in host defence against bacterial infection [55]. This theory is in keeping with the preference of $hnpsPLA_2$ for anionic phospholipid interfaces, as damaged or apoptotic cells will have the negatively charged phospholipid PS exposed on their outer leaflet. In a healthy mammalian cell, PS is maintained on the inner leaflet by an aminophospholipid transferase, which becomes down-regulated in apoptosis [56]. Likewise in bacterial cells, the major phospholipid, phosphatidyl glycerol (PG) is also anionic, in contrast to healthy mammalian cells which contain mostly zwitterionic phospholipids such as PC on their outer leaflet. This explains why $hnpsPLA_2$ will help to destroy invading bacteria, but under normal circumstances will not hydrolyse healthy mammalian cells. In summary, the group IIA $hnpsPLA_2$ is a highly complex,

widely distributed and tightly controlled enzyme, but its exact role in inflammation has yet to be fully characterised.

1.5.2 Sepsis and Antimicrobial Defence.

As early as 1978, non-pancreatic sPLA$_2$ (npsPLA$_2$) had been identified in association with inflamed sites in experimental peritonitis in rabbits, and antigenic challenge in sheep. NpsPLA$_2$ was seen to be vasoactive, consistent with this observation for snake venom PLA$_2$s and this led to the involvement of npsPLA$_2$ in systemic inflammatory conditions being investigated [7].

Endotoxin shock, a typical systemic inflammatory condition, was induced in rabbits and the levels of npsPLA$_2$ were reported to increase considerably with a concomitant fall in blood pressure. Inactivation of npsPLA$_2$ prior to induction of endotoxin shock in the animal reduced this hypotensive response [47]. Elevated levels of npsPLA$_2$ have been seen in a number of animal infection models including rats, horses and baboons as well as in humans, which suggests that increased expression of sPLA$_2$ is part of the host response to bacterial infection. In both Gram-negative and Gram-positive bacterial septic shock, patients have demonstrated hyperphospholipasemia, where the PLA$_2$ involved was shown to be the same as that isolated from synovial fluid of arthritic patients [47]. So it appears that inflammatory conditions resulting from bacterial infection can in part be characterised by profoundly elevated levels of circulating PLA$_2$.

The bactericidal effect of hnpsPLA$_2$ has been studied *in vitro*. It was found that in the case of Gram-negative bacteria, such as *E. coli*, hnpsPLA$_2$ was only able to hydrolyse the bacterial membrane phospholipids in the presence of bactericidal/permeability increasing protein (BPI) [57,58]. This basic protein disrupts the lipopolysaccharide coat of Gram-negative bacteria allowing hnpsPLA$_2$ access to the cell wall and phospholipid membrane [59]. However, in

18

the case of Gram-positive bacteria such as *S. aureus* and *M. luteus*, hnpsPLA$_2$ is bactericidal in the absence of any other factors [60,61]. It has been confirmed that the bactericidal effect of hnpsPLA$_2$ is due to the hydrolysis of bacterial membrane phospholipids, as the effects are calcium dependent, and are not seen in the presence of EGTA [62].

The antibacterial effects of hnpsPLA$_2$ have also been studied *in vivo*. It was demonstrated that transgenic mice expressing the hnpsPLA$_2$ were resistant to *S. aureus* infection, with serum levels of PLA$_2$ rising dramatically after injection with these bacteria. This result was confirmed using antibodies against hnpsPLA$_2$, which blocked the resistance [8].

It is likely that the ability of group IIA PLA$_2$ to elicit antibacterial effects is due largely to the global positive charge of the enzyme. This is believed to assist its progress through the negatively charged peptidoglycan cell wall, as shown in figure 1.4. sPLA$_2$s from porcine pancreas and cobra venom for example have lower pI's and show little or no activity towards Gram-positive bacteria [63]. The cationic nature of hnpsPLA$_2$ also leads to its specificity towards anionic phospholipids. As the predominant phospholipids in bacterial membranes are cardiolipin and PG, it is perhaps unsurprising that hnpsPLA$_2$ shows such antibacterial activity.

It is important to stress, however, that this specificity is due to the anionic nature of the phospholipid interface allowing interfacial binding. The enzyme shows minimal substrate specificity in terms of active site preference.
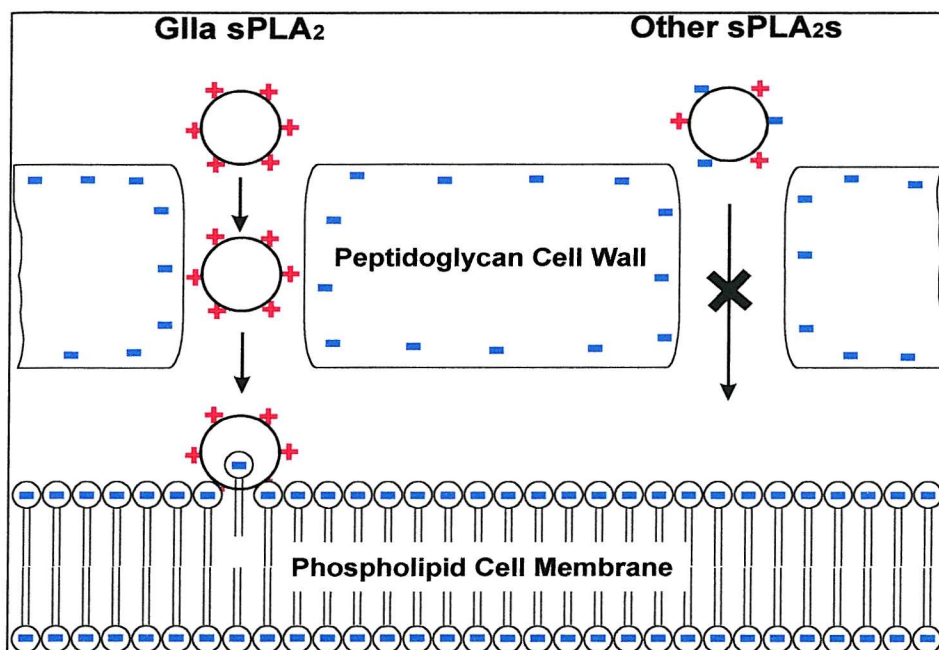
Figure 1.4 Schematic Representation of Group IIA sPLA$_2$ Accessing the Phospholipid Cell Membrane of Gram-positive Bacteria.

Taken from [63] with permission.

1.6 Structure of Human Non-pancreatic Secreted Phospholipase A$_2$.

HnpsPLA$_2$ is a small compact protein with a molecular mass of 13860 Da, and a sequence comprising 124 amino acids. Its dimensions are approximately 22 x 30 x 42 Å, with ~50 % of the protein consisting of α-helix and ~10 % β-strand which protrudes away from the body of the protein forming a so-called β-wing. HnpsPLA$_2$ and other group II sPLA$_2$s have a conserved core of homologous tertiary structure in common with the group I sPLA$_2$s. This includes the three major α-helices (residues 1-12, 37-54 and 90-109) and the backbone loop between residues 24 and 30. Side-chains from the amino acids in this core are critical for co-ordinating the calcium ion required for catalysis, defining the substrate binding site and mediating in catalysis itself [12].

A ribbon diagram of hnpsPLA$_2$ highlighting the key structural features is shown in figure 1.5.

The amino terminus of hnpsPLA$_2$ is also an important structural feature of the enzyme. Residues in this part of the protein are involved in a hydrogen-bonding network, which connects this area of the enzyme with the active site. The amino terminus is relatively mobile when the enzyme is free in solution, but forms a stable α-helix on interfacial binding. It was found that the mobility of this region was important for full catalytic activity; enzymes from group IB carry a propeptide attached to the N-terminal, which must be cleaved by trypsin to see full catalytic activity. Also, hnpsPLA$_2$ shows only ~ 1 % activity compared to the wild type if the initiator methionine residue is not removed from the amino terminus [12,64,65].

HnpsPLA$_2$ has seven disulphide bonds in keeping with its extracellular location, which contribute to its stable tertiary structure [12]. The group II sPLA$_2$s are distinguished from the group I enzymes by the position of one of these disulphides – the bond between cysteines 11 and 76 in group I sPLA$_2$s is absent in hnpsPLA$_2$, but is replaced by a salt-bridge which spans the lysine residue found at position 11 and the glutamate at position 77. This salt-bridge connects two conserved structural regions of the protein, thus retaining the overall fold of the enzyme and demonstrating how important the integrity of these regions is for function. A unique disulphide is found in group II sPLA$_2$s between the middle of the third helix (cysteine 50), and a C-terminal extension of seven residues (cysteine 133) leaving both groups of enzymes with a total of seven disulphides [12].

The C-terminal extension is a characteristic of group II but not group I sPLA$_2$s, whilst group II enzymes do not contain the elapid loop, so named due to its presence in the sPLA$_2$s structure of the cobra family *Elapidae*, which is a feature of group I and other classes of sPLA$_2$ [12].
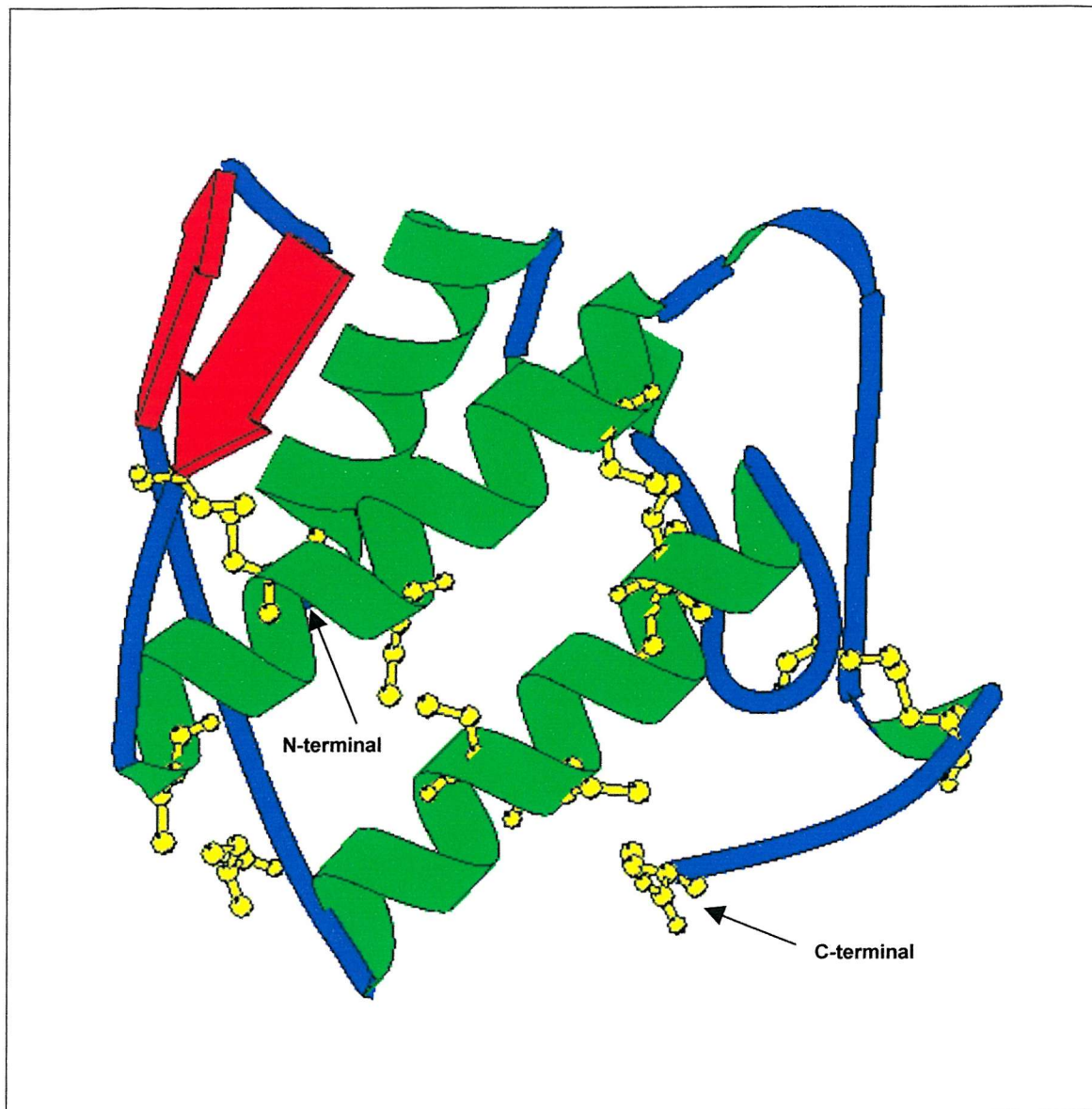
Figure 1.5 Ribbon Diagram of HnpsPLA$_2$.

Key secondary structures are coloured as follows:

Green - α-Helices,

Red - β-Wing,

Yellow - disulphide-forming cysteine residues

Arrows indicate the positions of the N- and C- terminal.

1.6.1 The Interfacial Binding Surface (IBS).

An important feature of hnpsPLA$_2$ and other secretory PLA$_2$s is their striking preference for aggregated substrates in the form of micelles, vesicles or membranes, on which their activity is many times higher than on monomeric substrate. This is perhaps unsurprising given the low concentrations of monomeric phospholipids found physiologically, and adds a further dimension to these enzymes, as before sPLA$_2$s can hydrolyse substrate phospholipid molecules, they must first productively bind to an aggregated phospholipid structure. This property of binding to a lipid/water interface is one shared with other enzymes including lipolytic enzymes and protein kinases, and hnpsPLA$_2$ has a conserved core of residues that make up this so-called interfacial binding surface. Other important functional parts of hnpsPLA$_2$ are the catalytic site and the calcium-binding loop, which are highly conserved throughout the major classes of sPLA$_2$s.

The interfacial binding surface (IBS) of secretory PLA$_2$s is the region of the protein responsible for its binding to aggregated substrate structures such as membranes and vesicles. The process of PLA$_2$ binding to the interface and then a substrate phospholipid entering the active site for hydrolysis is often denoted as shown in figure 1.6. It is important to note that the interfacial binding of hnpsPLA$_2$ to aggregated substrates is totally distinct from the hydrolysis of individual phospholipids, and that only when the enzyme is interfacially activated can catalysis occur. The IBS is a region found on the flat surface of hnpsPLA$_2$ and consists of a number of cationic residues including Arg-7, Lys-10, Lys-16, Lys-74, Lys-87, Arg-92, Lys-124 and Arg-127, which contribute to the binding via electrostatic interactions, and also influence the preference of hnpsPLA$_2$ for anionic substrate [66]. A number of exposed hydrophobic residues, which form a 'collar' around the active site are also involved in the binding of the enzyme to its interface [12].
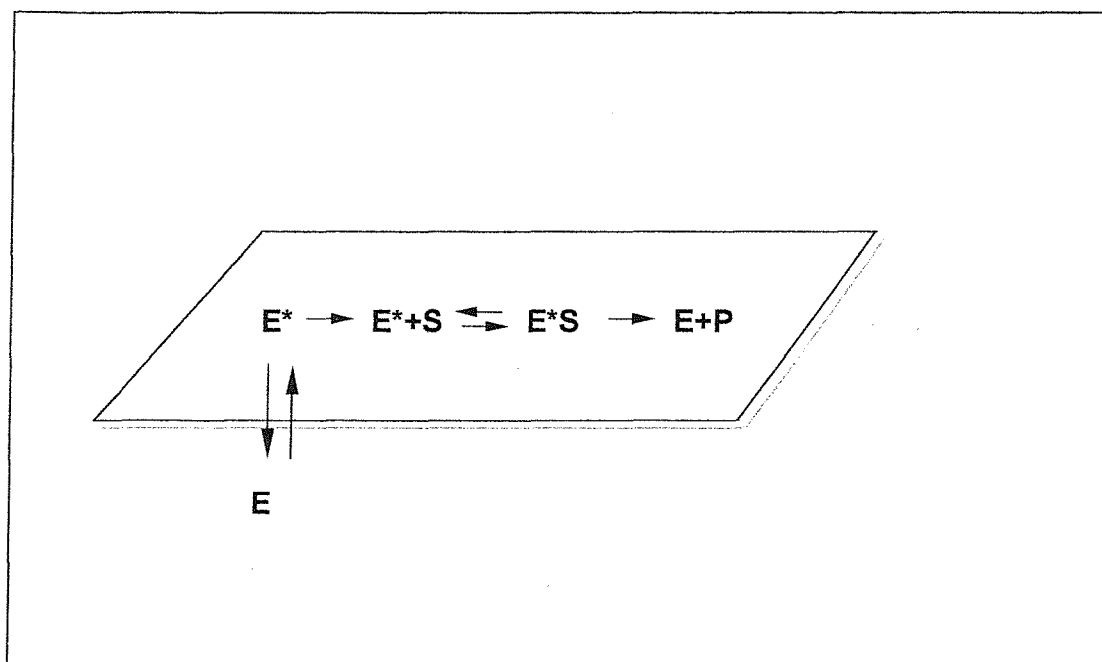
Figure 1.6 Schematic Representation of Interfacial Binding by sPLA$_2$.

sPLA$_2$ enzyme (E) binds to a substrate interface becoming interfacially activated (E*). Only now can the enzyme catalyse the hydrolysis of substrate (S) to products (P).

Figure 1.7 shows the distribution of charge on the IBS of hnpsPLA$_2$, together with the hydrophobic residues of the collar.

The role of cationic residues on the surface of hnpsPLA$_2$ has been investigated and characterised using site directed mutagenesis. The thirteen lysine and ten arginine residues on the surface were divided up into clusters and up to five residues at a time were subjected to charge reversal mutagenesis, in order to establish the role of electrostatic interactions in the process of interfacial binding [66,67]. This strategy was also used to identify specific heparin binding sites on the protein surface.
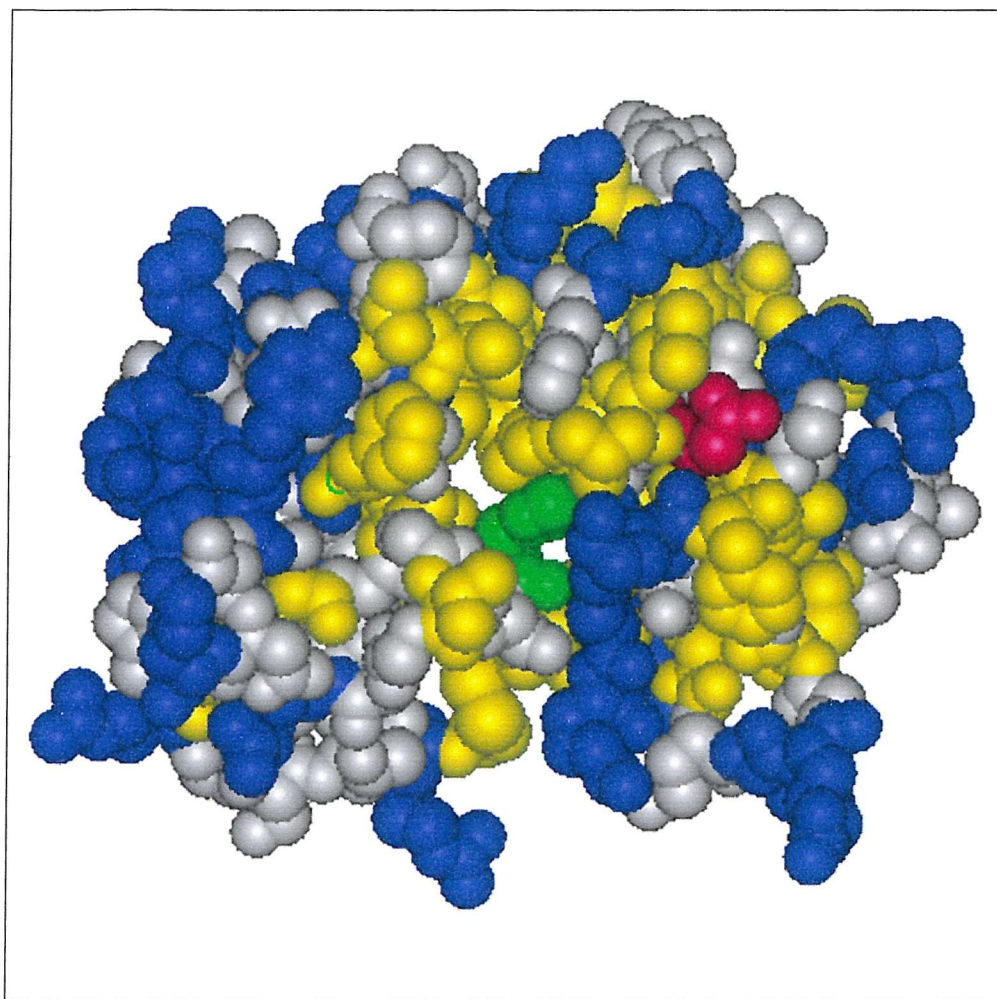
Figure 1.7 Space-filling Model of HnpsPLA₂.

The structure of hnpsPLA$_2$ has been coloured to show the basic residues and hydrophobic residues that are involved in interfacial binding. The picture is oriented so that the viewer is looking at the interface.

The enzyme is coloured as follows:

Blue - Basic residues

Yellow - Hydrophobic residues

The active site histidine (His-48) is coloured green, and the N-terminal residue red for purposes of orientation.

It was found that three residues in the N-terminal portion, Arg-7, Lys-10 and Lys-16 made the most significant contribution to binding, with the triple mutant R7E/K10E/K16E showing at least 290 times less binding affinity than the wild type [66,67]. The five-site mutant R7E/K10E/K16E/K124E/R127D was found to bind to anionic interfaces 2200-fold more weakly than the wild type [67]. However, a similar experiment concerning the group III bee venom sPLA2 showed that even after reversing the charge of five out of the six positive residues on the interfacial binding surface, there was little effect on the enzymes ability to bind and hydrolyse substrate [68]. Structural studies using electron spin resonance showed that it was in fact hydrophobic residues that were in direct contact with the interface, and the six basic residues did not actually contact the phospholipid surface [69].

It is anticipated therefore, that the different types of sPLA2 will show a preference for an interface indicative of their physiological function. For example, the high affinity of the cationic hnpsPLA2 for anionic phospholipids such as PG correlates well with an antibacterial role, whereas the *Naja naja* venom sPLA2 has a preference for zwitterionic PC interfaces consistent with killing and digestion of prey. It should be emphasised that the substrate preferences discussed relate to the interfacial binding step, and not to the affinity of the active site for a particular type of phospholipid.

1.6.2 The Hydrophobic Channel.

A deep hydrophobic pocket connects the IBS with the catalytic His-Asp pair of the active site, and this channel contains many of the conserved and invariant residues found in sPLA2s including Phe-106 at the base of the pocket, Leu-2 at the opening of the channel and Ile-9 and Phe-5 from the N-terminal [12]. The side chains from residues 2,5 and 9 constitute the right wall and mouth of the channel, with Phe-5 being the most critical, as its phenolic ring is trapped

between Ile-9 and the catalytic residue His-48 [70]. Ala-18, Leu-19, Cys-29 and Cys-45 are seen to line one side of the pocket, with a disulphide bond apparent between the two cysteines, and the residues Ala-17, Phe-24 and Val-31 are arranged on the opposite side of the pocket.

The residue at position 4 in the protein is responsible for anchoring the N-terminal helix with respect to the rest of the enzyme, but the conserved Gln residue seen here in most sPLA$_2$s is replaced by an Asn in hnpsPLA$_2$, leaving the helix less well anchored. The result is that the helix can move ~1 Å into the channel due to the interactions between Asn-4 and His-6, which is another exception to the core of invariant residues in this protein, as a Leu is found at position 6 in all sPLA$_2$s apart from hnpsPLA$_2$. The result of these interactions is that the mouth of the hydrophobic channel is slightly narrower in sPLA$_2$ from humans, in the absence of substrate [71]. The side chain of His-6 is inserted into the mouth of the hydrophobic channel when it is devoid of substrate, instead of being exposed to bulk solvent, which is a novel characteristic of hnpsPLA$_2$. There are several water molecules that are ordered within the pocket, which are displaced by fatty acyl chains on binding of substrate, thus allowing entry of the substrate into the active site [12]. The hydrophobic nature of the channel and the residues at its mouth, ensure a seemingly 'watertight' seal when the enzyme is bound to its substrate aggregate, thereby facilitating diffusion of the substrate phospholipid into the active site for hydrolysis.

1.6.3 The Calcium Binding Site.

The calcium ion required for catalysis is co-ordinated within the hydrophobic channel by the carboxylate oxygen atom of Asp-49 and the carbonyl oxygens of residues 28, 30 and 32, which are part of the calcium binding loop (residues 25-33). Two conserved structural water molecules complete the pentagonal bipyramid which co-ordinates the calcium ion (figure 1.8). The C-terminal

extension seen in hnpsPLA$_2$ is found close to the calcium binding loop, although it is not believed to be directly involved in calcium binding, interfacial recognition or catalysis [72].

1.6.4 The Disulphide Bonds.

HnpsPLA$_2$ contains seven disulphide bonds, and these are important features of extracellular enzymes as they contribute to the high levels of stability seen in sPLA$_2$. The importance of the disulphides present in the group I bovine pancreatic enzyme were investigated by the use of site-directed mutagenesis, where both cysteine residues of each disulphide in turn were mutated to alanines [73]. It was shown from these studies that the disulphide between Cys-84 and Cys-96 was required for the correct folding of the enzyme. In terms of stability, the disulphide between Cys-11 and Cys-77 was most important – this is not present in the group II enzymes, but is replaced by a salt-bridge again indicating the importance of structural integrity in this part of the protein [73].

1.6.5 The Active Site.

The active site of hnpsPLA$_2$ not surprisingly contains some of the most invariant and conserved residues in the protein, including the catalytic pair His-48 and Asp-99. The active site is found in a cleft below the surface of the protein, and is linked to the interfacial binding site by the hydrophobic channel. As well as the catalytic dyad, two conserved tyrosines, Tyr-52 and Tyr-73 are found here along with the water molecules that are proposed to be involved in catalysis.
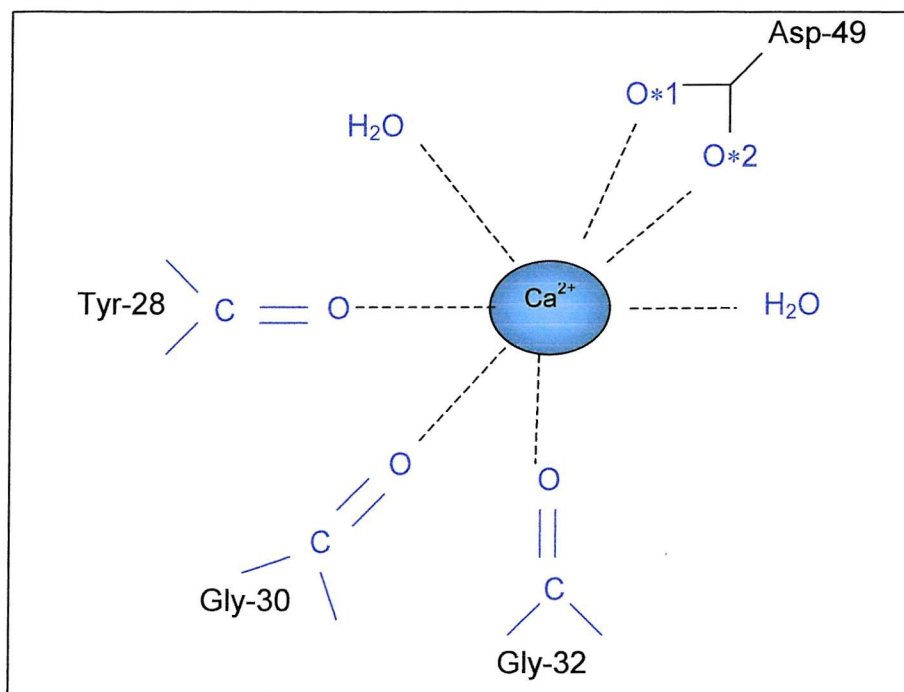
Figure 1.8 Schematic Representation of the Calcium-binding Ligands.
The calcium ion crucial for catalysis is shown co-ordinated by Asp-49, Tyr-28, Gly-30, Gly-32 and two water molecules.

1.7 Catalytic Mechanism.

Verheij *et al* first proposed the catalytic mechanism of sPLA$_2$ in 1980, after it had been deduced that the histidine at position 48 was crucial for catalysis [74]. This mechanism is likened to the 'catalytic triad' mechanism, due to its similarities with the so-named catalytic mechanism of serine proteases. These proteases also utilise a His/Asp pair for catalysis, but there is a serine residue involved, which completes the triad. The serine residue is replaced in sPLA$_2$ by a water molecule, which is proposed to be involved in the catalytic action. The mechanism is shown

29

in figure 1.9, and the positioning of the His/Asp pair and the catalytic water can be seen. The water is proposed to act as a nucleophile, attacking the carbonyl carbon of the substrates sn-2 group, and forming an oxyanion tetrahedral intermediate – the formation of this intermediate is the presumed rate-limiting step. The catalytic His-48 residue becomes protonated at the N-1 position, and is stabilised by the interaction with the negatively charged Asp-99. The tetrahedral intermediate can subsequently collapse with protonation by His-48 to release product. The calcium ion that is crucial for catalysis is thought to have a dual role in this mechanism, as it is involved in the orientation of the substrate molecule, as well as polarising the carbonyl carbon atom of the sn-2 group of the substrate. In the transition state, the oxyanion is stabilised by the calcium ion.

In 1997, Rogers *et al* proposed an alternative mechanism for catalysis, which differs from the original in that the rate-limiting step is the decomposition of the intermediate rather than its formation, and that two water molecules play a part in catalysis [75]. The proposed mechanism is shown in figure 1.10. In this mechanism, one of the water molecules acts as a nucleophile (OH^-) (w5 in figure 1.10) after being deprotonated, and is co-ordinated to the calcium ion, whilst the other water (w6) accepts a proton from the first water and is hydrogen-bonded to the catalytic His-48 residue. Catalysis proceeds when the nucleophilic water attacks the sn-2 group of the substrate phospholipid, forming the tetrahedral intermediate, which is stabilised in part by the crucial calcium ion. The collapse of the intermediate structure releases the fatty acid and lysophospholipid products. It is proposed that the collapse of the oxyanion intermediate is the rate-limiting step in this mechanism.

1.7.2 Modes of Catalysis.

Once interfacially bound, there are two modes of catalysis available to the $sPLA_2$ enzyme in order to cleave the ester bond of the phospholipid.

Figure 1.9 The 'One-Water' Catalytic Mechanism of PLA$_2$.

R1 and R2 represent the sn-1 and sn-2 fatty acyl chains; X represents the headgroup. (Taken from [74] with permission).

31
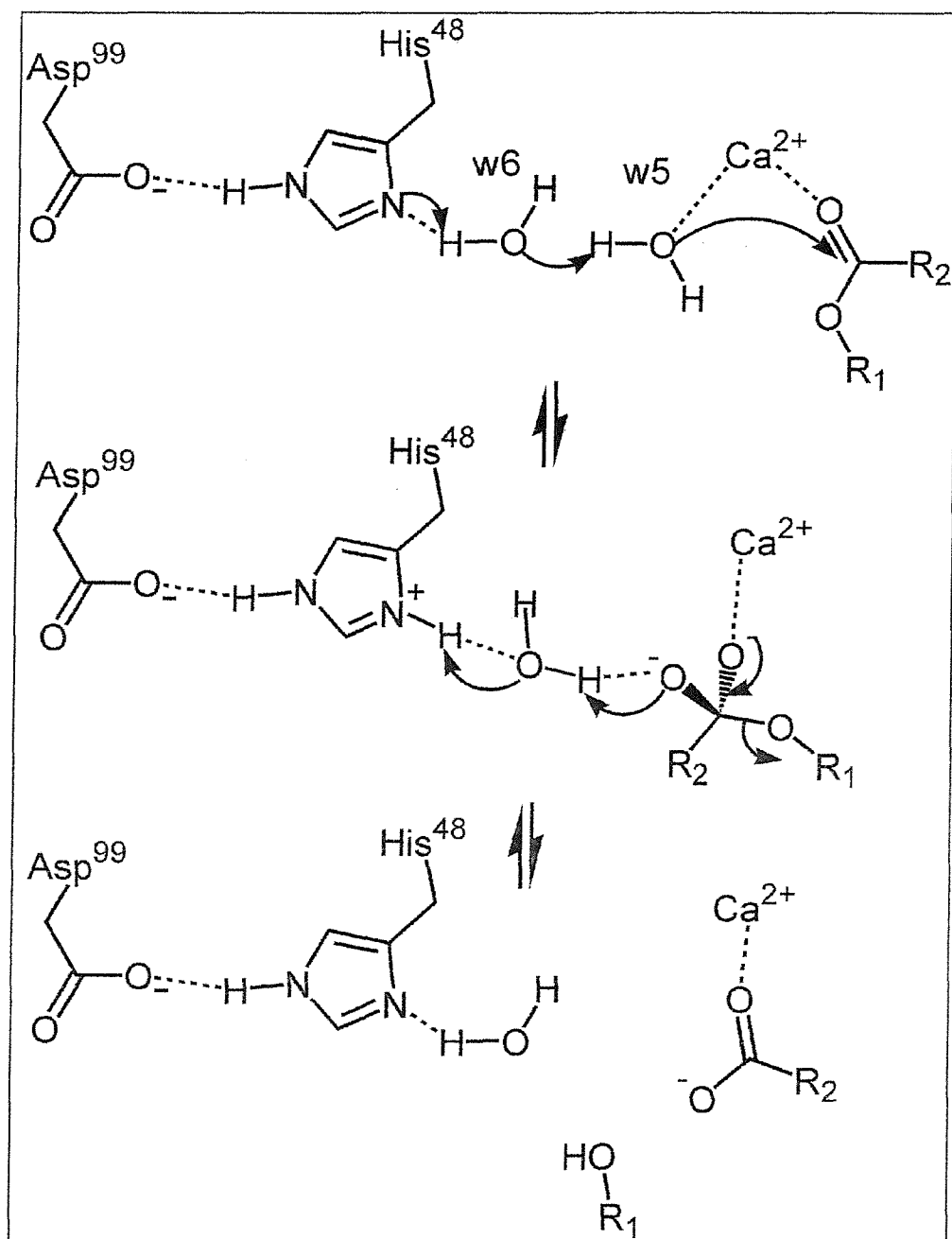
Figure 1.10 The 'Two-Water' Catalytic Mechanism

R1 represents the phospholipid molecule excluding the sn-2 fatty acyl chain; R2 represents the sn-2 fatty acyl chain. (Personal communication from Prof. M. K. Jain).

HnpsPLA$_2$ operates either via a 'hopping' mechanism where it binds (becoming interfacially activated), hydrolyses phospholipid and then dissociates from the substrate, or it binds and then 'scoots' across the surface of the aggregated substrate molecule hydrolysing the phospholipids in a processive manner without dissociating from the substrate at any time (figure 1.11) [76-78]. In scooting mode it has been shown, as exemplified by the porcine pancreatic sPLA$_2$, that the enzyme will remain attached to the interface of small, anionic vesicles while completely hydrolysing all the phospholipid in the outer monolayer. This is in the presence of excess substrate, with a maximum of one enzyme molecule bound per vesicle. Having hydrolysed all available phospholipid in this vesicle, the enzyme must now hop onto another vesicle before further catalysis can occur [76-78].
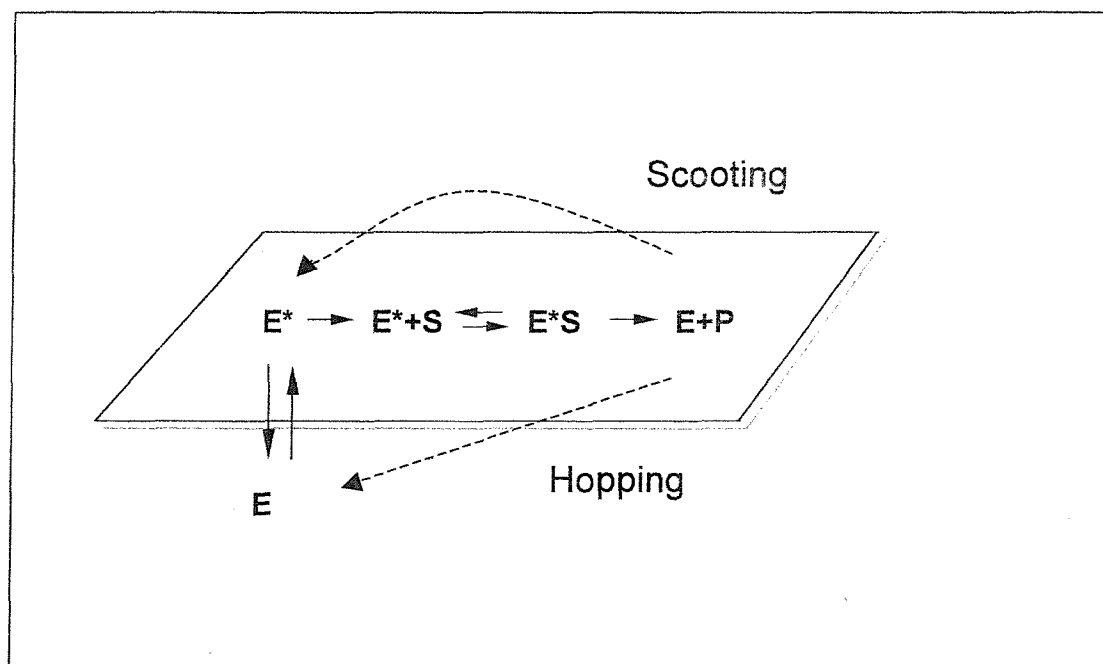
Figure 1.11 Schematic Diagram of the Hopping/Scooting Modes of Catalysis of HnpsPLA$_2$.

The hopping and scooting modes of catalysis of hnpsPLA$_2$ are indicated.

Key: E - enzyme, E* - interfacially activated enzyme, S - substrate, P - product.

1.8 Aims of the Thesis.

Interfacial binding of $sPLA_2$ to membrane surfaces is a major site for physiological regulation. Therefore, the major aim of this thesis was to study those structural features of $hnpsPLA_2$ that are involved in interfacial binding.

It was decided that the concept of interfacial competition (substrate depletion) would be used as a method of analysing interfacial binding, whereby the high affinity $sPLA_2$ competes with another high affinity protein for the interfacial surface. This technique has been used successfully in conjunction with the phospholipid-binding protein annexin V to gauge the relative binding affinities of various $sPLA_2$s for anionic vesicles.

The first objective of this project was the production of the active site mutants H48Q, H48N and H48A of $hnpsPLA_2$. These were constructed with the aim of obtaining structurally intact, but catalytically inactive mutants of $hnpsPLA_2$ that could be used in interfacial competition studies.

Surprisingly, the H48Q mutant was found to have significant residual activity. This was contrary to expectation, as the substitution of the catalytic histidine residue with a glutamine residue in other groups of $sPLA_2$ had provided an inactive mutant.

A detailed analysis of this mutant was required, including the solving of the crystal structure, in order to try and explain how this mutant could show catalytic activity even though it is lacking the catalytic histidine residue which has long been known to be crucial for catalysis.

Chapter Two - Materials and Methods

2.1 Chemicals.

All chemicals used were purchased from Sigma Chemical Company Ltd (Poole, Dorset) or BDH Ltd (Poole, Dorset) except for the following specialist items:

Amicon (Stonehouse, Gloucs.): Centricon and Centriplus concentrator

Avanti Polar Lipids (Alabama, USA): Dioleoyl phosphatidylglycerol, dioleoyl phosphatidylcholine, dioleolyl phosphatidylmethanol, 1-palmitoyl, 2-oleoyl phosphatidylglycerol

BioRad (Hemel Hempstead, Herts): M13 *in vitro* Site-Directed Mutagenesis Kit
Bradford Protein Assay Reagent

Boehringer Mannheim UK Ltd. (Lewes, E. Sussex): Restriction enzymes and buffers

Hichrom Ltd. (Reading, Berks.): Nucleosil NC300-5 C18 Column (HPLC)

Lab M (Bury, Lancs.): Tryptone, Yeast Extract, Agar No. 1

Molecular Probes (OR, USA): DAUDA (11-dansylaminoundecanoic acid)

Millipore (Stonehouse, Gloucs.): 0.22 μm filters

OSWEL (Southampton University, Southampton): Custom oligonucleotides, DNA sequencing

Pharmacia Biotech (Uppsalla, Sweden): 5 ml Hitrap SP-Sepharose (FPLC)
5 ml Hitrap Heparin-Sepharose columns (FPLC)

Promega (Chilworth, Southampton): Wizard Plus SV Miniprep Kit

Qiagen (Crawley, W. Sussex.): QiaQuick kits

Sartorius (Gottingen, Germany): Sterile 0.45 μm filters

2.2 Media.

<u>Luria-Bertani (LB) Broth   g/l</u>

Tryptone	10
Yeast Extract	5
NaCl	5

LB-Agar plates were used as solid growth media and contained 15 g Agar/l LB. Ampicillin/carbenicillin and chloramphenicol were used routinely as selectivity agents in concentrations of 50 µg/ml and 30 µg/ml respectively. Isopropyl-ß-thiogalactopyranoside (IPTG) was used to induce the growth of bacterial cells at a final concentration of 0.4 mM. Both the antibiotics and IPTG were filter sterilised prior to aseptic addition.

<u>H-Agar   g/l</u>

Tryptone	10
NaCl	5
Agar	15

<u>H-Top Agar   g/l</u>

Tryptone	10
NaCl	5
Agar	7

H-Agar plates were covered with H-Top Agar in order to grow M13 plaques as a bacterial lawn.

2.2.1 Sterilisation.

All broth and growth media, pipette tips and microfuge tubes were sterilised by autoclaving at 120 °C for 20 minutes. Ampicillin, IPTG and other heat labile chemicals were filter sterilised using disposable 0.45 µM filters.

37

2.2.2 Bacterial Strains.

Escherichia coli (*E.coli*) BL21 (DE3) cells transformed with pET11a containing the PLA$_2$ gene construct were maintained as streaks on LB-agar plates in the presence of 50 µg/ml ampicillin or carbenicillin for ~1 week at 4 °C. MV1190 cells were streaked on LB-agar plates in the absence of antibiotics for short-term storage. CJ236 cells were grown on LB-agar plates in the presence of chloramphenicol (30 µg/ml) as a selectivity agent. Long term storage of strains was achieved by adding 0.85 ml of an overnight culture of the cells to 0.15 ml sterile glycerol in a sterile cryotube, vortexing and storing at -70°C.

Bacterial Strain	Phenotype
BL21 (DE3)	F⁻ *ompT*, *hsd* S$_B$ (r⁻$_B$ m$_B$⁻), *gal*, *dcm*
MV1190	Δ(*lac-pro* AB), *thi*, supE, Δ(*sri-rec* A) 306:Tn10(tet^r) [F':*tra* D36, *pro* AB, *lac* I^{q}ZΔM15]
CJ236	*dut*-1, *ung*-1, *thi*-1, rel A-1; pCJ105 (Cm^r)

2.3 DNA Methods.

2.3.1 Site-directed Mutagenesis.

Site-directed mutagenesis was achieved by two methods: the Kunkel method, or a 2-stage PCR reaction.

The DNA sequence for human non-pancreatic secreted PLA$_2$ is shown in figure 2.1. The rational design of all oligonucleotide primers was based on this sequence.

```
                              TATGGCCCTGGTAAACTTCCACCGT
                              ACCGGGACCATTTGAAGGTGGCA
                              M   A   L   V   N   F   H   R

ATGATCAAGTTAACCACCGGTAAAGAAGCTGCTCTGTCTTACGGTTTCTA
TACTAGTTCAATTGGTGGCCATTTCTTCGACGAGACAGAATGCCAAAGAT
 M   I   K   L   T   T   G   K   E   A   A   L   S   Y   G   F   Y

CGGTTGCCACTGCGGTGTTGGCGGCCGCGGGTCCCCGAAAGACGCTACCG
GCCAACGGTGACGCCACAACCGCCGGCGCCCAGGGGCTTTCTGCGATGGC
 G   C   H   C   G   V   G   G   R   G   S   P   K   D   A   T


ACCGTTGCTGCGTTACCCACGACTGCTGCTACAAACGTCTCGAGAAACGT
TGGCAACGACGCAATGGGTGCTGACGACGATGTTTGCAGAGCTCTTTGCA
 D   R   C   C   V   T   H   D   C   C   Y   K   R   L   E   K   R

GGTTGCGGTACCAAATTCCTGTCTTACAAATTCTCTAACTCTGGTTCGCG
CCAACGCCATGGTTTAAGGACAGAATGTTTAAGAGATTGAGACCAAGCGC
  G   C   G   T   K   F   L   S   Y   K   F   S   N   S   G   S   R

AATCACCTGCGCTAAACAGGACTCTTGCCGTTCTCAGCTGTGCGAATGCG
TTAGTGGACGCGATTTGTCCTGAGAACGGCAAGAGTCGACACGCTTACGC
  I   T   C   A   K   Q   D   S   C   R   S   Q   L   C   E   C

ACAAAGCTGCAGCTACCTGCTTCGCTCGTAACAAAACCACCTACAACAAA
TGTTTCGACGTCGATGGACGAAGCGAGCATTGTTTTGGTGGATGTTGTTT
 D   K   A   A   A   T   C   F   A   R   N   K   T   T   Y   N   K

AAATACCAGTACTACTCTAACAAACACTGCCGTGGGTCTACCCCGCGTTG
TTTATGGTCATGATGAGATTGTTTGTGACGGCACCCAGATGGGGCGCAAC
 K   Y   Q   Y   Y   S   N   K   H   C   R   G   S   T   P   R   C

CTAATAGTGA
GATTATCACTTCGA
```

Figure 2.2 The Gene Coding for N1A HnpsPLA$_2$.

The gene is flanked by an Nde I restriction site (CATATG) at the 5′ end and a Hind III site at the 3′ end (AAGCTT) for cloning into the pET11a expression vector.

The Nde I site also contains the initiator methionine.

2.3.2 Primers Used for Mutagenesis.

Customised oligonucleotides were designed based on the gene sequence of human sPLA$_2$ and produced by Oswel (Southampton University).

Forward (5' end): AAAA GAA TTC CAT ATG GCC CTG GTA AAC TTC CAC

Reverse (3' end): AAAA AAG CTT ACT ATT AGC AAC GC

H48Q+: TGC TGC GTT ACC **CAG** GAC TGC TGC TAC

H48N (Kunkel): TGC TGC GTT ACC **AAC** GAC TGC TGC TAC

H48A (PCR): A* - GTA GCA GCA GTC **AGC** CGTAAC GCA GCA

                     B* - TGC TGC GTT ACC **GCT** GAC TGC TGC TAC

+ prepared previously (S. Baker)

Restriction sites are shown in green (*Eco RI*), and blue (*Nde I, Hind III*)

Mutations are shown underlined in bold.

2.3.3 The Kunkel Method.

The Kunkel method of mutagenesis makes use of the filamentous bacteriophage M13. M13 is an ideal cloning vehicle, as its genome is a desirable size (<10 kb) and the double stranded form (the replicative form, RF) can be treated like a plasmid for experimental purposes. The bacteriophage can be prepared easily from infected *E. coli* and can be reintroduced as readily by transformation. Genes cloned within an M13-based vector can be obtained in a single-stranded form which is useful for sequencing and *in vitro* mutagenesis. The Kunkel method of mutagenesis is based on the ability to select for a mutagenized strand of double-stranded DNA, as opposed to the parent DNA strand, which is facilitated by the use of *E. coli* strains lacking the enzymes d-UTPase (*dut⁻*) and uracil N-glycosylase (*ung⁻*) [79]. The *dut⁻* mutation results in uracils being incorporated into thymine positions in the nascent DNA, and the *ung⁻* mutation means that the

enzyme responsible for removing these uracils is not present. The uracil-containing strand may then be used as a template for the synthesis of an oligonucleotide-primed complementary strand containing the desired mutation. The resulting double-stranded moiety can then be transformed into an *E. coli* strain with a proficient uracil N-glycosylase which will inactivate the uracil-containing template strand, leaving the non-uracil containing mutated strand to replicate. The presence of the desired mutation can then be confirmed by sequencing, and the mutated gene transferred into a suitable vector for expression.

2.3.4 Preparation of a Single-stranded M13 Template for Mutagenesis.

The first stage of the production of a single-stranded M13 template requires amplification of the gene which will be used as the template, in this case the gene coding for the N1A hnpsPLA$_2$. Plasmid DNA containing the PLA$_2$ gene was isolated using a Promega Wizard SV Miniprep kit as described in 2.3.9. The gene was then amplified by PCR using the forward and reverse oligonucleotide primers shown in 2.3.2. The forward primer contains *Eco RI* and *Nde I* restriction sites for cloning into M13 and pET11a respectively. The reverse primer contains a *Hind III* site for cloning into both vectors. PCR was effected by repeating 35 cycles of denaturation, annealing and synthesis at 94 °C, 56 °C and 72 °C respectively, using the thermostable DNA polymerase from *Pyrococcus furiosus* (*pfu*). This enzyme possesses a 3'→5' exonuclease (proofreading) function in addition to its polymerase activity. Excess nucleotides and polymerase were removed from the PCR product using a QIAquick PCR Purification kit (section 2.3.10). The PLA$_2$ gene and M13mp19 bacteriophage (shown in figure 2.2) in which to clone the gene were digested with the restriction enzymes *Eco RI* and *Hind III* (see 2.3.11), with excess nucleotides being removed using a QIAquick Nucleotide Removal kit (2.3.12).
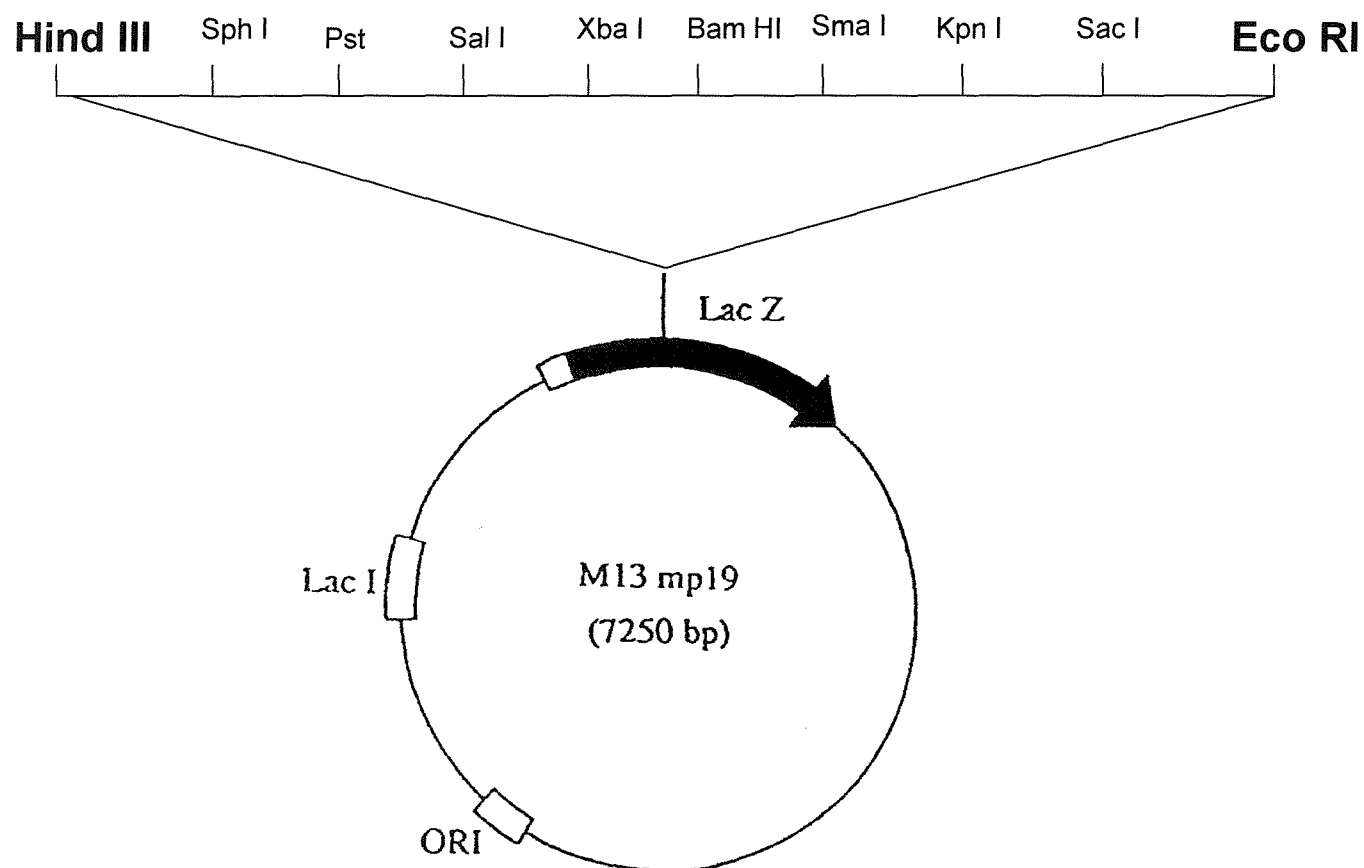
Figure 2.2 The M13 Bacteriophage Used to Create a Single-stranded DNA Template for Mutagenesis.

The gene coding for hnpsPLA$_2$ was cloned into M13 via the *Eco RI* and *Hind III* restriction sites indicated in bold.

The PLA$_2$ gene was then ligated into the M13 vector (section 2.3.13) and transformed into calcium-competent *E. coli* MV1190 cells (section 2.3,2.3). 50 μl of 2 % X-gal (dissolved in dimethyl formamide) and 20 μl 100 mM IPTG were added to the cells before plating, to enable distinction between cells containing the M13/PLA$_2$ construct (clear plaques) and those without (blue plaques). Six clear plaques were selected from the transformation plate and added to 1 ml sterile TE buffer (10 mM Tris.HCl, pH 8.0, 1 mM EDTA) to form the phage stock which is stable for ~ 2 months at 4 °C. The phage stock was then used to infect a *duf*, *ung* *E. coli* strain in order to produce a uracil-containing M13 molecule containing the PLA$_2$ gene, which can be used as a template for production of mutant DNA. The *duf*, *ung* *E. coli* strain CJ236 was grown overnight on LB-agar plates supplemented with 30 μg/ml chloramphenicol. A single colony was used to inoculate 10 ml LB containing 30 μg/ml chloramphenicol, which was grown for 6 hours at 37 °C with shaking. 100 μl of the previously prepared phage stock was added to the culture and grown overnight at 37 °C with shaking. The single-stranded uracil-containing M13 DNA template was isolated from the CJ236 cells using a QIAprep Spin M13 clean-up kit (section 2.3.14).

2.3.5 Annealing of Mutagenic Primers and Synthesis of Mutant DNA.

The oligonucleotide primer for an H48A mutant of hnpsPLA$_2$ is shown in 2.3.2. The primer was phosphorylated (section 2.3.15) before being annealed to the single-stranded M13 template (2.3.16). Synthesis of the mutant DNA strand was achieved as described in section 2.3.17, before the M13 was transformed into calcium competent MV1190 cells (as before) which have an operable uracil N-glycosylase. This will degrade the uracil-containing template strand, leaving the newly synthesised mutant strand to replicate. Transformants were then cultured and the DNA isolated by minprep and sequenced to confirm the presence of the mutation. Mutant DNA was then transformed as before into MV1190 cells, isolated by minprep and digested with *Nde I* and *Hind III* to isolate the mutated

gene for ligation into the pET11a plasmid (figure 2.3) used for expression of the gene. pET11a plasmid was also digested using the same restriction enzymes, and de-phosphorylated to prevent re-ligation of the plasmid (2.3.18). Both the gene and plasmid were run on a large agarose gel (section 2.3.19) and extracted from the gel as described in section 2.3.20. The gene and plasmid were ligated as before, and the resulting plasmid containing the mutant hnpsPLA$_2$ gene was transformed into BL21 (DE3) *E. coli* cells used to overexpress the gene.

2.3.6 The PCR Method of Mutagenesis.

This method of mutagenesis uses the polymerase chain reaction to amplify DNA whilst introducing a mutation at the desired site [80]. The polymerase chain reaction works on a repeated cycle of denaturation, annealing and synthesis of the DNA in question, which is primed using synthetic oligonucleotides complementary to the DNA. Mutations can be introduced into DNA using oligonucleotide primers that are complementary to the DNA except for the desired mutation. This method provides a time-efficient way to produce mutant DNA and eliminates the need to clone the gene to be mutated into an alternative cloning vehicle such as M13, as all PCR reactions can be carried out in the plasmid used for overexpression of the gene (pET11a in the case of this report). The reaction is summarised in figure 2.4.

In the first stage (1) the DNA is primed with mutagenic oligonucleotides to amplify the DNA with the required mutation incorporated. This is achieved in two reactions, one containing primers A and A', the other B and B'. A and B are primers complementary to either end of the gene, A' and B' are primers complementary to the region of DNA surrounding the codon to be mutated, and contain the mutant codon within them.
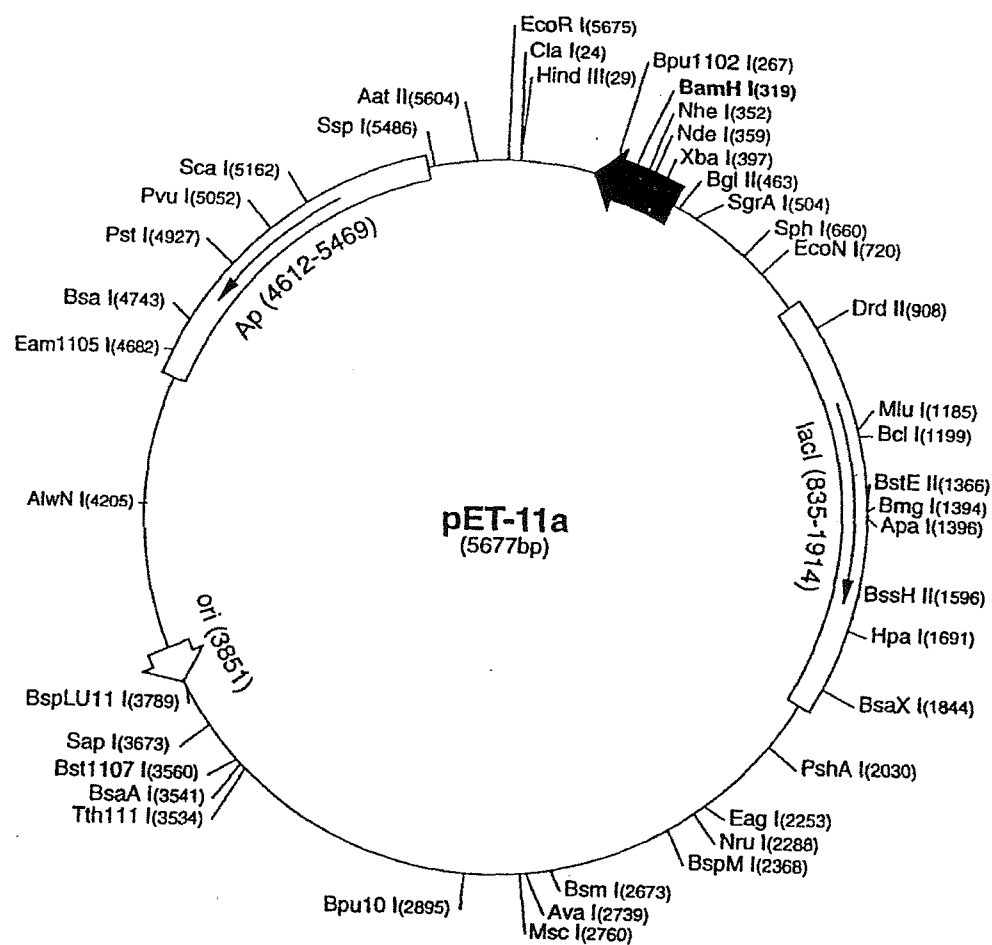
Figure 2.3 The pET11a Plasmid.

The gene coding for hnpsPLA$_2$ was cloned into the pET11a vector via *Nde I* and *Hind III* restriction sites, for overexpression in *E. coli BL21 (DE3)* cells.
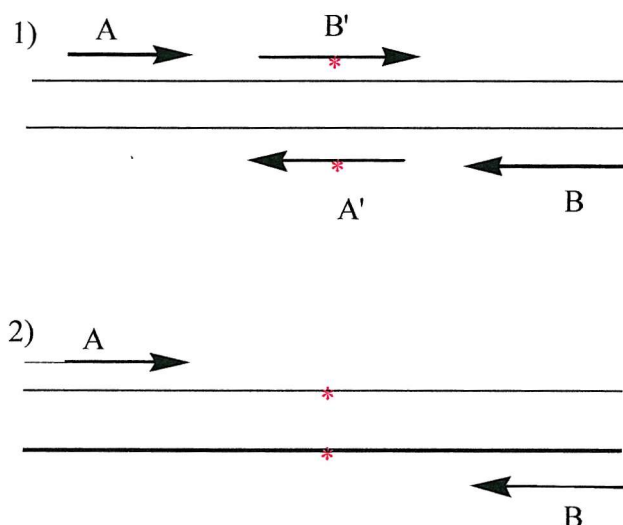
Figure 2.4 Schematic diagram of the 2-step PCR mutagenesis method:

1) A and B are oligonucleotides complementary to the ends of the DNA to be mutated. A' and B' are primers containing the required mutation (*).

2) The mutated DNA is amplified using A and B.

An equal amount of each reaction is then combined and the PCR repeated, to amplify the entire mutated piece of DNA (2). The mutated DNA is then digested from the plasmid via the *Nde I* and *Hind III* restriction sites coded for at either end of the gene, and ligated into freshly digested pET11a plasmid for sequencing and expression.

2.3.7 Production of Mutant DNA Using PCR.

The PCR mutagenesis method was used to produce the H48N mutant of hnpsPLA$_2$. The first step of the protocol involved amplification of the target gene using oligonucleotide primers that contain the required mutation within them. This was achieved in two separate reactions in order to produce two overlapping

fragments of mutant DNA which could then be combined to produce one continuous length of DNA. Reaction 1 contained 200 nmoles of the PLA_2 gene to be used as a template, 100 nmoles each of primers A and A', 16 nmoles of dNTPs and H_2O to a total volume of 50 µl. Reaction 2 contained the same as reaction 1 except that primers A and A' were replaced by primers B and B' (section 2.3.2 for primers, figure 2.5 for schematic diagram of reactions). After being heated to 94 °C for 1 minute (hot start), 2.5 U of *pfu* DNA polymerase was added, and 25 cycles of PCR were performed under the following conditions:

94 °C	1 minute (denaturation)
66 °C	1 minute (annealing)
72 °C	1 minute (synthesis)

Equal molar quantities of reactions 1 and 2 were then combined, and the PCR repeated as above to produce a continuous length of DNA containing the mutation. The PCR reaction was then purified using a QIAquick PCR Purification kit described previously.

2.3.8 Cloning of Mutant DNA into pET11a Plasmid for Expression.

The cleaned PCR reaction was digested with *Nde I* and *Hind III* restriction enzymes (2.3.11), and excess nucleotides removed as described in 2.3.12. The pET11a plasmid (figure 2.3) into which the mutant DNA was to be cloned was also digested with the same enzymes and cleaned in the same way. The mutant DNA was then ligated into the plasmid (2.3.13) and transformed into electrocompetent BL21 (DE3) *E. coli* cells. The presence of the required mutation was confirmed by sequencing.

2.3.9 Isolation of Plasmid DNA.

1-5 ml overnight cultures of cells were pelleted by centrifugation at 12,100 g for 10 minutes. The supernatant was discarded and the plasmid DNA isolated using a Promega Wizard SV miniprep kit according to the manufacturers instructions.

2.3.10 Purification of PCR Reactions.

Excess nucleotides, polymerase etc. were removed from PCR reactions using a QIAquick PCR Purification kit according to the manufacturers instructions.

2.3.11 Restriction Digests.

Restriction enzymes were used with the buffers supplied, and in accordance with the manufacturers instructions.

2.3.12 Purification of Restriction Digests.

Restriction enzyme digests were purified using a QIAquick Nucleotide removal kit according to the manufacturers instructions.

2.3.13 Ligation of DNA.

Ligations were performed using T4 DNA ligase in conjunction with the buffers supplied by the manufacturer in small (~20 µl) volumes containing 1-2 U of ligase and 100-200 ng of plasmid DNA. The reaction was incubated at 16 °C overnight.

2.3.14 Purification of M13 Template.

The uracil-containing M13 template was purified from CJ236 *E. coli* cells using a QIAprep Spin M13 kit according to the manufacturers instructions.

2.3.15 Phosphorylation of Oligonucleotides.

Custom-made oligonucleotides were phosphorylated before use by mixing 200 pmol of the oligonucleotide with 100 mM Tris.HCl, pH 8.0, 10 mM $MgCl_2$, 5 mM DTT, 0.4 mM ATP. 4.5 units of T4 Polynucleotide kinase were added and the reaction incubated at 37 °C for 45 minutes. Heating the mixture at 65 °C for 10 minutes stopped the reaction

2.3.16 Annealing of Mutagenic Primers to M13 Template.

The phosphorylated oligonucleotides were annealed to the M13 template under the following conditions. 2-3 pmoles of mutant oligonucleotide was added to 200 ng of uracil-containing M13 DNA and 1 μl of 10X annealing buffer (20 mM Tris.HCl, pH 7.4, 2 mM $MgCl_2$, 50 mM NaCl). Sterile H_2O was added up to a volume of 10 μl. The reaction was placed in a water bath pre-heated to 70 °C, which was immediately switched off and allowed to cool to 35 °C over approximately 1 hour. After this time, the reaction was transferred to an ice/water bath ready for the synthesis of a complementary strand of mutant DNA.

2.3.17 Synthesis of Mutant DNA from Oligonucleotide Primed M13.

Synthesis of a complementary strand of DNA containing the required mutation was effected in the following way:

To the annealing reaction, 1 μl 10X synthesis buffer, 1μl T4 DNA ligase and 0.5 U T7 DNA polymerase were added. The reaction was kept on ice for 5 minutes, then transferred to room temperature for 5 minutes before being incubated at 37 °C for 90 minutes. The reaction was stopped by addition of 90 μl TE buffer.

49

2.3.18 Dephosphorylation of pET11a.

Digested plasmid (pET11a) into which the mutated gene is cloned was dephosphorylated by adding 5 µl of calf intestinal alkaline phosphatase (CIAP) to 1 µg of digested plasmid. The reaction was incubated at 37 °C for 20 minutes, and then transferred to 65 °C for 20 minutes. 5 mM EDTA and 0.5 % SDS were added and the reaction incubated at 75 °C for 10 minutes before being cooled to room temperature.

2.3.19 Agarose Gel Electrophoresis.

Agarose was used at 1% (w/v) in TAE buffer (40 mM Tris.HCl, 1.14 ml glacial acetic acid/100 ml, 1 mM EDTA) containing 1 µg/ml ethidium bromide. 15 ml of gel solution was poured onto a mini gel plate, and a comb inserted to form wells. Gels were run in a horizontal electrophoresis tank with TAE buffer containing 1 µg/ml ethidium bromide. Samples containing 0.5 volumes of loading buffer (0.25 % (w/v) bromophenol blue, 30 % glycerol) were loaded into wells and gels were run at 100 V until the dye front was 2/3 of the way down the gel. The DNA was visualised using a UV transilluminator.

2.3.20 Gel Extraction.

An agarose gel was run as previously described, and the DNA of interest excised from the gel using a sterile scalpel under UV light. The DNA was then purified using a Qiagen gel extraction kit.

2.3.21 Estimation of DNA Concentration.

DNA concentration was estimated by measuring its absorbance at 260 nm, with this value being converted using the equation:

1 O.D.$_{260}$ unit = ~50 ng/µl (double-stranded DNA)

1 O.D.$_{260}$ unit = ~33 ng/µl (single-stranded DNA)

2.3.22 Preparation of Calcium-competent Cells

10 ml of LB broth was inoculated with the host *E. coli strain* and incubated overnight at 37 °C with shaking. 500 µl of the overnight culture was used to inoculate 10 ml LB, which was incubated at 37 °C with shaking until the O.D.$_{600}$ was ~0.6. The cells were then pelleted by centrifugation at 5,620 g for 5 minutes at 4 °C, and resuspended in 5 ml cold sterile 50 mM CaCl$_2$ [81]. The cells were chilled on ice for 20 minutes before being collected as above. The pellet was resuspended in 500 µl cold sterile 50 mM CaCl$_2$ and aliquoted into 250 µl quantities. Calcium-competent cells were made fresh for each set of transformations.

2.3.23 Transformation by Heat-shock.

3-6µl of DNA to be transformed was mixed with 250 µl of calcium-competent cells, and chilled on ice for 60-75 minutes. The cells were heat-shocked by placing in a water bath at 42 °C for 3 minutes and then returned to ice. 30-170 µl of heat shocked cells were then mixed with 300 µl of an overnight culture of host strain and plated onto H-agar plates in top-agar [81].

2.3.24 Preparation of Electrocompetent Cells

100 ml of LB broth was inoculated with the host *E. coli* strain and incubated with shaking overnight at 37 °C. 500 ml of fresh LB was inoculated with 20 ml of the overnight culture and grown at 37 °C until the $O.D._{600}$ was ~0.6. The cells were chilled on ice for 5 minutes before being pelleted by centrifugation at 5,620 g for 15 minutes at 4 °C. The cells were washed with 1 l of cold sterile water before being collected as above. The final wash was with 20 ml of cold sterile 10 % glycerol, and after centrifugation as before, the cells are resuspended in 2-3 ml cold sterile 10 % glycerol, before being aliquoted into 50 μl quantities for use [82]. Unused aliquots of electrocompetent cells were stored at -70 °C.

2.3.25 Transformation by Electroporation.

Cells were transformed following the method of Dower [82]. DNA to be transformed was first dialysed against 10 % glycerol on 0.025 μm filters for 20 minutes. 1 μl of DNA was mixed well with 50 μl of electrocompetent cells and chilled on ice for 2 minutes. The mixture was then transferred to a 0.1 cm gap cuvette, and electroporated using a BioRad Gene Pulsar at the appropriate settings (1.25 kV, 200 μF capacitor, 200 ε) and applying one pulse. Immediately, 1 ml of sterile SOC medium (10 mM NaCl, 2.5 mM $MgCl_2$, 10 mM $MgSO_4$, 20 mM glucose, 20 g/l tryptone, 5 g/l yeast extract) was added to the cuvette to resuspend the cells. The cells were then transferred to a universal tube and incubated at 37 °C for 30 minutes with shaking before being plated onto LB-agar plates containing the appropriate selective antibiotic.

2.3.26 Sequencing.

DNA sequencing was carried out by OSWEL (Southampton University).

2.4 Overexpression and Purification of HnpsPLA$_2$.

2.4.1 Overexpression of HnpsPLA$_2$.

E.coli cells BL21 (DE3) transformed with the pET11a plasmid containing the hnpsPLA$_2$ gene were grown initially on LB-agar plates supplemented with 50 μg/ml ampicillin at 37 °C overnight. Single bacterial colonies were picked off and grown overnight in 10 ml LB containing 50 μg/ml ampicillin at 37 °C. An overnight-culture was added to a fluted flask containing 1 l LB and 50 μg/ml ampicillin and incubated at 37 °C with shaking until the OD$_{600}$ was ~0.6. The cells were then induced with IPTG to a final concentration of 0.4 mM for a further 4-5 hours, before being harvested by centrifugation at 5,000 g at 4 °C for 20 minutes.

During the course of this study, the selective antibiotic was changed from ampicillin to carbenicillin. Over-night cultures were replaced as innoculum by 10 ml cultures of LB containing a single bacterial colony grown for ~6 hours (OD $_{600}$ ~0.6) in the presence of 50 μg/ml carbenicillin. In all other cases, 50 μg/ml carbenicillin replaced 50 μg/ml ampicillin.

2.4.2 Isolation of Inclusion Bodies.

The inclusion bodies were isolated using a method based on that of Bhat *et al* [83]. The pelleted cells were resuspended in 50 ml of Buffer X (50 mM Tris.HCl pH 8.0, 50 mM NaCl, 1 mM ethylenediaminetetraacetic acid (EDTA), 0.5 mM phenylmethylsulfonyl fluoride (PMSF)) containing 0.4 % (v/v) Triton-X 100 and 0.4 % (w/v) sodium deoxycholate and washed for 20 minutes at 4 °C. The cells were then sonicated for 15 seconds on, 15 seconds off for 15 cycles using an MSE-Soniprep 150 at medium amplitude before being collected by centrifugation at 12,000 g for 10 minutes at 4 °C.

53

The pellet was washed as before, but with 0.8 % (v/v) Triton-X 100 and 0.8 % (w/v) sodium deoxycholate before being sonicated and centrifuged as before. The pellet was then washed twice more at room temperature with first 1 % (v/v) Triton-X 100 and then Buffer X alone, with the pellet collected by centrifugation between washes.

2.4.3 Solubilization of Inclusion Bodies.

The inclusion bodies were solubilized overnight at 4 °C in 25 ml Buffer X containing 6 M Guanidine.HCl and 5 % β-mercaptoethanol, and collected as the supernatant after centrifugation at 27,000 g for 15 minutes at 4 °C.

2.4.4 Protein Refolding.

The protein was refolded at a concentration of ≤1.5 mg/ml by dialysing against 4 l of refolding buffer (25 mM Tris.HCl pH 8.0, 5 mM $CaCl_2$, 5 mM cysteine, 900 mM Guanidine.HCl) at 4 °C for 72 hours, with buffer changed every 12 hours, based on a method adapted from that of van Scharrenburg [84]. The refolded protein was then dialysed overnight at 4 °C against 4 l of dialysis buffer (20 mM Tris.HCl pH 8.0, 2.5 mM KCl) in order to remove excess Guanidine.HCl prior to column purification.

2.4.5 SP-Sepharose Chromatography Column Purification.

A 5 ml Hitrap SP-Sepharose column was loaded with refolded protein solution at 1 ml/min. and washed with Buffer A (10 mM Sodium Acetate pH 6.0) until the absorbance at 280 nm was zero. The protein was eluted with Buffer B (Buffer A + 2 M KCl) over a linear gradient from 0 – 100 %.

PLA$_2$ eluted from the column at ~ 1 M KCl. 1.5 ml fractions were collected throughout and assessed for protein content by measuring the absorbance at 280 nm and the continuous fluorescence displacement assay (see later) was used to determine PLA$_2$ activity - fractions containing PLA$_2$ were pooled.

2.4.6 Heparin-Sepharose Chromatography Column Purification.

The pooled fractions from the SP-Sepharose column were diluted 3X with Buffer C (20 mM Tris.HCl pH 7.4) to reduce the concentration of KCl before being applied to a 5 ml Hitrap heparin-Sepharose column. The column was washed with Buffer C until the absorbance at 280 nm was zero, before a gradient of Buffer D (Buffer C + 1 M KCl) was run to achieve 40 % at 20 ml and 100 % at 80 ml. PLA$_2$ eluted from the column at 0.6 M KCl. The fractions were collected and assayed for PLA$_2$ content as before, with the fractions containing PLA$_2$ being pooled.

2.5 Preparation of Recombinant Rat Liver Fatty Acid Binding Protein (FABP).

2.5.1 Overexpression of FABP.

Recombinant rat liver FABP was expressed from a synthetic gene for the enzyme, which is cloned into the pET11a expression vector and contained within E. coli BL21 (DE3) cells. E. coli cells containing the pET11a plasmid were grown, and FABP overexpressed from these cells in exactly the same way as described for the hnpsPLA$_2$ (see section 2.4.1 for method). The resulting cells were pelleted by centrifugation at 5, 000 g for 20 minutes at 4 °C.

2.5.2 Isolation of FABP.

The pelleted *E. coli* cells were resuspended in 3 ml cell lysis buffer/g of *E. coli* (50 mM Tris.HCl pH 8.0, 1 mM EDTA, 100 mM NaCl) (J. Davies, personal communication). To this, 4 µl of 100 mM PMSF and 80 µl lysozyme (10 mg/ml) were added per g *E. coli* and incubated at 4 °C with stirring for 20 minutes before addition of 4 mg deoxycholate/g *E. coli* and further incubation for 30 minutes. The cells were then sonicated using a MSE-Soniprep 150 at medium amplitude for 5 cycles of 20 seconds on, 20 seconds off before being collected by centrifugation at 12,100 g for 25 minutes at 4 °C. A 30 % ammonium sulphate cut was effected at 4 °C for 1 hour, followed by a 60 % cut for a further hour. Precipitate was removed by centrifugation at 12,100 g for 30 minutes between cuts. The resulting protein solution was dialysed against 20 mM KH_2PO_4, pH 7.4 overnight to remove remaining ammonium sulphate.

2.5.3 Affinity Chromatography Purification of FABP Using Dodecyl-agarose.

10 ml of dodecyl-agarose was equilibrated with 100 mM KH_2PO_4 buffer (pH 7.4) by repeated steps of centrifugation at 12,100 g for 1 minute at 4 °C. 10 mg FABP solution was added to the equilibrated dodecyl-agarose, and spun as above to bind the FABP to the agarose. This was then washed repeatedly as above to remove any unbound proteins, before pure FABP was eluted from the agarose by addition of 50 mM KH_2PO_4 buffer (pH 7.4) containing 25 % EtOH. The resulting FABP was dialysed against 20 mM KH_2PO_4 (pH 7.4) overnight at 4 °C to remove the EtOH.

An SDS-PAGE showing the purity of FABP at the different stages of the purification is shown in figure 2.5.
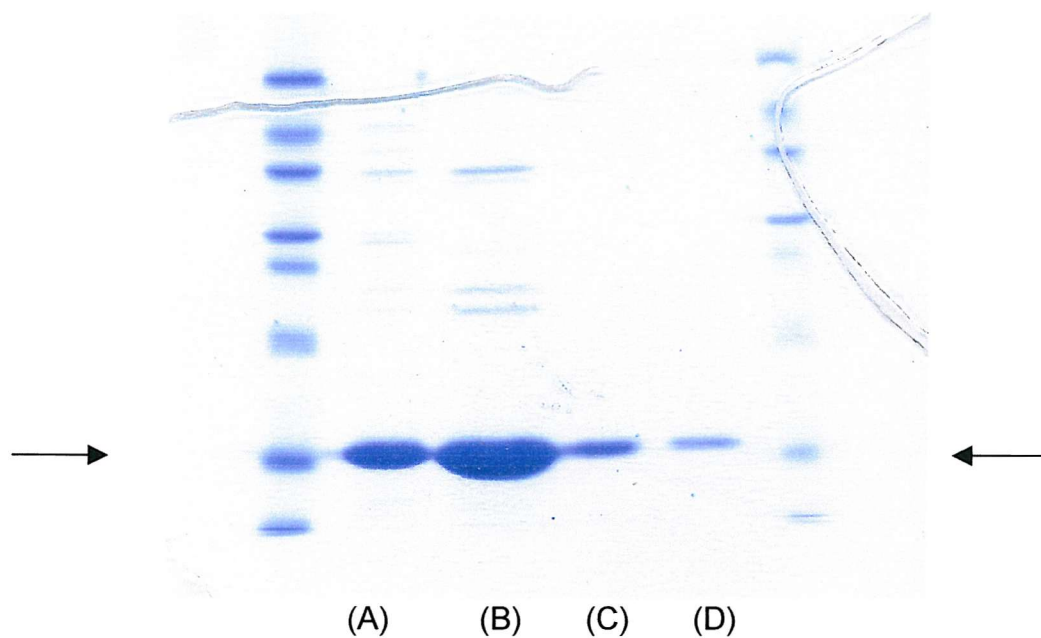
Figure 2.5 SDS-PAGE Showing the Purification of FABP.

SDS-PAGE was carried out as described in section 2.6.10.

Lanes A and B show FABP from BL21 DE3 cells, and after the 30 % ammonium sulphate cut respectively. Lanes C and D show FABP before and after dodecyl-agarose purification respectively.

The arrows indicate the expected position of the FABP band. Molecular weight markers shown in the far left and right lanes are (from top), 66, 45, 36, 29, 24, 20 and 14.5 and 6.5 kDa.

2.6 Analytical Techniques.

2.6.1 Measurement of PLA₂ Activity Using a Continuous Fluorescence Displacement Assay.

This assay, developed by Wilton [85], provides a continuous, sensitive method to determine the activity of PLA_2. It utilises the fluorescent probe 11-(5-dimethylaminonapthalenesulphonylamino) undecanoic acid (DAUDA) (figure 2.6), and the high fluorescence seen when this fatty acid analogue binds to recombinant rat liver fatty acid binding protein (FABP), which is does with high affinity (K_d ~0.1 µM) [85].
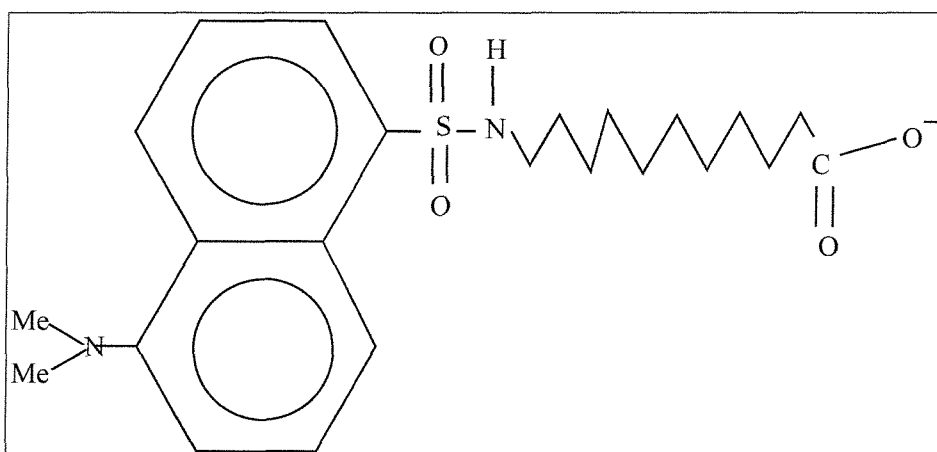
Figure 2.6 11-(5-dimethylaminonapthalenesulphonylamino) Undecanoic Acid (DAUDA).

The assay involves vesicles of phospholipid presented usually as small unilamellar vesicles (SUVs), which will be hydrolysed on addition of PLA_2 with the subsequent release of fatty acids. These free fatty acids will compete for binding to FABP, causing displacement of the DAUDA, and a resulting decrease in fluorescence intensity (excitation 350 nm, emission measured at 500 nm). This rate of decrease in fluorescence is proportional to the activity of PLA_2 (figure 2.7).
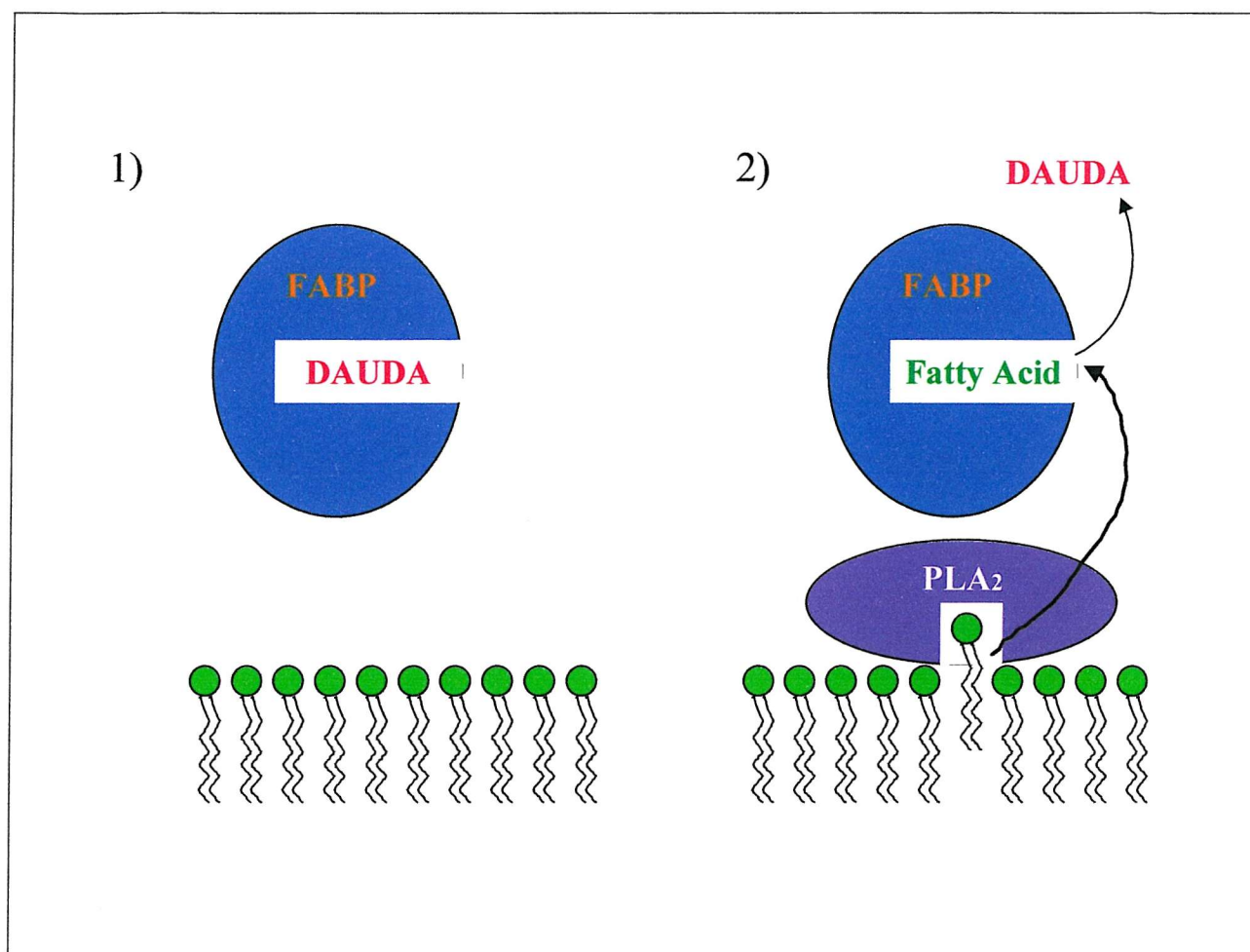
Figure 2.7 Cartoon diagram of the Fluorescence Displacement Assay.

1) Fatty-acid analogue DAUDA bound to FABP giving high fluorescence

2) DAUDA displaced from FABP by fatty acids released on phospholipid hydrolysis by PLA_2, causing a proportional decrease in fluorescence.

The assay is carried out usually at 25 °C using a Hitachi F-2000 Fluorescence Spectrophotometer. Each assay contains 0.1 M Tris.HCl pH 8.0, 0.1 M NaCl, 2.5 mM $CaCl_2$, 1 μM DAUDA, 50 μg/ml phospholipid and ~12 μg/ml FABP. The reaction is started by the addition of PLA_2. The assay system is sensitive to ng quantities of PLA_2., and has a sensitivity limit of approximately 10 pmol long

chain fatty acid released per minute [85]. Assays are calibrated by the addition of a known amount of oleic acid (or other relevant fatty acid), and all assays are performed in triplicate.

2.6.2 Measurement of PLA$_2$ Activity Using Pyrene-PG.

An alternative method to measure the activity of PLA$_2$ used the fluorescent substrate 1-palmitoyl,2-(10-pyrenyldecanoyl)-sn-glycero-3-phosphoglycerol (pyrene-PG) presented as SUVs [86]. Hydrolysis of the phospholipid by sPLA$_2$ releases pyrene-labelled fatty acid, which when bound to BSA present in the assay cause an increase in fluorescence (excitation 345 nm, emission measured at 398 nm). The maximum fluorescent signal was obtained by addition of 5 µg snake venom. The assay was calibrated by titrating a known amount of 10-pyrenyldecanoic acid into the system.

The assay is carried out at 25 °C using a Hitachi F-2000 Fluorescence Spectrophotometer. A typical assay contained 1.5 ml Buffer T (50 mM Tris.HCl, pH 7.4, 100 mM NaCl, 1 mM EGTA), 2 µM pyrene-PG, 15 µl 10 % fatty-acid free BSA and the required amount of PLA$_2$. The base line (blank) was recorded for 2 minutes, after which the reaction was started by the addition of 15 µl 1 M CaCl$_2$.

2.6.3 Measurement of sPLA$_2$ Activity using *Micrococcus luteus*.

PLA$_2$ activity was also measured using the Gram-positive bacteria *Micrococcus luteus* as substrate. Single bacterial colonies were grown overnight in 10 ml LB at 37 °C with shaking. The overnight culture was diluted 10-fold, and grown to OD$_{600}$ ~0.45. The bacteria were centrifuged at 2,500 g for 15 minutes and resuspended in ~2.5 ml Hanks balanced salt solution (HBSS) so that the OD$_{600}$ of a 20-fold dilution in HBSS was ~0.11.

This equates to an approximate bacterial concentration of 2×10^7 cells/ml, or ~1 nmole phospholipid/ml assay [63]. The bacteria are kept on ice until required. The assay is carried out at 37 °C using a Hitachi F-2000 Fluorescence Spectrophotometer. A typical assay contains 1 ml HBSS, 1 µM DAUDA, 2.5 mM $CaCl_2$ and 2×10^7 cells/ml. The reaction is started by addition of the required amount of PLA_2.

2.6.4 Total Phospholipid Extraction and Analysis by Mass Spectrometry.

Total lipid extraction was carried out based on a method by Bligh and Dyer [87], and was used to determine the amount of phospholipid that had been hydrolysed over a time course. Enzyme activity was measured using the fluorescence displacement assay (2.6.1), with 64 µM DOPG SUVs as substrate, and the reaction allowed to continue until a specific time point had been reached. At the required time points, the reaction was stopped by the addition of ice-cold 5 mM EGTA, and the entire reaction was decanted into 1.25 ml ice-cold methanol whilst vortexing. The internal standard required for mass spectrometry analysis (20 nmole DMPG) was added at this stage, and total phospholipid extraction carried out.

To each enzyme reaction, 1.25 ml methanol and 1.25 ml chloroform were added whilst vortexing. A further 1.25 ml chloroform was added, followed by 1.25 ml H_2O whilst vortexing. The reactions were then incubated at –20 °C until total separation of the two phases could be observed. The lower layer, containing phospholipid, was then removed and dried down under a stream of nitrogen and resuspended in 200 µl chloroform for mass spectrometry analysis. All experiments were carried out in triplicate, and the control in each case consisted of a reaction that contained all reagents except enzyme. Mass spectrometry was carried out as described in section 2.6.14.

2.6.5 Binding Studies Using *N*-Dansyl-1,2-Palmitoyl-*sn*-glycero-3-phosphoethanolamine (Dansyl–DPPE).

Binding of enzyme to phospholipid vesicles was studied by measuring the fluorescence change of the fluorescent probe dansyl-DPPE incorporated into vesicles at 4 mol % [67]. Vesicles were prepared by drying down a mixture of 5 μM DOPG and 0.2 μM dansyl-DPPE under a stream of nitrogen. Phospholipid was then resuspended in methanol and vesicles formed by rapid injection into reaction medium (0.1 M Tris.HCl, pH 8.0, 0.1 M NaCl, 1 mM EDTA).

Fluorescence measurements were taken using a Hitachi F-2000 fluorescence spectrophotometer, with excitation at 345 nm and emission measured between 450-600 nm. Assays were performed in triplicate, and in each case a blank scan (buffer only) and control scan (F_0, no enzyme) were measured.

2.6.6 Preparation of Small Unilamellar Vesicles (SUVs).

SUVs of the required phospholipid were prepared by microinjection of a methanol solution of phospholipid into the assay cocktail using a Hamilton microsyringe. The force of injection is enough to ensure sufficient mixing, so the methanol is diluted and the phospholipid molecules are evenly dispersed. The resulting vesicles have a diameter of ~ 25-50 nm (as measured on a Coulter N4 Plus particle sizer), and SUVs were freshly prepared for each set of assays. Typically, 100 μl of a 10 mg/ml solution of phospholipid in methanol is injected into 20 ml of assay buffer to provide a phospholipid concentration of 50 μg/ml.

2.6.7 Preparation of Multi-lamellar Vesicles (MLVs).

MLVs were prepared by drying down a known amount of the required phospholipid under nitrogen, and resuspending in a known amount of 0.2 M Tris.HCl buffer (pH 8.0) containing 0.2M NaCl. After standing on ice for 5 minutes, the solution was rigorously vortexed for 2 minutes. MLVs were kept on ice until use. The resulting MLVs have a diameter of between ~100-3000 nm, (as measured on a Coulter N4 Plus particle sizer) and were freshly prepared for each set of assays.

2.6.8 Preparation of SUVs from MLVs

An alternative method of producing SUVs when the phospholipid in question is not soluble in methanol or ethanol requires that MLVs of the phospholipid are first produced (see above). The MLVs are then subjected to 10 cycles of freeze/thaw using liquid N_2 before being sonicated for 20 cycles of 30 seconds on, 30 seconds off using a Heat Systems Ultrasonic processor at medium amplitude. The MLV solution clarifies once all MLVs are broken down to SUVs.

2.6.9 Estimation of Protein Concentration.

Protein concentration was estimated using either the bicinchoninic acid (BCA) assay [88], or the BioRad reagent assay, based on the method of Bradford [89], depending on the sensitivity of the protein solution to the reagents.

The BCA assay is based on the intense purple complex that BCA forms with cuprous ion (Cu^{1+}) in alkaline conditions. Production of Cu^{1+} from the reaction between protein and alkaline Cu^{2+} (biuret reaction) can be measured using this reagent.

The Bradford assay uses the dye Coomassie Brilliant Blue G-250, and exploits the shift in absorption maximum from 465 to 595 nm seen when this dye binds protein. It is this increase in absorption at 595 nm that is measured in order to estimate protein concentration. In each case measurements were made in triplicate, with bovine serum albumin (BSA) providing the standard protein concentration.

Estimations of protein concentration were also made using the absorbance reading at 280 nm and the absorption coefficient ($A_{280}^{1\%,1\text{ cm}}$) which calculates the extinction coefficient according to the number of tryptophan, tyrosine and cystines within that protein [90]:

$$E = 5550 \sum Trp + 1340 \sum Tyr + 150 \sum Cys$$

The Beer-Lambert law (A = E.c.l.) can then be applied to estimate protein concentration

2.6.10 SDS-Polyacrylamide Gel Electrophoresis (SDS-PAGE).

SDS-PAGE was used to assess protein purity according to the method of Laemmli [91]. 30 % acrylamide gels were prepared from 15 % resolving gel (5 ml 30 % acrylamide, 5 ml resolving gel buffer (750 mM Tris.HCl, pH 8.8, 2 ml 10 % SDS), 5 μl N,N,N',N'-tetramethyl-ethylenediamine (TEMED), microspatula ammonium persulphate crystals) and 4 % stacking gel (1 ml acrylamide, 3.75 ml stacking gel buffer (250 mM Tris.HCl, pH 6.8, 2 ml 10 % SDS), 2.75 ml H_2O, 10 μl TEMED, microspatula ammonium persulphate crystals). Approximately 25 μl of protein sample was boiled for 10 minutes with 5 μl sample buffer (0.3125 M Tris.HCl, pH 6.8, 10 % SDS, 10% sucrose, 0.0025 % bromophenol blue, 5 % β-mercaptoethanol) before being loaded onto the gel.

Gels were run vertically immersed in reservoir buffer (5x stock: 1 % SDS, 100 mM Tris.HCl, 770 mM glycine) at 30 mA, stained with Coomassie Blue and destained overnight in 45% methanol and 5% acetic acid.

2.6.11 Reverse Phase High Pressure Liquid Chromatography (RP-HPLC).

RP-HPLC was achieved using a Gilson HPLC equipped with a Nucleosil NC300-5 C18 column. Approximately 100 µg of protein sample was loaded onto the column, which was equilibrated with 0.1% trifluoroacetic acid (TFA) at room temperature. A linear gradient of acetonitrile was applied to the column, and protein elution was seen as a single peak at ~36% acetonitrile.

2.6.12 Heat Denaturation.

The thermal stability of PLA$_2$s were assessed by incubating protein at temperatures between 25 °C - 75 °C for 6 hours. After this time, aliquots were removed and kept on ice prior to being assayed for residual activity using the continuous fluorescence displacement assay with DOPG SUVs as substrate. A sample of protein at 25 °C acted as the control. Each assay was performed in triplicate.

2.6.13 Inactivation of PLA$_2$ Using *para*-Bromophenacyl Bromide (*p*BPB).

The alkylation of histidine residues in PLA$_2$ was achieved by incubating a sample of protein in 100 mM sodium cacodylate buffer, pH 6.0 at room temperature. A molar excess of *p*BPB (dissolved in acetone) to protein ranging from 1-100:1 was then added.

Residual activity was assayed using the continuous fluorescence displacement assay at regular time intervals with DOPG SUVs as substrate. Protein incubated with acetone alone constituted the control.

2.6.14 Electrospray Ionisation Mass Spectrometry (ESI-MS)

All electrospray experiments were carried out using a Micromass LCT™ orthogonal acceleration time of flight mass spectrometer fitted with a nanoElectrospray source. The mass spectrometer was operated in positive ion mode at a source temperature of 80° C with a cone voltage of 43 V. Control, data acquisition and post-processing were performed using Masslynx 3.4 software. Maximum entropy calculations were achieved using Maxent3™. Samples were desalted into 50 % acetonitrile and 5 % formic acid prior to analysis using a micro column (bed volume 200 nl) containing R2 porous resin.

2.6.15 Circular Dichroism (CD).

CD spectra of enzymes were measured using the method of Lee [92] with a Jasco J-270 spectropolarimeter. For comparative secondary structure CD, 300 μl of a 0.2 mg/ml solution of protein in 10 mM phosphate buffer, pH 7.4 was measured between 190 nm and 250 nm. Spectra were averaged from 7 accumulations.

For thermal denaturation studies, CD spectra of enzyme in conditions described above were measured at increasing temperatures from 25 °C to 82 °C, and spectra were averaged from 3 accumulations.

2.7 Crystallography.

2.7.1 Crystallisation.

Pure enzyme at a concentration of 20 mg/ml was dialysed into crystallisation buffer (0.1 M Tris.HCl pH 7.4, 5 mM $CaCl_2$). Crystals were grown in 8-10 months at 4 °C by the hanging drop method, from 10 µl droplets containing 10 mg/ml enzyme, 0.1 M Tris.HCl, pH 7.5, 2.5 M NaCl, 5 mM $CaCl_2$, 0.5 mM β-octyl-glucopyranoside. These droplets were plated onto siliconised cover slips and sealed over reservoirs containing 1 ml of 5.5 M NaCl, 0.1 M Tris.HCl, pH 7.5.

2.7.2 X-ray Data Collection and Processing.

Diffraction data were collected at 100 K on a MAR image plate, using monochromatic CuKα radiation (λ = 1.5418 Å) from a rotating anode generator (N1A), or were collected at a Synchrotron source (Grenoble) (H48Q).

2.7.3 Molecular Replacement.

Initial phases were calculated from a molecular replacement solution obtained with the wild type PLA_2 (PDB entry 1POD) as the search model. Rigid body refinement was done in CNS. The program QUANTA was used for visualisation purposes.

2.7.4 Refinement.

The program CNS was used for the refinement. To monitor the progress of the refinement, 5 % of the data was used to calculate R_{free}.

Chapter Three - The H48Q Mutant of HnpsPLA$_2$

3.1 Studying the Interfacial Binding of HnpsPLA₂.

HnpsPLA$_2$ is one of a small number of enzymes whose ability to catalyse the hydrolysis of phospholipid substrate is totally dependent on it first binding to a lipid/water interface. This phenomenon of interfacial binding is totally distinct from the ability of the enzyme to catalyse the hydrolysis of individual phospholipid molecules within this interface.

As mentioned previously, hnpsPLA$_2$ is a highly cationic protein, with many of its 23 positively charged residues being found on the interfacial binding surface. The IBS of hnpsPLA$_2$ was in part characterised by using charge-reversal site-directed mutagenesis, to help define the contribution of electrostatic interactions and ascertain which individual residues or clusters of residues were most important in interfacial binding [66]. In addition, some studies using an N-terminal mutant of hnpsPLA$_2$ (this region of the protein is also implicated in interfacial binding) have been carried out and the findings are discussed below.

However, the binding of hnpsPLA$_2$ to an interface has yet to be clearly defined and remains the focus of this thesis.

3.1.1 The V3W Mutant of HnpsPLA₂.

The N-terminal region of sPLA$_2$s has been implicated in interfacial binding. Pro-enzymes (such as the pancreatic PLA$_2$) with an N-terminal extension are unable to effectively bind to an interface, while NMR studies of mature pancreatic PLA$_2$s suggest that the N-terminal region of the enzyme only forms a stable α-helical conformation when interfacially bound – when free in solution, this region is less well defined [64].

The porcine pancreatic PLA$_2$ has a Trp residue at position 3, and when used as a fluorescence reporter group, an increase in fluorescence signal is seen

upon interfacial binding of this enzyme, again implicating this area of the enzyme in binding. The human group IIA form of the enzyme does not contain any tryptophan residues, so a V3W mutant of hnpsPLA$_2$ was constructed in order that binding of the human enzyme may also be studied using fluorescence changes [93,94]. This mutant showed enhanced activity on vesicles of phosphatidylcholine, and was 10-fold more active against whole cell membranes as compared to the wild type [93,94]. It was concluded from these studies that the Trp residue could act as a type of anchor for the enzyme, by inserting into the interface to allow catalysis to take place, and again infers that this N-terminal region of the human sPLA$_2$ is also involved in interfacial binding.

3.1.2 The Use of His-48 Mutants to Study Interfacial Binding of HnpsPLA$_2$.

Interfacial binding of hnpsPLA$_2$ to its substrate interface is a critical step, as the enzyme cannot hydrolyse phospholipid molecules until it is interfacially bound. This interfacial binding can be of very high affinity, and therefore difficult to measure. Techniques used to measure interfacial binding include separating the bound and free enzyme, or studying spectral changes that occur on binding. These techniques have little application for hnpsPLA$_2$, as separation of bound and free enzyme involves centrifugation, which is not applicable to small phospholipid vesicles, and even when using heavier vesicles such as sucrose-loaded large unilamellar vesicles, the vesicles are still fragile and may be damaged by the process. HnpsPLA$_2$ does not contain any tryptophan residues which could be used to study spectral changes on binding, as was the case for the porcine pancreatic enzyme described above [95].

The very high affinity nature of the binding of hnpsPLA$_2$ to its substrate interface (Kd $\sim \leq 10^{-8}$ M) also means that most fluorescent methods will not be exploitable, as the sensitivity of these methods are too low to be able to

detect binding of this enzyme to an interface at concentrations of enzyme below 10 $^{-8}$ M. An ideal way to overcome the problems associated with studying interfacial binding would be to prevent the catalytic activity of hnpsPLA$_2$, leaving an intact enzyme that could be used in competitive binding assays to try and characterise the interfacial properties of this enzyme. Methods that could be used to provide an enzyme system lacking catalytic activity include using a non-hydrolysable substrate analogue, or chemically altering the catalytic residues, but both of these methods would be open to criticism in terms of physiological relevance. Another option is to remove the calcium ion that is crucial for catalysis, but this may leave the active site channel where the calcium is co-ordinated in a changed conformation, which could invalidate the results.

The residue found to be crucial for catalysis, His-48, is the key amino acid to target for alteration. Therefore, the method of choice to remove the catalytic activity of hnpsPLA$_2$ was by mutating the catalytic residue His-48, leaving an inactive version of the enzyme to be studied.

3.1.3 His-48 Mutants of Other sPLA$_2$s.

Since it was deduced that His-48 was the catalytically important residue in pancreatic sPLA$_2$, His-48 mutants have been produced in various types of the enzyme including the bovine pancreatic and bee venom sPLA$_2$s. In the case of the bovine pancreatic enzyme, three active site mutants were constructed in which the His-48 was substituted with a Gln, Asn or Ala residue in order to ascertain the catalytic properties of His-48 in detail [96]. These mutants were analysed by NMR and were subject to activity and denaturing experiments in order to measure their structural integrity and to determine if any residual activity was present in the absence of His-48. The H48A mutant was judged not to be structurally intact, and the H48N showed some residual catalytic activity, but the H48Q mutant was both intact and inactive [96]. A similar result was obtained for the bee venom sPLA$_2$ when the equivalent catalytic histidine, His-34, was mutated [97].

The decision to construct the active site mutants H48Q, H48N and H48A of hnpsPLA$_2$ was made based on these findings, with priority on the H48Q as this would seem most likely to provide an inactive enzyme [96,97], which was still able to refold, and would therefore be structurally intact and still capable of binding to the phospholipid interface.

3.2 Preparation of Recombinant HnpsPLA$_2$.

The hnpsPLA$_2$ used throughout this study is a recombinant form of the enzyme produced by R. Othman [93]. The gene for hnpsPLA$_2$ was constructed by the single-step ligation of 12 synthetic oligonucleotides, and was cloned into the pET11a expression vector via Hind III and Eco RI restriction sites which were introduced during the design of the construct. The gene coding for recombinant hnpsPLA$_2$ is under the control of the T7 RNA promoter, and is regulated by the *lac* operon to allow *E. coli* growth with controlled expression of the gene by addition of IPTG.

In order that the initiator Met could be removed by the aminopeptidase of the *E. coli* used for overexpression of the protein, the second amino acid Asn was mutated to Ala. HnpsPLA$_2$ with the initiator Met still present was studied, but showed only ~10 % activity as compared with wild-type protein [93]. This N1A mutant was found to share near identical structural and catalytic properties with the wild-type protein [93], and provides a useful model with which to pursue site-directed mutagenesis studies.

The expression and purification protocol for recombinant hnpsPLA$_2$ was previously established [93] and the method is described in section 2.3. Having a recombinant form of hnpsPLA$_2$ is desirable, but overexpression of the enzyme in *E. coli* is limited by the 7 di-S bonds contained in the fully folded structure, which cannot be formed in the highly reducing conditions of the bacteria. This results in denatured hnpsPLA$_2$ being expressed in inclusion bodies, which must be broken down to release the protein. The subsequent refolding of the protein is achieved by dialysis of the diluted, denatured protein

against 0.9 M Guanidine hydrochloride, using a method refined from that of Van Scharrenberg which was originally used to refold the porcine pancreatic form of the enzyme [84]. The refolding process was refined from that reported previously, by increasing the refolding time from 48 to 72 hours, and by significantly reducing the concentration at which the protein was refolded from 0.6 mg/ml to $\leq$ 0.15 mg/ml. These refinements helped to improve the yield of folded protein, and minimise the extensive loss of protein seen on refolding due to aggregation and non-specific interactions, which can occur when refolding proteins at higher concentrations. Once refolded, the protein solution was dialysed to remove the Guanidine hydrochloride, which would otherwise prevent binding of the protein to chromatography columns. The first chromatography step uses the strong cation exchange media SP-Sepharose in an ion-exchange capacity at pH 6.0, which utilises the highly cationic nature of the enzyme. Protein elutes at ~ 1 M KCl, and this is followed by affinity-chromatography using a heparin-Sepharose column at pH 7.4 to further purify the protein. A heparin column is used as part of the purification process, as it is bound by hnpsPLA$_2$ *in vivo*, and PLA$_2$ elutes from this column at ~ 0.6 M KCl. The recombinant protein was judged to be pure by SDS-PAGE, with a typical yield of protein from 1 litre LB being 8 mg (table 3.1). Protein purity was further analysed by RP-HPLC, using a Nucleosil-C18 column equilibrated with 0.1 % TFA to which ~ 100 µg of N1A was loaded, and a linear gradient of acetonitrile (0-100 % in 0.1 % TFA) applied. The protein eluted as a single peak at ~ 36 % acetonitrile and a typical elution profile is shown in figure 3.1.

The specific activity of N1A hnpsPLA$_2$ was measured using the continuous fluorescence displacement assay (detailed in section 2.6.1) and figure 3.2 shows a representative fluorescent trace obtained from this assay with 64 µM DOPG SUVs as substrate. A dose response curve for N1A when assayed under these conditions is shown in figure 3.3. The initial activity of the enzyme was measured at a fixed concentration of DOPG (64 µM) and enzyme concentrations between 20-200 ng, and shows a linear relationship between the initial activity of N1A and the enzyme concentration.

	Amount of Protein (mg)	% Recovery of Protein
Solubilized Inclusion Bodies	32	100
Refolded Protein	31.8	99.6
Refolded, Dialysed Protein	18.4	57.5
SP-Sepharose	18.1	56.5
Heparin-Sepharose	~9	~28

Table 3.1. Recovery of N1A HnpsPLA$_2$ at Key Stages of the Preparation

Samples were taken at key stages of the preparation of N1A hnpsPLA$_2$ and protein concentration ascertained using either the BCA assay [88] or the Bradford assay [89] (section 2.6.9) depending on the sensitivity of the particular method to reagents used at each stage. The results shown are from the processing of 1 litre of culture.
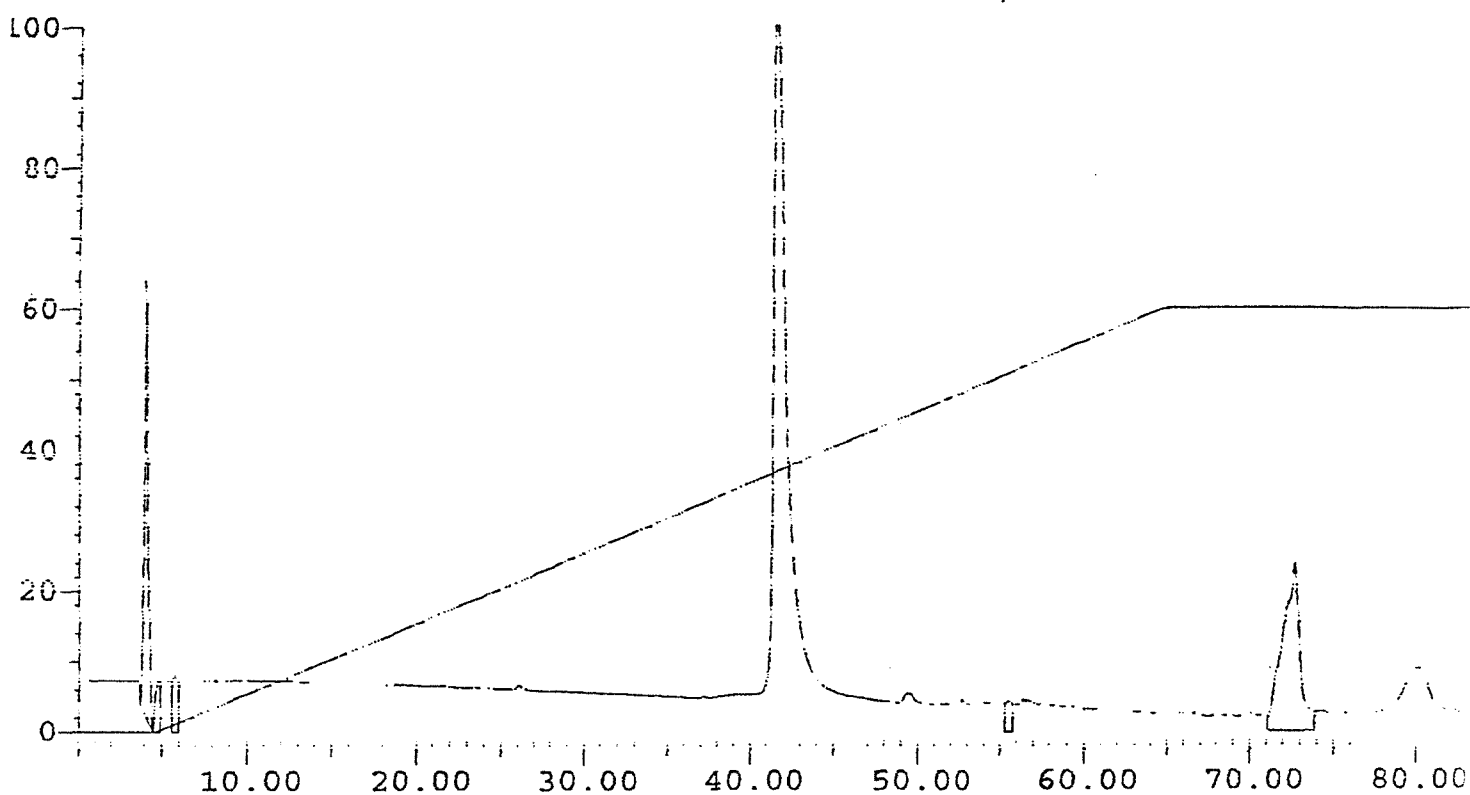
Figure 3.1. Reversed Phase HPLC Analysis of N1A HnpsPLA$_2$.

RP-HPLC was carried out as described in section 2.6.11.

100 µg of N1A was applied to a Nucleosil C-18 RP-HPLC column. A linear gradient of acetonitrile in 0.1 % TFA was run through the column (0-60 %) starting 5 minutes after protein injection.

Protein was detected by monitoring the O.D. at 230 nm.

Pure protein eluted in a single peak at ~36 % acetonitrile.
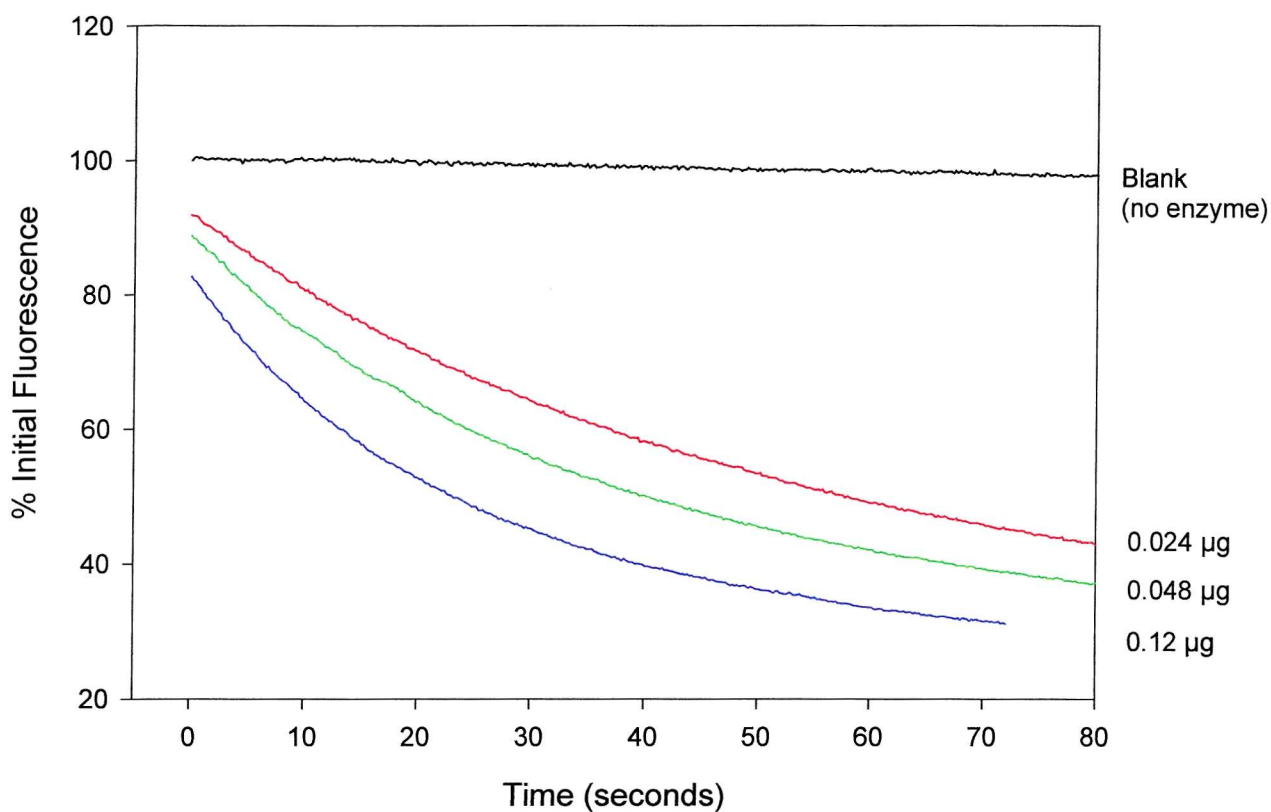
Figure 3.2. Fluorescence Traces Showing the Hydrolysis of DOPG SUVs by N1A HnpsPLA$_2$.

Activity of N1A was measured using the fluorescence displacement assay as described in section 2.6.1, with 64 µM DOPG SUVs as substrate.

Assays contained either:

—— - No enzyme
—— - 0.024 µg
—— - 0.048 µg or
—— - 0.12 µg of N1A hnpsPLA$_2$.

Enzyme was added at time = 0.
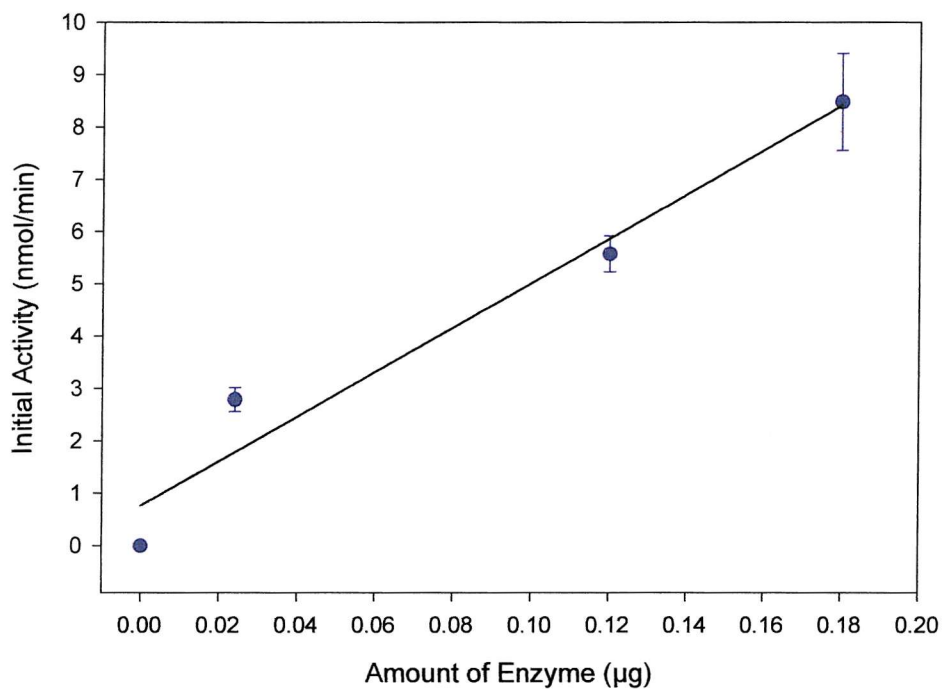
Figure 3.3 Dose Response Curve for the Hydrolysis of DOPG SUVs by N1A HnpsPLA$_2$.

Enzyme activity was measured using the fluorescence displacement assay as previously described, with 64 μM DOPG SUVs as substrate.

● - N1A HnpsPLA$_2$

Each data set is the mean of 3 separate measurements ± s.d

3.3 The H48Q Mutant of HnpsPLA$_2$.

As discussed previously, substitution of the catalytically crucial histidine residue with a glutamine residue in both the group IB bovine pancreatic (His-48), and the group III bee venom (His-34) sPLA$_2$s resulted in a structurally intact and catalytically inactive enzyme [96,97]. As such a protein was desirable for use as an interfacial binding probe, the N1A, H48Q mutant of hnpsPLA$_2$ was prepared. The N1A, H48Q mutation was introduced into the hnpsPLA$_2$ gene using the Kunkel method of mutagenesis [98].

(For simplicity the N1A, H48Q mutant (and all further double mutants) of hnpsPLA$_2$ will be referred to as e.g. the H48Q mutant, as all mutants carry the N1A mutation).

3.3.1 Purification and Characterisation of H48Q HnpsPLA$_2$.

The H48Q hnpsPLA$_2$ was prepared and purified in an identical manner to the N1A. The yield of H48Q per litre LB is similar to that obtained with the N1A, indicating a similar level of expression and recovery for the two forms of the enzyme. Analysis by SDS-PAGE showed the H48Q mutant to be pure figure 3.4). To further confirm the structural similarity between the N1A and H48Q, the mutant was analysed by RP-HPLC, and the elution of pure H48Q from a C-18 Nucleosil column is identical to that of the N1A and is shown in figure 3.5. The eluted peak was subject to ESI-MS analysis, which confirmed the mass of H48Q as 13851 Da, giving the expected mass difference of 9 units between the N1A and H48Q; the difference in mass between a histidine and glutamine residue. The spectrum for H48Q is shown in figure 3.6 and a spectrum for N1A is shown in figure 3.7 for comparison. These results, taken together indicate that the H48Q mutation in hnpsPLA$_2$ has not caused any significant change in the gross structure of the enzyme, as compared to the N1A, with the active site mutant showing similar properties to the N1A throughout the preparation and purification.
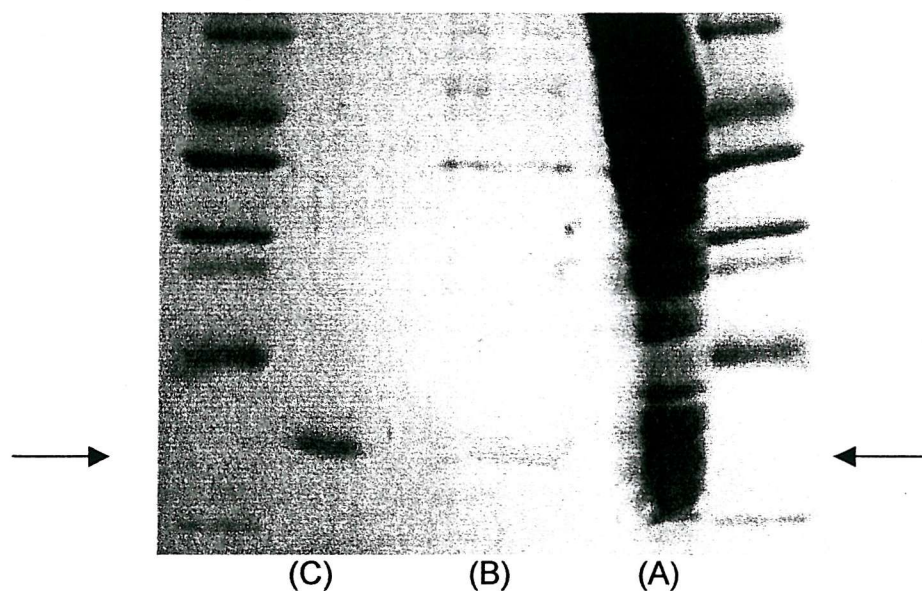
Figure 3.4 SDS-PAGE Showing the Purification of H48Q HnpsPLA$_2$.

SDS-PAGE was carried out as described in section 2.6.10.

Lanes A and B show H48Q hnpsPLA$_2$ released from BL21 DE3 *E. coli* cells by sonication, and purified inclusion bodies containing H48Q hnpsPLA$_2$ respectively. Lane C shows H48Q hnpsPLA$_2$ protein collected after purification on a heparin-Sepharose chromatography column.

The arrows indicate the expected position of the H48Q hnpsPLA$_2$ band. A characteristic of this protein is that it runs at approximately 17 kDa on SDS-PAGE.

Molecular weight markers shown in the far left and right lanes are (from top), 66, 45, 36, 29, 24, 20 and 14.5 kDa.
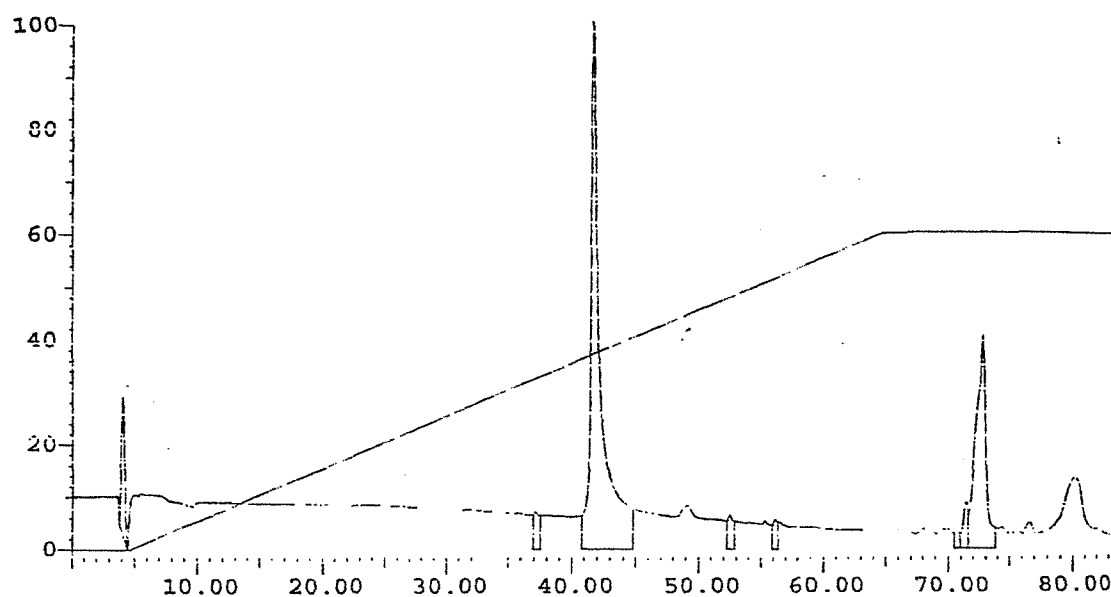
Figure 3.5 Reversed Phase HPLC Analysis of H48Q HnpsPLA$_2$.

RP-HPLC was carried out as described in section 2.6.11.

100 µg of H48Q was applied to a Nucleosil C-18 RP-HPLC column. A linear gradient of acetonitrile in 0.1 % TFA was run through the column (0-60 %) starting 5 minutes after protein injection.

Protein was detected by monitoring the O.D. at 230 nm.

Pure protein eluted in a single peak at ~36% acetonitrile.
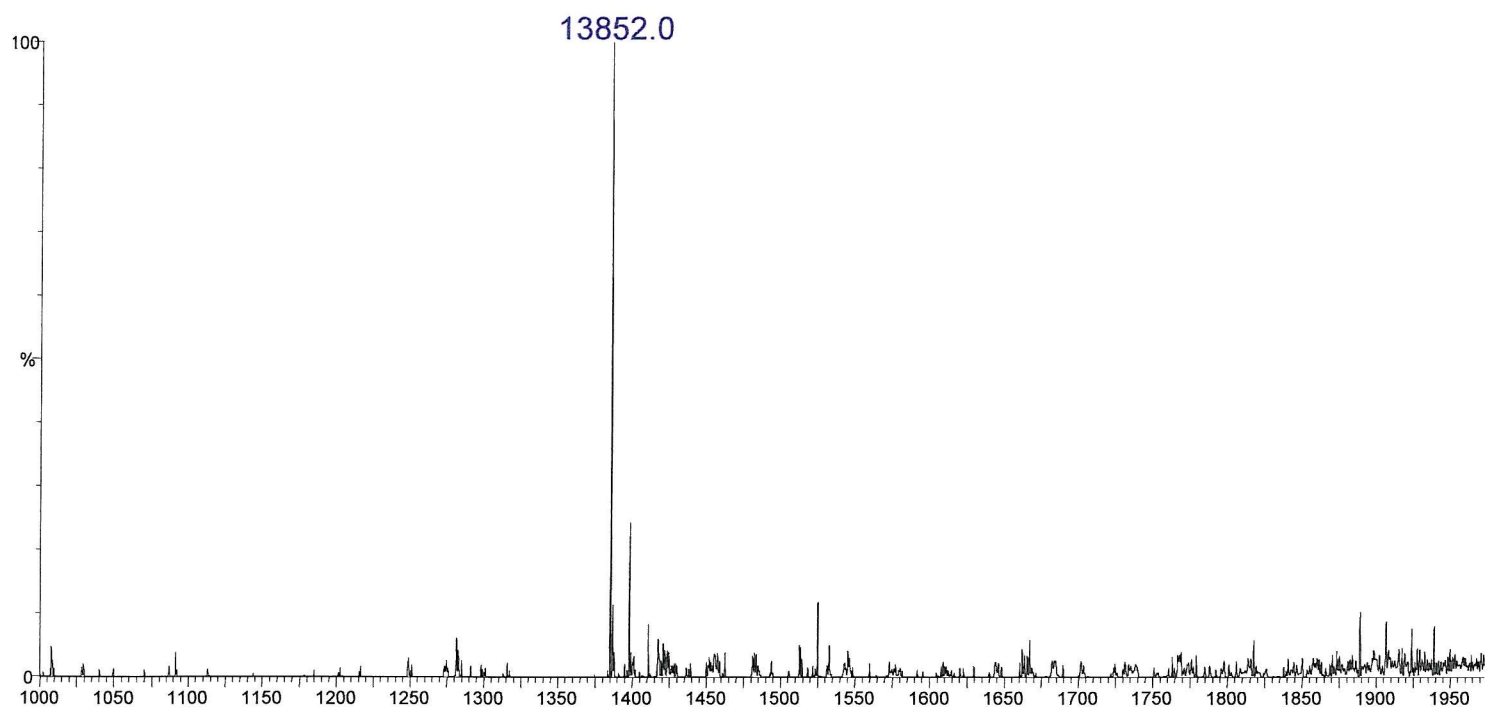
13852.0

Figure 3.6 Analysis of H48Q HnpsPLA$_2$ using Mass Spectrometry.

Electrospray ionisation mass spectrometry was carried out as described in section 2.6.14.

The molecular mass of H48Q HnpsPLA$_2$ as judged by mass spectrometry is 13852 ± 1.0, against a predicted mass of 13851.
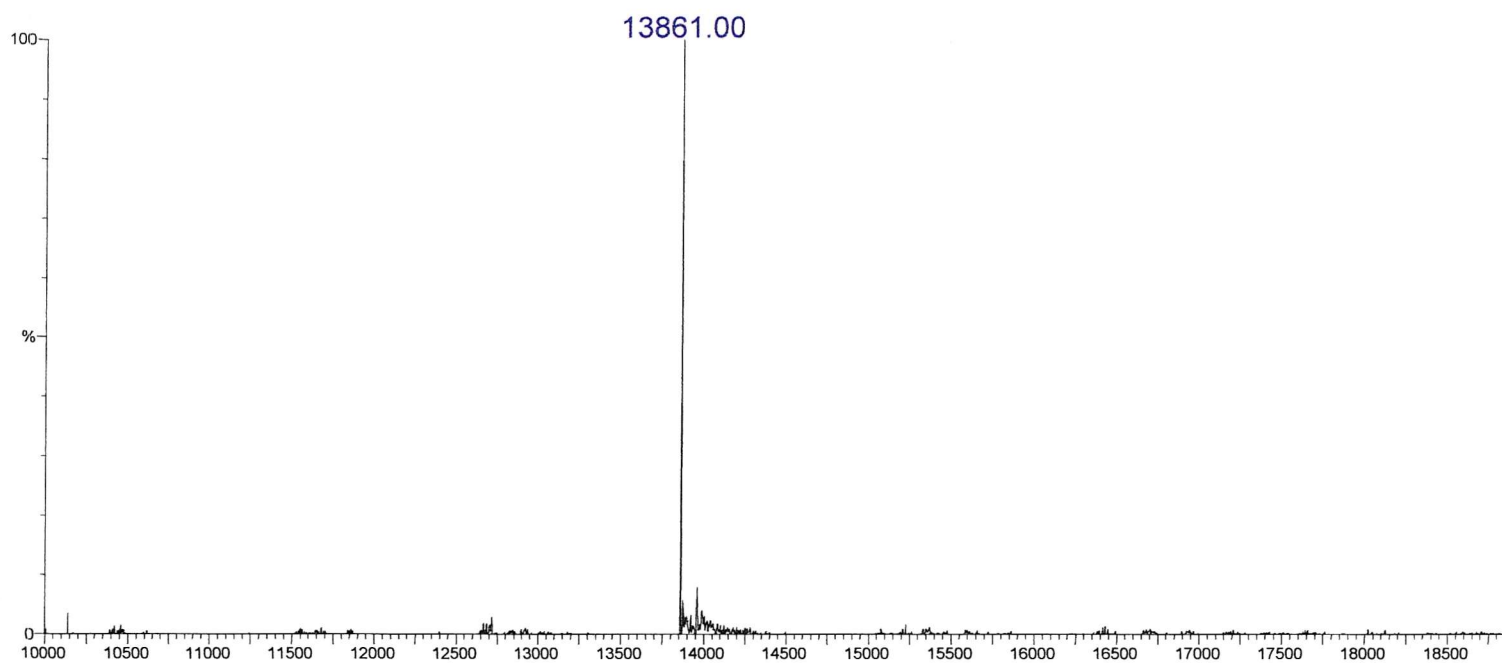
Figure 3.7 Analysis of N1A HnpsPLA₂ using Mass Spectrometry.

Electrospray ionisation mass spectrometry was carried out as described in section 2.6.14.

The molecular mass of N1A HnpsPLA₂ as judged by mass spectrometry is 13861 ± 1.0, against a predicted mass of 13860.

3.3.2 Kinetic Properties of H48Q HnpsPLA$_2$.

As previously stated the H48Q mutant was produced with the aim of obtaining a structurally intact, inactive, active site mutant as had been achieved with the bovine pancreatic and bee venom enzymes. Therefore, it was somewhat surprising on assaying this mutant for catalytic activity to find that it did still show catalytic activity at a rate of ~ 4 % as compared to the N1A. Figure 3.8 compares the elution of N1A and H48Q hnpsPLA$_2$ from a heparin-Sepharose column, which is the final stage of the purification procedure. The profile shows that both proteins elute at the same concentration of salt, and differ only in the amount of activity shown. A fluorescence trace obtained when assaying H48Q using the continuous fluorescence displacement assay with DOPG SUVs as substrate is shown in figure 3.9 and shows the significant catalytic activity retained by the mutant.

Figure 3.10 shows a dose response curve for H48Q when assayed on SUVs of DOPG at a fixed concentration of 64 µM. A linear relationship can be seen between the initial activity of the mutant and concentration of enzyme, at enzyme concentrations between 1.25 and 3.75 µg/ml. the graph of activity versus DOPG concentration in figure 3.11 shows that substrate concentration is not a factor in the activity of H48Q. To ensure that the activity shown by the H48Q was neither an anomaly or caused by contamination by N1A, the preparation and purification protocol was repeated three times initially. In each case, expression was from single bacterial colonies and separate equipment, including chromatography columns was used for the mutant. The gene was also re-sequenced, and confirmed that the H48Q mutation was present and also that this was the only difference in the sequence as compared to the N1A. The sequence is shown in figure 3.12.

The very significant activity (~ 4 %) shown by the H48Q mutant was not compatible with previous published data for the pancreatic and bee venom enzymes [96,97]. In addition, it was not consistent with the catalytic mechanism proposed for the enzyme, which requires that His-48 acts as a base in the predicted rate limiting step, in which a water molecule is

deprotonated during the formation of an oxyanion intermediate (see figure 1.10) [75]. Therefore, a detailed comparison of the structural and catalytic properties of the N1A and H48Q was necessary.

3.3.3 Comparison of the Secondary Structures of H48Q and N1A HnpsPLA₂.

Having demonstrated that the H48Q mutant behaves in a similar way to the N1A in terms of preparation and purification, and having eliminated contamination by the N1A as a potential reason for the small but significant activity shown by this mutant, it was then necessary to determine in more detail the structural integrity of the mutant.

Circular dichroism (CD) was employed as a method of comparing the secondary structure of H48Q with N1A. CD is a technique used to gain structural information about macromolecules such as proteins, including the relative amounts of α-helix, β-sheet and random coil contained within them. It can also be used to measure the unfolding of proteins, by monitoring the changes in structure that occur during denaturation [99]. The technique of CD uses circularly polarised light (CPL), which can be right or left-handed. Right and left-handed CPL are mirror images of each other i.e. they are chiral, and these two forms of light are absorbed differently by molecules which are asymmetric, for example amino acids that have chirality around the α-carbon bond [100]. CD is measured as the difference in absorbance of right and left-handed CPL by the protein or molecule in question. CD is measured in the UV part of the spectrum, and at far-UV (170-250 nm) the CD of a protein will report on its mainchain conformation. Key secondary structure features of proteins have characteristic CD – for example, α-helices have large negative CD bands at 208 and 222 nm, and a large positive band at 192 nm which is different to a characteristic CD for β-sheet.
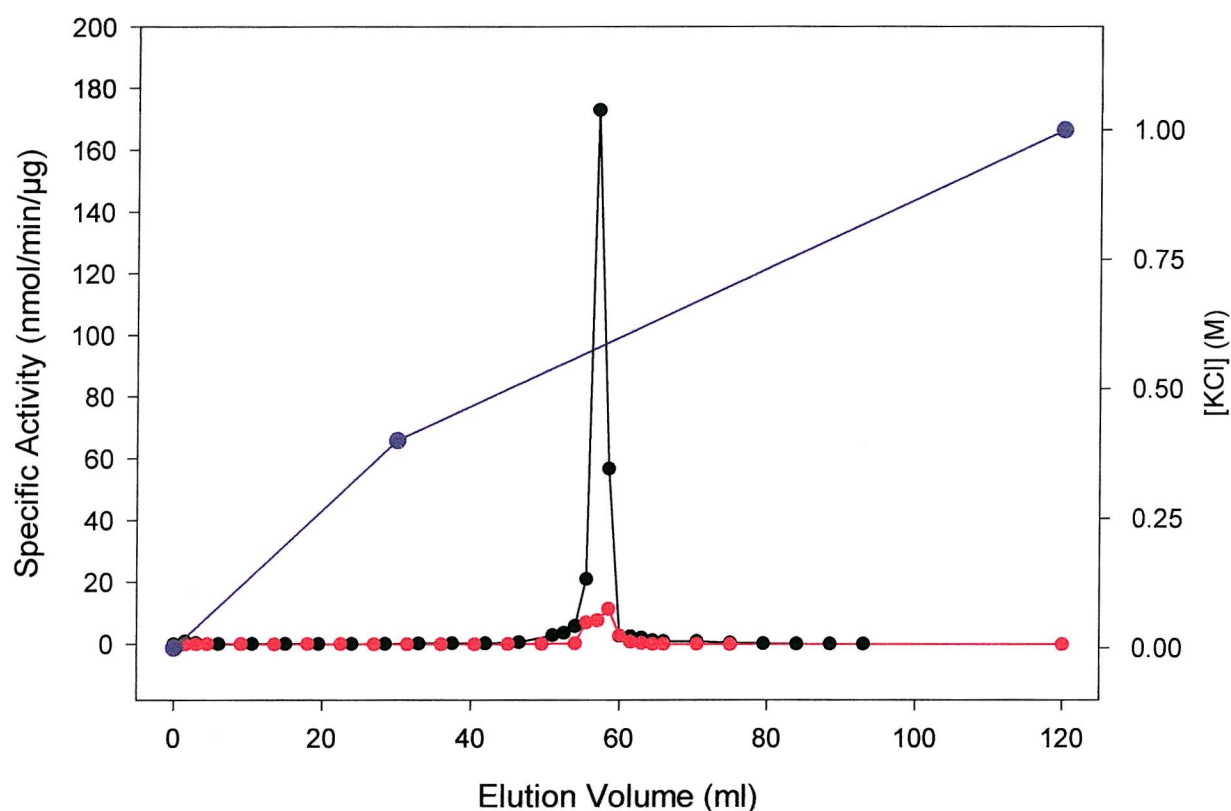
Figure 3.8 Elution of N1A and H48Q HnpsPLA$_2$ from a Heparin-Sepharose Chromatography Column.

See section 2.4.6 for column protocol. Enzyme activity was measured using the fluorescence displacement assay with SUVs of DOPG (64 µM) as substrate (section 2.6.1)

● - N1A HnpsPLA$_2$

● - H48Q HnpsPLA$_2$

● - KCL Concentration

Protein elution was measured by continuous monitoring of the absorbance at 280 nm.
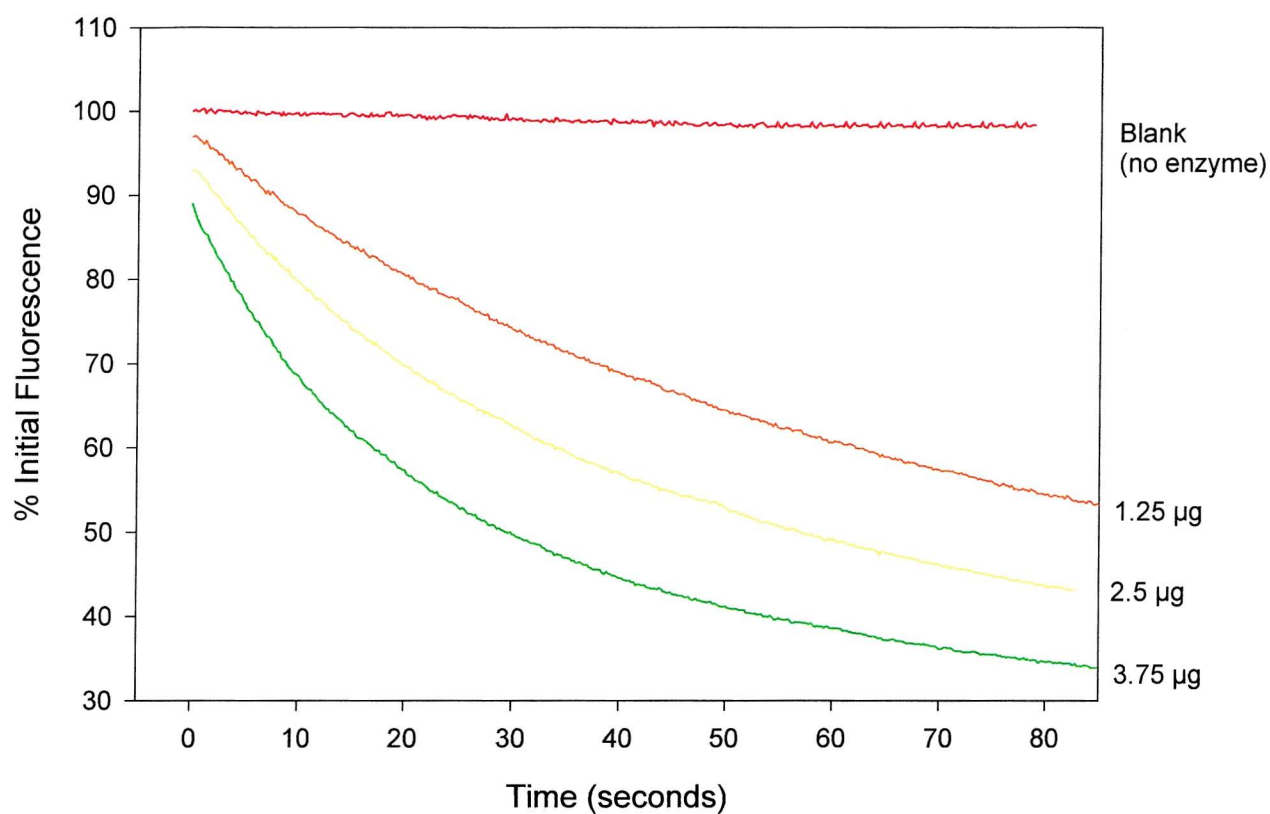
Figure 3.9 Fluorescence Trace Showing the Hydrolysis of DOPG SUVs by H48Q HnpsPLA$_2$.

Activity of H48Q was measured using the fluorescence displacement assay as before.

Assays contained either:

——— - No enzyme

——— - 1.25 µg

——— - 2.5 µg or

——— - 3.75 µg of H48Q hnpsPLA$_2$.

Enzyme was added at time = 0.
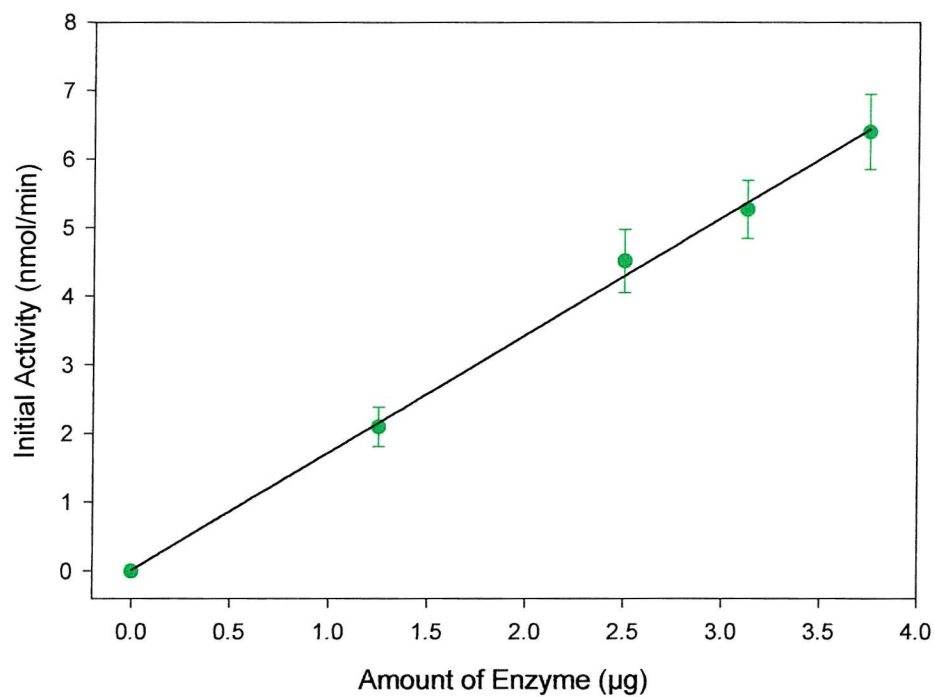
Figure 3.10 Dose Response Curve for the Hydrolysis of DOPG SUVs by H48Q HnpsPLA$_2$.

Enzyme activity was measured using the fluorescence displacement assay as before, with 64 µM DOPG.

● - H48Q HnpsPLA$_2$

Each data set is the mean of 3 separate measurements ± s.d.
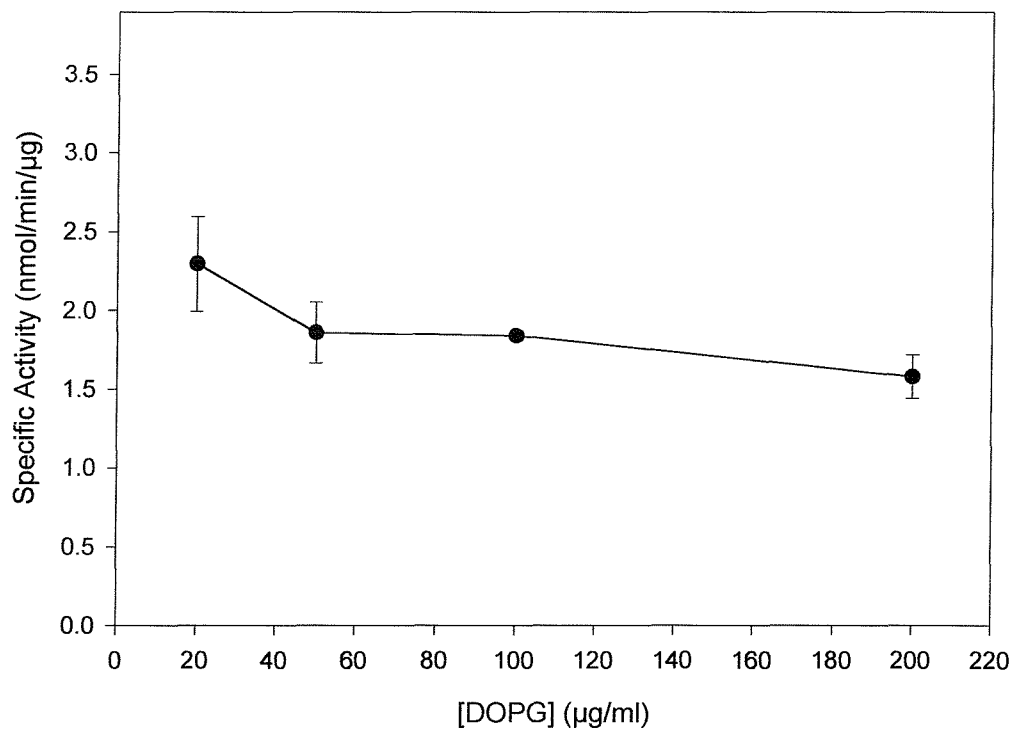
Figure 3.11 Effect of Substrate Concentration on the Hydrolysis of DOPG SUVs by H48Q HnpsPLA₂.

Enzyme activity was measured using the fluorescence displacement assay as before, with varying substrate concentrations as indicated.

• - H48Q HnpsPLA₂

Each data set is the mean of 3 separate measurements ± s.d.
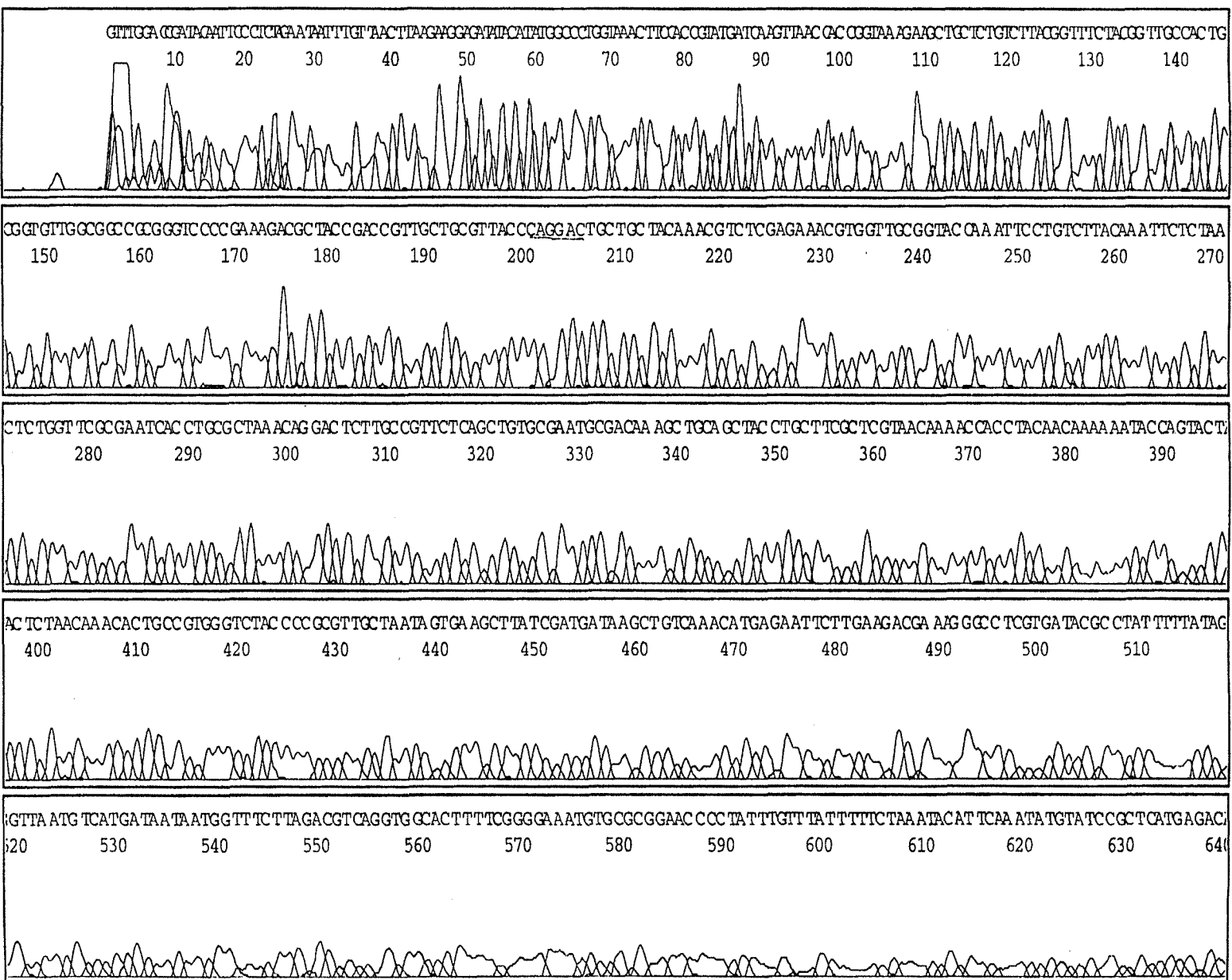
Figure 3.12 The Gene Sequence Coding for the H48Q Mutant of HnpsPLA₂.

89

Figure 3.13 shows the CD spectrum of both N1A and H48Q, which indicates that the H48Q mutation has not caused any significant conformational changes in the protein structure.

3.3.4 Thermal Denaturation of N1A and H48Q HnpsPLA$_2$.

Having demonstrated the similarity between the N1A and H48Q in terms of structure, the stability of the H48Q structure was compared to that of the N1A by thermal denaturation. Mutations in enzymes can often render them less stable than the wild type, and assessing their thermal stability can effectively compare differences between native and mutant proteins. Incubating the two proteins at temperatures between 25 - 75 °C, and comparing the residual activity of both at each temperature in part achieved this. Such high temperatures are required due to the stability that 7 disulphide bonds confer on hnpsPLA$_2$. The results are shown in figure 3.14, and show that both proteins show an identical pattern of loss of activity. This implies that the H48Q has a structure that is very similar if not identical to that of the N1A in terms of stability.

The thermal stability of the two forms of hnpsPLA$_2$ was further analysed using CD as a means of comparing the structural integrity of the enzymes with increasing temperature. A representative CD spectra for N1A measured at temperatures ranging from 25 °C to 82 °C is shown in figure 3.15. As temperature increases, the transition from α-helical to random coil structure can be seen. To obtain melting curves for the two proteins, the CD data was analysed and the CD at 222 nm was plotted against the experimental temperature. The graphs are shown in figure 3.16. The results demonstrate that the melting temperature (Tm) of N1A is marginally higher than that of H48Q - 66 °C compared with 63 °C.

This indicates that both forms of the enzyme have a similarly stable structure, with transition from α-helical to random coil structure occurring at a near identical temperature.

90
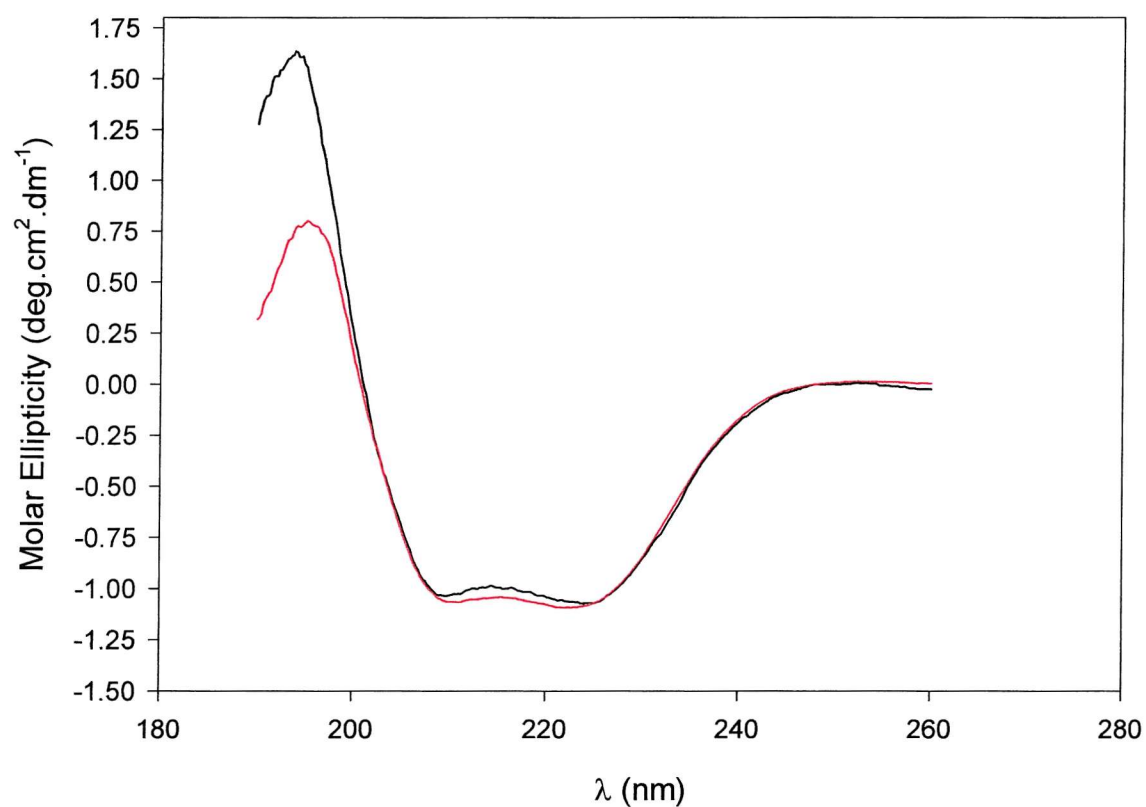
Figure 3.13 C.D. Spectra of N1A and H48Q HnpsPLA₂.

CD was carried out as specified in section 2.6.15.

Concentration of enzyme was 0.18 mg/ml in each case, and spectra have been corrected for blank (10 mM phosphate buffer).

——— - N1A

——— - H48Q

Spectra shown are averaged from 5 accumulations.
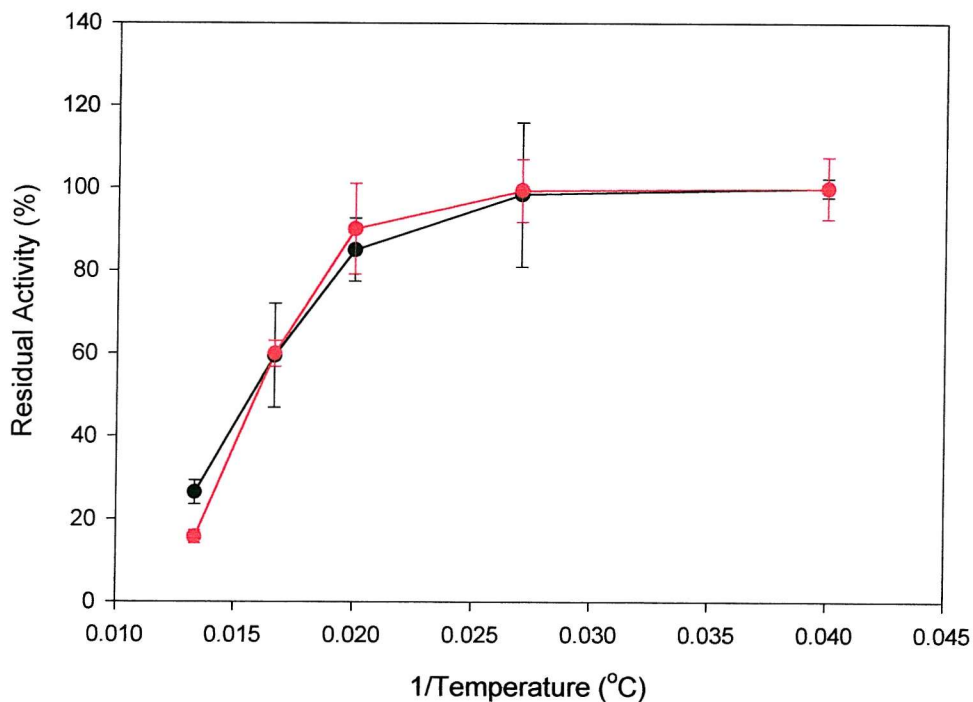
Figure 3.14 Specific Activity of N1A and H48Q HnpsPLA$_2$ after Incubation at Temperatures Between 25 - 75 ^{o}C.

Enzyme activity was measured at each temperature using the fluorescence displacement assay described previously with SUVs of DOPG (64 µM) as substrate. Protein was incubated at each temperature for 30 minutes prior to being assayed.

The control consisted of a sample of each enzyme incubated on ice for 6 hrs. Activity assays on the control samples confirmed that there was no significant loss of activity.

• - N1A HnpsPLA$_2$

• - H48Q HnpsPLA$_2$

Each data set is the mean of three separate measurements ± s.d.
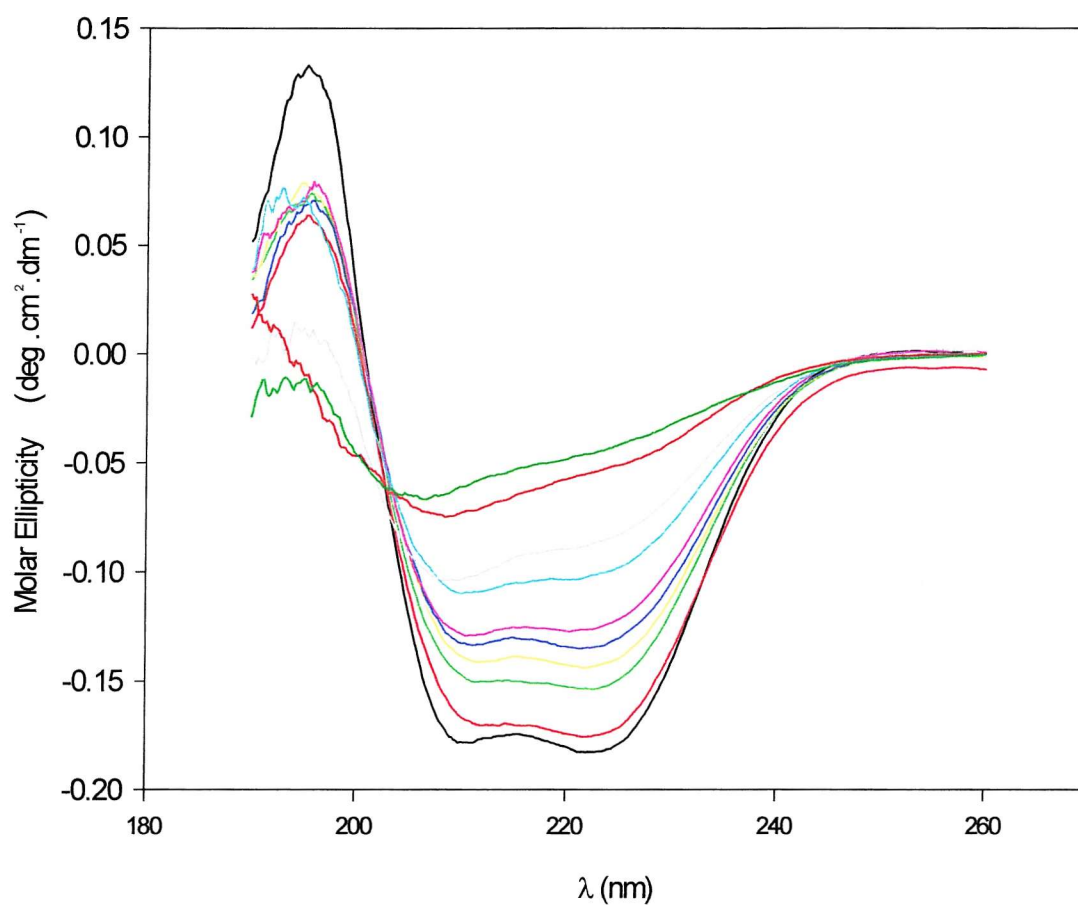
Figure 3.15 CD Spectra for N1A HnpsPLA$_2$ Measured from 25 ^{o}C to 82 ^{o}C.

CD was carried out as described in section 2.6.15. Concentration of N1A was 0.18 mg/ml. Spectra have been corrected for blank (10 mM phosphate buffer).

——	25 ^{o}C
——	31 ^{o}C
——	35 ^{o}C
——	40 ^{o}C
——	47 ^{o}C
——	55 ^{o}C
——	62 ^{o}C
——	68 ^{o}C
——	75 ^{o}C
——	82 ^{o}C
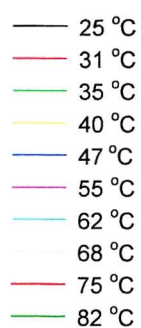
Spectra shown are averaged from 3 accumulations.
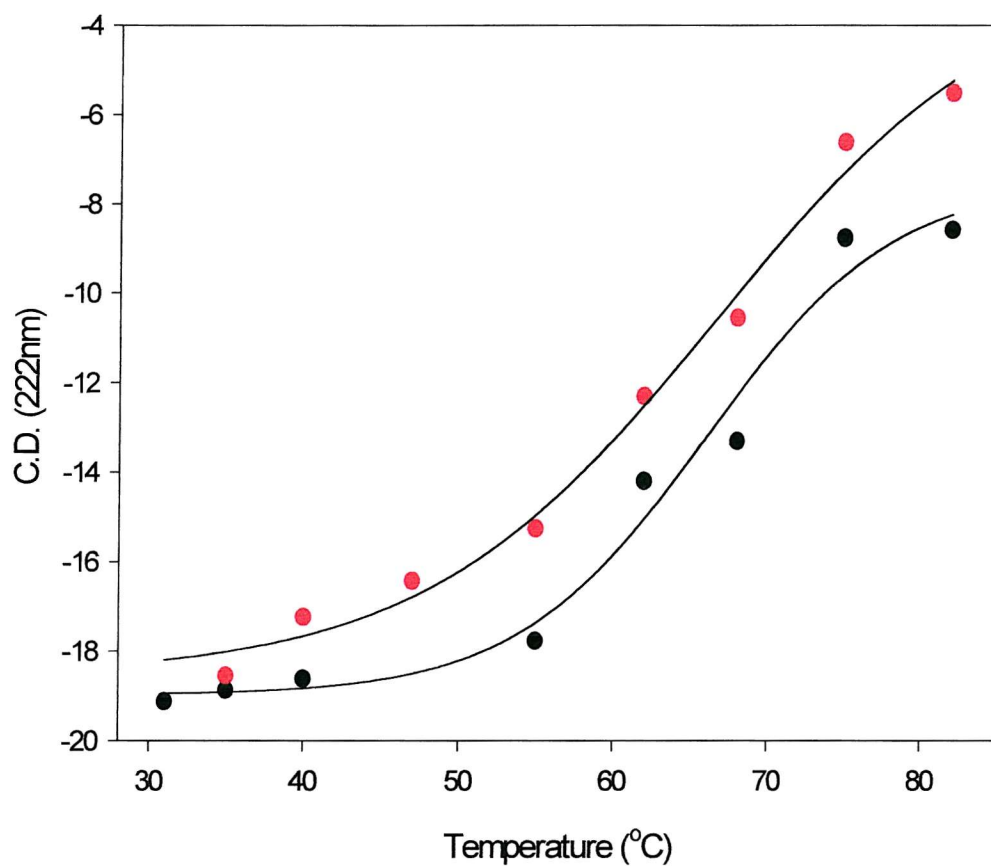
Figure 3.16 Melting Curves for N1A and H48Q HnpsPLA$_2$

Data was calculated from CD spectra of N1A and H48Q hnpsPLA$_2$ measured at temperatures between 25 - 82 °C (see previous figure).

• - N1A hnpsPLA$_2$

• - H48Q hnpsPLA$_2$

Data was obtained from the average spectra of 3 accumulations.

3.3.5 Comparison of the Interfacial Binding of N1A and H48Q HnpsPLA$_2$ to DOPG Vesicles.

Having assessed the structural integrity of the two forms of the enzyme, it was necessary to study the binding capacity of H48Q to ensure that the mutant enzyme is able to bind productively to the substrate interface. Human non-pancreatic sPLA$_2$ does not contain any tryptophan residues, which could be used to measure fluorescent changes upon binding to substrate interfaces. One method used to study interfacial binding, which overcomes the need for an intrinsic fluorescent reporter, utilises the fluorescent phospholipid probe dansyl-DPPE (figure 3.17).
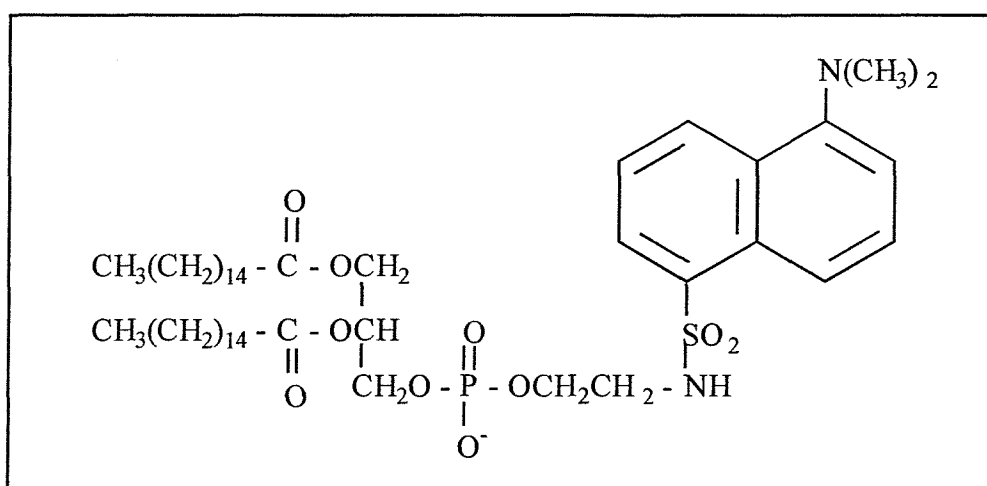
Figure 3.17 Structure of N-Dansyl-1,2-Palmitoyl-sn-glycero-3-phosphoethanolamine (Dansyl–DPPE).

When incorporated into a bilayer, the dansyl group will be at least partially solvent exposed. When desolvation of this dansyl fluorophore occurs, such as when enzyme binds to an interface where it is contained, a blue shift in fluorescence is seen, with an increase in fluorescence intensity of the probe. This probe has previously been used in vesicles of DTPM (a non-hydrolysable phospholipid) to compare the interfacial binding of N1A with met-PLA$_2$, (a recombinant form of the enzyme with the initiator Met still intact), V3W and the

porcine pancreatic sPLA$_2$ (pp-sPLA$_2$) [93,94]. These studies investigated the role of free calcium in interfacial binding, and showed that in the presence of free calcium, there was a steeper saturation curve than when calcium was absent, indicating that there was less binding affinity for the interface in the absence of calcium.

In this study, dansyl-DPPE was mixed with DOPG at a ratio of 4-mol%, a quantity which ensures that sufficient probe will be available on the outer layer of the SUVs to report on binding, when they are prepared by methanol injection. EDTA was present in the assay cocktail to chelate calcium and other ions, in order to prevent hydrolysis of the vesicles. Figure 3.18 compares the binding of H48Q and N1A to DOPG vesicles by comparison of the desolvation of the fluorescent probe on interfacial binding. The graph for the pp-sPLA$_2$ form is also shown for comparison.

The results show that the binding characteristics for the N1A and the H48Q are very similar. The results for the pp-sPLA$_2$ show that this enzyme has a lower affinity for DOPG vesicles than the human group IIA sPLA$_2$. This is in good agreement with studies that used the phospholipid-binding protein annexin V in a competitive manner to determine the relative affinity of pp-sPLA$_2$ and hnpsPLA2 for DOPG vesicles. The conclusion of these studies was that pp-sPLA$_2$ has a lower affinity for DOPG interfaces than hnpsPLA$_2$ [101].

3.3.6 Effect of NaCl Concentration on the Ability of N1A and H48Q HnpsPLA$_2$ to Hydrolyse DOPG SUVs.

To further test the binding of H48Q compared to N1A, both enzymes were assayed in the presence of increasing NaCl concentrations. This would interrupt the electrostatic interactions thought to be mainly responsible for interfacial binding, and allow discrepancies between the binding of H48Q and N1A to be seen.

96
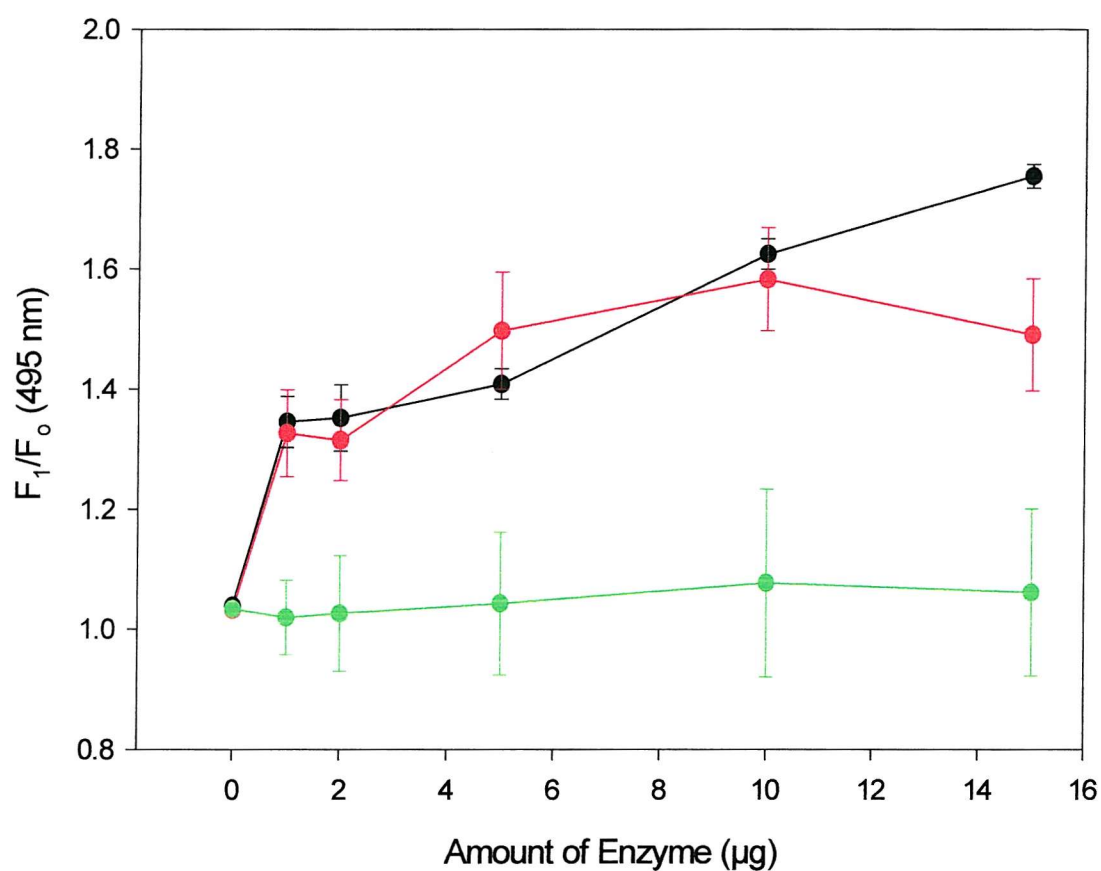
Figure 3.18 Comparison of the Binding of N1A and H48Q HnpsPLA$_2$ to DOPG Vesicles.

Preparation of 15 µM DOPG vesicles containing 4 %mol dansyl-DPPE was carried out as described in section 2.6.5. Enzyme binding was monitored as an increase in fluorescence at 495 nm.

All assays contained 1 mM EDTA.

● - N1A HnpsPLA$_2$

● - H48Q HnpsPLA$_2$

● - pp-sPLA$_2$

Each data set represents the mean of three separate measurements ± s.d.

Figure 3.19 shows the resulting graph, and the similar activities seen suggest that H48Q is able to interfacially bind as efficiently as the N1A at NaCl concentrations tested.

The increase in activity seen up to 100 mM NaCl may be due to the partial disruption of electrostatic interactions between the enzyme and vesicle which may in fact increase the catalytic rate, as the enzyme will be able to scoot more freely over the surface of the vesicle. Above this concentration of NaCl, the activity is fairly constant, and may represent an equilibrium-like state between the contribution of electrostatic interactions and hydrophobic interactions to interfacial binding. The relative activities measured in the presence of increasing NaCl for N1A and H48Q (% of 100 mM NaCl) are essentially the same, indicating that the mutant is as able to productively bind to a substrate interface as the N1A, thus ruling out impaired substrate binding as a reason for the low catalytic activity seen.

Having demonstrated that the H48Q mutant has a structure similar to that of the N1A both in terms of its overall fold and stability and is able to bind interfacially to a similar extent, it was then necessary to investigate the nature of the activity seen with the H48Q more fully.

3.3.7 Ability of H48Q to Hydrolyse Pyrene-labelled Phospholipid.

During the characterisation of the H48Q mutant, the preparation of an H48Q mutant of human group IIA sPLA$_2$ by C.M. Mournier (Pasteur Institute, Paris, France - personal communication) was reported, and this mutant too was found to be active. However the rate quoted was 0.5 % as compared to the wild type enzyme, which is substantially less than was found with our version of the mutant. The group in question assay their enzyme for phospholipase A$_2$ activity using a method reported by Radvanyi, which utilises pyrene-labelled phospholipids as a probe for activity [86]. These phospholipids are labelled at the sn-2-acyl position with 10-pyrenyldecanoic acid, which will be released upon phospholipid hydrolysis (figure 3.20).
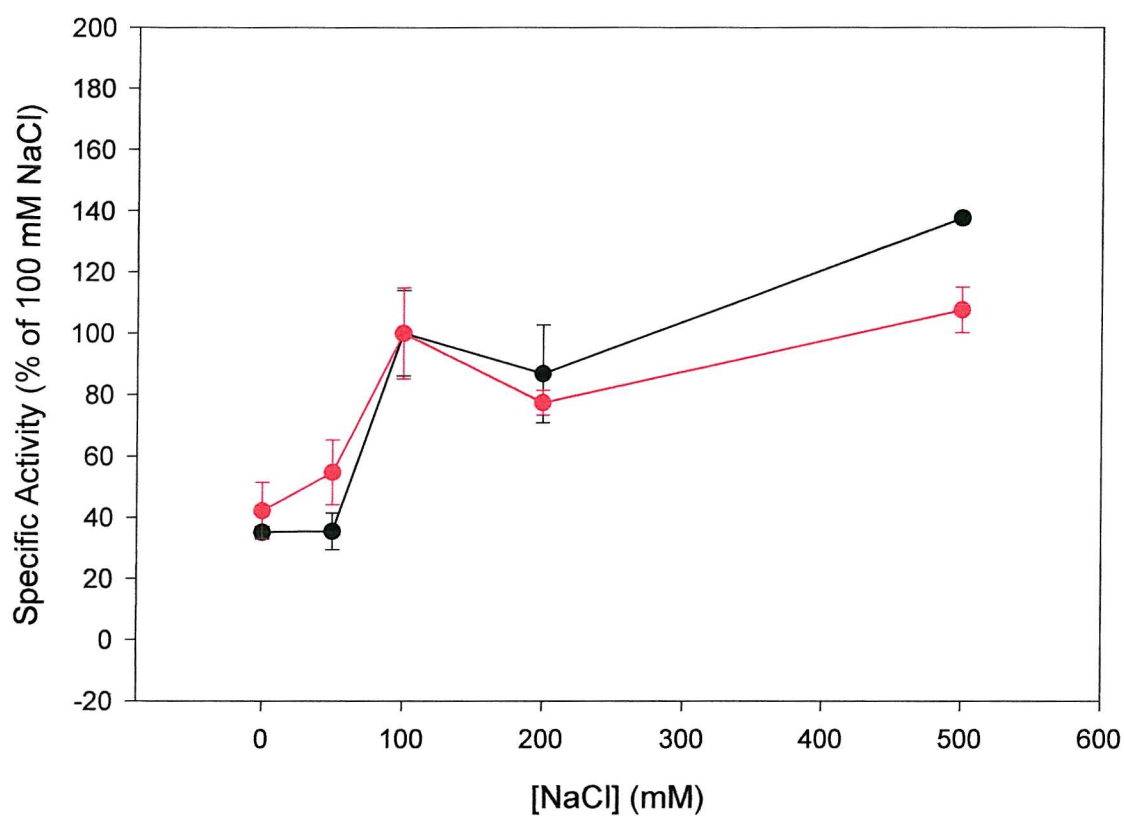
Figure 3.19 Effect of NaCl on Ability of N1A and H48Q HnpsPLA$_2$ to Hydrolyse DOPG Vesicles.

Specific activity was assayed using the fluorescence displacement assay (section 2.6.1) with SUVs of DOPG (64 µM) as substrate.

● - N1A

● - H48Q

Each data set is the mean of three separate measurements ± s.d.

The free 10-pyrenyldecanoic acids will tightly bind albumin, which is present in the assay, and give pyrene fluorescence when excited at 345 nm, which can be monitored at 398 nm and used to measure the specific activity of phospholipases.

$$CH_3(CH_2)_{14} - \overset{\overset{\textstyle O}{\textstyle \|}}{C} - OCH_2$$

$$(CH_2)_9 - \overset{\overset{\textstyle \|}{\textstyle C}}{O} - OCH \quad \overset{O}{\|}$$

$$CH_2O - \overset{\textstyle P}{\underset{\textstyle \cdot O}{}} - OCH_2$$

$$HCOH$$

$$CH_2OH$$
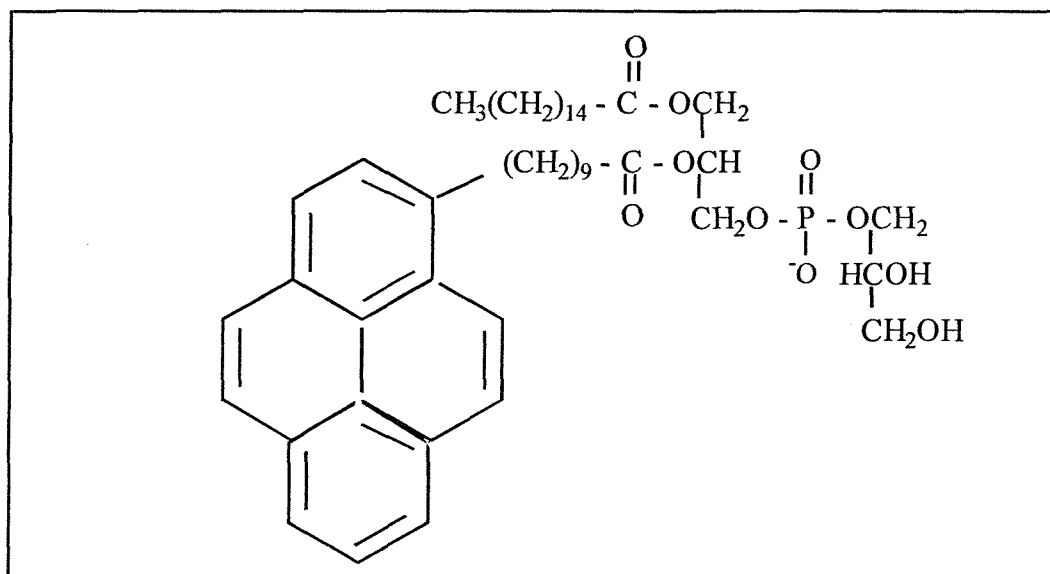
Figure 3.20 Structure of 1-Palmitoyl-2-Pyrenedecanoyl-*sn*-Glycero-3-Phosphoglycerol (Pyrene-PG).

As the H48Q mutant prepared by C.M. Mournier was reported to have activity, but at a lower rate than ours, the Radvanyi assay technique was used with pyrene-labelled PG in order to compare the two H48Q mutants in terms of activity. Figures 3.21 and 3.23 show typical fluorescence traces obtained when assaying N1A and H48Q hnpsPLA₂ using this assay. Dose response curves for N1A and H48Q hnpsPLA₂ using pyrene-labelled PG as substrate show a linear relationship between initial activity and concentration of enzyme at a fixed substrate concentration (figures 3.22 and 3.24). The specific activities measured for the N1A and H48Q in this way were 112.16 ± 19.95 and 3.2 ± 0.75 respectively, giving the H48Q a rate of 2.85 % as compared to the N1A. That the rate seen by C.M. Mournier is less than this may be due to enzyme purity etc.
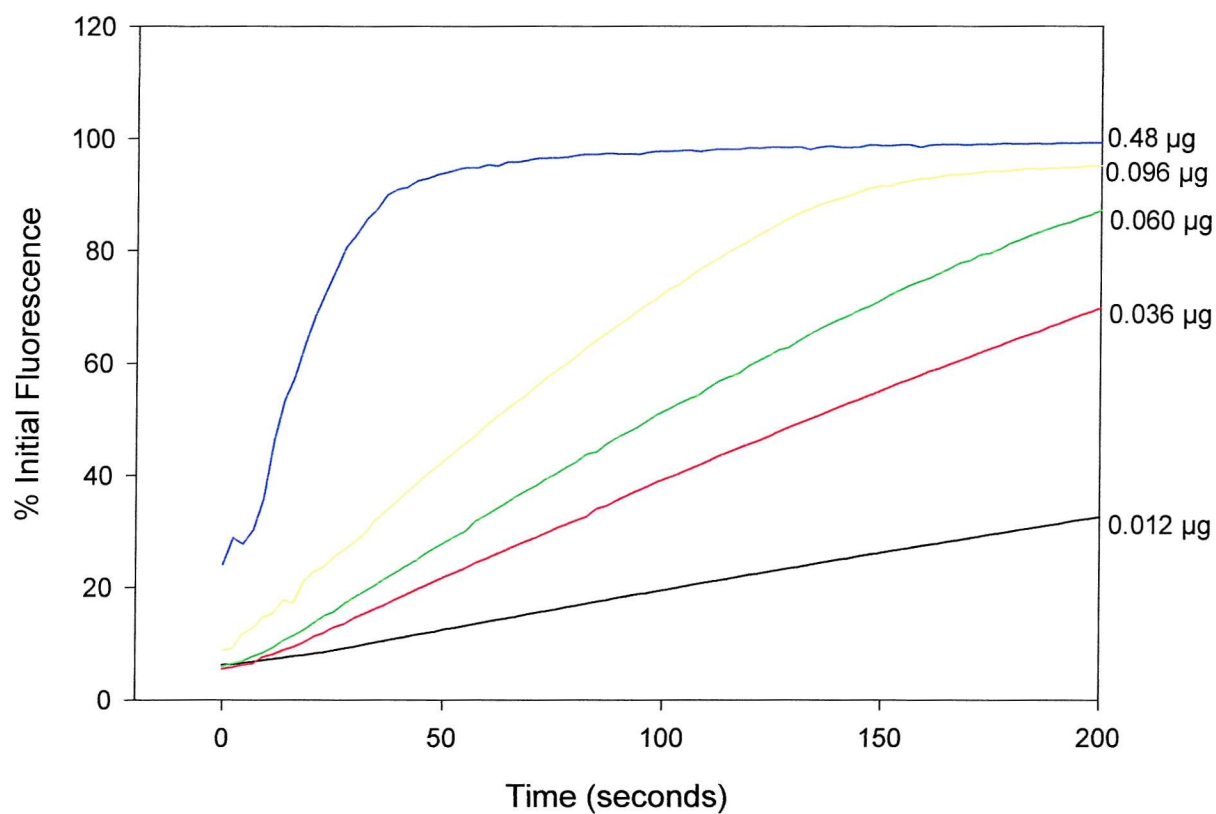
Figure 3.21 Fluorescence Traces Showing the Hydrolysis of Pyrene-PG by Varying Amounts of N1A HnpsPLA$_2$.

Enzyme activity was measured as described in section 2.6.2, with 2 µM substrate.

Assays contained either:

— - 0.012 µg
— - 0.036 µg
— - 0.060 µg
— - 0.096 µg or
— - 0.48 µg N1A HnpsPLA$_2$

Enzyme was added at time = 0.
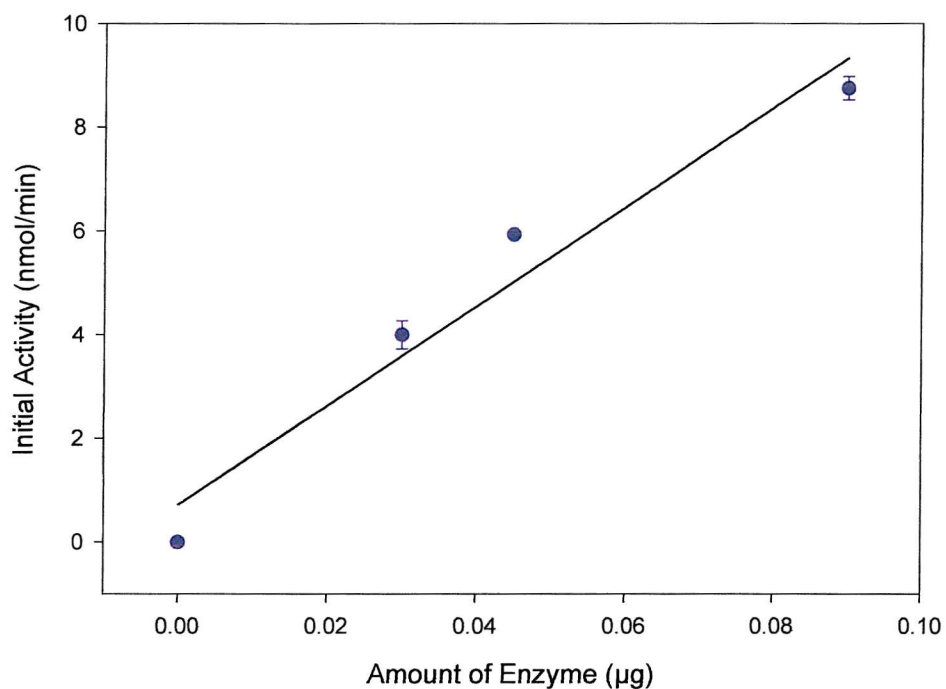
Figure 3.22 Dose Response Curve for the Hydrolysis of Pyrene-labelled PG by N1A HnpsPLA$_2$.

Enzyme activity was measured according to the method described in section 2.6.2, with 2 µM substrate. Data used is obtained from pyrene fluorescence as shown in figure 3.20.

● - N1A HnpsPLA$_2$

Each data set is the mean of three separate measurements ± s.d.
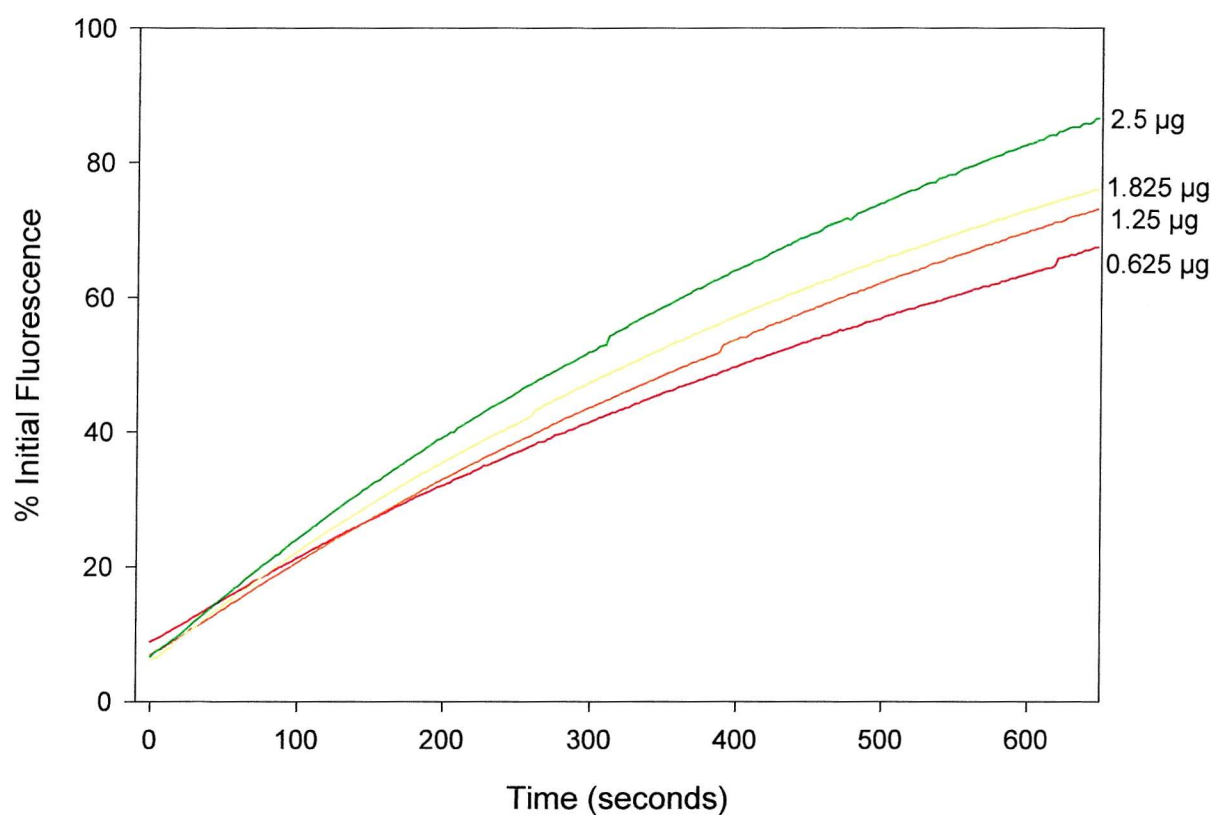
Figure 3.23 Fluorescence Traces Showing the Hydrolysis of Pyrene-PG by Varying Amounts of H48Q HnpsPLA₂.

Enzyme activity was measured as described previously.

Assays contained either:

    — -   0.625 µg

    — -   1.25 µg

    — -   1.825 µg or

    — -   2.5 µg H48Q HnpsPLA₂

Enzyme was added at time = 0.
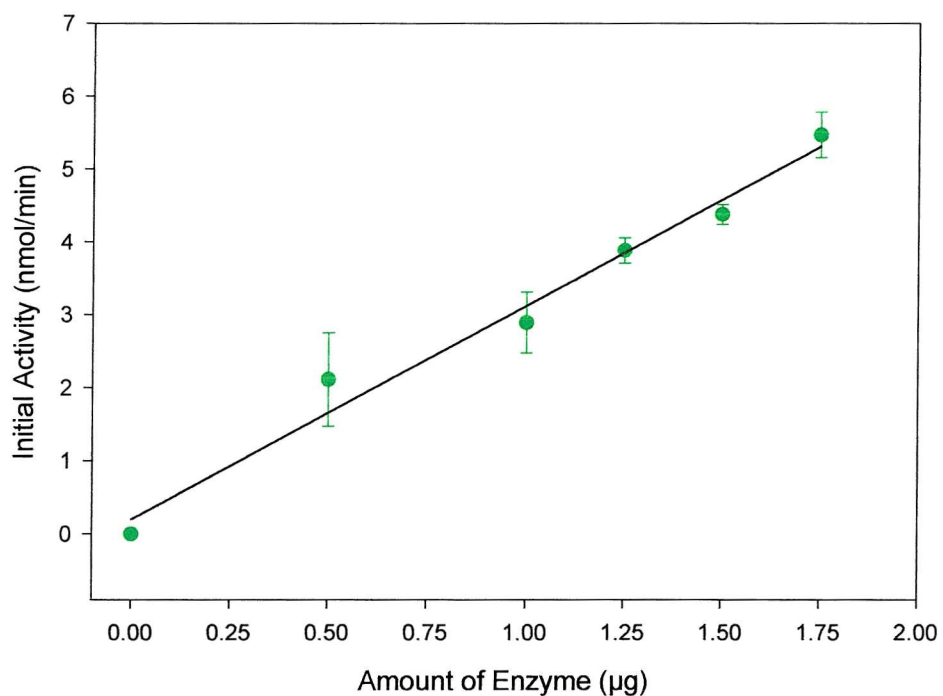
Figure 3.24 Dose Response Curve for the Hydrolysis of Pyrene-labelled PG by H48Q HnpsPLA$_2$.

Enzyme activity was measured according to the method described in section 2.6.2. Data used is obtained from pyrene fluorescence as shown in figure 3.22.

● - H48Q HnpsPLA$_2$

Each data set is the mean of three separate measurements ± s.d.

3.3.8 Effect of pH on Ability of N1A and H48Q to Hydrolyse DOPG Vesicles.

The histidine residue crucial for catalytic activity (His-48) is found within the active site of hnpsPLA$_2$, which is located in a pocket connected to the surface by a hydrophobic channel [12]. Protonation of this histidine residue in N1A at decreasing pH (pKa His ~ 6) will prevent it acting as a proton acceptor in the crucial stage of catalysis. As the H48Q lacks the catalytically crucial histidine residue in its active site, it should be less sensitive to lower pH than the N1A. To test this theory, both the N1A and the H48Q were assayed using the fluorescence displacement assay at varying pH, and the results are shown in figure 3.25. The results show that the H48Q is less susceptible to changes in pH than the N1A, as expected, most probably due to the protonation of the His-48 in N1A at ~ pH 6.0.

It was not possible to measure the activity at pHs lower than pH 5.5, due to the sensitivity of the assay system to low pH, and also because the activity of the H48Q becomes too low to accurately measure.

3.3.9. Comparison of the Catalytic Activity of N1A and H48Q using Calcium and other Divalent Cations.

The calcium ion that is crucial for catalysis is co-ordinated within the channel that connects the active site with the interfacial binding surface [12]. The substitution of His-48 with a Gln residue may have altered this region of the protein, particularly the H-bonding network found here. This could affect the ability of the H48Q to bind calcium efficiently.

As the overall structural stability and the interfacial binding of H48Q has been determined, it is also necessary to confirm that the mutant is able to co-ordinate calcium efficiently to rule this out as a reason for catalytic activity at such a reduced rate.
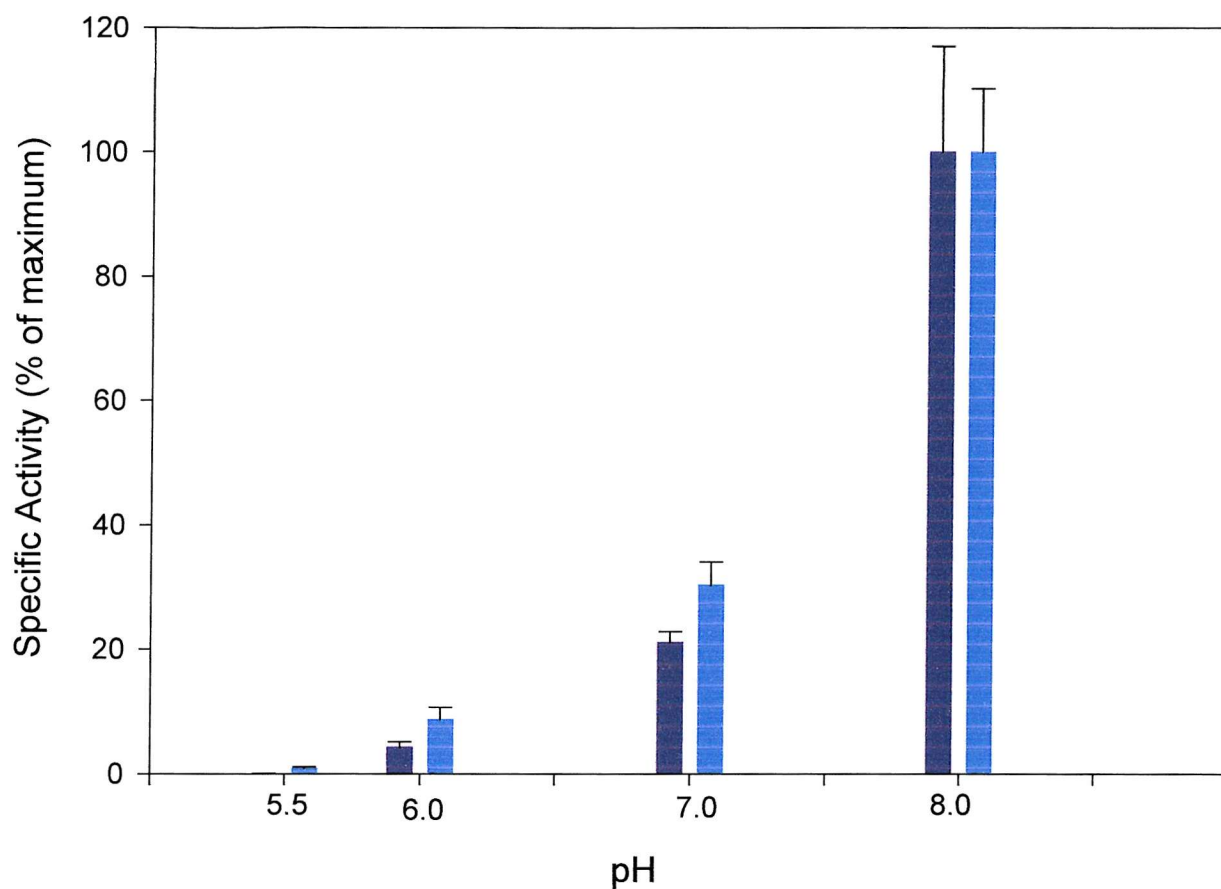
Figure 3.25 Effect of pH on the Hydrolysis of DOPG Vesicles by N1A and H48Q HnpsPLA$_2$.

Enzyme activity was measured using the continuous fluorescence displacement assay as described in materials & methods (2.6.1) with 64 μM DOPG SUVs as substrate.

▬▬▬ - N1A HnpsPLA$_2$
▬▬▬ - H48Q HnpsPLA$_2$

Each data set is the mean of three separate measurements ± s.d.

The N1A and H48Q were assayed for activity using the fluorescence displacement assay using a range of calcium concentrations and the results are shown in figure 3.26. The results indicate that even with low Ca^{2+} concentrations, both the N1A and H48Q can support catalysis, and no significant difference could be seen between the two.

The porcine pancreatic $sPLA_2$ is able to support catalysis with Co^{2+} instead of Ca^{2+}, albeit at a reduced rate due to its lower affinity for Co^{2+}, and also shows activity with Ni^{2+} at even lower rates [102]. The N1A and H48Q $sPLA_2$s were also assayed in the presence of these cations to test whether or not the human $sPLA_2$ can support activity with them in the same way that the pp enzyme can. It is possible that the H48Q mutant has a lower affinity for calcium than the N1A due to the mutation in the active site, but it may still be able to bind it sufficiently well to support catalysis, thus disguising any differences in affinity associated with a changed conformation in the active site. If the N1A has a lower affinity for Co^{2+} or Ni^{2+} than Ca^{2+}, as judged by its catalytic ability, in theory this will amplify any difference in the affinity of H48Q for these cations. The porcine pancreatic form of the enzyme was also assayed for comparison, and the results are shown in figures 3.27-3.29.

The results for the N1A and the H48Q show that these enzymes are able to catalyse the hydrolysis of DOPG SUVs with cobalt or nickel ions as cofactor. However, the rate of catalysis seen is markedly less than in the presence of calcium. The increase in catalytic rate of the $pp-sPLA_2$ enzyme in the presence of increasing calcium is notably slower than with the N1A or H48Q. Also, this enzyme too shows a low catalytic rate when measured on Co^{2+} ions and Ni^{2+} ions.

This result is in good agreement with the published data [102].
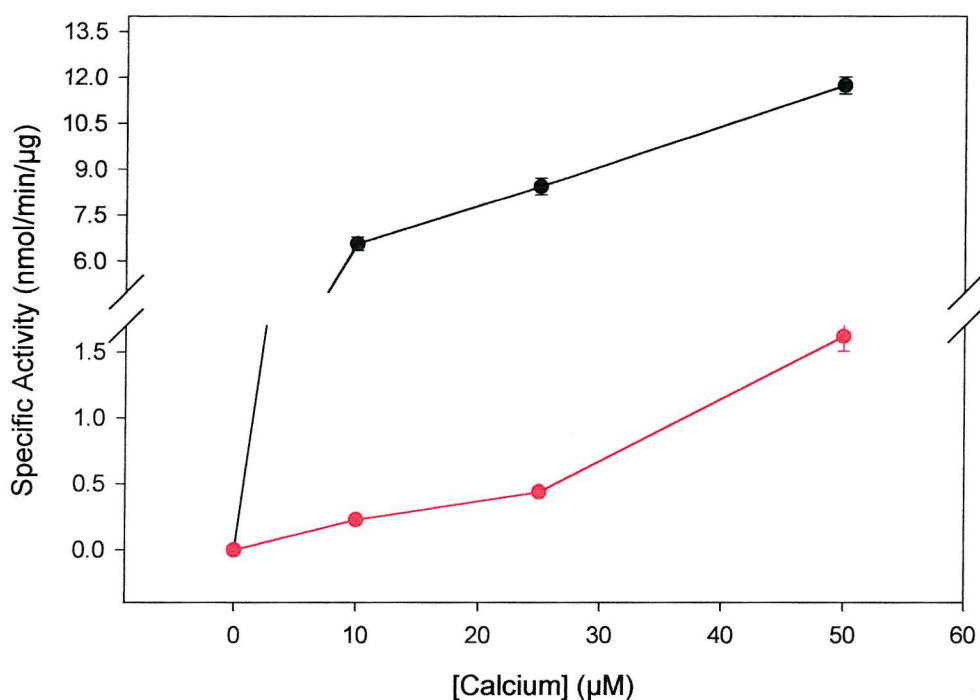
Figure 3.26 Comparison of the Hydrolysis of DOPG SUVs by N1A and H48Q HnpsPLA$_2$ at Different CaCl$_2$ Concentrations.

Enzyme activity was measured using the fluorescence displacement assay as previously described (section 2.6.1).

All data is corrected for the minor activity seen in the absence of any added calcium.

● - N1A HnpsPLA$_2$

● - H48Q HnpsPLA$_2$

Each data set is the mean of three separate measurements ± s.d.
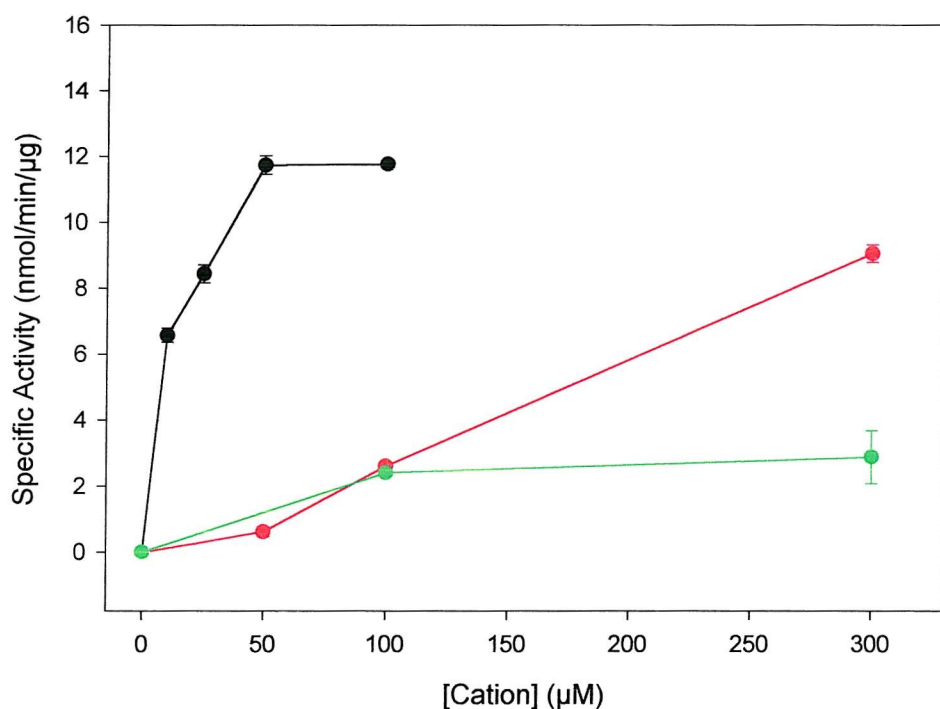
Figure 3.27 Comparison of the Hydrolysis of DOPG SUVs by N1A HnpsPLA$_2$ at different Concentrations of CaCl$_2$, CoCl$_2$ and NiCl$_2$.

Enzyme activity was measured using the fluorescence displacement assay as described (section 2.6.1).

All data is corrected for the minor activity seen in the absence of any added cation.

● - CaCl$_2$

● - CoCl$_2$

● - NiCl$_2$

Each data set is the mean of three separate measurements ± s.d.
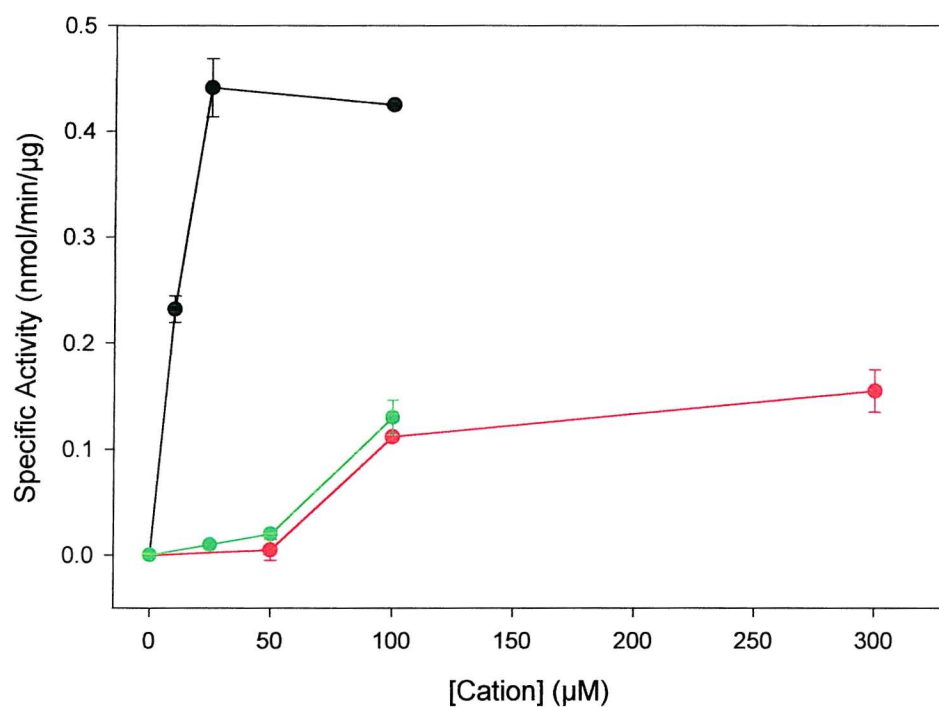
Figure 3.28 Comparison of the Hydrolysis of DOPG SUVs by H48Q HnpsPLA$_2$ at different Concentrations of CaCl$_2$, CoCl$_2$ and NiCl$_2$.

Enzyme activity was measured using the fluorescence displacement assay as described (section 2.6.1).

All data is corrected for the minor activity seen in the absence of any added cation.

● - CaCl$_2$

● - CoCl$_2$

● - NiCl$_2$

Each data set is the mean of three separate measurements ± s.d.
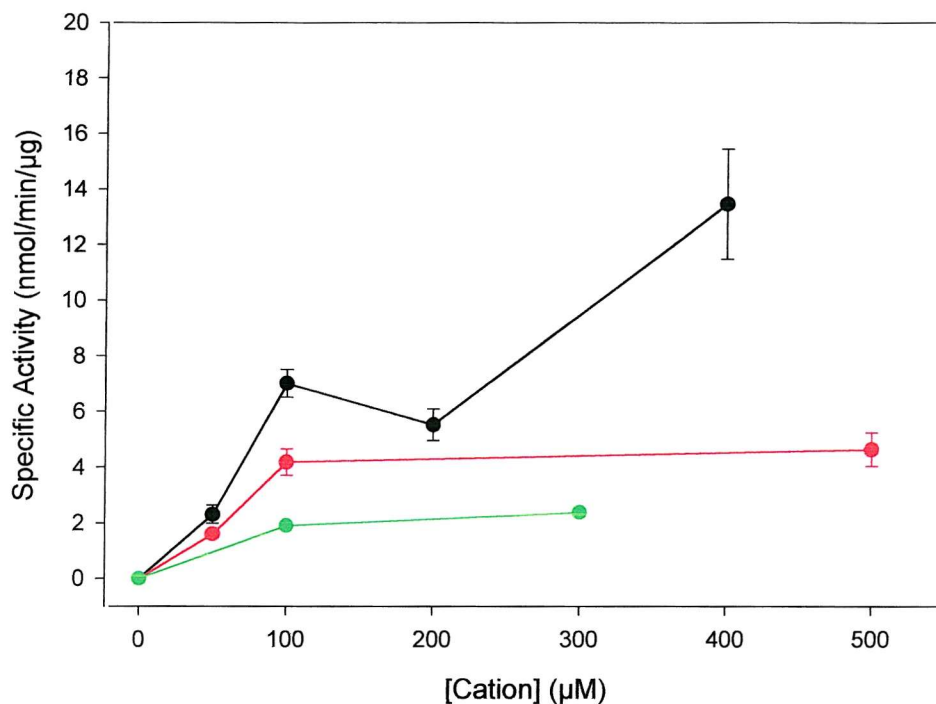
Figure 3.29 Comparison of the Hydrolysis of DOPG SUVs by pp-sPLA$_2$ at different Concentrations of CaCl$_2$, CoCl$_2$ and NiCl$_2$.

Enzyme activity was measured using the fluorescence displacement assay as described (section 2.6.1).

All data is corrected for the minor activity seen in the absence of any added cation.

● - CaCl$_2$

● - CoCl$_2$

● - NiCl$_2$

Each data set is the mean of three separate measurements ± s.d.

3.3.10 Effect of the Physical Properties of the Vesicle on Specific Activity of N1A and H48Q HnpsPLA$_2$.

All previous work using the fluorescence displacement assay has used SUVs of DOPG to compare the activity of the H48Q mutant with the N1A. It was of interest to compare the activity using MLVs of DOPG. These are much larger vesicles, and have diameters ranging from ~ 100-3000 nm, compared with a range of ~ 25-100 nm for SUVs.

The specific activities for the two enzymes when assayed on these substrate presentations are shown in figures 3.30 and 3.31. The results show that the specific activities of the enzymes are higher when assayed on MLVs as compared with SUVs. The reason for the enhanced activity of the N1A, and to a lesser extent, the H48Q mutant on MLVs is not clear, but must reflect differences in the interfacial binding of the enzymes to the different types of vesicle. It is thought that the enzymes will bind very tightly to SUVs, and that this tight binding will impede the overall rate of catalysis. For example, if the enzyme is limited to scooting kinetics with SUVs, this may be less optimal in terms of catalytic ability than conditions where hopping kinetics can occur, as may be the case with MLVs.

The SUVs used in the majority of the assays reported here are made by the rapid injection of a methanol solution of phospholipid into aqueous solution. An alternative method involves first making MLVs and then breaking these up by cycles of freeze/thaw and sonication to form SUVs. This method is popular when the phospholipid in question is not soluble in methanol (or ethanol), or when the assay system used is sensitive to methanol [103]. The fluorescence displacement assay used predominantly throughout this thesis can tolerate the small amount of methanol introduced on injection of phospholipid, and the majority of phospholipids used are soluble in methanol. Thus methanol injection is used predominantly to form SUVs, being a reproducible and less time-consuming method than the alternative.

Figure 3.30: N1A
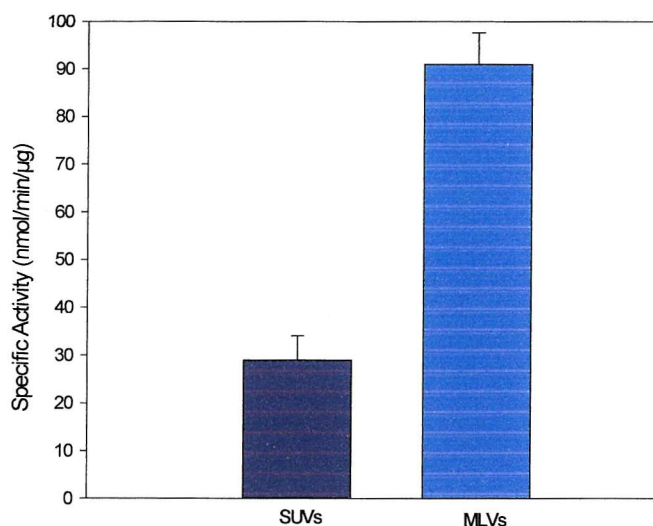
Figure 3.31: H48Q
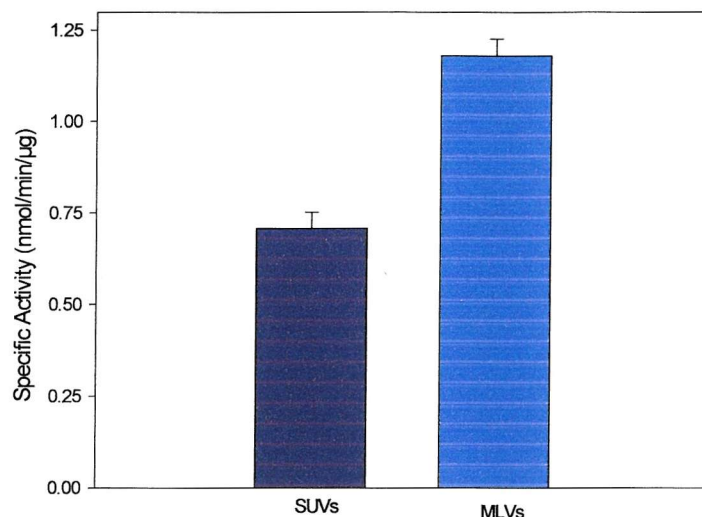
Figures 3.30 and 3.31 Specific Activity of N1A and H48Q HnpsPLA$_2$ when Assayed on SUVs and MLVs of DOPG.

Activity of N1A and H48Q hnpsPLA$_2$ was measured on SUVs and MLVs of DOPG (64 µM) using the fluorescence displacement assay (section 2.6.1). MLVs and SUVs were prepared as described in sections 2.6.6 and 2.6.7.

Specific activities for N1A are: SUVs - 28.98 ± 5.03 nmol/min/µg

MLVs - 90.89 ± 6.71 nmol/min/µg

Specific activities for H48Q are: SUVs - 0.71 ± 0.043 nmol/min/µg

MLVs - 1.18 ± .047 nmol/min/µg

Each data set represents the mean of three separate measurements ± s.d.

Having measured the activity of N1A and H48Q on MLVs of DOPG, and having seen an enhanced rate of activity with both compared to SUVs, the experiment was then repeated. This time the MLVs used to measure specific activity were then sonicated to form SUVs as described above, in order to compare directly the activity on MLVs and SUVs. Methanol injected SUVs were also prepared, and the activity of the three mutants was assayed on these for comparison. The results in figure 3.32 and 3.33 show that the specific activity of N1A and H48Q decreases when the substrate changes from MLV to SUV conformation, although the change of rate for the H48Q is modest. This is likely due to the change in the curvature of the vesicle as discussed above. The fact that SUVs prepared by sonication of MLVs show slightly higher activity than SUVs prepared by methanol injection may be due to the fact that there may be some larger species of vesicle remaining in the system even after the freeze/thaw and sonication procedure, or sonication may produce slightly larger sized vesicles.

3.3.11 Comparison of the Specific Activities of H48Q and N1A on SUVs of DOPM and POPG.

The ability of H48Q to productively bind DOPG SUVs, co-ordinate calcium and support activity at low pH has been compared with that of N1A, as has their secondary structure and stability. Similarly, different physical preparations of the same substrate, DOPG, have been compared as substrate.

A final comparison employed assays containing different anionic phospholipids as substrate, and this involved using SUVs prepared from POPG and DOPM. Figure 3.34 shows the difference in specific activity seen with the H48Q and N1A. Both enzymes were assayed with the same preparation of vesicles to eliminate any error caused by differences in the interface of the substrate vesicle. Results for DOPG are shown for comparison.

114

Figure 3.32: N1A

Figure 3.33: H48Q
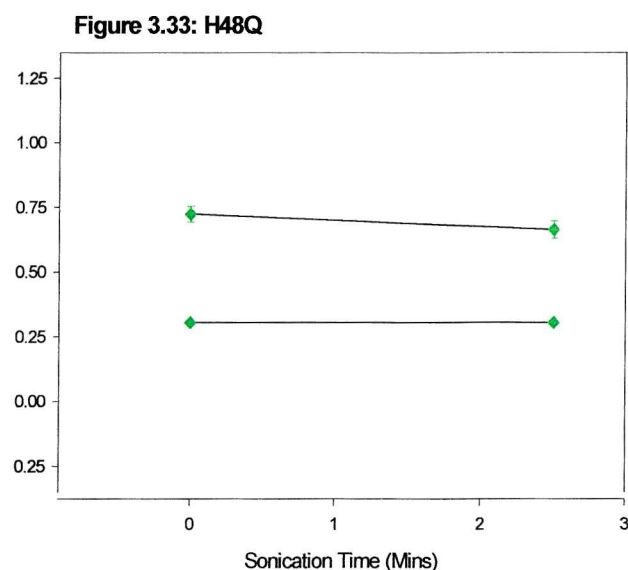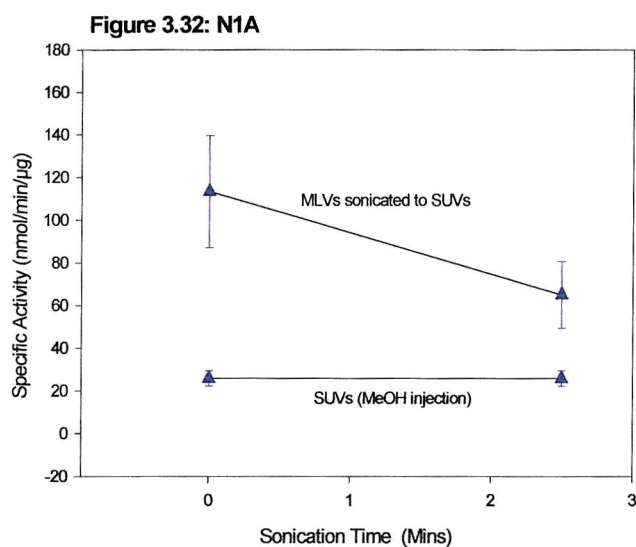
Figures 3.32 and 3.33 Specific Activity of N1A and H48Q HnpsPLA$_2$ Assayed on DOPG MLVs, MLVs Sonicated to form SUVs and SUVs Prepared by Methanol Injection.

Activity of N1A and H48Q hnpsPLA$_2$ was measured using the fluorescence displacement assay with 64 µM vesicles. All DOPG vesicles were prepared as described in section 2.6.6-8.

The top line in each graph represents MLVs sonicated to form SUVs. SUVs prepared by MeOH injection are the lower line of each graph, and are shown for comparison only.

▲   -   N1A HnpsPLA$_2$

●   -   H48Q HnpsPLA$_2$

Each data set is the mean of three separate measurements ± s.d.

115
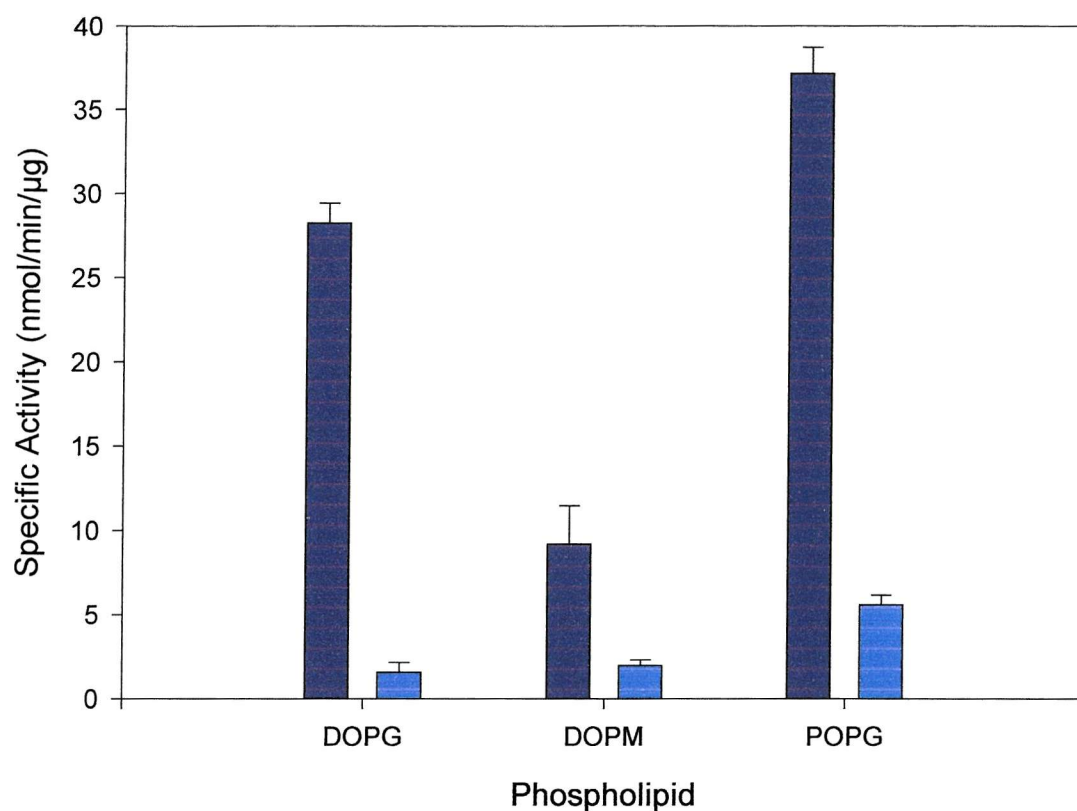
Figure 3.34 Specific Activity of N1A and H48Q HnpsPLA$_2$ when Assayed on Vesicles of DOPG, DOPM and POPG.

Enzyme activity was measured using the fluorescence displacement assay described in section 2.6.1. For each different substrate, MLVs were prepared at a concentration of 50 µg/ml phospholipid, and then reduced to SUVs by freeze/thaw and sonication (section 2.6.8).

- N1A HnpsPLA$_2$

- H48Q HnpsPLA$_2$

Each set of data represents three separate measurements ± s.d.

The results show that the specific activity for N1A measured on DOPM is lower than for DOPG, and the rate for POPG is highest of all. DOPM has a smaller head group than DOPG (methanol compared with glycerol), which will give this phospholipid a more triangular shape than the DOPG (i.e. the head group is smaller than the fatty acyl chains), which would result in a less tightly packed surface on SUVs of this phospholipid. It is possible that this would result in high affinity binding to the vesicles, thus maximising scooting kinetics and further reducing hopping between vesicles as previously discussed (see section 3.3.10).

In contrast, SUVs of POPG will have the most tightly packed surface of the three, due to the presence of only one unsaturated fatty acid in this phospholipid (compared with DOPG and DOPM which have two), which will result in the phospholipid molecules packing more tightly together. Therefore, the activity of N1A on SUVs of POPG compared with DOPM and DOPG would be expected to be higher as the enzyme will be able to bind less efficiently to the surface and hopping kinetics will be enhanced.

The results for H48Q show that this mutant has a higher activity on POPG than DOPG, presumably for reasons similar to the N1A, but fails to show such a decrease in activity on DOPM. This could be a problem of trying to accurately measure a significant reduction in activity from the already low level observed with DOPG as substrate.

3.3.12 Hydrolysis of *Micrococcus luteus* by N1A and H48Q HnpsPLA$_2$.

Gram positive (Gram-+ve) bacteria such as *Micrococcus luteus* and *Staphylococcus aureus* are known to be hydrolysed by human group IIA sPLA$_2$ [8,60,61,104,105]. Such bacteria have a PG-rich anionic cell membrane contained beneath a peptidoglycan cell wall. In the case of *M luteus*, more than 70 % of the total phospholipid content is accounted for by PG and cardiolipin (diphosphatidylglycerol), with virtually all of the phospholipids being contained in the cell membrane [104]. HnpsPLA$_2$ is able

to access this cell membrane and hydrolyse the phospholipids contained within it, but other sPLA$_2$s such as nn- and pp-sPLA$_2$ are unable to catalyse phospholipid hydrolysis unless the cells are first treated with lysozyme, which will disrupt the outer wall. This is thought to be due to the relative pI of these enzymes; human sPLA$_2$ has a isoelectric point in excess of 10.5, but nn- and pp-sPLA$_2$s have more neutral pIs (5 and 6.5 respectively) [12,60,63]. The high global cationic charge of the human sPLA$_2$ allows it to penetrate the anionic cell wall effectively, but lysozyme is required to permeabilize the peptidoglycan layer before e.g. nn/pp-sPLA$_2$ can catalyse the hydrolysis of cell membrane phospholipids [63].

M. luteus provide a physiological substrate on which to test the activity of the H48Q mutant of hnpsPLA$_2$ in comparison with the N1A. The fluorescence displacement assay system is used to measure the activity of N1A and H48Q on *M. luteus*. The assay consists of a stock cocktail containing ~ 2×10^7 cells/ml in HBSS as substrate in place of the phospholipid normally used (see section 2.6.3 for bacterial preparation). The results of the hydrolysis of *M. luteus* phospholipids by the two forms of hnpsPLA$_2$ are shown in figure 3.35. The specific activities of the N1A and H48Q are 1.94 ± 0.34 and 0.06 ± 0.003 respectively, which gives the rate of activity of the H48Q as 3.1 % with respect to the N1A.

This assay not only confirms that when using a physiological substrate the H48Q mutant has a significant catalytic rate, which is comparable to that seen on alternative substrate presentations, but also that it is as capable as the N1A of penetrating the bacterial cell wall in order to access the phospholipid-containing cell membrane. This again confirms the similarity of the overall structure of the mutant to the N1A.
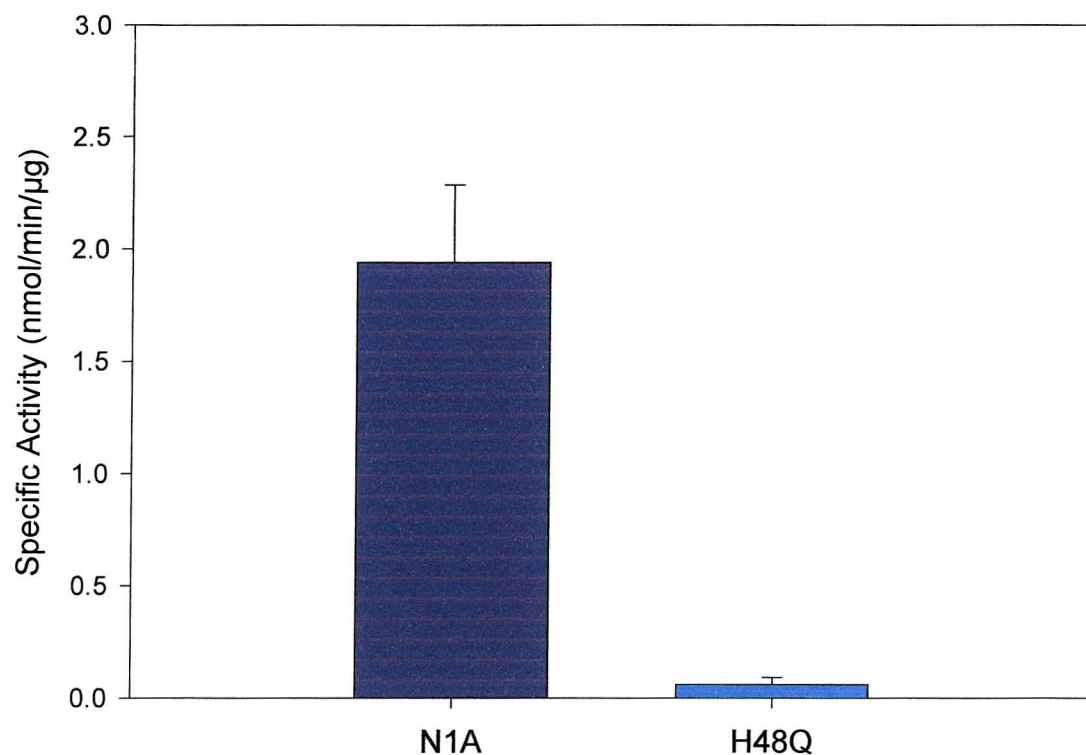
Figure 3.35 Specific Activity of N1A and H48Q HnpsPLA$_2$ when Assayed on *Micrococcus luteus*.

Enzyme activity was measured using the fluorescent displacement assay (section 2.5.1) with *Micrococcus luteus* as substrate (see section 2.6.3).

Each data set is the mean of three separate measurements ± s.d.

3.3.13 The Use of Lipid Extraction and Mass Spectrometry to Directly Measure Enzyme Activity.

All of the methods reported so far to measure the activity of the N1A and H48Q have been indirect, in so much that they provide a means of calculating the amount of product produced rather than directly measuring the loss of phospholipid substrate due to hydrolysis. One method that can be used to directly measure the amount of substrate hydrolysed involves phospholipid extraction, and quantification using mass spectrometry.

The extraction method is based on the fact that a mixture of chloroform and methanol, when added to the phospholipid-containing reaction medium will form a monophasic solution. Dilution of this with chloroform and water yields a biphasic solution, where the lower chloroform layer can be isolated and dried down under a stream of nitrogen. The lipid species will be contained here, and can be quantified by mass spectrometry analysis [87].

For this assay, DOPG SUVs were incubated with either N1A, H48Q or no enzyme (control sample) for between 0.5 – 60 minutes. The hydrolysis of phospholipids by enzyme was halted at each time point by the addition of 5 mM EGTA to chelate the calcium required for catalysis, and the entire reaction mixture was then dropped into ice-cold methanol. The phospholipids were extracted as detailed in section 2. 6.4. 20 nmoles of DMPG was added to the reaction mixture once it had been mixed with methanol, to act as an internal standard with which to calculate the amount of DOPG hydrolysed by each form of the enzyme.

Figure 3.36 shows that after only five minutes, the maximum hydrolysis has been achieved by the N1A, whereas the H48Q has not achieved this level of hydrolysis even after sixty minutes has passed. This result is in good agreement with the previous results in terms of the overall rate of catalysis by the H48Q, and it confirms that the rate seen with this mutant is due to its ability to catalyse the hydrolysis of phospholipids.
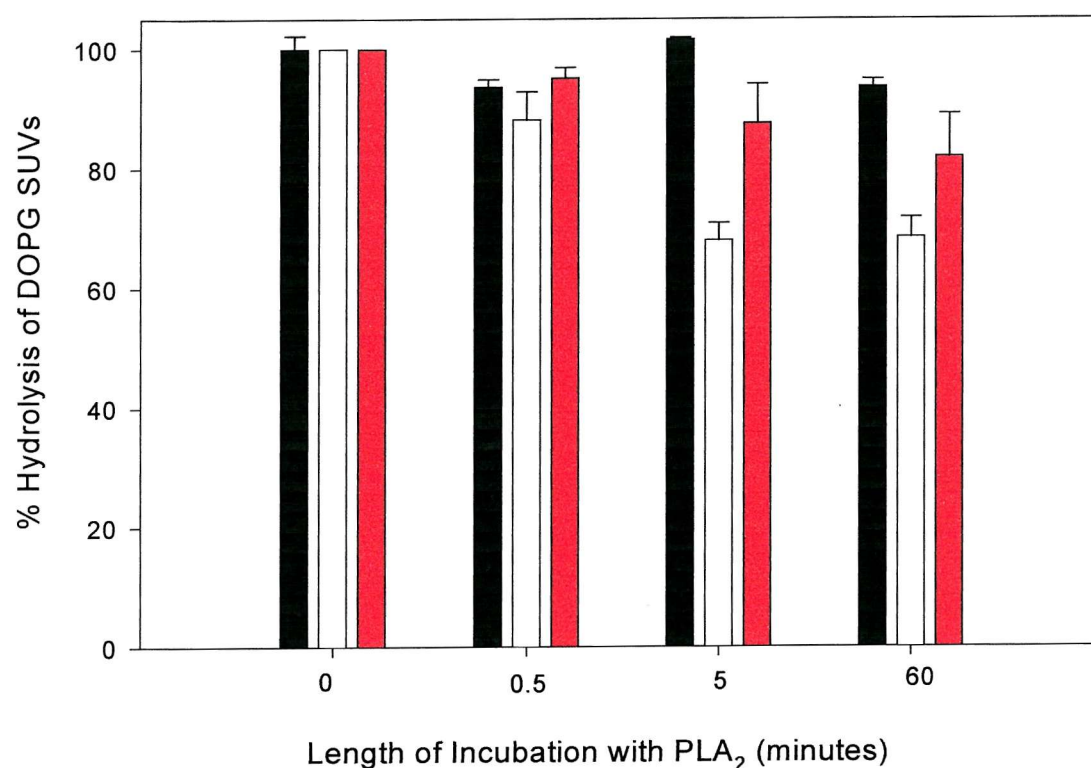
Figure 3.36 Hydrolysis of DOPG by N1A and H48Q HnpsPLA₂ as determined by ESI-MS.

SUVs of DOPG were incubated with either no enzyme (control), N1A or H48Q hnpsPLA₂ for the length of time stated. The reaction was stopped by the addition of 5 mM EGTA and lipid extractions carried out as stated in section 2.6.4. Mass spectrometry was performed using a mass spectrometer under the conditions described in section 2.5.14.

The control in each case consists of all reagents except enzyme.

■ - Control

☐ - N1A HnpsPLA₂ (0.45 µg)

■ - H48Q HnpsPLA₂ (3.5 µg)

Each data set is the mean of three separate measurements ± s.d.

3.4 Effect of the Alkylating Agent *para*-Bromophenacyl Bromide on N1A and H48Q HnpsPLA$_2$.

The experiment, which involved assaying the N1A and H48Q at decreasing pH, demonstrated the relative insensitivity to low pH shown by the H48Q as compared to the N1A. This presumably is due to the effect of pH on the His-48 residue, which is not present in the H48Q mutant. This confirms that the catalytic activity seen with the H48Q must depend on residues other than His-48. To further this theory, the alkylating agent *para*-bromophenacyl bromide (*p*BPB) was employed. *p*BPB has been widely used to inhibit the catalytic activity of sPLA$_2$s and assess the role of sPLA$_2$ activity in snake venoms etc [40,106]. It was deduced by amino acid analyses that the *p*BPB selectively alkylates histidine residues, and the inhibitory effect of *p*BPB on sPLA$_2$ is due to the alkylation of the His-48 residue in the active site [39].

In a study concerning the effect of *p*BPB on both the N1A and H48Q hnpsPLA$_2$s, the N1A would be expected to show sensitivity to this reagent, and lose catalytic activity commensurate with the alkylation of the His-48 residue. Conversely, the H48Q mutant would not be expected to show sensitivity to *p*BPB, as the His-48 residue has been substituted with a glutamine residue. The results in figure 3.37 however, show unexpectedly that after incubation of both N1A and H48Q hnpsPLA$_2$ with a 50-fold molar excess of *p*BPB at pH 8.0/37 $^{\circ}$C both enzymes displayed a similar loss of catalytic activity ($t^{\frac{1}{2}}$ N1A ~ 9 min, H48Q ~ 8 min). The control experiments consisting of N1A and H48Q incubated in the presence of acetone (solvent used to dissolve *p*BPB) and alone, at 37 $^{\circ}$C clearly indicate that it is the *p*BPB causing the loss of activity.

One aspect of the experiment that may have masked any clear differences between the loss of activity of the N1A and the H48Q was the speed of inhibition. To eliminate this problem, the experiments were repeated at pH 6.0 and 25 $^{\circ}$C as opposed to pH 8.0 and 37 $^{\circ}$C, and this gave the desired result of considerably slowing the reaction down (figure 3.38).
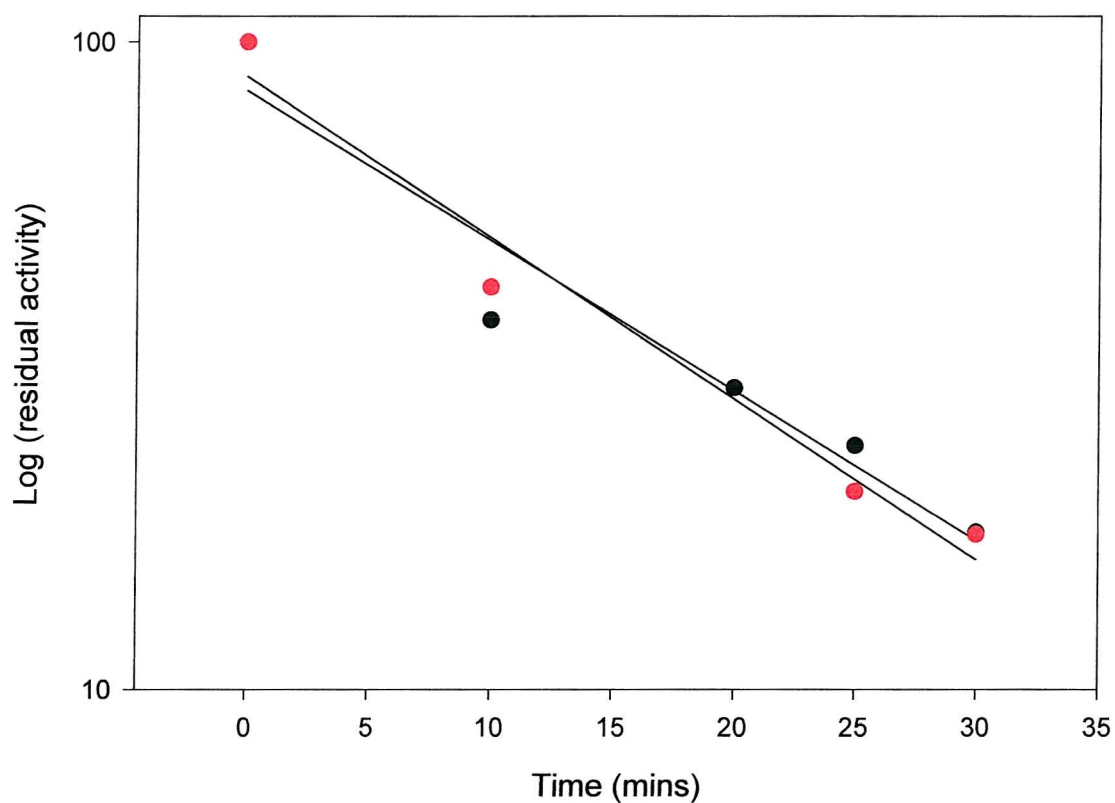
Figure 3.37 Inactivation of N1A and H48Q HnpsPLA$_2$ with a 50:1 Molar Excess of _p_BPB (pH 8.0, 37 °C).

Inactivation of enzyme by _p_BPB was carried out as described in section 2.6.13. Residual activity of enzyme was measured using the fluorescence displacement assay (section 2.6.1).

Control consisted of enzyme incubated alone or with the appropriate amount of acetone.

● - N1A HnpsPLA$_2$

● - H48Q HnpsPLA$_2$

Data represents the typical inactivation seen under these conditions as judged by at least three separate experiments.
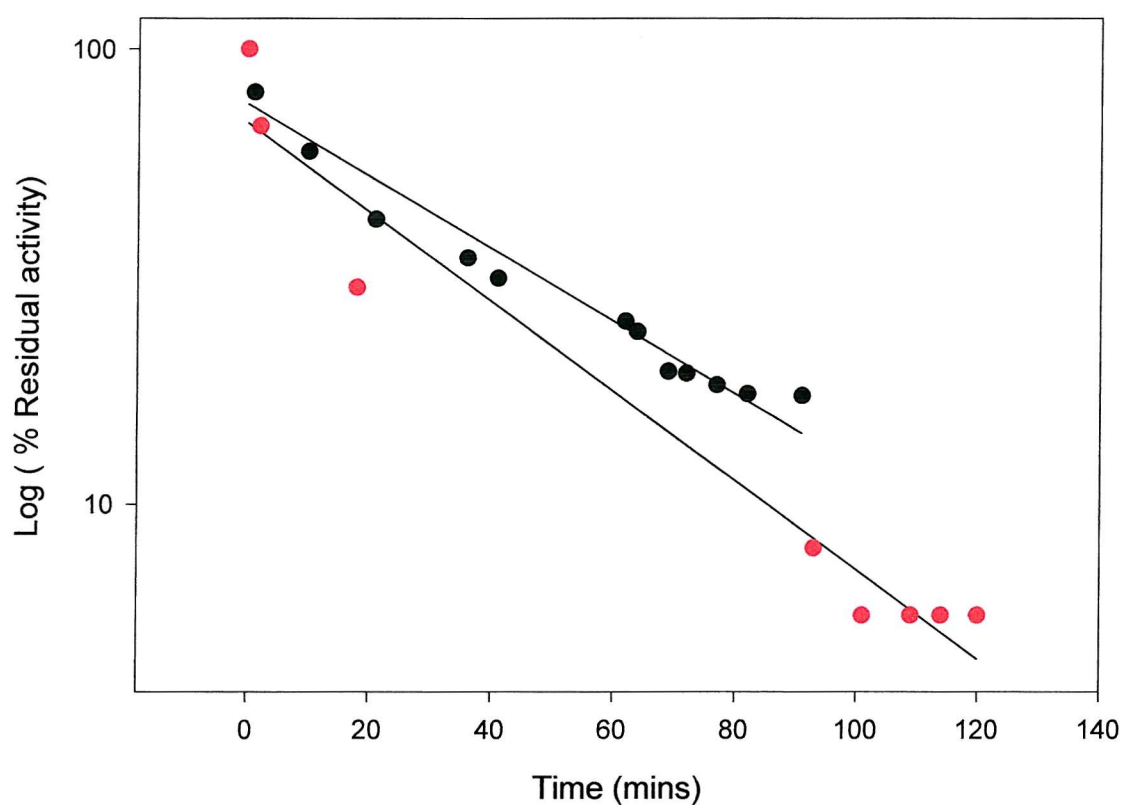
Figure 3.38 Inactivation of N1A and H48Q HnsPLA$_2$ with a 10:1 Molar Excess of pBPB (pH 6.0, 25 °C).

Inactivation of enzyme by pBPB was carried out as described in section 2.6.13. Residual activity of enzyme was measured using the fluorescence displacement assay (section 2.6.1).

Control consisted of enzyme incubated alone or with the appropriate amount of acetone.

● - N1A HnpsPLA$_2$

● - H48Q HnpsPLA$_2$

Data represents the typical inactivation as judged by three separate experiments.

However, even at such a reduced rate of inhibition, it was not possible to ascertain a significant difference in the rate of inactivation of N1A and H48Q hnpsPLA$_2$ ($t^{\frac{1}{2}}$ N1A ~ 19 min, H48Q ~ 16 min). (All future experiments were carried out at pH 6.0, 25 °C).

3.4.1 Inactivation of N1A and H48Q hnpsPLA$_2$ by pBPB at Molar Ratios of 2:1 and 1:1.

One of the unique features of the human non-pancreatic form of sPLA$_2$ is the presence of a histidine residue at position 6, which is peculiar to this group of the enzyme, as a leucine is conserved here in other varieties of the enzyme [12]. The side chain of this His-6 residue lies at the opening to the hydrophobic channel, and it was postulated that pBPB could perhaps alkylate this residue, thereby effectively blocking the access of the substrate to the active site proper. If this were the case, and if this effect was secondary to the alkylation of His-48 (in the case of the N1A), then by performing the reaction under the relatively slower conditions detailed above, and comparing the inhibition profiles of N1A and H48Q with 2:1 and 1:1 molar ratios of pBPB, any difference in the inactivation of the two enzymes attributable to the alkylation of His-6 should become apparent.

In fact it was not possible to ascertain any significant difference between the loss of catalytic activity of the N1A and H48Q when assayed after incubation with a 2:1 molar excess of pBPB (figure 3.39) ($t^{\frac{1}{2}}$ N1A ~ 90 min, H48Q ~ 100 min). No significant difference between the inactivation of N1A and H48Q with a 1:1 molar excess of pBPB was seen either.
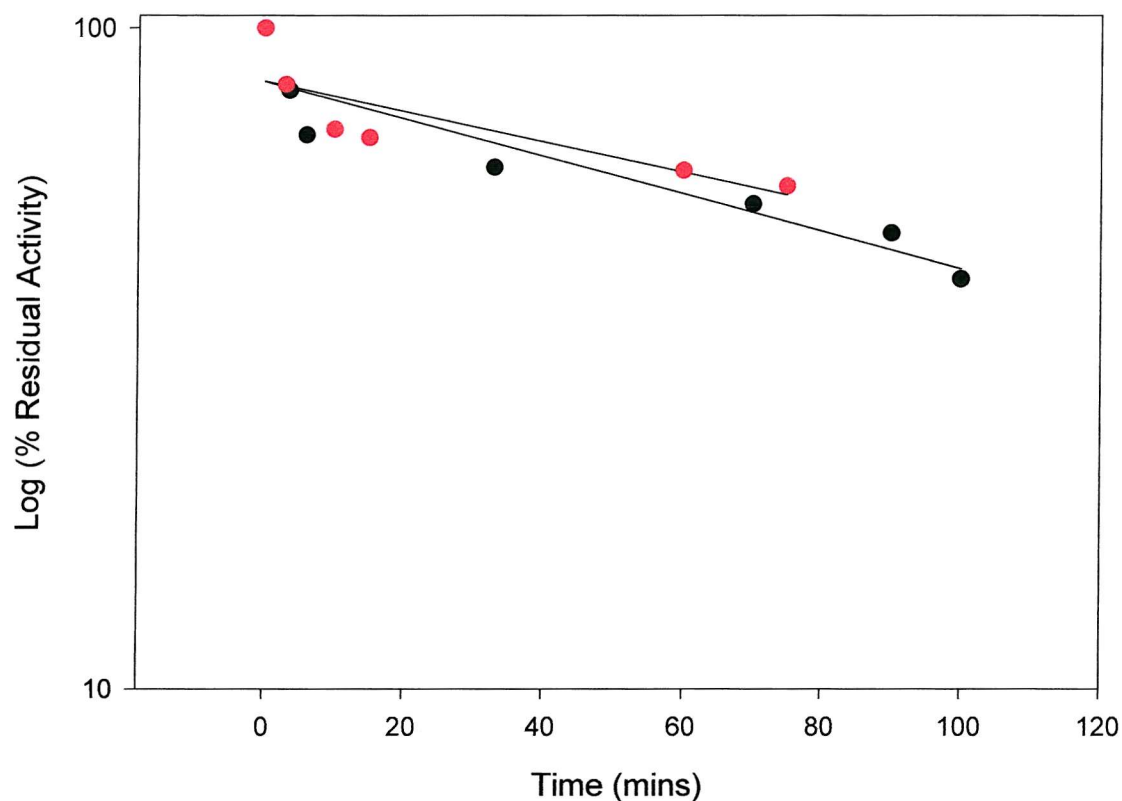
Figure 3.39 Inactivation of N1A and H48Q HnpsPLA$_2$ with a 2:1 Molar Excess of pBPB (pH 6.0, 25 $^{\circ}$C).

Inactivation of enzyme by pBPB was carried out as described in section 2.6.13. Residual activity of enzyme was measured using the fluorescence displacement assay (section 2.6.1).

Control consisted of enzyme incubated alone or with the appropriate amount of acetone.

● - N1A HnpsPLA$_2$

● - H48Q HnpsPLA$_2$

Data represents the typical inactivation as judged by three separate experiments.

3.4.2 Effect of Calcium on Inactivation of N1A and H48Q HnpsPLA$_2$.

In a further attempt to determine whether or not the pBPB was eliciting its effect within the active site, calcium was added to the reaction. It has been shown previously that the presence of calcium in the active site of sPLA$_2$s reduces the rate of inactivation by pBPB considerably by virtue of the protective effect that calcium exerts when bound [39]. Theoretically, if the pBPB were alkylating the active site residue, then the presence of calcium would noticeably reduce the alkylation. However, if His-6 were targeted by pBPB, then the presence of calcium in the active site would not have any effect on the inactivation by pBPB.

The results in figures 3.40 and 3.41 show that both proteins are protected from inactivation by pBPB when calcium is present to a similar extent, which indicates that the pBPB is in fact exerting its effect from within the active site. The porcine pancreatic sPLA$_2$, also known to be sensitive to alkylation by pBPB was treated in the same way for comparison and the results of incubating pp-sPLA$_2$ in the presence and absence of calcium are shown in figures 3.42. It can be seen from these results that this sPLA$_2$ also behaves in an analogous manner to the hnps forms of PLA$_2$.

3.4.3 Analysis of pBPB Effect using Mass Spectrometry.

In order to try and establish how many histidine residues in the N1A and H48Q were being affected by pBPB, both proteins were incubated with a 10:1 molar excess of pBPB until a maximal loss (> 75 %) of activity was seen. The protein samples were then analysed by mass spectrometry. The molecular weight of pBPB is 277.9, and as the alkylation of histidine residues results in the loss of a bromine molecule from the reagent an increase in mass of 197 would indicate that one molecule of pBPB had been incorporated into the sPLA$_2$ enzyme.
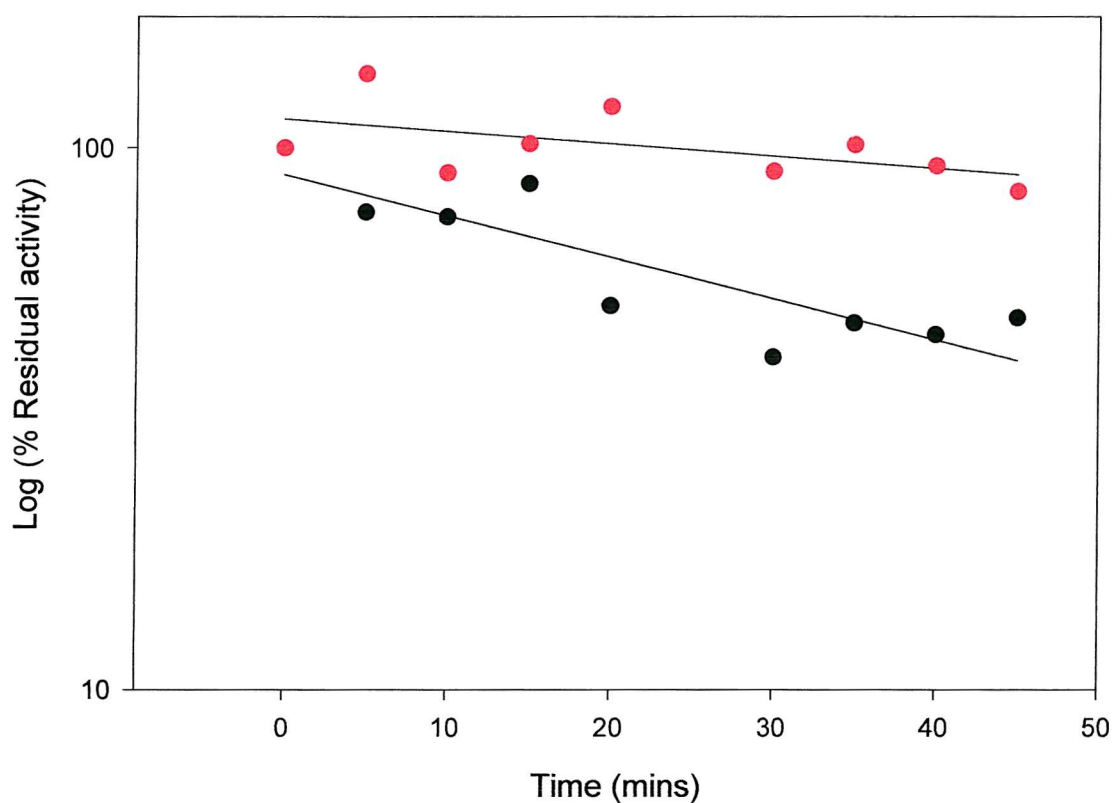
Figure 3.40 Inactivation of N1A HnpsPLA$_2$ by 10:1 Molar Excess of *p*BPB in the Presence and Absence of 10 mM Calcium.

Inactivation of enzyme by *p*BPB was carried out as described in section 2.6.13 in the presence or absence of 10 mM CaCl$_2$. Residual activity of enzyme was measured using the fluorescence displacement assay (section 2.6.1).

Control consisted of enzyme incubated alone or with the appropriate amount of acetone.

● - N1A HnpsPLA$_2$ (t$^{\frac{1}{2}}$ ~20 min)

● - N1A HnpsPLA$_2$ + 10 mM CaCl$_2$ (t$^{\frac{1}{2}}$ ~ 55)

Data represents the typical inactivation as judged by three separate experiments.
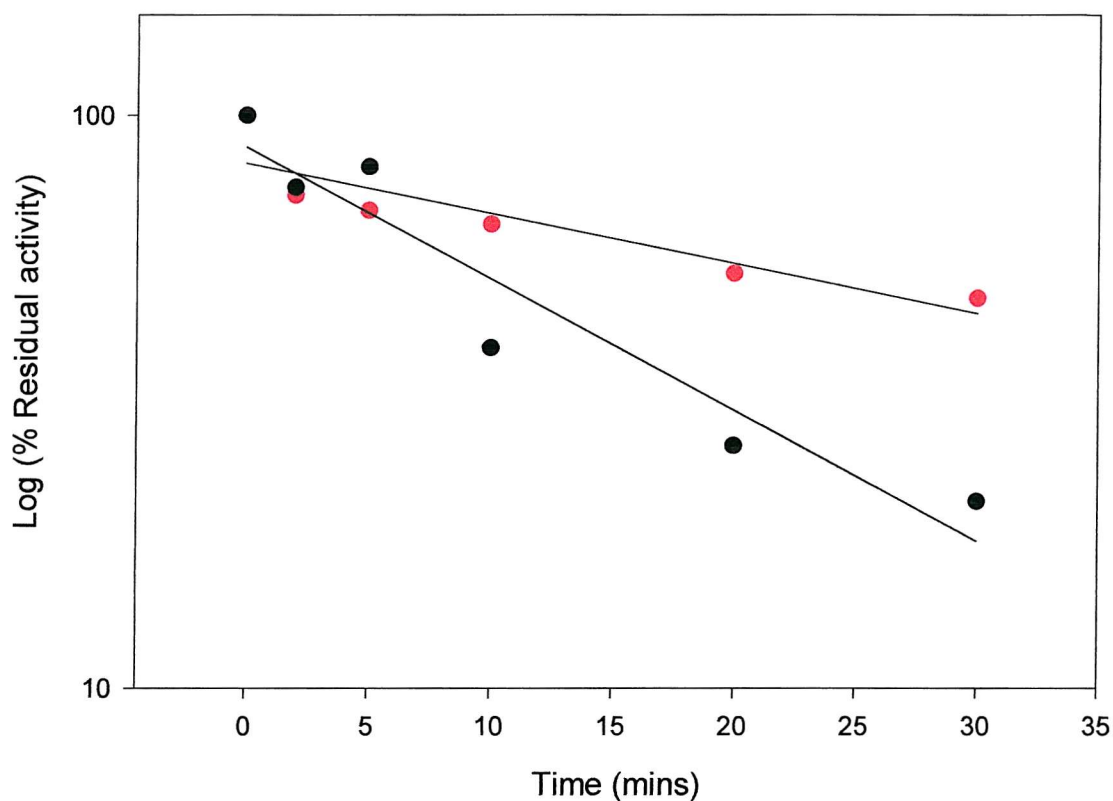
Figure 3.41 Inactivation of H48Q HnpsPLA$_2$ by 10:1 Molar Excess of pBPB in the Presence and Absence of 10 mM Calcium.

Inactivation of enzyme by pBPB was carried out as described in section 2.6.13 in the presence or absence of 10 mM CaCl$_2$. Residual activity of enzyme was measured using the fluorescence displacement assay (section 2.6.1).

Control consisted of enzyme incubated alone or with the appropriate amount of acetone.

● - H48Q HnpsPLA$_2$ (t$^{\frac{1}{2}}$ ~ 9 min)

● - H48Q HnpsPLA$_2$ + 10 mM CaCl$_2$ (t$^{\frac{1}{2}}$ ~ 24 min)

Data represents the typical inactivation as judged by three separate experiments.
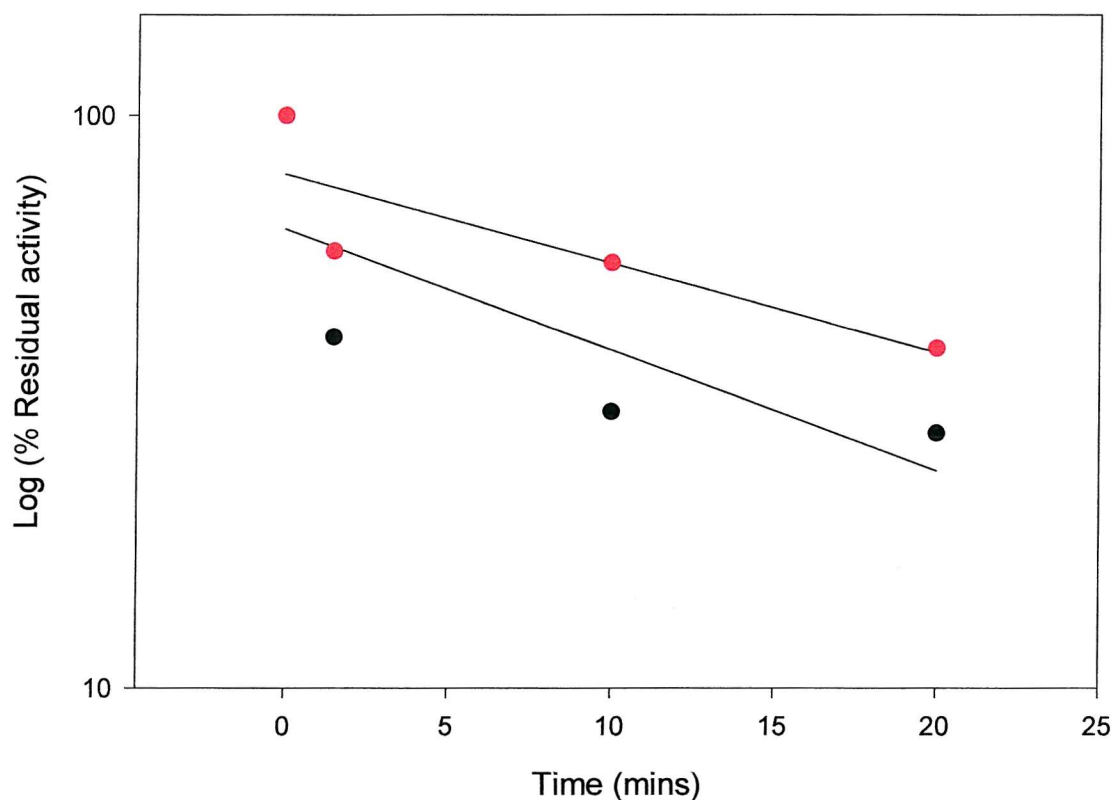
Figure 3.42 Inactivation of pp-sPLA$_2$ by 10:1 Molar Excess of pBPB in the Presence and Absence of 10 mM Calcium.

Inactivation of enzyme by pBPB was carried out as described in section 2.6.13 in the presence or absence of 10 mM CaCl$_2$. Residual activity of enzyme was measured using the fluorescence displacement assay (section 2.6.1).

Control consisted of enzyme incubated alone or with the appropriate amount of acetone.

● - pp-sPLA$_2$ (t$^{1/2}$ ~ 4 min)
● - pp-sPLA$_2$ + 10 mM CaCl$_2$ (t$^{1/2}$ ~ 14 min)

Data represents the typical inactivation as judged by three separate experiments.

The results of the mass spectrometry of pBPB-modified N1A and H48Q are shown in figures 3.43 and 3.44 respectively. The results reveal that only the N1A has a pBPB molecule incorporated, as demonstrated by the increase in molecular weight from 13861 to 14058. This is contrary to the almost identical inhibition patterns seen with the N1A and H48Q.

One possible explanation for the similar inactivation profiles seen with the N1A and H48Q which may explain the lack of incorporation of pBPB into H48Q is that the pBPB reversibly ester bonds to the invariant Asp-99 residue also found in the active site of hnpsPLA$_2$. This would be disrupted by the presence of formic acid that is used in the mass spectrometry. In order to test this theory, the alkylation was repeated, and after ~ 50 % loss of activity TFA was added to the reaction to disrupt the putative ester bond between the pBPB and the Asp-99. This should result in the recovery of activity by the H48Q mutant. However, any attempts at recovery of enzyme activity by treatment at low pH followed by assay at normal pH were unsuccessful (data not shown).

3.5 Discussion

The H48Q mutant of hnpsPLA$_2$ was prepared in order to provide an inactive active site mutant, which was structurally intact and could be used to probe the interfacial binding properties of sPLA$_2$s. When this mutant was found to possess catalytic activity, even only at a much-reduced rate as compared to the N1A, it became clear that the H48Q could not be used in this capacity.

It was also very significant that this mutant was still capable of catalytic activity without possessing the histidine at its active site, as His-48 has long been known to be the residue that is crucial for catalysis. Therefore, it was important to confirm that the considerable residual activity of the H48Q mutant was genuine and could be demonstrated under a variety of assay conditions.
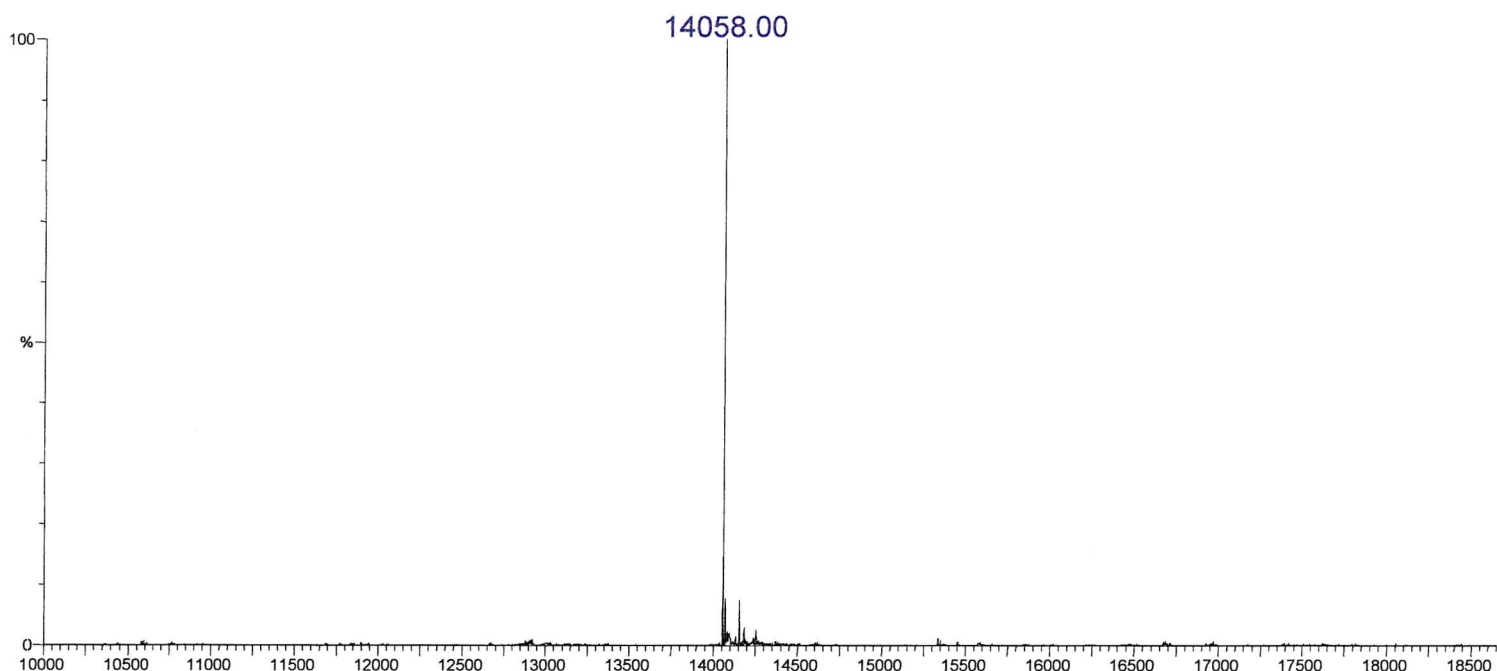
Figure 3.43 Analysis of N1A HnpsPLA$_2$ Incubated with 10:1 Molar Excess of _p_BPB by Mass Spectrometry.

Inactivation of enzyme was carried out as described in section 2.6.13. Electrospray ionisation mass spectrometry was carried out as described in section 2.6.14

The molecular mass of N1A hnpsPLA$_2$ after incubation with 10:1 molar ratio of _p_BPB is 14058 ± 1.0.

The mass spectrometry was performed three times on three separate experiments to ensure the result was correct.
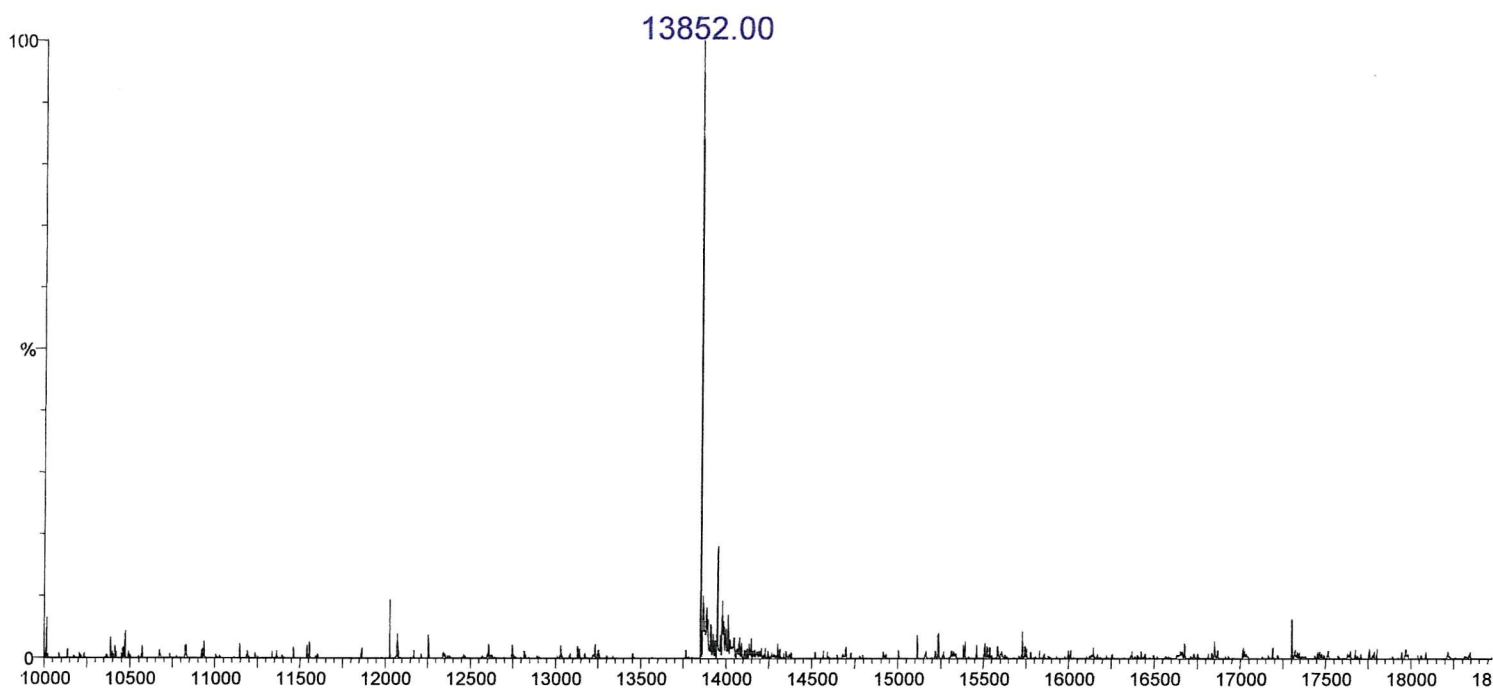
Figure 3.44 Analysis of H48Q HnpsPLA$_2$ Incubated with 10:1 Molar Excess of *p*BPB by Mass Spectrometry.

Inactivation of enzyme was carried out as described in section 2.6.13. Electrospray ionisation mass spectrometry was carried out as described in section 2.6.14.

The molecular mass of H48Q hnpsPLA$_2$ after incubation with 10:1 molar ratio of *p*BPB is 13852 $\pm$ 1.0.

The mass spectrometry was performed three times on three separate experiments to ensure the result was correct.

The results shown thus far have confirmed that the H48Q has a stable structure, which is correctly folded and very similar, if not identical to the N1A. The H48Q has shown catalytic activity when presented with a number of different substrates in various forms, and has exhibited a comparable ability to bind calcium and other cations as the N1A. The interfacial binding of H48Q has been studied using the fluorescent phospholipid probe dansyl-PE, where it demonstrated an identical binding profile to the parent enzyme, and the lipid extraction/mass spectrometry experiment confirmed the actual hydrolysis of phospholipid by this mutant. These results taken together suggest that the activity shown by the H48Q is significant and is not the result of an inferior ability to bind productively to the substrate interface, or a lack of structural integrity. The implications of this considerable residual activity in the absence of a functional active site residue are discussed in chapter five.

The effect of the alkylating agent pBPB has been reported, and presents a further intriguing property of this mutant. Not only does the H48Q lose activity in a similar manner to the N1A, but also when incubated with pBPB in the presence of calcium, it appears to be protected to a similar extent as the N1A. This would suggest that in the H48Q as in the N1A, the pBPB is exerting its effect at the active site. It was surprising then to find that no pBPB was incorporated into the mutant as judged by MS, whereas one molecule of the pBPB derivative is incorporated into the N1A. This is an important result, as it establishes that His-6, which is unique to the human IIA enzyme, and forms part of the active site channel, is not alkylated under the assay conditions used. Moreover, the failure to demonstrate any incorporation of the pBPB derivative into the H48Q mutant confirms that such alkylation of His-6 cannot be the cause of the inactivation of the H48Q.

The observation that the rate of inactivation of the H48Q closely parallels that N1A suggests that a similar mechanism is operating at the active site, although no incorporation can be seen by MS analysis of the inactivated H48Q. One possibility is that the pBPB is able to inactivate the catalytic aspartate residue (Asp-99), which can ester bond to the alkylating agent according to the scheme shown below (figure 3.45).

134
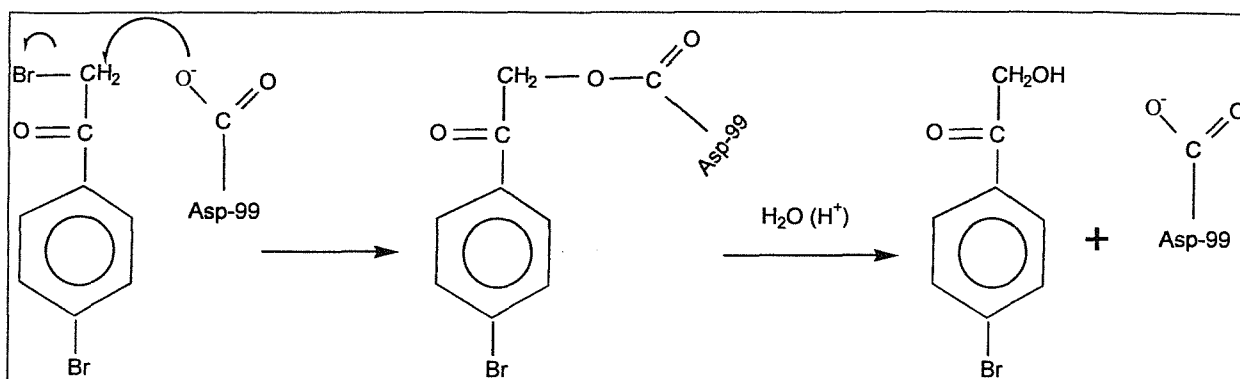
Figure 3.44 Schematic Representation of the Incorporation of pBPB into the Asp-99 residue in the Active Site of H48Q HnpsPLA$_2$.

Although the lack of incorporation of pBPB into the H48Q could be due to the acid lability of the ester, which would be lost during the processing prior to MS, attempts to recover such activity by using acid conditions *in vitro* were not successful.

The activity shown by the H48Q is of considerable importance, and further analysis is required in order to elucidate a method by which this mutant can retain significant catalytic activity. To this end, the H48Q has been subject to crystallographic analysis, the results of which are reported in chapter five.

Chapter Four - The H48A and H48N Mutants of HnpsPLA$_2$

4.1 The H48A and H48N Mutants of HnpsPLA$_2$.

The primary aim of this thesis was to study the interfacial binding phenomenon of hnpsPLA$_2$. As previously discussed (section 3.1.2), an ideal tool with which to probe interfacial binding is an inactive mutant of the enzyme that could be employed to compete with active forms of the enzyme for the interface. A competition assay utilising such an inactive mutant could be used to gauge the relative affinities of different types of PLA$_2$s for different substrate interfaces, as interfacial competition would be reflected in the catalytic rate of the sPLA$_2$s measured in the presence of the competing, inactive mutant. Interfacial competition, unlike active site competition requires that enough of the inactive competitor is available to deplete the binding surface sufficiently to restrict availability of this surface to the active enzymes being studied. Therefore, a high molar ratio of inhibitor to substrate is required before significant inhibition is observed. This requirement for large amounts of inhibitor protein could be overcome by using very low substrate concentrations, but this is undesirable as the sensitivity of the assay system used to measure catalytic activity would prevent accurate rate measurements from being taken.

The published work of Gelb and co-workers using the bee venom enzyme [97] and Tsai and co-workers using the bovine pancreatic sPLA$_2$ [96] described how the mutation of the catalytic histidine to a glutamine gave rise to an inactive, intact mutant (see section 3.1.3). However, as shown in the preceding chapter, the equivalent mutant of hnpsPLA$_2$ showed activity at a rate of 3-4 %. Although small, this rate is significant enough to prevent the H48Q mutant of hnpsPLA$_2$ from being used as a competitive binding agent, especially since the competitive protein is used in excess of the normal enzyme. In addition to producing the inactive glutamine mutants, the Gelb and Tsai laboratories also mutated the catalytic histidine of the bee and bovine pancreatic enzymes to both alanine and asparagine. These mutants were also found to be inactive, and in both cases the alanine mutant was deemed not to be structurally intact. In the bovine pancreatic study, the asparagine

mutant showed slight activity, but this was five orders of magnitude lower than the wild type. Though this mutant appeared to be slightly less stable than the wild type enzyme, it seemed that substitution of the active site histidine with an asparagine rather than an alanine produced a more viable mutant, in terms of structure and activity [96]. In this chapter, the production and characterisation of the H48A and H48N mutants of hnpsPLA$_2$ are described. These mutants were produced with the aim of obtaining a mutant with which to fulfil the primary aims of this thesis, namely a structurally intact but inactive form of hnpsPLA$_2$ that could be used to probe interfacial binding.

4.2 Preparation and Characterisation of the H48A Mutant of HnpsPLA$_2$.

The H48A mutant of hnpsPLA$_2$ was produced in order to ascertain whether it would provide an inactive, active site mutant of hnpsPLA$_2$, which could be used to probe interfacial binding. The mutation was introduced into the hnpsPLA$_2$ gene using a 2-stage PCR method of mutagenesis. The protocol for this method is detailed in chapter 2, section 2.3.6. The gene sequence coding for the mutant H48A is shown in figure 4.1. The sequence contains the codon GCT (Ala) in place of CAC (His) at sequence position 207-209, which corresponds to residue 48, and confirms the mutation is present. The gene was cloned into the pET11a expression plasmid, and *E. coli* BL21 DE3 cells were transformed with this vector for overexpression of the H48A mutant.

Repeated attempts were made to produce mutant H48A hnpsPLA$_2$ protein, but in each case they were unsuccessful. SDS-PAGE analysis showed that there was some hnpsPLA$_2$ present after solubilising the inclusion bodies containing the unfolded enzyme (figure 4.2), but no protein was collected from the SP-Sepharose column used as the first stage of chromatography purification. It was presumed from this that although some H48A mutant protein was expressed, it was unable to fold correctly due to the mutation, with the result that no pure protein could be obtained.
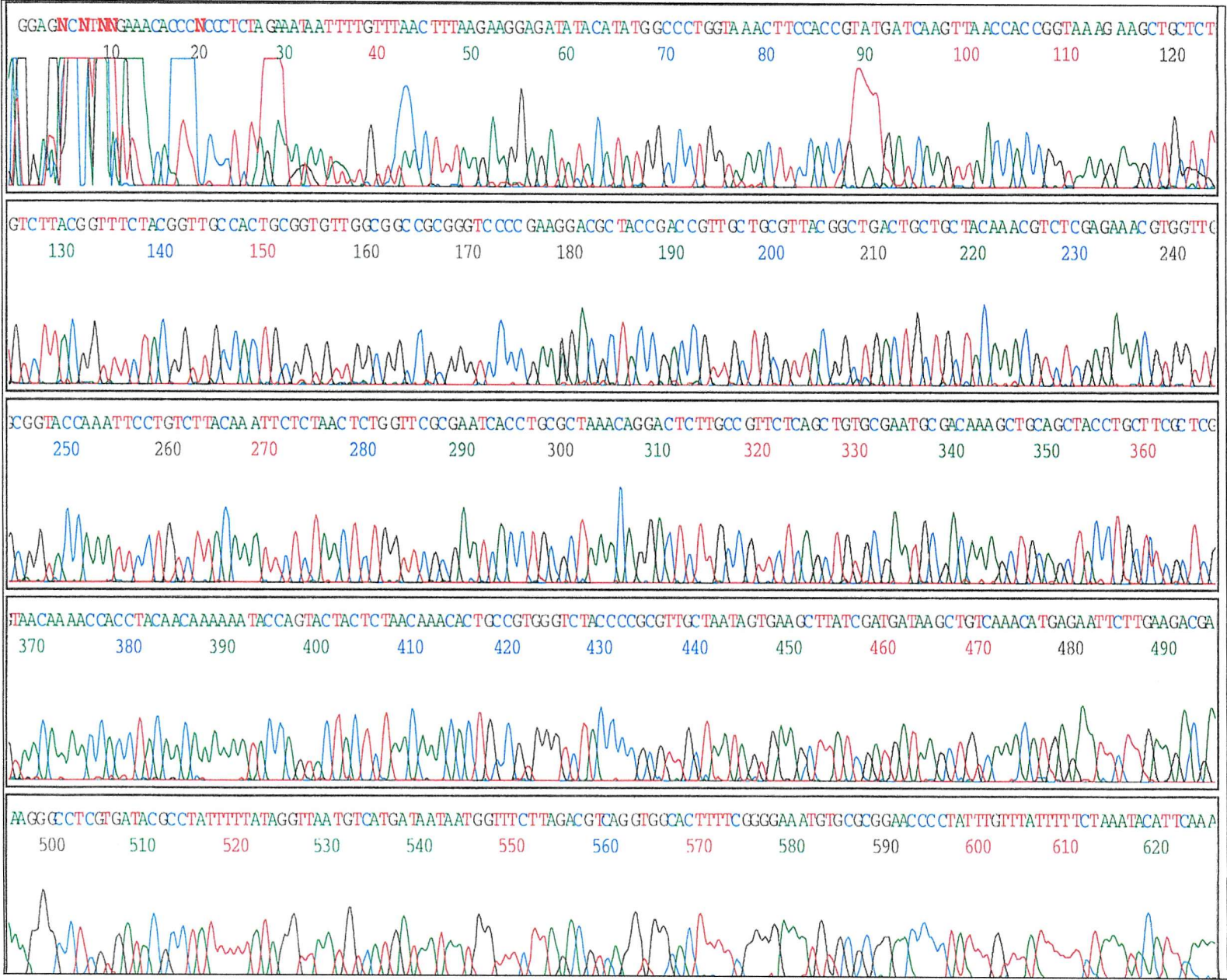
Figure 4.1 Gene Sequence Coding for the H48A Mutant of HnpsPLA₂.

139
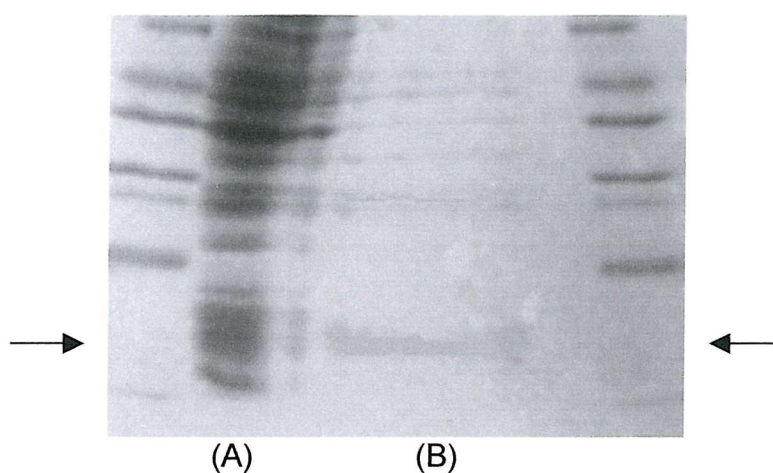
Figure 4.2 SDS-PAGE Showing the Purification of H48A HnpsPLA$_2$.

SDS-PAGE was carried out as described in section 2.6.10.

Lanes A and B show H48A hnpsPLA$_2$ released from BL21 DE3 *E. coli* cells by sonication, and purified inclusion bodies containing H48A hnpsPLA$_2$ respectively.

The arrows indicate the expected position of the H48A hnpsPLA$_2$ band. A characteristic of this protein is that it runs at approximately 17 kDa on SDS-PAGE.

Molecular weight markers shown in the far left and right lanes are (from top), 66, 45, 36, 29, 24, 20 and 14.5 kDa.

This result is consistent with the results from the bovine pancreatic and bee venom H48A sPLA$_2$s, which also found that substituting the catalytic His-48 residue with a small, uncharged amino acid severely compromised the structural integrity of the enzyme [96,97]. As it was not possible to obtain a reasonable amount of H48A with which to characterise this mutant, no further experimentation was carried out on this modified form of the enzyme, as clearly it would not be possible to use this mutant in the desired capacity.

4.3 Preparation and Characterisation of the H48N Mutant of HnpsPLA$_2$.

The final member of the trio of active site mutants to be constructed was the H48N. This mutation was introduced into the gene coding for hnpsPLA$_2$ using the Kunkel method of mutagenesis, which is described in detail in section 2.3.3. The gene sequence for the H48N mutant of hnpsPLA$_2$ is shown in figure 4.3, and the codon CAC (His) is replaced by AAC (Asn) at sequence position 209-211, which corresponds to residue 48 and confirms the presence of the mutation. The H48N was expressed and purified in the same way as the N1A (section 2.4), and a similar yield of protein was achieved. Protein purity was confirmed using SDS-PAGE (shown in figure 4.4).

Elution of H48N from the chromatography columns used to purify hnpsPLA$_2$ occurred at the same salt concentration as the N1A, and analysis of the mutant by RP-HPLC (figure 4.5) showed that this enzyme elutes as a single peak at the same acetonitrile concentration as the N1A. To confirm the mass of the H48N was that expected due to the substitution of a His residue with an Asn, the peak eluted from the HPLC was subject to ESI-MS analysis, and this confirmed the mass of the mutant as 13838 ± 1.0 (figure 4.6), consistent with the predicted mass of 13837.

Figure 4.3 Gene Sequence Coding for the H48N Mutant of HnpsPLA$_2$.

142
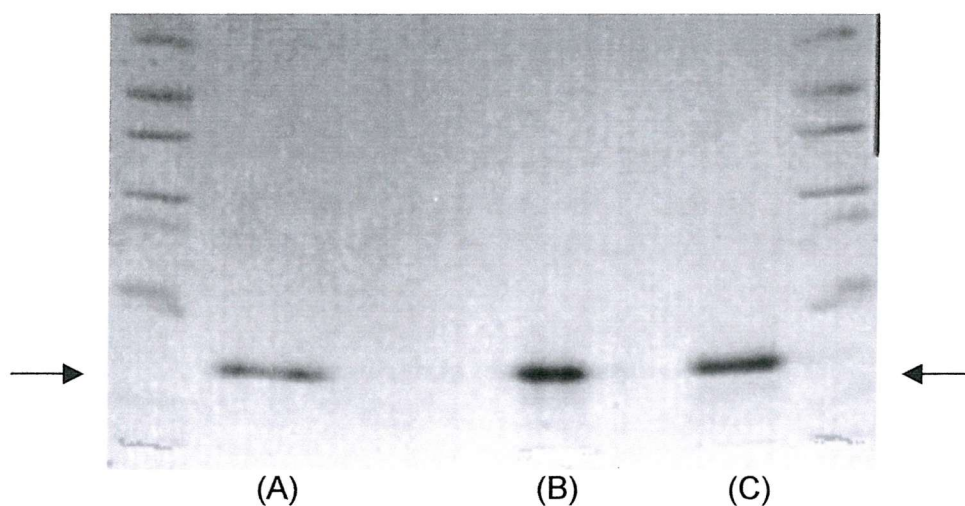
Figure 4.4 SDS-PAGE Analysis of Purified H48N HnpsPLA$_2$.

SDS-PAGE was carried out as described in section 2.6.10.

The purity of the H48N mutant (lane A) is compared with that of the N1A (lane B) and H48Q (lane C) mutants. All mutants shown represent the active fractions obtained from the Heparin-Sepharose chromatography column.

Arrows indicate the expected position of the hnpsPLA$_2$ mutants at 17 kDa (see figure 4.2)

Molecular weight markers shown in the far left and right lanes are (from top), 66, 45, 36, 29, 24, 20 and 14.5 kDa.
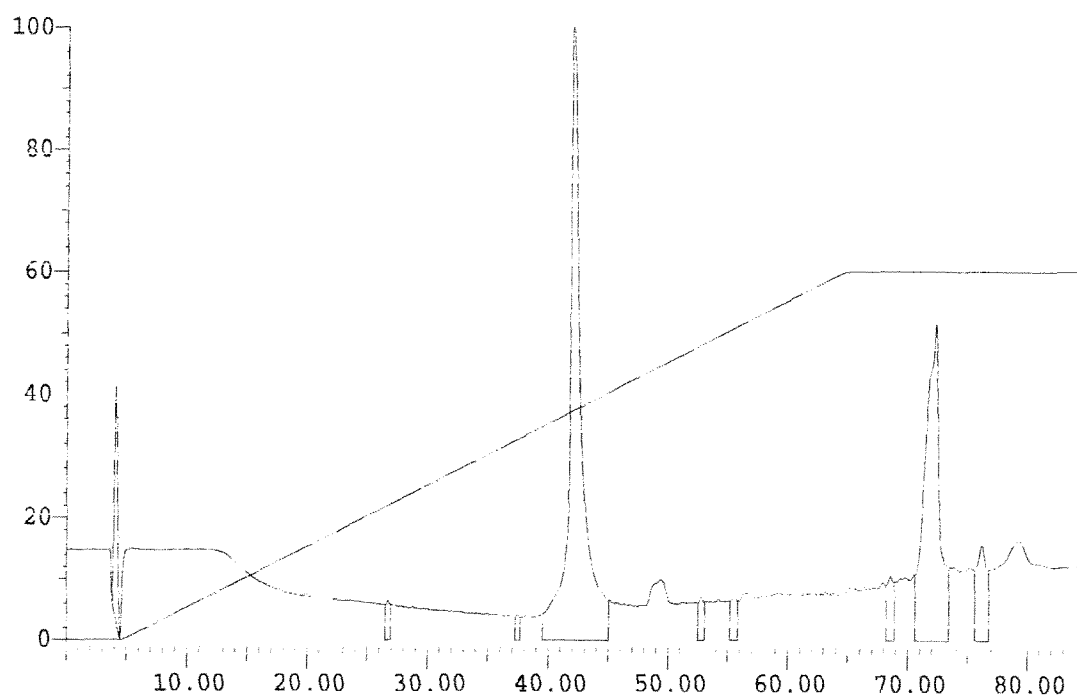
Figure 4.5 RP-HPLC Analysis of H48N HnpsPLA₂.

RP-HPLC was carried out as described in section 2.6.1.

~ 100 μg of H48N hnpsPLA₂ was loaded onto a Nucleosil C-18 RP-HPLC column. A linear gradient of acetonitrile in 0.1 % TFA was run through the column 5 minutes after protein injection. Protein was detected by monitoring the O.D. at 230 nm.

Protein eluted as a single peak at ~ 36 % acetonitrile.
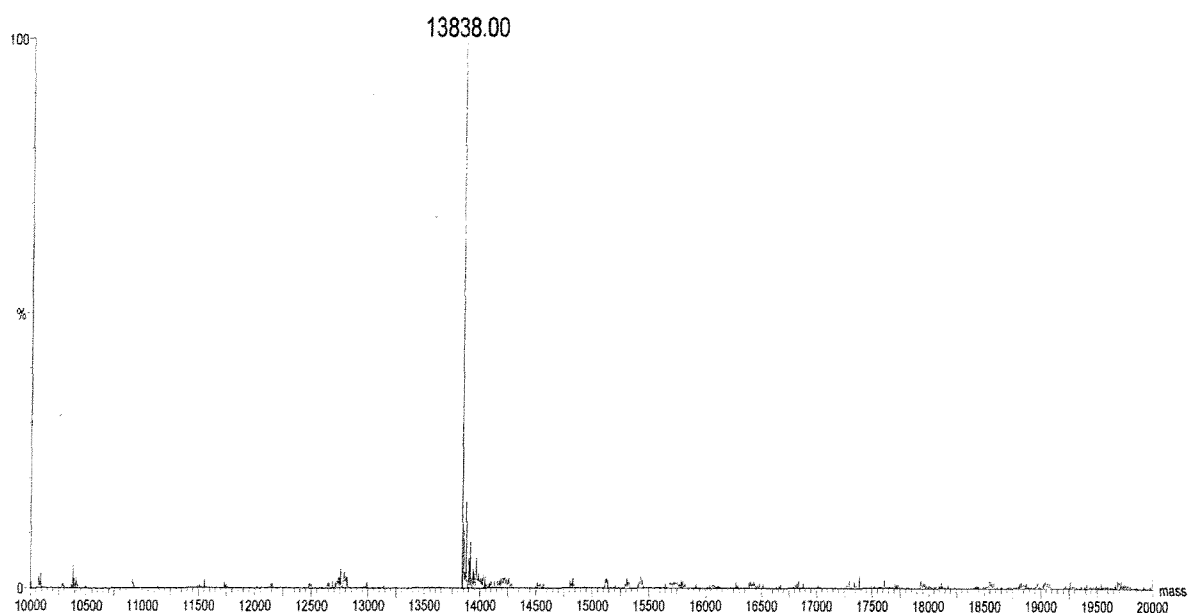
Figure 4.6 Analysis of H48N HnpsPLA$_2$ using Mass Spectrometry.

Electrospray ionisation mass spectrometry was carried out as described in section 2.6.14.

The molecular mass of H48N HnpsPLA$_2$ as judged by mass spectrometry is 13838 ± 1.0.

4.3.1 Kinetic Properties of H48N HnpsPLA$_2$.

When the H48N mutant of hnpsPLA$_2$ was assayed for activity using the fluorescence displacement assay with SUVs of DOPG as substrate, minor residual activity could be measured, at a rate of < 0.25 % as compared to the N1A

A typical fluorescence trace obtained from the hydrolysis of DOPG SUVs (64 μM) by H48N is shown in figure 4.7. A dose response curve constructed from this data is shown in figure 4.8, and a linear relationship can be seen between the initial activity of the enzyme, and the concentrations of enzyme used. To highlight the low catalytic activity shown by this H48N mutant, a typical fluorescence trace obtained with 3.5 μg of H48N is compared with those measured with 0.05 μg of N1A and 2.5 μg of the H48Q mutant, and is shown in figure 4.9. Under the conditions used, the specific activities of H48N, N1A and H48Q are 0.143 ± 0.004, 64.35 ± 4.78 and 1.80 ± 0.013 nmol/min/μg respectively. This activity is at least 10-fold less than that seen with the H48Q mutant, and is low enough to enable this mutant to be used as a competitive probe for interfacial binding, which was the initial aim of this thesis.

4.3.2 Comparison of the Secondary Structure of H48N with N1A.

The use of the H48N mutant of hnpsPLA$_2$ as a competitive binding agent relies not only on its relative inactivity, but also requires that the enzyme is structurally intact and correctly folded. The mutant is very similar to the N1A in terms of its preparation, yield and elution from chromatography columns, indicating that it is structurally similar to its parent enzyme. However, its proposed experimental role demands that its structure is examined in more detail, and CD is the method of choice (see chapter 3, section 3.3.3). This technique was used to compare the structure of H48N with the N1A, and also to determine its relative stability.
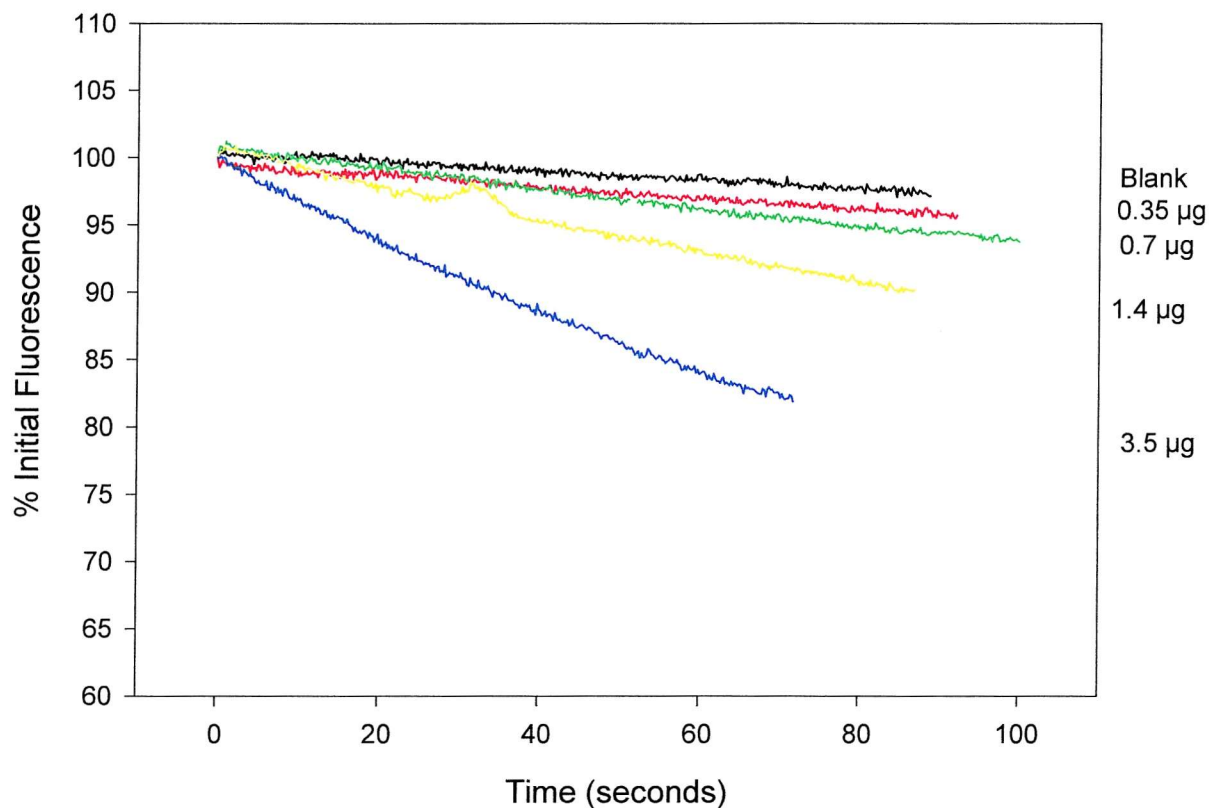
Figure 4.7 Fluorescence Trace Showing the Hydrolysis of DOPG SUVs by H48N HnpsPLA$_2$.

Enzyme activity was measured using the fluorescence displacement assay previously described (2.6.1) with 64 µM DOPG SUVs as substrate.

Assays contained either:

— - No enzyme

—— - 0.35 µg

—— - 0.7 µg

—— - 1.4 µg

—— - 3.5 µg H48N HnpsPLA$_2$

Enzyme was added at time 0.
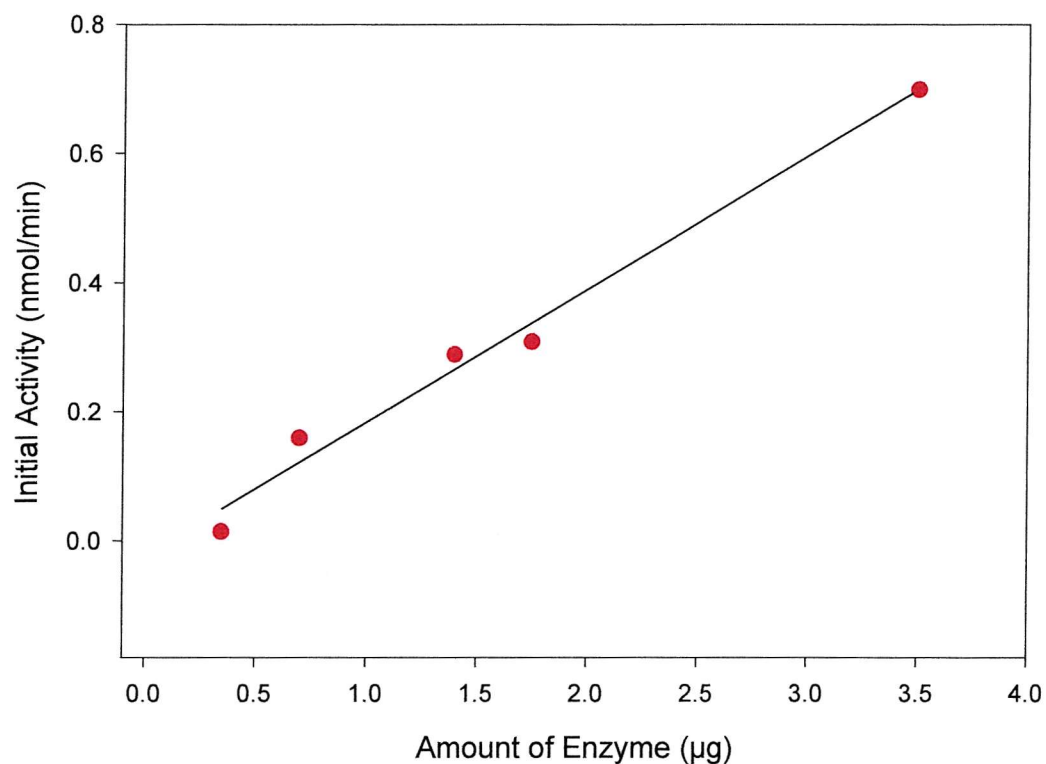
Figure 4.8 Dose Response Curve for the Hydrolysis of DOPG SUVs by H48N HnpsPLA$_2$.

Enzyme activity was measured using the fluorescence displacement assay described in section 2.6.1 with 64 µM DOPG SUVs as substrate.

● - H48N HnpsPLA$_2$

Each data set is the mean of 3 separate measurements ± s.d.
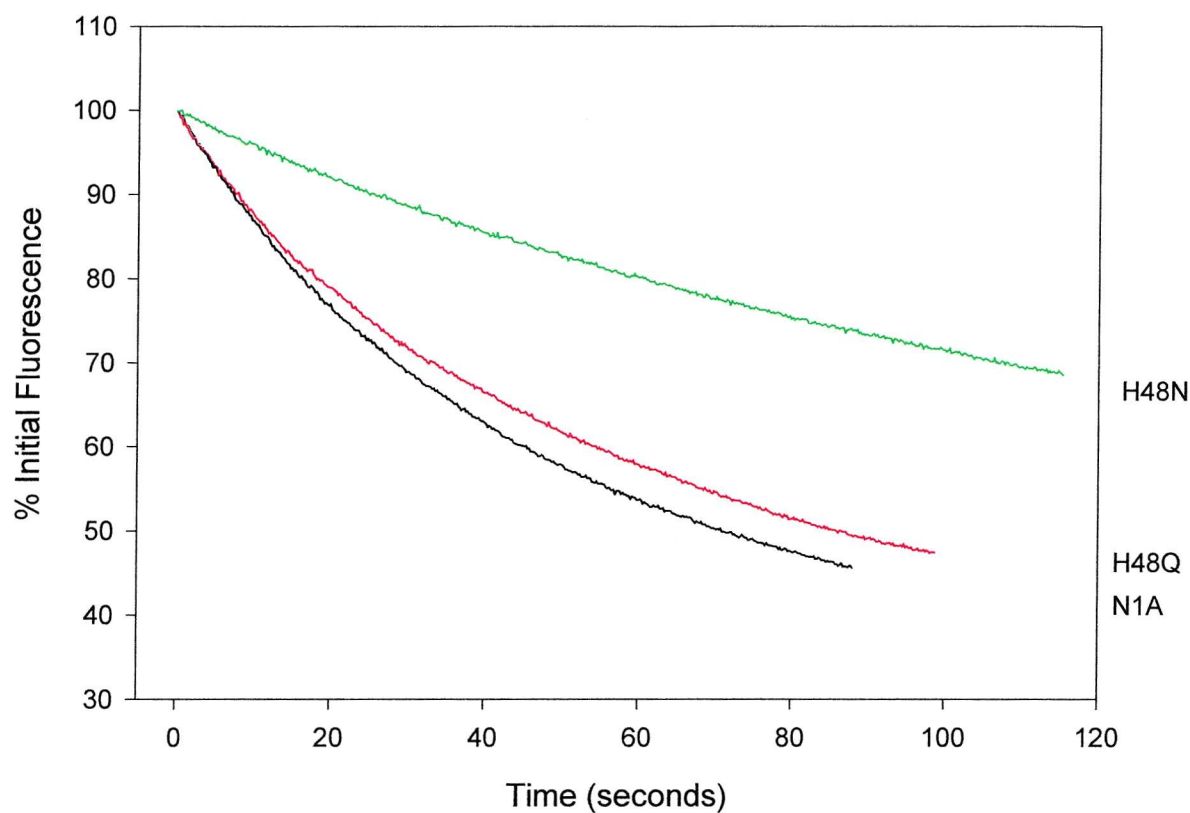
Figure 4.9 Comparison of the Hydrolysis of DOPG SUVs by N1A, H48Q and H48N HnpsPLA$_2$.

Enzyme activity was measured using the fluorescence displacement assay (2.6.1) with 64 µM DOPG SUVs as substrate.

——— - 0.05 µg N1A HnpsPLA2

——— - 2.5 µg H48Q HnpsPLA$_2$

——— - 3.5 µg H48N HnpsPLA$_2$

Enzyme was added at time 0.

The CD spectra of the secondary structure of H48N and N1A are shown in figure 4.10, and indicate that although there are slight differences in the structures of the H48N and the N1A, no major structural changes have been caused by substitution of the active site histidine.

4.3.3 Thermal Denaturation of H48N HnpsPLA$_2$.

CD was also used to assess the thermal stability of H48N. Spectra were measured at temperatures between 25 °C and 82 °C (figure 4.11), and the CD at 222 nm (a characteristic trough in the trace of an α-helix) was plotted against the temperature (figure 4.12).

The Tm calculated from this melting curve was ~58 °C for the H48N, as compared with 66 °C for the N1A. The Tm indicates the temperature at which the transition of the structure from α-helix to random coil occurs, and is similar for the N1A and H48N mutant. This demonstrates that the mutant has a structure that is similar to that of the N1A in terms of stability, and confirms that the H48N mutation has not caused any major disruptions to the structure of the enzyme.

4.3.4 The Use of *N*-Dansyl-1, 2-Palmitoyl-*sn*-glycero-3-phosphoethanolamine (Dansyl–DPPE) to Study the Interfacial Binding of H48N.

The CD data described above indicated that the gross structure of the H48N mutant was very similar to the structure of the N1A enzyme while the proteins showed similar thermal stability. However, the H48N had minimal catalytic activity and therefore, this mutant has the necessary characteristics to be used as an interfacial probe to study the interfacial binding properties of the catalytically active wild type and mutant hnpsPLA$_2$s.

150
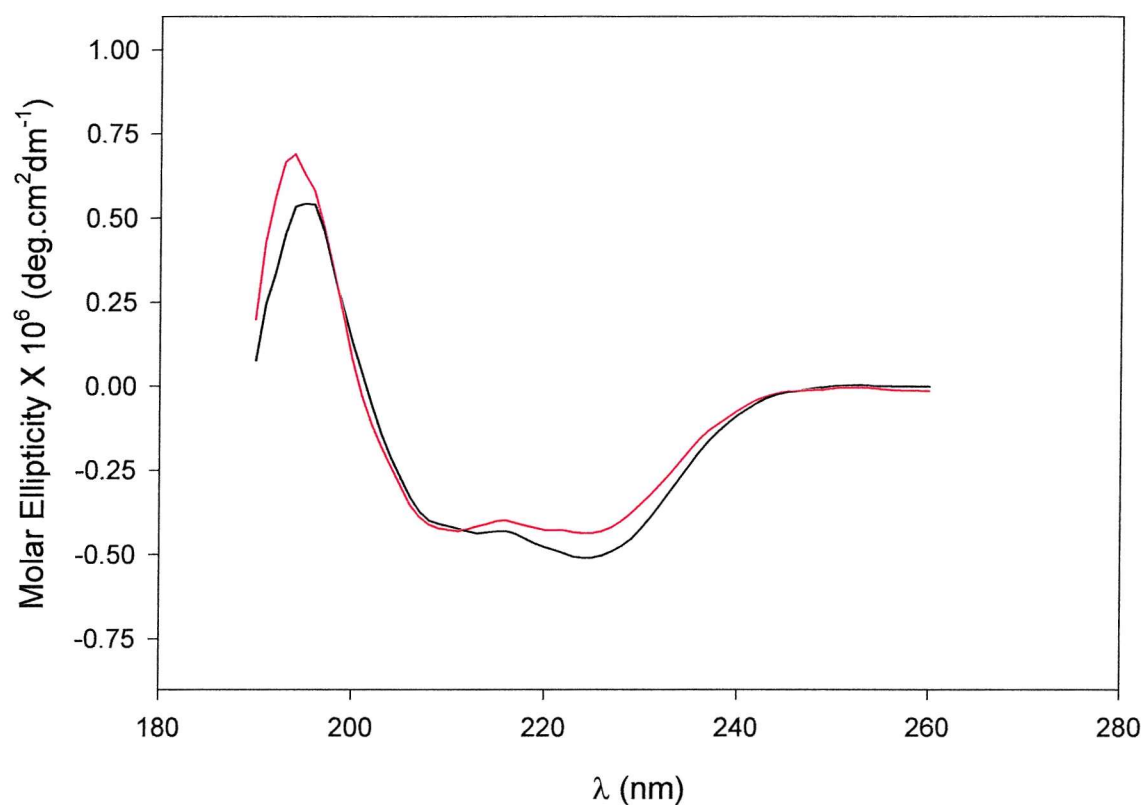
Figure 4.10 CD Spectra of N1A and H48N HnpsPLA$_2$.

CD was carried out as described in section 2.6.15.

Enzyme concentration was 0.18 mg/ml in each case, and spectra have been corrected for blank (10 mM phosphate buffer).

———— - N1A HnpsPLA$_2$

———— - H48N HnpsPLA$_2$

Spectra shown are averaged from 5 accumulations.
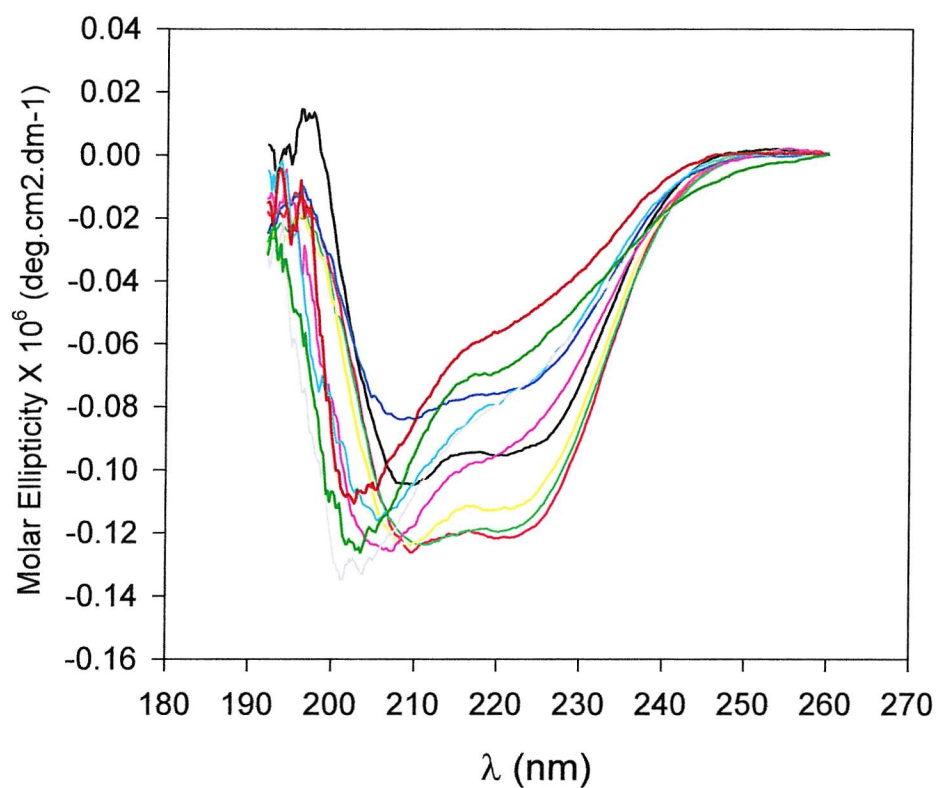
Figure 4.11 CD Spectra of H48N HnpsPLA$_2$ Measured at Temperatures between 25 °C and 82 °C.

CD was carried out as described in section 2.6.15. Concentration of H48N was 0.18 mg/ml. Spectra have been corrected for blank (10 mM phosphate buffer).

——	- 31 °C
——	- 35 °C
——	- 40 °C
——	- 47 °C
——	- 55 °C
——	- 62 °C
——	- 68 °C
——	- 75 °C
——	- 82 °C

Spectra shown are averaged from 3 accumulations.
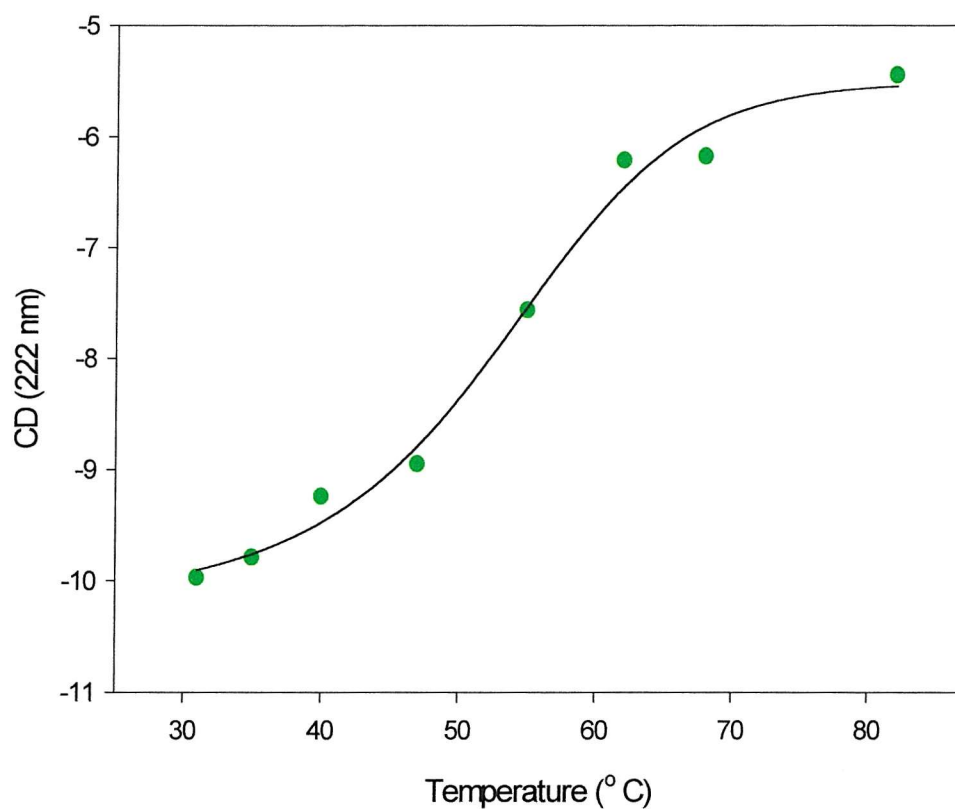
Figure 4.12 Tm Curve for H48N HnpsPLA$_2$ Calculated from CD Spectra Measured at Temperatures between 25 °C and 82 °C.

CD was carried out as described in section 2.6.15.

Concentration of H48N was 0.18 mg/ml. Spectra have been corrected for blank (10 mM phosphate buffer).

The calculated Tm is ~ 58 ^{o}C.

● - H48N HnpsPLA$_2$

Spectra shown are averaged from 3 accumulations.

In order to confirm its interfacial binding characteristics, the binding of the H48N to vesicles was studied using the fluorescent phospholipid dansyl-DPPE. The structure is shown in figure 3.13, and the use of this probe to measure interfacial binding of the H48Q mutants is described in Chapter 3, section 3.3.5. Dansyl-DPPE was incorporated into SUVs of DOPG at 4 mol%, and its fluorescent properties were used to report on enzyme binding by measuring the increase in fluorescence at 495 nm. EDTA was present in the assay system to prevent any hydrolysis of the vesicles. The results are shown in figure 4.13.

The H48N mutant of hnpsPLA$_2$ appears not only to be correctly folded and structurally stable but is also able to bind effectively to an interface. In addition, this mutant has very low activity as compared to the N1A and H48Q mutant, making it ideal for use as an interfacial binding probe than can compete with the N1A and other active enzymes for binding to the phospholipid interface.

4.4 The Use of Annexin V as a Competitive Interfacial Binding Probe.

In the previous sections evidence has been provided that the hnpsPLA$_2$ mutant H48N is structurally very similar if not identical to the wild type enzyme yet is essentially devoid of catalytic activity. Therefore this mutant has the necessary properties to be used in interfacial competition (substrate depletion) assays. In order to confirm the viability of such assays, preliminary experiments were performed with annexin V, a protein with similar membrane binding properties to PLA$_2$. The annexins are a family of phospholipid and calcium binding proteins. The role of these proteins *in vivo* has not been clearly defined, but they are known to inhibit the activity of phospholipases A$_2$ [107-109]. At least 10 mammalian forms of annexin have been identified, and crystal structures are available for some annexins, including human annexin V, which is well characterised [110,111].
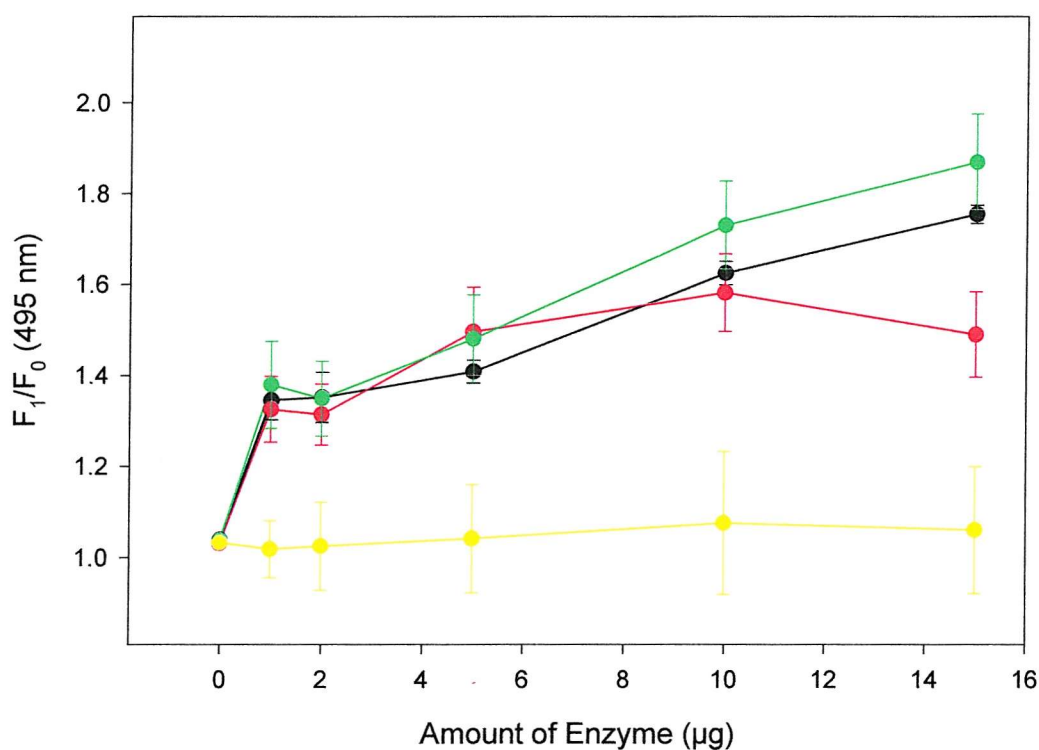
Figure 4.13 Comparison of the Binding of N1A and H48Q HnpsPLA$_2$ to DOPG Vesicles.

Preparation of DOPG vesicles containing 4 %mol dansyl-DPPE was carried out as described in section 2.5.7.

Enzyme binding was monitored as an increase in fluorescence at 495 nm. All assays contained 1 mM EDTA.

● - N1A HnpsPLA$_2$

● - H48Q HnpsPLA$_2$

● - H48N HnpsPLA$_2$

● - pp sPLA$_2$

Each data set represents the mean of three separate measurements ± s.d.

155

The ability of annexin V to bind phospholipid aggregates is dependent on it first binding calcium, and association of annexin V with phospholipid membranes can be reversed using calcium chelators such as EDTA [107]. The anti-PLA$_2$ activity shown by annexin V is thought to be largely due to the decreasing amount of substrate available to the PLA$_2$ as more annexin V binds phospholipid (substrate depletion), and not due to a direct effect the annexin V has on PLA$_2$. The inhibitory effect of annexin V is lost if assays are performed at higher substrate concentrations [112].

The use of annexin V as a competitive interfacial binding agent has been reported and this competitive effect was used to obtain information regarding the affinity of different sPLA$_2$s for their substrate interface [101]. Since it was anticipated that annexin V and the H48N mutant would show very similar properties, preliminary experiments were performed with annexin V to confirm the viability of the method that could then be applied to the H48N mutant

The fluorescence displacement assay was used under conditions of limiting substrate (2.5 nmoles DOPG), with increasing amounts of annexin V added to the vesicles prior to addition of PLA$_2$ enzyme. In this way, the relative affinities of pp- and nn-sPLA$_2$ and hnpsPLA$_2$ for DOPG SUVs were determined. The results are shown in figure 4.14. The amounts of annexin V needed to cause 50 % inhibition of activity of nn-sPLA$_2$ and pp-sPLA$_2$ are ~ 4.5 µg and ~ 1.25 µg respectively, while in the case of the N1A, only ~ 30 % inhibition was seen in the presence of 9 µg of annexin V. The amount of annexin V used to achieve near maximal inhibition of pp-sPLA$_2$ was ~ 3 µg, or ~ 80 pmoles. Under conditions of limiting substrate (2.5 nmoles), this gives a phospholipid : annexin V ratio of ~ 24 : 1, if assuming ~ 70 % of the phospholipid in the vesicle is on the outer monolayer. This is close to published stoichiometries, and is the amount of annexin V that is required to completely cover the surface of the vesicles, hence causing almost complete inhibition of pp-sPLA$_2$ activity [107]. These results show that N1A > nn-sPLA$_2$ > pp-sPLA$_2$ in terms of affinity of these enzymes for DOPG interfaces, and are in good agreement with published data [101].

156
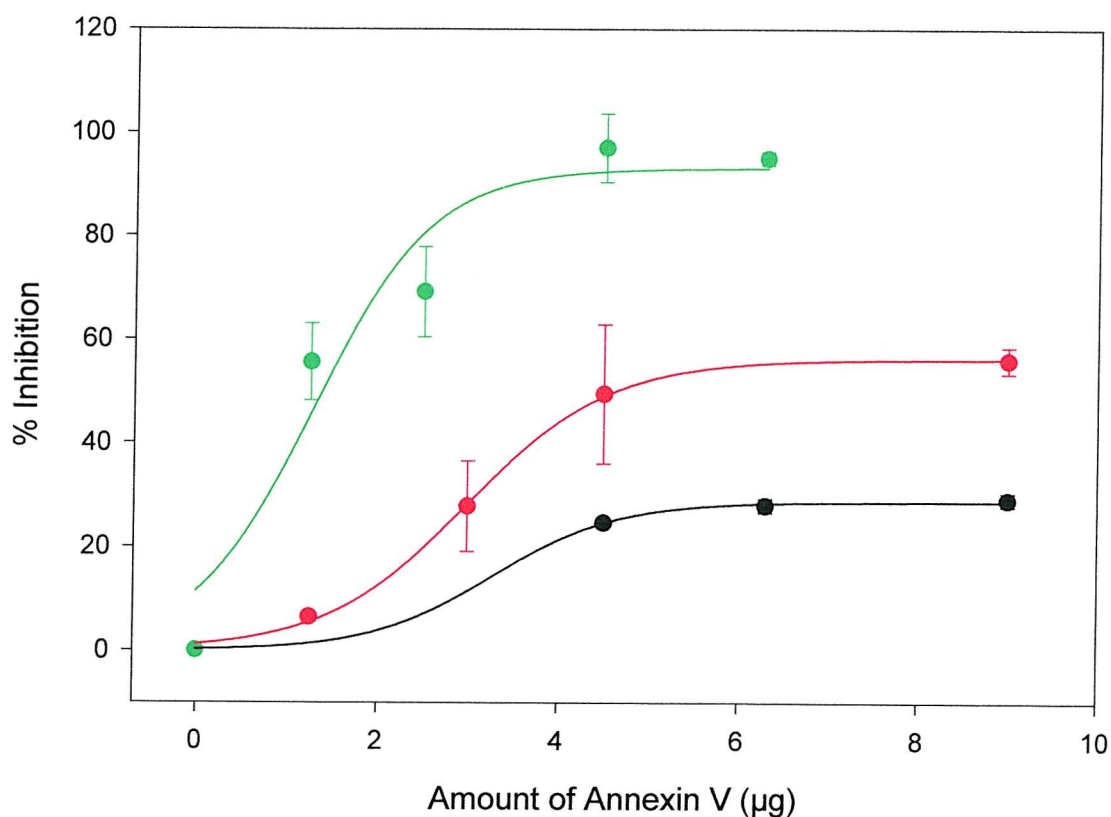
Figure 4.14 Inhibition of N1A, pp-sPLA$_2$ and nn-sPLA$_2$ by Annexin V.

Enzyme activity was measured using the fluorescence displacement assay (2.6.1) with 2.5 nmoles DOPG SUVs as substrate. 0.024 µg of N1A, 0.016 µg of pp- and 0.020 µg of nn-sPLA$_2$ were used per assay.

Activity measured in the presence of annexin V is expressed as a percentage of activity measured without annexin V present.

●   - N1A HnpsPLA$_2$

●   - pp-sPLA$_2$

●   - nn-sPLA$_2$

Each data set represents the mean of three experiments ± s.d.

4.5 The Use of H48N HnpsPLA$_2$ as a Competitive Binding Inhibitor to Study the Binding of N1A HnpsPLA$_2$, pp-sPLA$_2$ and nn-sPLA$_2$ to SUVs of DOPG.

The experimental protocol used to study the competitive effect of annexin V on the interfacial binding of N1A, nn- and pp-sPLA$_2$s could now be applied to the H48N mutant. The fluorescence displacement assay was used as before with limiting substrate (2.5 nmoles DOPG SUVs), and the initial experiment involved competing the H48N against N1A, nn- and pp-sPLA$_2$, to compare the pattern of inhibition with that seen with annexin V. The results are shown in figure 4.15, and a similar inhibitory effect seen with annexin V is found with the H48N mutant.

The enzyme that was most sensitive to the inhibitory effect of H48N, and therefore having the lowest affinity for DOPG SUV interfaces was the pp-sPLA$_2$, as was the case when annexin V was the competitive binding agent. In this instance, ~ 0.65 μg of H48N was sufficient to achieve maximal inhibition of pp-sPLA$_2$ activity. This amount of H48N equates to ~ 50 pmoles of enzyme, and presuming that approximately 70 % of the phospholipid in the vesicle is available for enzyme binding, gives a molar ratio of phospholipid : H48N of ~ 35 : 1, in keeping with the established stoichiometries.

The amount of H48N needed to cause ~ 50 % inhibition of pp- and nn-sPLA$_2$s was ~ 0.35 μg and ~ 0.55 μg respectively, reflecting the substantially lower affinity for DOPG interfaces these enzymes have as compared to the N1A where greater than 0.75 μg was required to cause the same level of inhibition. The results confirm the data that was produced using annexin V and again highlight the high affinity of hnpsPLA$_2$ for anionic vesicles relative to the *Naja naja* venom and porcine pancreatic enzymes. This high affinity is not unexpected considering the very high pI of this protein and its known preference for anionic interfaces, allowing among other functions its antibacterial role.
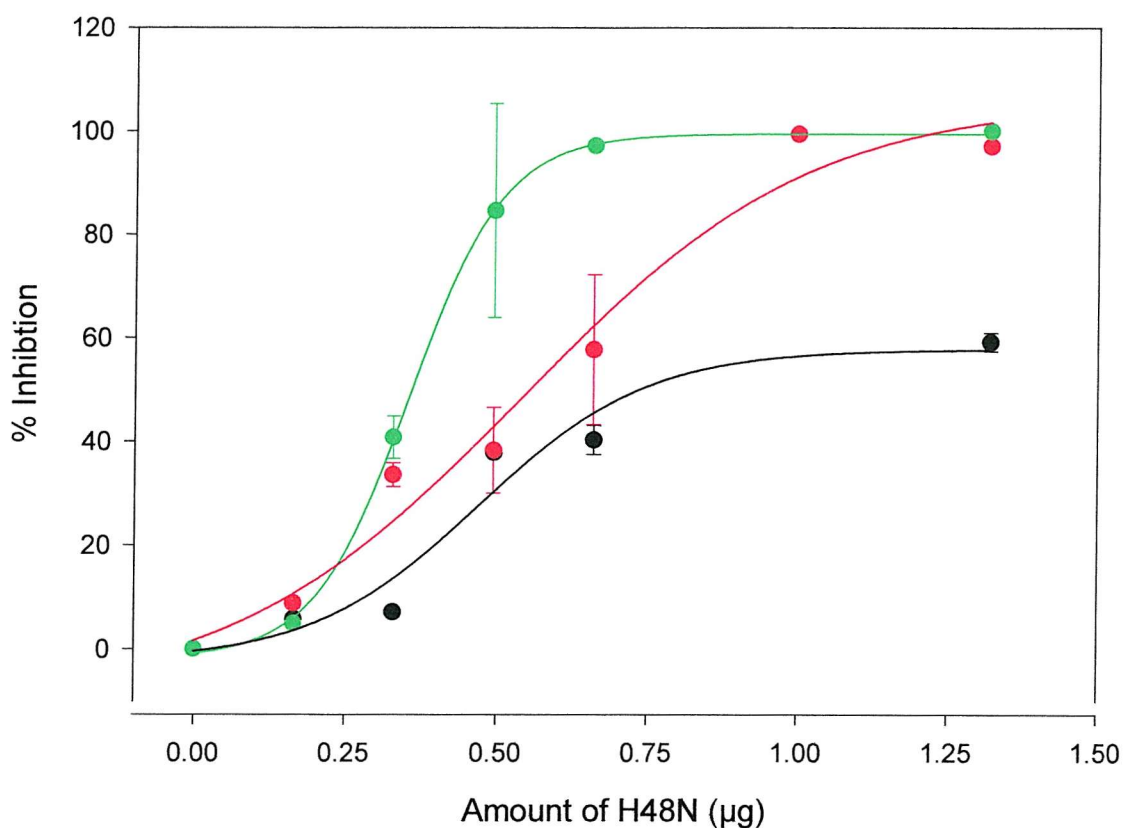
Figure 4.15 Inhibition of N1A, pp-sPLA$_2$ and nn-sPLA$_2$ by H48N HnpsPLA$_2$.

Enzyme activity was measured using the fluorescence displacement assay (2.6.1) with 2.5 nmoles DOPG SUVs as substrate. 0.024 µg of N1A, 0.016 µg of pp and 0.020 µg of nn sPLA$_2$ were used per assay.

Activity measured in the presence of H48N is expressed as a percentage of activity measured without H48N present.

● - N1A HnpsPLA$_2$

● - nn-sPLA$_2$

● - pp-sPLA$_2$

Each data set represents the mean of three experiments ± s.d.

159

4.6 The Inhibitory Effect of H48N HnpsPLA$_2$ on N1A and H48Q HnpsPLA$_2$ Measured on MLVs and SUVs of DOPG.

The specific activity of N1A and the active site mutant H48Q when assayed on both SUVs and MLVs of DOPG was reported in the previous chapter. It was shown that both enzymes displayed higher specific activities when assayed on the larger flatter MLVs than on the smaller, more curved SUVs. It is possible that this difference in activity is due to differences in interfacial binding affinity. Therefore, the effect of H48N on the activity of both MLVs and SUVs was studied, in order to ascertain the binding affinities of the N1A and H48Q for the two types of vesicle. Each enzyme was assayed on both SUVs and MLVs in the presence of increasing amounts of H48N in order to compare the binding affinities for SUVs and MLVs of the two enzymes.

The results in figure 4.16 show that the N1A appears to bind more tightly to the MLV preparation of DOPG than the SUV preparation, in that low concentrations of H48N inhibit the activity of the enzyme more effectively with the SUV preparation. This difference appears to disappear on addition of higher concentrations of H48N. However, in view of the inherent difficulties of these assays and the errors that are intrinsic to the method, it could be argued that the N1A binds with similar affinity to both types of vesicle.

The situation with the H48Q seems to be more clear cut (figure 4.17) in that this mutant binds more tightly to the SUVs, and is more readily displaced from the MLVs by the H48N. However, under these assay conditions, which involve large amounts of H48Q to obtain measurable enzyme activity, the amount of available phospholipid interface becomes critical. Since the total amount of phospholipid is the same for the SUV and MLV preparations, the fact that MLVs contain several phospholipid bilayers means that the surface concentration of phospholipid is much less than with the SUVs. Because of this, the MLV preparation will be more sensitive to inhibition by the H48N than the SUV preparation.
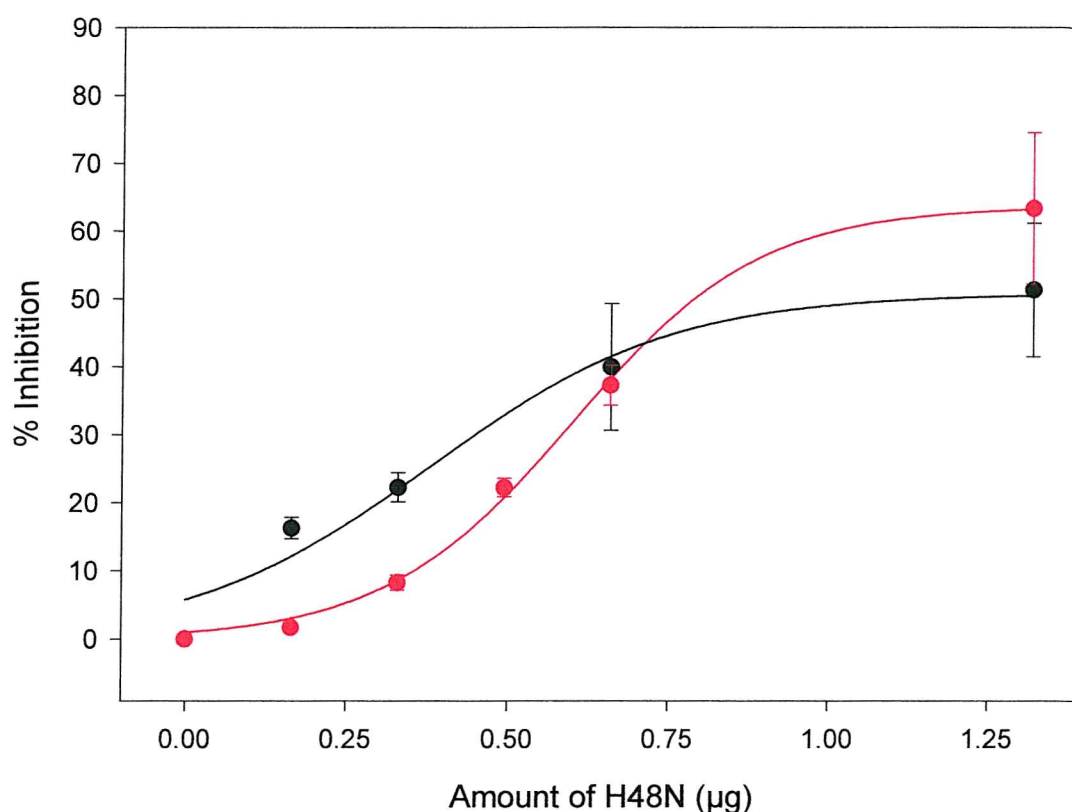
Figure 4.16 Effect of H48N on Hydrolysis of SUVs and MLVs of DOPG by N1A HnpsPLA$_2$.

Enzyme activity was measured using the fluorescence displacement assay (2.6.1) with 2.5 nmoles DOPG SUVs or MLVs as substrate. 0.048 µg of N1A was used per assay.

Activity measured in the presence of H48N is expressed as a percentage of activity measured without H48N present.

● - SUVs

● - MLVs

Each data set represents the mean of three separate experiments ± s.d.
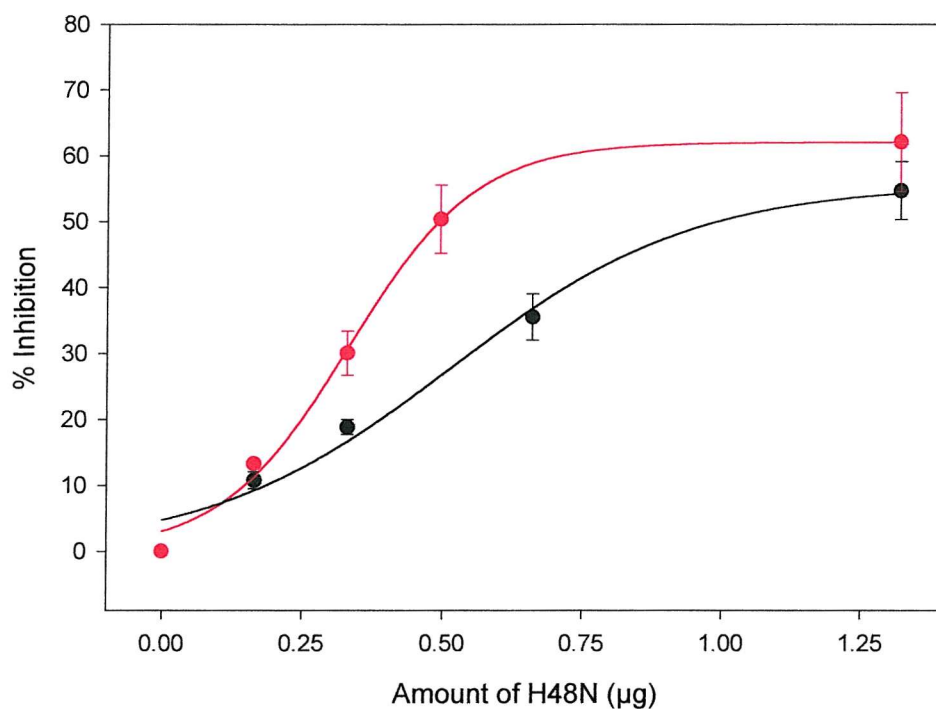
Figure 4.17 Effect of H48N on Hydrolysis of SUVs and MLVS of DOPG by H48Q HnpsPLA$_2$.

Enzyme activity was measured using the fluorescence displacement assay (2.6.1) with 2.5 nmoles DOPG SUVs or MLVs as substrate. 2.5 μg of H48Q was used per assay.

Activity measured in the presence of H48N is expressed as a percentage of activity measured without H48N present.

● - SUVs

● - MLVs

Each data set represents the mean of three separate experiments ± s.d.

This explanation is upheld in figures 4.18 and 4.19, where the two enzymes are directly compared on SUVs and MLVs respectively. There is no difference between the N1A and H48Q with SUVs, but a clear difference is seen with MLVs. This reflects the limiting amount of surface phospholipid present in the MLV preparation and the fact that a much larger number of molecules of the H48Q have to be bound to see significant activity, requiring more surface phospholipid.

4.7 The Ability of H48N HnpsPLA$_2$ to Inhibit Hydrolysis of Cardiolipin by N1A HnpsPLA$_2$, nn-sPLA$_2$ and pp-sPLA$_2$.

The affinities of the N1A hnpsPLA$_2$, nn-sPLA$_2$ and pp-sPLA$_2$ for the complex phospholipid cardiolipin were tested using the H48N mutant of hnpsPLA$_2$ as a competitive agent. The structure of cardiolipin is shown in figure 4.20, and consists of a PG molecule attached via the glycerol headgroup to a PA molecule.
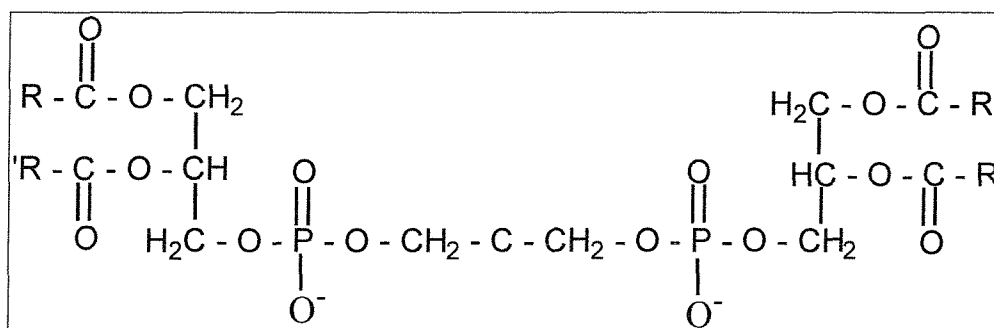
Figure 4.20 The Structure of Cardiolipin.

R/R' represent long chain fatty acids.
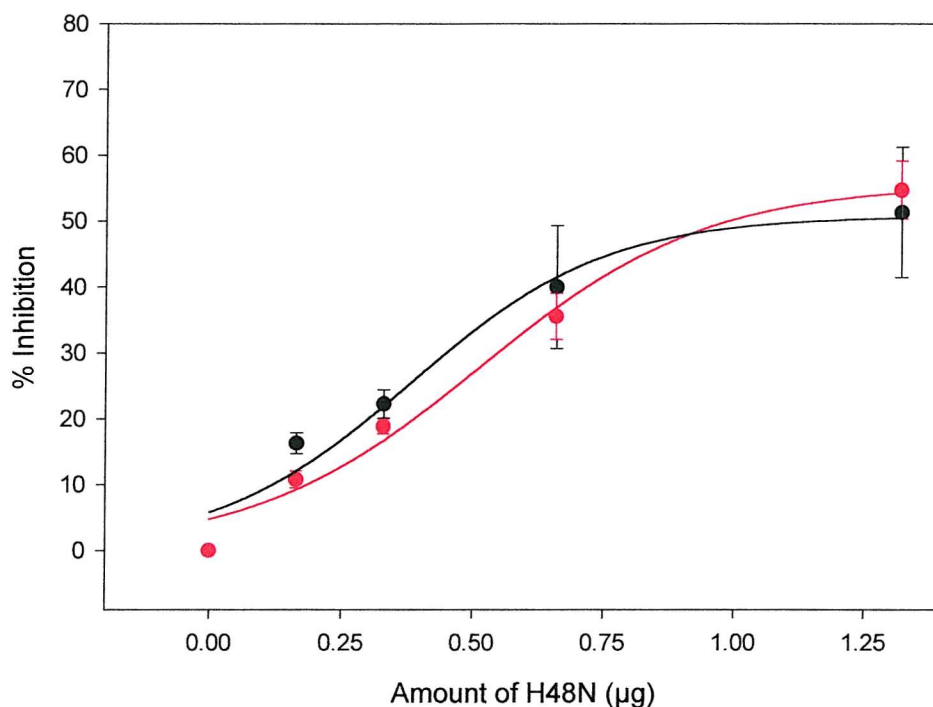
Figure 4.18 Effect of H48N on Hydrolysis of SUVs of DOPG by N1A and H48Q HnpsPLA$_2$.

Enzyme activity was measured using the fluorescence displacement assay (2.6.1) with 2.5 nmoles DOPG SUVs or MLVs as substrate. 0.048 µg of N1A and 2.5 µg of H48Q were used per assay.

Activity measured in the presence of H48N is expressed as a percentage of activity measured without H48N present.

● - N1A HnpsPLA$_2$

● - H48Q HnpsPLA$_2$

Each data set represents the mean of three separate experiments ± s.d.
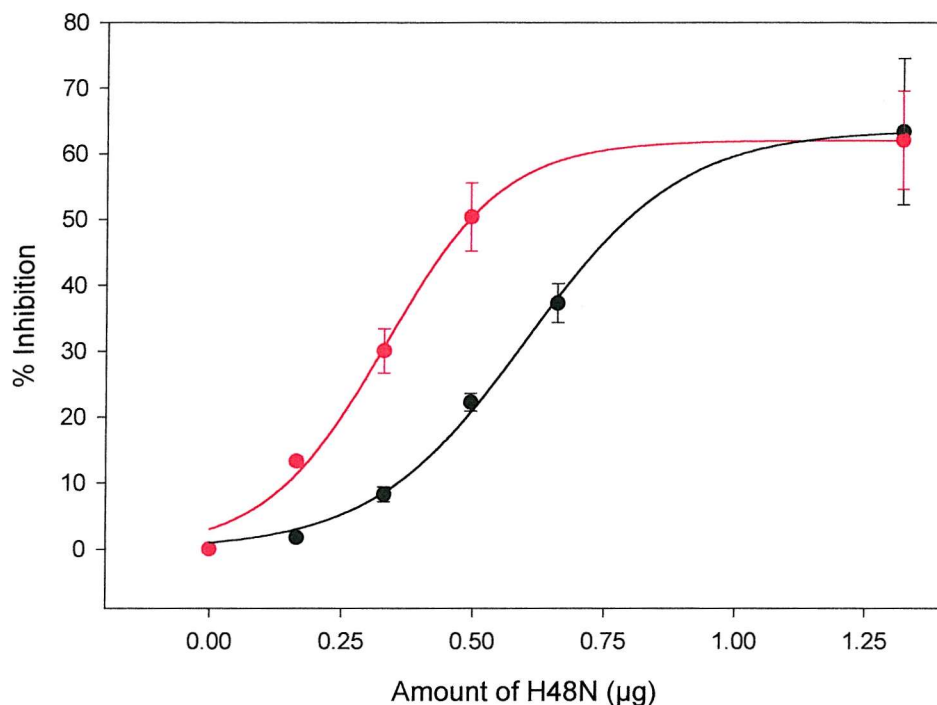
Figure 4.19 Effect of H48N on Hydrolysis of MLVS of DOPG by N1A and H48Q HnpsPLA$_2$.

Enzyme activity was measured using the fluorescence displacement assay (2.6.1) with 2.5 nmoles DOPG SUVs or MLVs as substrate. 0.048 µg of N1A and 2.5 µg of H48Q were used per assay.

Activity measured in the presence of H48N is expressed as a percentage of activity measured without H48N present.

● - N1A HnpsPLA$_2$

● - H48Q HnpsPLA$_2$

Each data set represents the mean of three separate experiments ± s.d.

This phospholipid is found in high concentrations in bacterial cell membranes and the inner and outer membranes of mitochondria, and as it contains a net negative charge of two, it would seem likely to be a good substrate interface for hnpsPLA$_2$ [113]. In fact, only low catalytic activity is seen when N1A is assayed on this phospholipid, which is likely due to the size of the active site channel. In hnpsPLA$_2$, this channel is slightly narrower than found in other PLA$_2$s, and so would have difficulty accommodating this bulky phospholipid. Conversely, the pp-sPLA$_2$ can hydrolyse cardiolipin, and the active site channel in this enzyme is less constrained than the N1A, presumably allowing entry of this phospholipid into the active site. The venom sPLA$_2$ from *Naja naja* shows very little catalytic activity on cardiolipin similar to the N1A, although this enzyme has high affinity for the related phospholipid DOPG [113]. The effects of adding increasing concentrations of H48N on the hydrolysis of cardiolipin by the three enzymes may provide some insight into the relative abilities these enzymes have to productively bind to a cardiolipin interface, and the results of such a competition study are shown in figure 4.21.

The pp-sPLA$_2$, which is catalytically active on cardiolipin, is also most inhibited by the H48N indicating a relatively lower affinity for the cardiolipin interface. The nn- and N1A sPLA$_2$s both show similar low levels of inhibition, which is likely to be a reflection on their ability to productively bind an interface consisting of cardiolipin.

That the H48N can cause significant inhibition of pp-sPLA$_2$ activity must indicate that the hnpsPLA$_2$ mutant is able to bind to the cardiolipin interface. This adds support to the theory that hydrolysis of cardiolipin by N1A is limited by its inability to hydrolyse a single cardiolipin molecule, rather than by its ability to bind to this phospholipid interface.
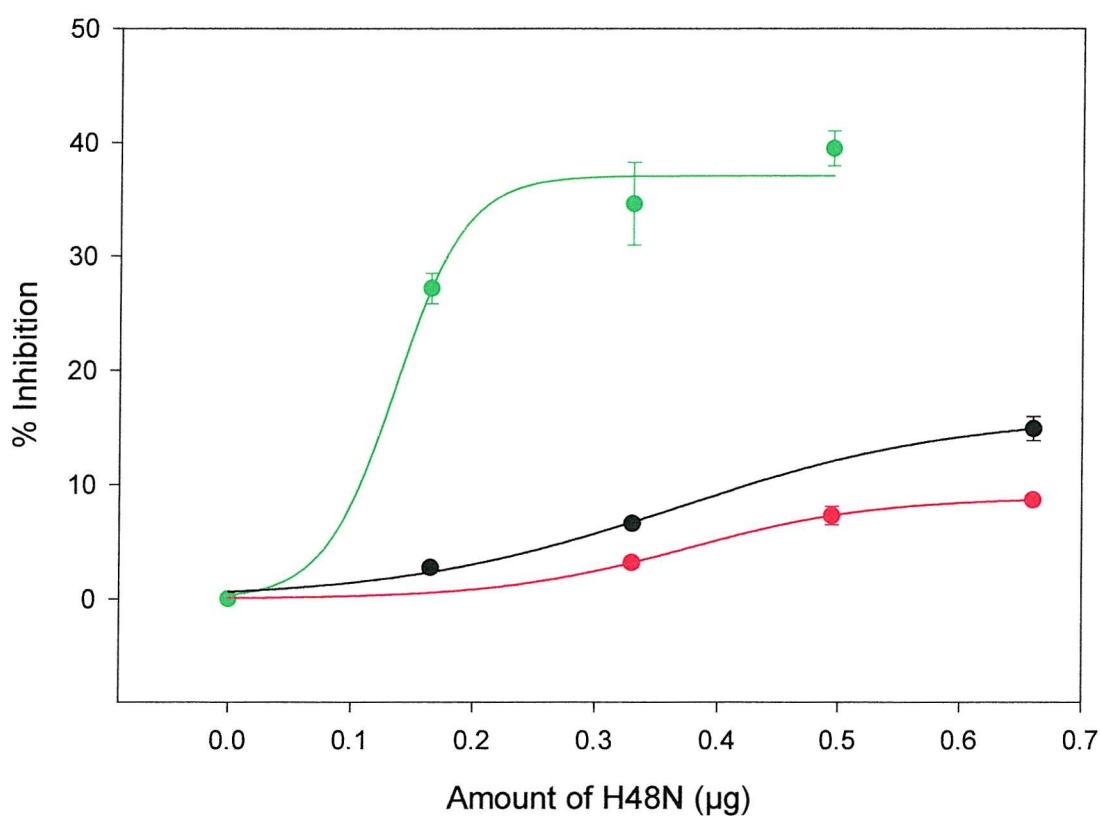
Figure 4.21 Effect of H48N on the Hydrolysis of Cardiolipin SUVs by N1A, nn-sPLA$_2$ and pp-sPLA$_2$.

Enzyme activity was measured using the fluorescence displacement assay (2.6.1) with 2.5 nmoles cardiolipin SUVs as substrate. 0.96 μg of N1A, 0.815 μg of pp and 1.00 μg of nn sPLA$_2$ were used per assay.

Activity measured in the presence of H48N is expressed as a percentage of activity measured without H48N present.

● - N1A HnpsPLA$_2$

● - nn-sPLA$_2$

● - pp-sPLA$_2$

Each data set represents the mean of three experiments ± s.d.

4.8 The Ability of N1A HnpsPLA$_2$ to Hydrolyse the Bacterium *M. luteus* in the Presence of H48N HnpsPLA$_2$.

The hnpsPLA$_2$ enzyme is able to hydrolyse suspensions of *M. luteus* as described in the previous chapter, a feature not seen with other sPLA$_2$s [60]. This unique property of hnpsPLA$_2$ has been attributed to the large excess of cationic residues on the surface of the protein, because charge reversal mutagenesis of up to five of these cationic residues completely removed the ability of the enzyme to hydrolyse the *M. luteus* suspensions (Beers, Buckland, Wilton - unpublished data). It is thought that the surface cationic residues facilitate the penetration of hnpsPLA$_2$ through the negatively charged cell wall, allowing access to the underlying cell membrane (see figure 1.4). If this is the case, then the inactive H48N should still be able to access the cell membrane, and a competitive effect should be seen when assaying the N1A in the presence of increasing amounts of H48N.

The graph in figure 4.22 shows the results of this competition study. The competitive effects of the H48N are clearly shown and this confirms that the ability of N1A to reach the bacterial cell membrane is not due to its catalytic activity, as the H48N which is inactive is still able to access this layer and compete with the N1A for the interface provided by the cell membrane.

4.9 Comparison of the Interfacial Binding of Tryptophan Mutants of HnpsPLA$_2$ to DOPG SUVs.

The inability of hnpsPLA$_2$ to hydrolyse PC-containing zwitterionic interfaces is attributable not only to the role of electrostatic interactions in defining binding affinity, but also to the lack of tryptophan residues in this type of sPLA$_2$. The importance of tryptophan residues in binding proteins to the phospholipid interface particularly when the interface is zwitterionic has been highlighted [95,114].
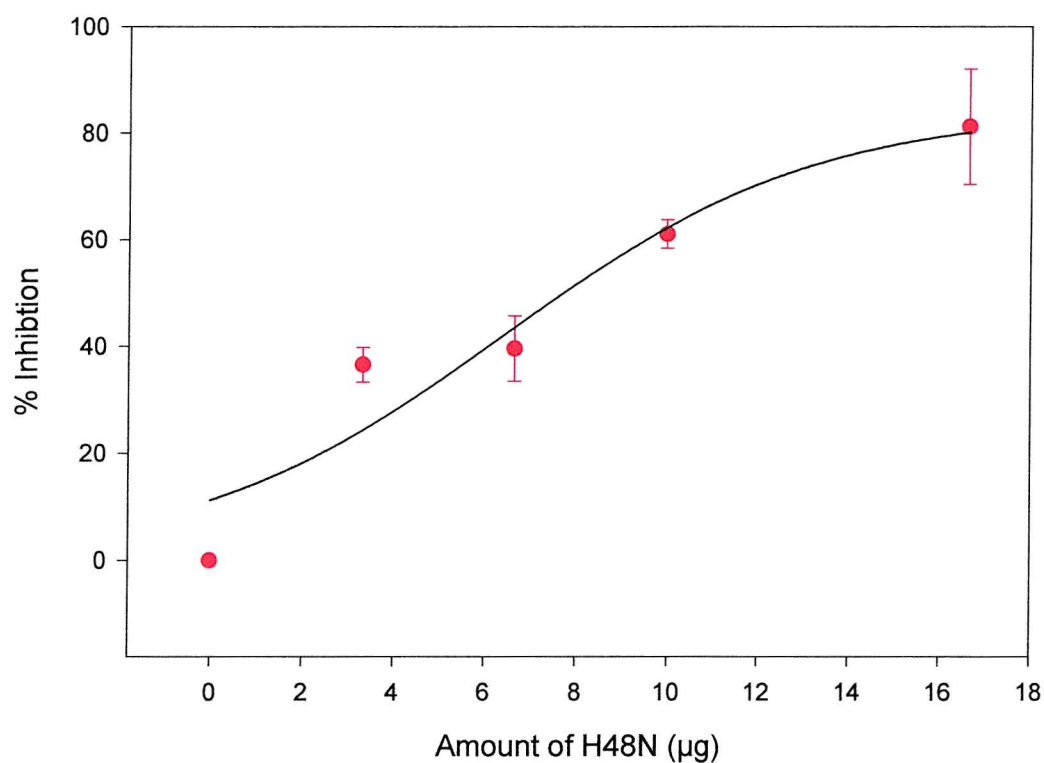
Figure 4.22 Effect of H48N on the Ability of N1A HnpsPLA$_2$ to Hydrolyse *M. luteus*.

Enzyme activity was measured using the fluorescence displacement assay as before, with *M. luteus* as substrate. *M. luteus* were prepared according to section 2.6.3. Each assay contained 2.4 µg of N1A.

Activity measured in the presence of H48N is expressed as a percentage of activity measured without H48N present.

● - N1A HnpsPLA$_2$

All data sets are the average of three separate experiments ± s.d.

The pp-sPLA$_2$ contains a surface-exposed tryptophan at position three, and this residue is believed to play a major role in the interaction of this enzyme with its substrate interface [94]. In addition, the group V enzyme contains four tryptophan residues, of which Trp-31 is believed to be a major factor in this sPLA$_2$s ability to hydrolyse PC-containing interfaces [26]. Similarly, the tryptophan at position 20 in the *Naja naja* venom enzyme of group IA is believed to be the key residue in this enzyme for promoting binding to PC interfaces.

The insertion of a tryptophan residue into these equivalent positions in the hnpsPLA$_2$ has been performed in order to determine how such mutations might affect the ability of this enzyme to hydrolyse PC interfaces. These V3W, L20W and V31W mutants were assayed for their ability to hydrolyse both DOPC and DOPG vesicles and of specific interest was the fact that all mutants expressed similar activity to the wild type on DOPG vesicles (Beers, Buckland, Wilton - unpublished data). Because the enzyme binds with high affinity to such vesicles and this binding involves primarily electrostatic interaction, it was predicted that there would not be major differences in the binding of these tryptophan mutants to DOPG vesicles. The positions of these mutations are indicated on the space-filling model of hnpsPLA$_2$ in figure 4.23.

The results of the competition study involving the three mutants containing tryptophan are shown in figure 4.24 and confirm these predictions. When these results are compared with the N1A itself, (figure 4.15) it can be seen that all the curves are similar in failing to produce 100% inhibition with the highest concentration of H48N. However, the V31W mutant is most similar to the N1A while the V3W and L20W appear to bind tighter to the DOPG vesicles as these two mutants are less easily inhibited by the H48N.
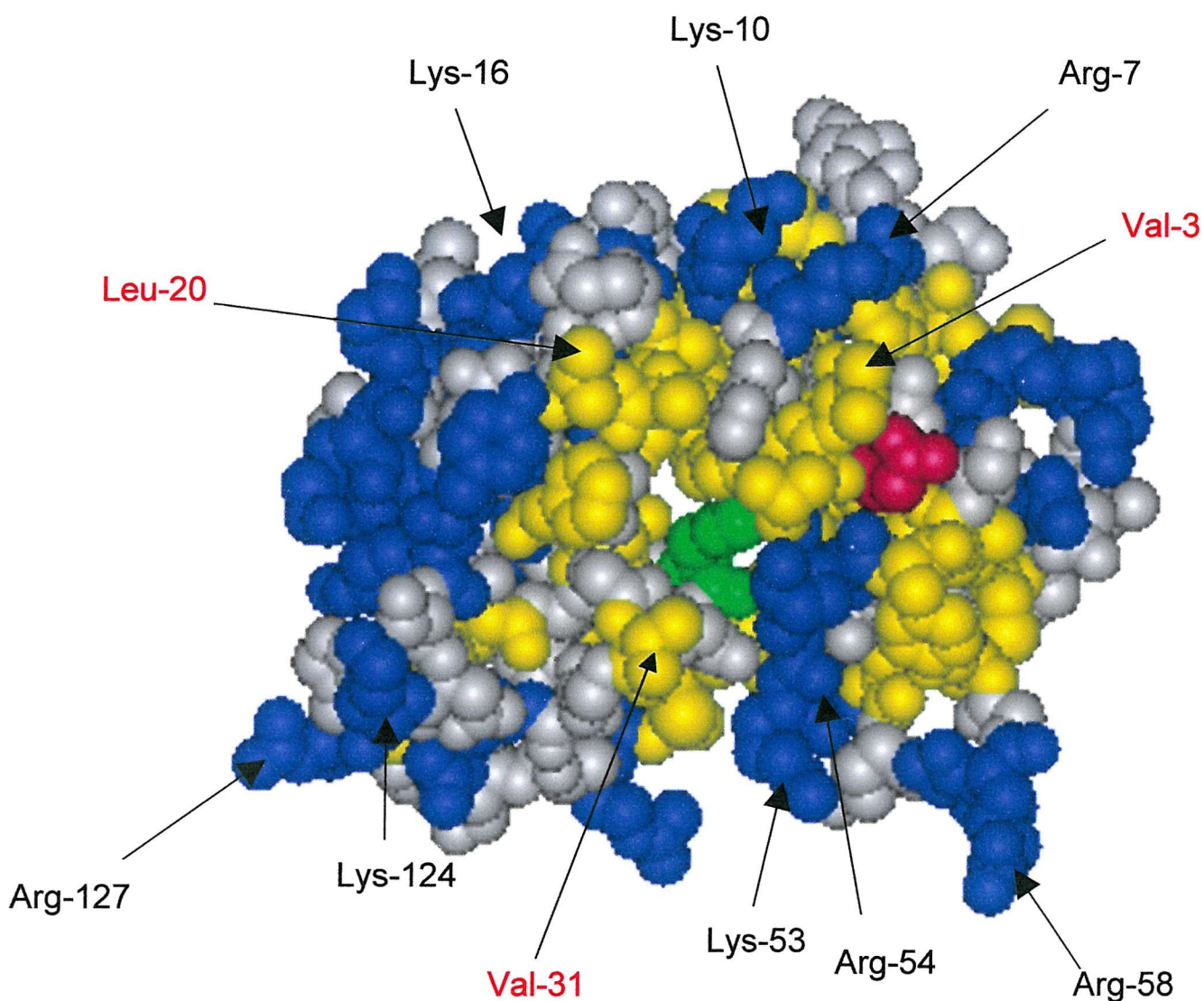
Figure 4.23 Space-filling Model of HnpsPLA₂.

The model is positioned so that the viewer is looking at the interfacial binding surface. Basic residues are highlighted in blue, hydrophobic residues in yellow. The N-terminal Ala and the active site His-48 are coloured red and green respectively, for orientation purposes. Residues indicated are sites of mutagenesis, which are described in the text.

171
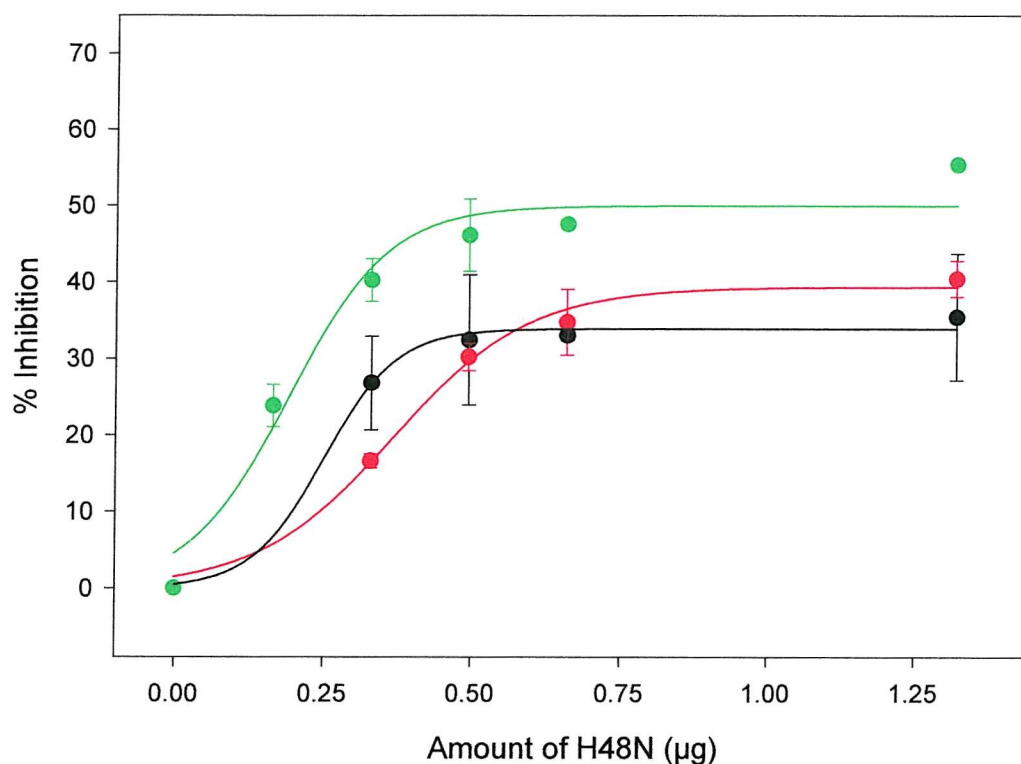
Figure 4.24 Effect of H48N on the Hydrolysis of DOPG SUVs by the Tryptophan Mutants V3W, V31W and L20W of HnpsPLA$_2$.

Enzyme activity was measured using the fluorescence displacement assay as before, with 2.5 µM DOPG as substrate. Assays contained either 0.058 µg of V3W, 0.064 µg of V31W or 0.061 µg of L20W hnpsPLA$_2$.

Activity measured in the presence of H48N is expressed as a percentage of activity measured without H48N present.

● - V3W HnpsPLA$_2$

● - L20W HnpsPLA$_2$

● - V31W HnpsPLA$_2$

All data sets are the average of three separate experiments ± s.d.

Overall the results show that the insertion of tryptophan into the N1A has no major effects on the binding of these mutants to DOPG vesicles and this is line with the fact that such mutants express similar activity to the N1A on such vesicles. Although it would be anticipated that these mutants would bind to PC vesicles with higher affinity than the N1A, because the H48N does not bind to PC, it is not possible to perform interfacial competition assays with this substrate.

4.10 The Effect of H48N HnpsPLA$_2$ on the Hydrolysis of DOPG SUVs by Charge-Reversal Mutants.

A major contributing factor to the affinity for substrate interfaces shown by sPLA$_2$s is their global charge, and interfacial binding has been found to be predominantly driven by electrostatic interactions. A number of charge reversal mutants have been produced and these mutants have been used to assess the contribution of charge to heparin/HSPG binding and the antibacterial nature of hnpsPLA$_2$ [66,67]. In the course of that work it was observed that several charge reversal mutants were significantly more active on DOPG vesicles than the N1A. This enhanced activity was also seen when using lysozyme-permeabilised suspensions of M. luteus, where all sPLA$_2$s have direct access to the cell membrane. The enhanced activity of these mutants on DOPG vesicles is shown in figure 4.25. It is possible that these charge reversal mutants bind less tightly to DOPG vesicles and M. luteus cell membranes, and it is this lower binding affinity that facilitates the higher rate of hydrolysis. Such enhanced hydrolysis may be linked to the enzyme molecule being able to 'hop' between vesicles, rather than staying on the same vesicle and 'scooting' over the surface to effect hydrolysis. This explanation requires that hopping is a rapid event relative to scooting, thus allowing the enhanced catalytic activity. It was important therefore, to study the affinities of these charge reversal mutants for binding DOPG interfaces, especially those mutants with enhanced catalytic activity as compared to N1A.

173
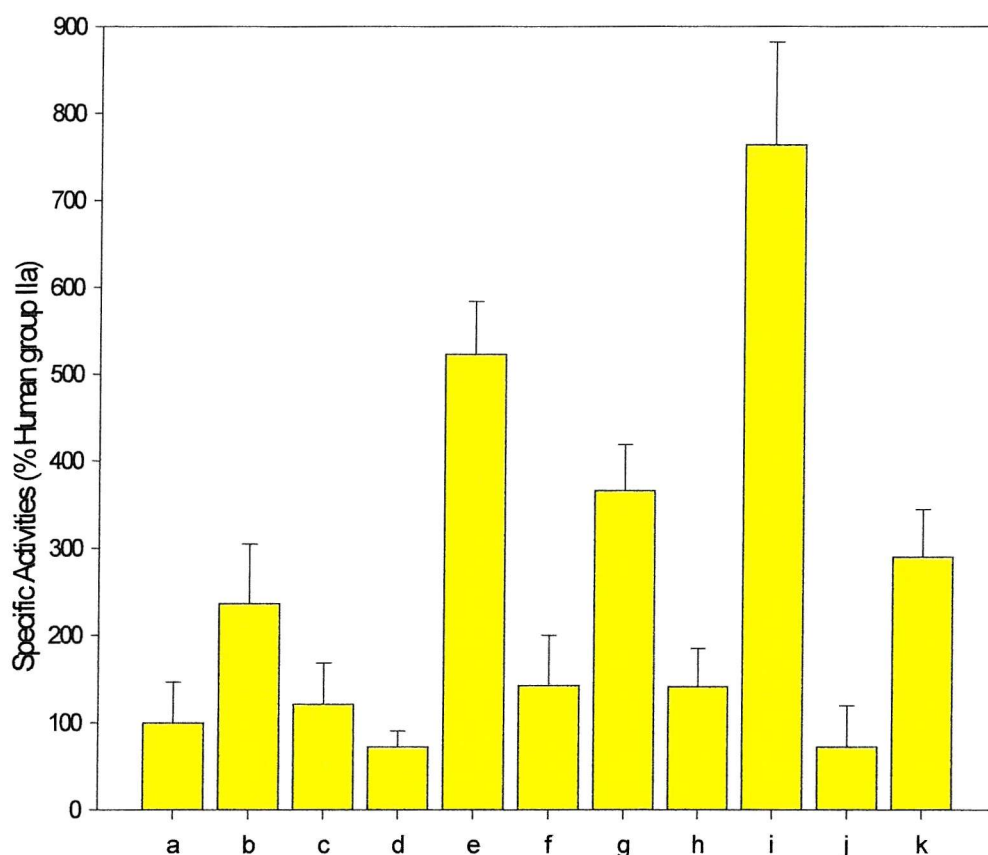
Figure 4.25 Comparison of the Activity of N1A and Charge-reversal Mutants of HnpsPLA$_2$ assayed on SUVs of DOPG.

Specific activities were determined for N1A and charge reversal mutants of hnpsPLA$_2$ against DOPG SUVs (63 µM).

a - N1A   g - K53E/R54E/R58E

b - R7E/K10E   h - K74E/K87E/R92E

c - K110E/K115E   i - R7E/K10E/K16E

d - K38/K116E   j - K38E/K124E/R127D

e - K10E/K16E   k - K53E/R54E/R58E/K124E/R127D

f - K124E/R127D

Data shown are means of three separate experiments ± s.d. (S. Beers, personal communication).

The mutants that were available for investigation were: R7E/K10E, K124E/R127E, R7E/K10E/K16E and R7E/K10E/K16E/K124E/R127E (series one), and K124E/R127E, K53E/R54E/R58E and K53E/R54E/R58E/K124E/R127E (series two). The positions of these mutations are indicated on the space-filling model of the interfacial binding surface of hnpsPLA$_2$ shown in figure 4.23.

The results of the binding assays are shown in figures 4.26 and 4.27. The results clearly show that it is the number of sites of charge reversal that has the biggest effect on binding. The mutants that showed the greatest enhancement in activity, namely the R7E/K10E and the R7E/K10E/K16E, showed only modest effects in terms of reduced binding in the presence of H48N. Similar inhibitory effects on binding were seen with the K124E/R127D mutant, and this mutant had showed no significant enhancement in activity.

Therefore, the important conclusion for this study is that the enhanced activity of some of these charge reversal mutants cannot be attributed to non-specific reduced interfacial binding. It would appear that charge reversal of specific residues must affect how the enzyme sits on the interface and certain changes in topology are beneficial to catalysis.

4.11 Discussion.

The production of the H48A and H48N mutants of hnpsPLA$_2$ has been reported. No H48A protein was obtained however, and this would suggest that such a major mutation in the active site of the enzyme has severely comprised the ability of the enzyme to fold into the correct orientation.

The H48N mutant of hnpsPLA$_2$ appeared to be structurally intact, as shown by its purification, and more accurately by CD studies. This mutant, like the H48Q mutant was found to be slightly active, but the rate was # 0.25 % of that of the N1A.
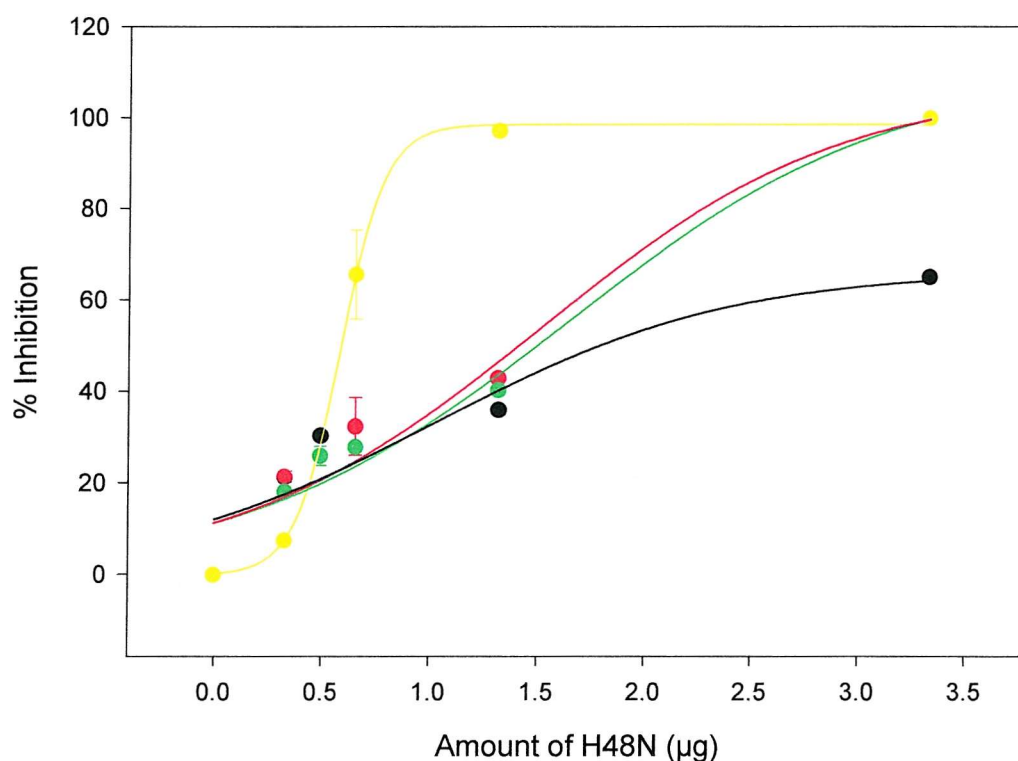
Figure 4.26 The Effect of H48N on Hydrolysis of DOPG SUVs by Charge Reversal Mutants - Series One.

Enzyme activity was measured using the fluorescence displacement assay (2.6.1) with 2.5 µM DOPG SUVs as substrate. Assays contained 0.006 µg of the relevant mutant. Activity measured in the presence of H48N is expressed as a percentage of activity obtained without H48N present.

- ● - R7E/K10E
- ● - K124E/R127E
- ● - R7E/K10E/K16E
- ● - R7E/K10E/K16E/K124E/R127E

Each data set represents the mean of three experiments ± s.d.

176
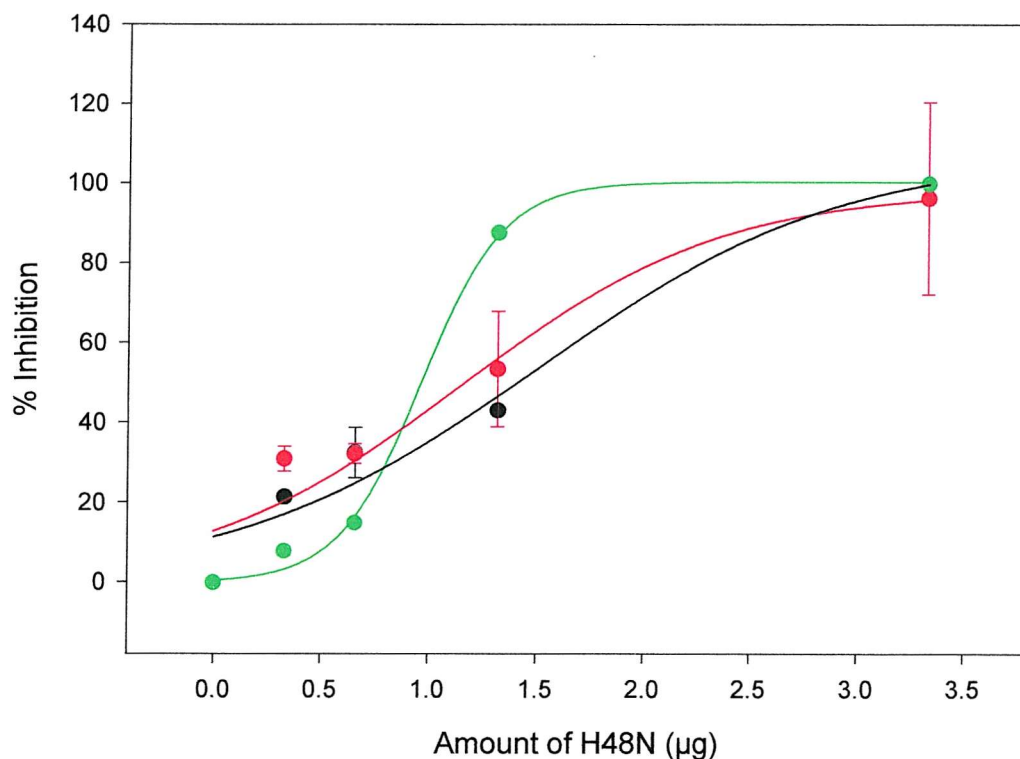
Figure 4.27 The Effect of H48N on Hydrolysis of DOPG SUVs by Charge Reversal Mutants - Series Two.

Enzyme activity was measured using the fluorescence displacement assay (2.6.1) with 2.5 µM DOPG SUVs as substrate. Assays contained 0.006 µg of the relevant mutant. Activity measured in the presence of H48N is expressed as a percentage of activity obtained without H48N present.

● - K124E/R127E

● - K53E/R54E/R58E

● - K53E/R54E/R58E/K124E/R127E

Each data set represents the mean of three experiments ± s.d.

This activity was not significant enough to prevent the H48N mutant from being used as an interfacial binding probe, which was the initial aim of this thesis.

Preliminary interfacial binding studies were carried out using the phospholipid-binding protein annexin V, and these experiments were then repeated using the H48N as the competing factor. As the results obtained with the H48N were comparable with those obtained using annexin V, it was concluded that the H48N could effectively compete for a phospholipid interface, and therefore be used to gauge the relative affinities of different types of PLA_2 for substrate interfaces.

The competitive effect of H48N on hydrolysis of cardiolipin vesicles by different $sPLA_2$s was studied. The results showed that the porcine pancreatic form of the enzyme was more inhibited by the H48N than the other $sPLA_2$s tested (nn-$sPLA_2$ and N1A hnpsPLA_2). That the pp-$sPLA_2$ was inhibited by the H48N clearly demonstrates that the human non-pancreatic secreted form of the enzyme can effectively bind to a cardiolipin interface, and therefore its lack of hydrolytic activity on this interface must be due to the enzymes inability to accommodate the bulky cardiolipin molecule into its active site in the correct orientation for hydrolysis.

The experiment concerning the competitive effect of H48N on the ability of N1A to hydrolyse the cell membrane of M. luteus highlighted the role of charge, and not activity on accessing this membrane. As a competitive effect was clearly seen in the presence of H48N, this confirms that the mutant enzyme can access the cell membrane effectively, even though it is essentially inactive. This adds weight to the theory that it is the cationic charges on the surface of hnpsPLA_2 that is responsible for its ability to access the bacterial cell membrane.

The results from the experiment which concerned the inhibitory effect of H48N on the hydrolysis of DOPG vesicles by tryptophan mutants of hnpsPLA_2 helped confirm that the binding of these mutants to DOPG interfaces is not

significantly enhanced by the presence of a Trp residue. This is in good agreement with the data produced from activity studies on these mutants when measured on DOPG. It is thought that hnpsPLA$_2$ can bind tightly to DOPG SUVs, and so the presence of a Trp residue should neither enhance nor hinder this binding. It would be of interest to study the binding of these mutants to vesicles of DOPC, in order to ascertain the contribution of the tryptophan residues to interfacial binding to this zwitterionic interface. Unfortunately, the H48N mutant does not bind to PC interfaces, and so cannot be used for this purpose.

The final experiment, which made use of the H48N mutant as a competitive binding agent, involved a number of charge-reversal mutants. These mutants were made in the laboratories of M.H. Gelb (Department of Chemistry, University of Washington, US) in order to study the contribution of electrostatic charge to interfacial binding. Many of the mutants showed higher catalytic activity than the N1A itself when assayed on vesicles of DOPG. This is thought to be due to the presence of negative charges, and the lessening of positive charges, which will prevent the enzymes from binding as tightly to the vesicles as the N1A. To get a more accurate picture of this changed interfacial binding, a number of these mutants were competed with the H48N for binding to DOPG. The overall inference from these studies is that it is the number of reversed charges that influences the binding affinity of these mutants, rather than any specific sites of mutation.

The H48N mutant has fulfilled the primary aim of this thesis, which was to produce an intact, catalytically inactive mutant of hnpsPLA$_2$ that could be used as a competitive binding agent to probe the interfacial binding of different sPLA$_2$s. It will provide a useful tool with which to help characterise the interfacial binding of future mutants of hnpsPLA$_2$ as well as to study the binding of different types of sPLA$_2$ to different substrate interfaces. However, the assay is most effective when comparing different enzymes on the same interface or different mutants of an enzyme provided that such mutants express sufficient activity that similar amounts of native and mutant protein can be compared in the assay.

179

Chapter Five - Crystallographic Studies of N1A and H48Q HnpsPLA$_2$

5.1 Introduction.

The H48Q mutant of hnpsPLA$_2$ was produced with the expectation that the resulting enzyme would be essentially inactive. Two previous examples of an equivalent mutation in both the bovine pancreatic and the bee venom enzymes were reported to be both structurally intact and catalytically inactive (< 0.001 % of the wild type) [96,97]. Based on these findings, the H48Q mutation seemed to be the ideal substitution for the catalytically critical His-48 residue in order to obtain such an inactive, active site mutant that could be used in interfacial binding studies.

However, as reported in detail in chapter three, characterisation of this mutant revealed that significant catalytic activity remained, even though this mutant lacks the histidine residue long known to be the crucial residue for catalytic activity. The H48Q mutant was shown to be structurally intact and was very similar to the N1A in terms of stability. The undertaking of a detailed crystallographic study of the H48Q was required in order to try and understand the mechanism by which this active site mutant can show significant activity.

As mentioned previously, the H48Q mutant also contains the mutation N1A to allow successful expression of the enzyme in *E. coli*. In order for a crystallographic study of the H48Q mutant to be valid, the N1A mutant must also be crystallised. This would enable an examination of the N-terminal region of the enzyme, to ensure that the N1A mutation does not significantly alter the conformation of this part of the enzyme, and to provide a model with which to compare the H48Q structure.

5.2 Crystallographic Methods.

5.2.1 Growing Protein Crystals.

Protein crystals are ordered 3-D arrays of protein molecules, which are formed by slow, controlled precipitation of the protein. The method used to grow crystals in the case of this report was the 'hanging-drop' method [115,116]. In this method, a reservoir containing buffer and precipitant, the concentration of which is optimal for crystal growth, are sealed in a container, usually a well in a 24-well Linbro plate, by a greased cover slip. A droplet containing 50 % protein solution, 50 % reservoir solution is suspended from this cover slip. Within this closed system, the droplet and reservoir will equilibrate by vapour diffusion, until the concentration of precipitant in the droplet has increased to that which is optimal for crystal growth, i.e. the concentration of the reservoir solution.

5.2.2 Data Collection.

Data from the N1A crystal were collected in house, and data from the H48Q mutant were collected from a synchrotron source at Grenoble as described in section 2.7 [117,118]. Data was collected using the oscillation method, which involves rotating the crystal through small angles e.g. ~ 0.25 $^{\circ}$ - 1.5 $^{\circ}$, and collecting the images produced from each oscillation [119]. The total number of images collected depends on the space group of the crystal, and is chosen in order to maximise the total number of reflections that can be recorded. Seven different crystal classes are possible for protein crystals, and assigning of a space group to a data set requires examination of the diffraction pattern to find symmetry and systematic absences that are characteristic of the different space groups. The 'International Tables for Crystallography' must be consulted in order to identify the space group based on these symmetry patterns [120].

5.2.3 Data Processing.

Data processing involves converting the raw data into a list of indexed reflections with corresponding amplitudes. The initial aim of processing is to determine the orientation and unit cell of the crystal. With this knowledge, it is possible to predict the positions where reflections will be found, and then measure the intensity of each reflection. After the data have been collected they must be processed, so that each of the recorded reflections has an index, which take the form of Miller coordinates (h,k,l). As each image may have a slightly different incident fluctuation due to fluctuations in the beam, the images have to be scaled so that equivalent reflections are measured according to the same scale. Equivalent reflections i.e. those with the same Miller indices, or symmetry equivalent ones can then be averaged. A further problem encountered when collecting data is that of measuring partial reflections. Due to the rotation of the crystal during data collection some reflections will only be measured partially, but these reflections may be measured fully elsewhere. By estimating the partiality of these reflections, it is possible to estimate the intensity of the reflection had it been fully recorded. In the case of this report, the program MOSFLM [121] was used to process the data, and the program Scala from the Collaborative Computing Project Number 4 (CCP4) suite was used to merge and scale the data [122].

5.2.4 Molecular Replacement.

Molecular replacement is a technique that allows the initial phases of an unknown structure to be calculated based on those of a known, homologous structure [123]. In this method, the known structure is fitted into the unit cell of the unknown structure by way of rotation and translation functions that position the known structure as accurately as possible onto the structure under investigation.

The program MOLREP was used for molecular replacement in the case of this report [124].

5.2.5 Refinement.

Following molecular replacement the model will contain errors, and these can be minimised by manually rebuilding and refining the model in order to improve the agreement between the experimental observations and the model itself. The expected structure factors can be calculated from the model - F_{calc} - and this can then be compared with the observed structure factors - F_{obs} [125]. Refinement of the model will reduce the difference between these two parameters. Initial refinement of the model involved using rigid-body refinement, along with grouped temperature factor refinement, to adjust the gross structural features of the model. This was followed by cycles of simulated annealing, which can use either torsion or Cartesian refinement, and which involves simulating heating the model to 2500 K, and cooling to 300 K in steps of 25 K to allow freer movement and better placing of the atoms [126,127]. Individual temperature factor refinement was also carried out using the CNS program suite [128]. If the resolution of the data does not extend to ~ 2.5 Å, then only grouped temperature refinement should be performed. R-factors were used throughout the refinement procedure to ensure that the refinement was proceeding in the correct direction. The R-factor is a measure of the agreement between the observed data and the calculated data - as this agreement improves the R-factor will tend to zero. The R_{free}-factor is a further indication of the accuracy of the fit. This is calculated using only 5 % of the data, which is then excluded from refinement and so can report only on genuine improvements in the model. An increase in either R-factor at any time during the refinement indicates that the data is being over fit, and refinement must not proceed.

5.2.6 Electron Density Maps.

Electron density maps were calculated using the CCP4 suite. Electron density maps were either 2Fo - Fc maps or Fo - Fc maps, where Fo is the observed structure factors for the model, and Fc represent the calculated structure factors (see F_{obs}, F_{calc} above). The program QUANTA was used for visualisation purposes [129].

5.3 Crystallography of N1A HnpsPLA₂.

The conditions used to grow crystals of the N1A and H48Q mutants of hnpsPLA₂ were modified from those published by Scott *et al* describing the crystallisation conditions for the wild type hnpsPLA₂ isolated from the synovial fluid of arthritic patients [71]. Crystals of N1A were grown at 4 °C from droplets containing ~ 10 mg/ml protein, 5 mM Ca^{2+}, 0.1 M Tris. HCl (pH 7.5), 5.5 M NaCl and 0.5 mM ∃-octylglucoside. A typical N1A crystal is shown in figure 5.1. A single crystal was used for data collection, which was carried out as described in section 2.7. Data collection proceeded through 60 °, with an oscillation angle of 1 °. The crystal belonged to space group $P6_122$, as determined by the symmetry and systematic absences in the diffraction pattern. The unit cell parameters were a = 74.79, b = 74.79 and c = 88.891, and there was one molecule in the asymmetric unit. Figure 5.2 shows the packing of molecules in a unit cell with $P6_122$ space group. The data set contains 31180 reflections (4693 unique), with an R_{merge} of 0.066 and a completeness of 99.5 % at 2.6 Å. The 2.2 Å resolution crystal structure of wild type hnpsPLA₂ was used as a search model. The only difference in sequence between the two is the N1A mutation. As the space group of the wild type model is also $P6_122$, and the unit cell dimensions were the same, no molecular replacement was required to fit the N1A data onto the model. The initial R-factor was 0.33 (R_{free} = 0.38). A summary of the crystal data and relevant parameters are shown in table 5.1.
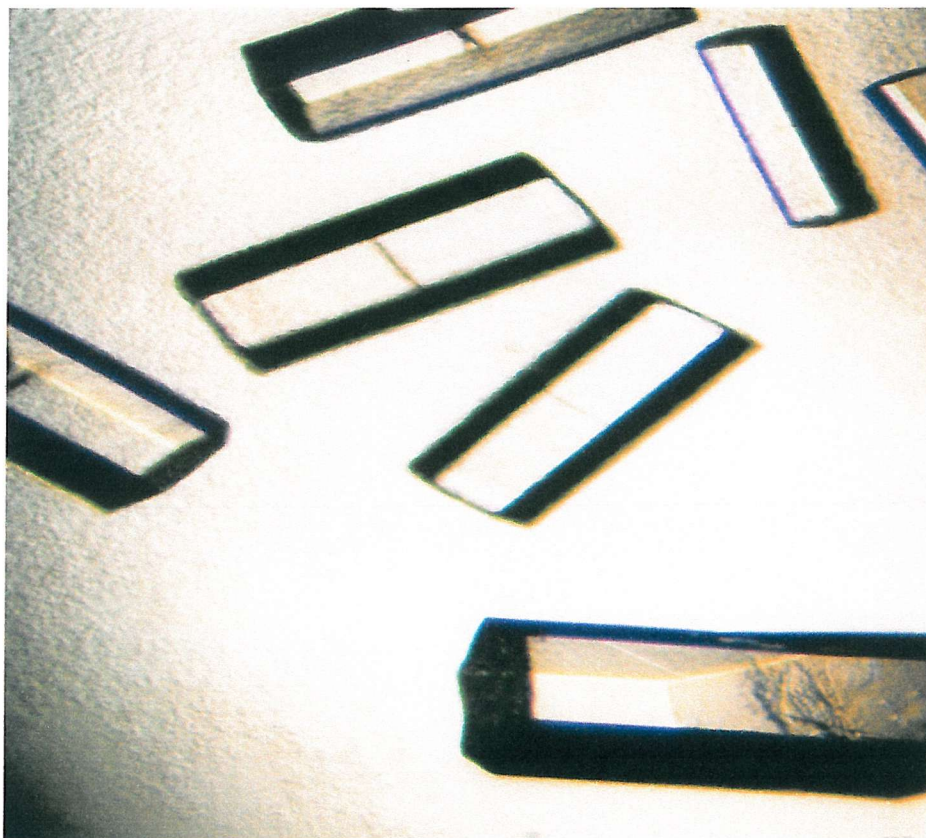
Figure 5.1 Photograph of a Typical Crystal of N1A HnpsPLA$_2$.

Crystals were grown as described previously.
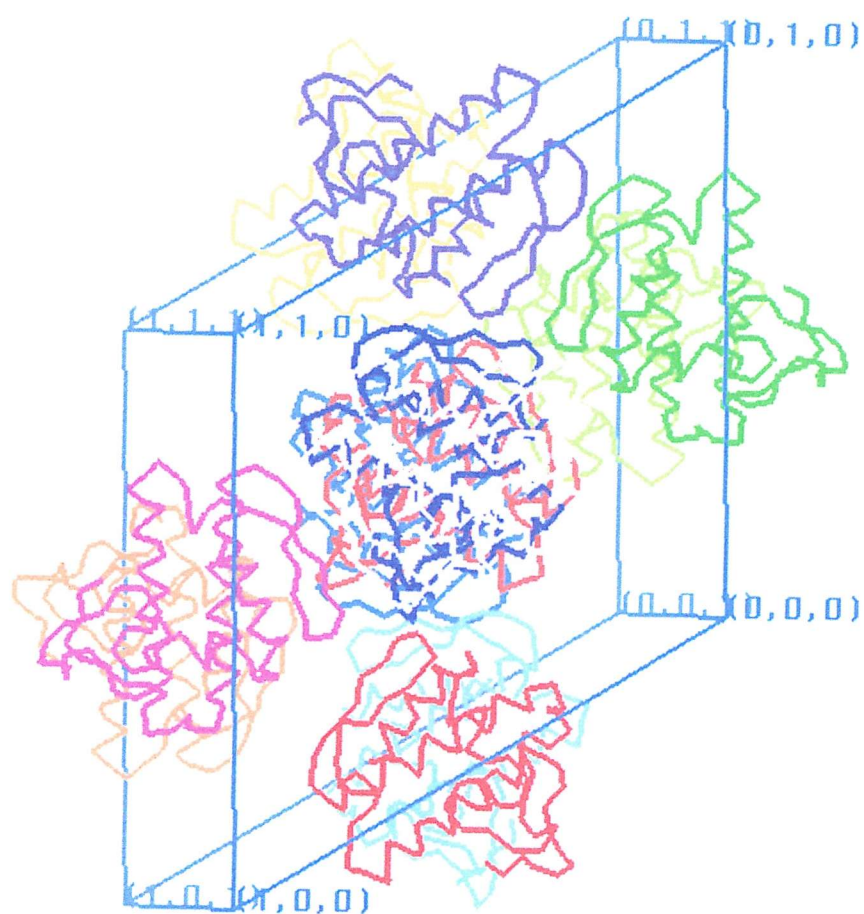
Figure 5.2 Packing Diagram Showing N1A HnpsPLA$_2$ in the P6$_1$22 Space Group.

The diagram was generated using the graphics program Quanta [129].

Space Group	$P6_122$
Cell Parameters	a=b=74.79, c=88.89
Cell Angles	$\alpha=\beta=90$, $\gamma=120$
Resolution Range	15 - 2.6 Å
R-factor (R-free) - Initial	0.3324 (0.3755)
R-factor (R-free) - Final	0.2161 (0.2984)
Number of Reflections Measured	31180
Number of Unique Reflections	4693
R_{symm}	0.066
Multiplicity	3.4
Completeness (%)	99.5
Number of Protein Atoms	931
Number of Ca^{2+} Ions	2
Number of Waters	93

Table 5.1 Summary of N1A HnpsPLA$_2$ Crystal Data

5.3.1 The Crystal Structure of N1A HnpsPLA₂.

The N1A mutant of hnpsPLA$_2$ was crystallised in order that this could be used as a model to compare the structure of the H48Q mutant with, as the H48Q also contains the N1A mutation. In order to do this, the N1A structure must first be compared with the true wild type structure to ensure there are no significant differences between the two. HnpsPLA$_2$ isolated from the synovial fluid of arthritic patients has been solved to a resolution of 2.2 Å, and this structure was used as a model with which to solve the structure of the N1A [71]. The initial comparison was of the C-α backbone of the N1A with the wild type. This is shown in figure 5.3, and there are no obvious differences in the N1A model as compared with the wild type. The secondary structure comparison in figure 5.4 confirms that the two structures are essentially the same. Any minor discrepancies between the two structures are most likely due to the difference in resolution of the models. This will limit the accuracy of some regions of the structure. The grey spheres in the diagram are the two calcium residues that were modelled into the N1A.

The most important region of the N1A structure to compare with the wild type is the N-terminal region, where the Asn → Ala substitution is contained. Figure 5.5 shows a close-up of this area, and the Asn-1 of the wild type and the Ala-1 of the N1A mutant can be seen. It is clear from this that the N-terminal residues are in the same orientation as one another, and that the N1A mutation has not caused any disruption to the protein structure in this region.

The picture in figure 5.6 shows an overlay of the active site residue His-48 and the calcium-binding residue Asp-49 from the wild type and N1A structures. In this crucial part of the structure, the active site residues from the N1A mutant occupy identical locations to those from the wild type structure, again confirming the accuracy of the N1A model. The two catalytic waters and the calcium ion that is required for catalysis are shown in the N1A structure.
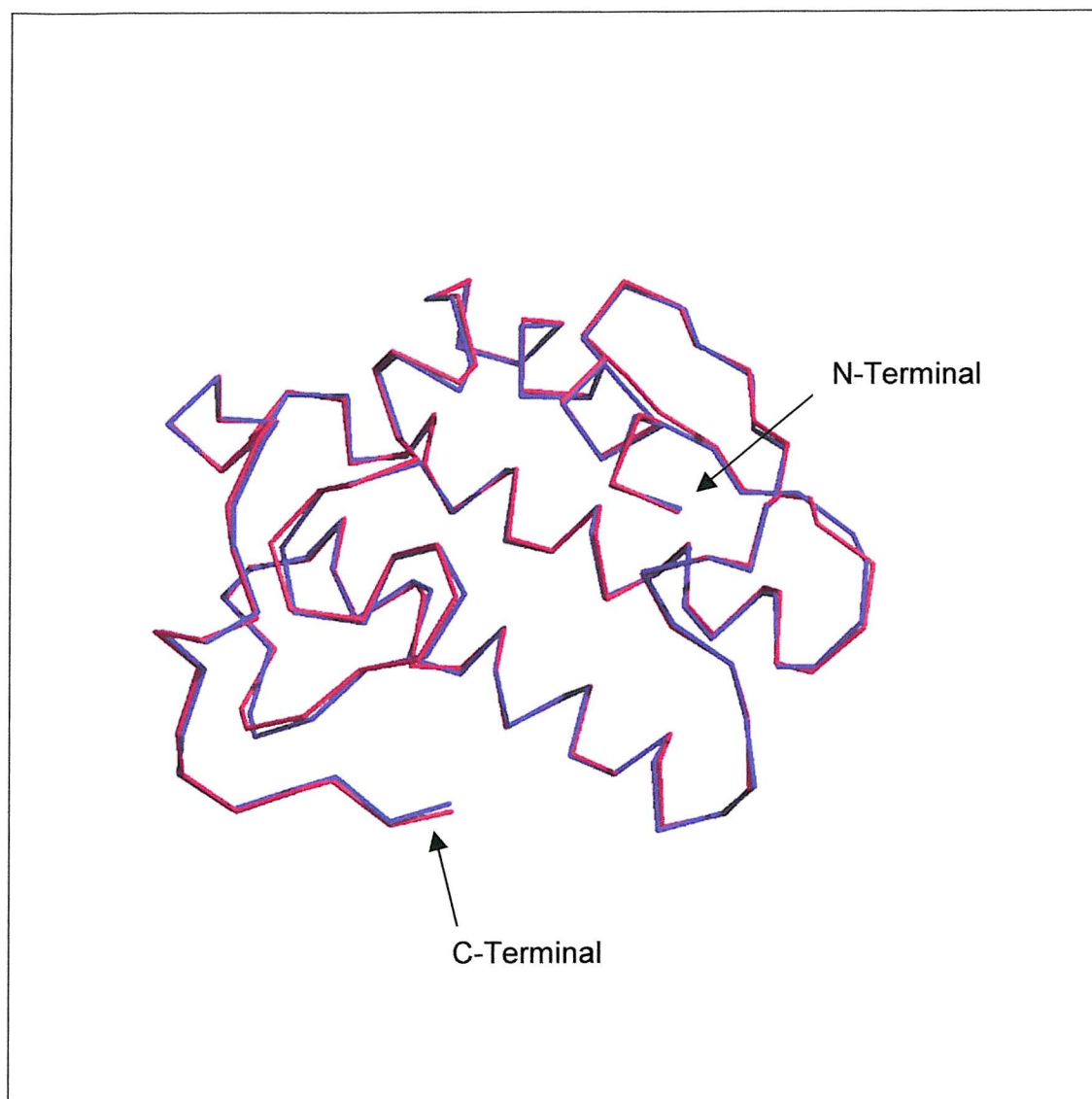
Figure 5.3 A Comparison of the C-α Trace of N1A and Wild type HnpsPLA₂.

The programs Xtalview and Raster3d were used to create the model [131,132].

Purple - N1A hnpsPLA₂

Pink - Wild type hnpsPLA₂
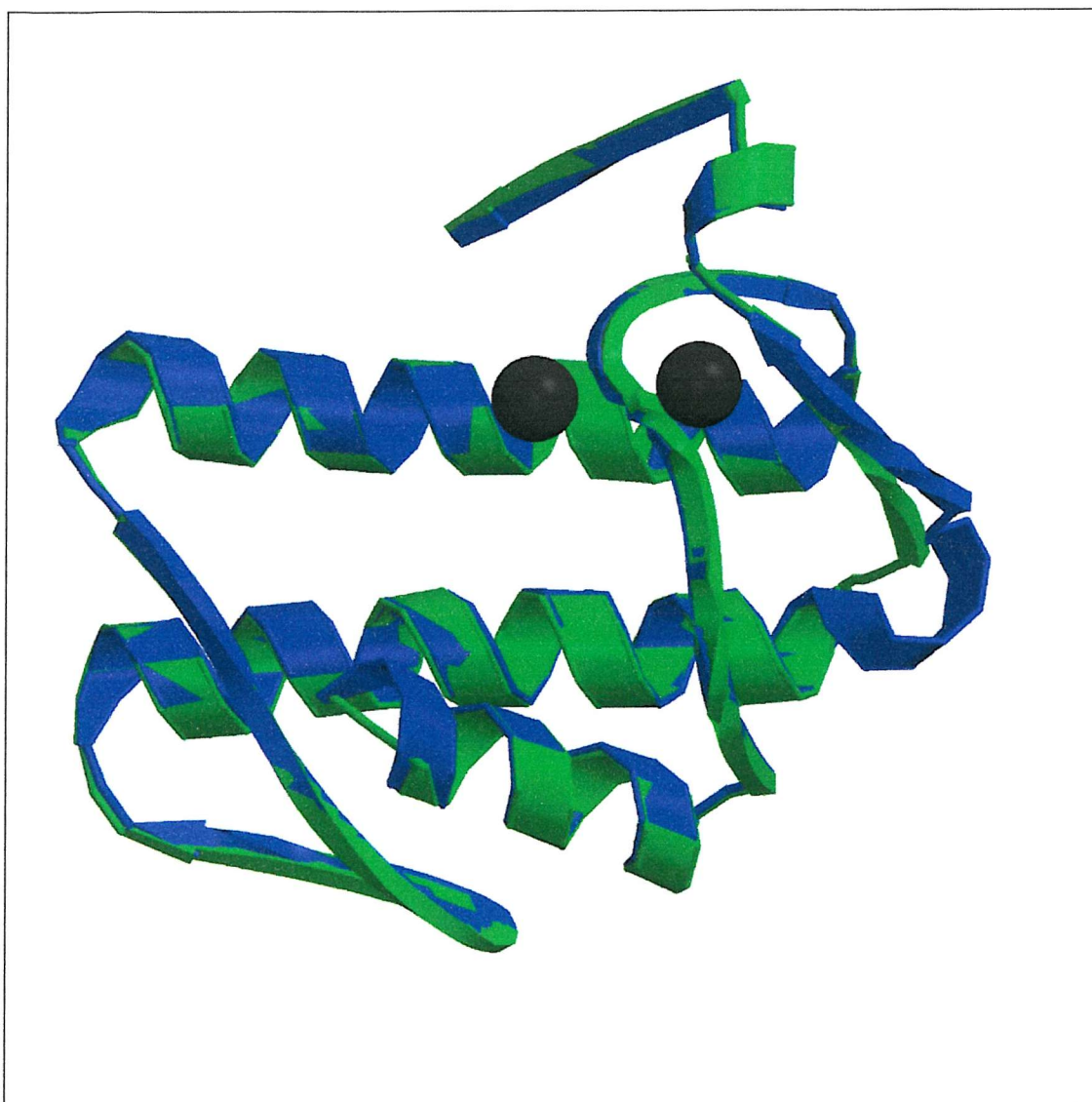
Figure 5.4 A Comparison of the Secondary Structures of N1A and Wild type HnpsPLA$_2$.

The program MOLSCRIPT was used to produce the picture [133].

The grey spheres represent two calcium ions found in the N1A structure.

Blue - N1A hnpsPLA$_2$

Green - Wild type hnpsPLA$_2$
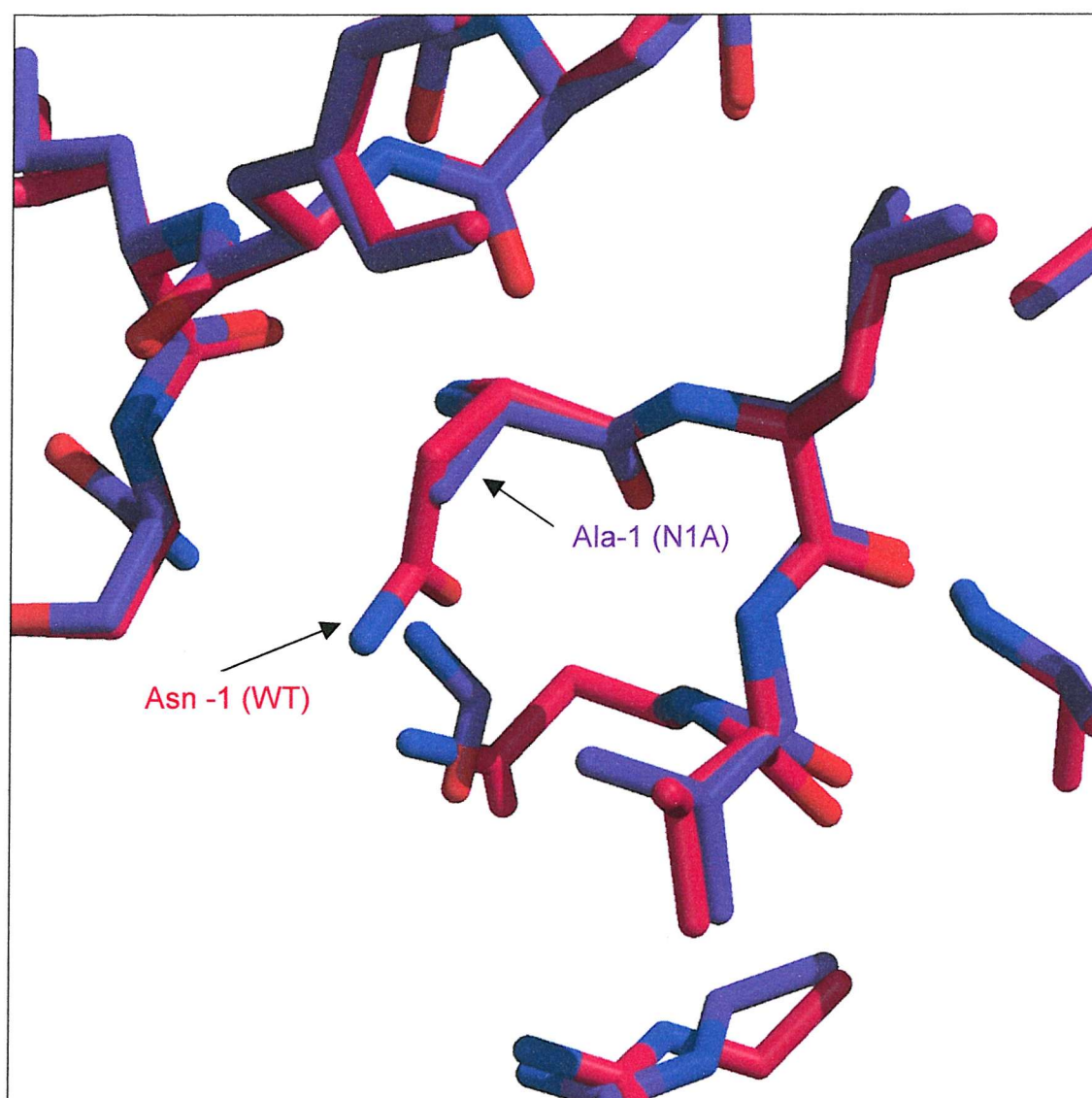
Figure 5.5 Representation of the N-Terminal Residues of N1A and Wild Type HnpsPLA$_2$.

The diagram was generated using the programs Xtalview and Raster3d [131,132].

Purple - N1A hnpsPLA$_2$

Red - Wild type hnpsPLA$_2$
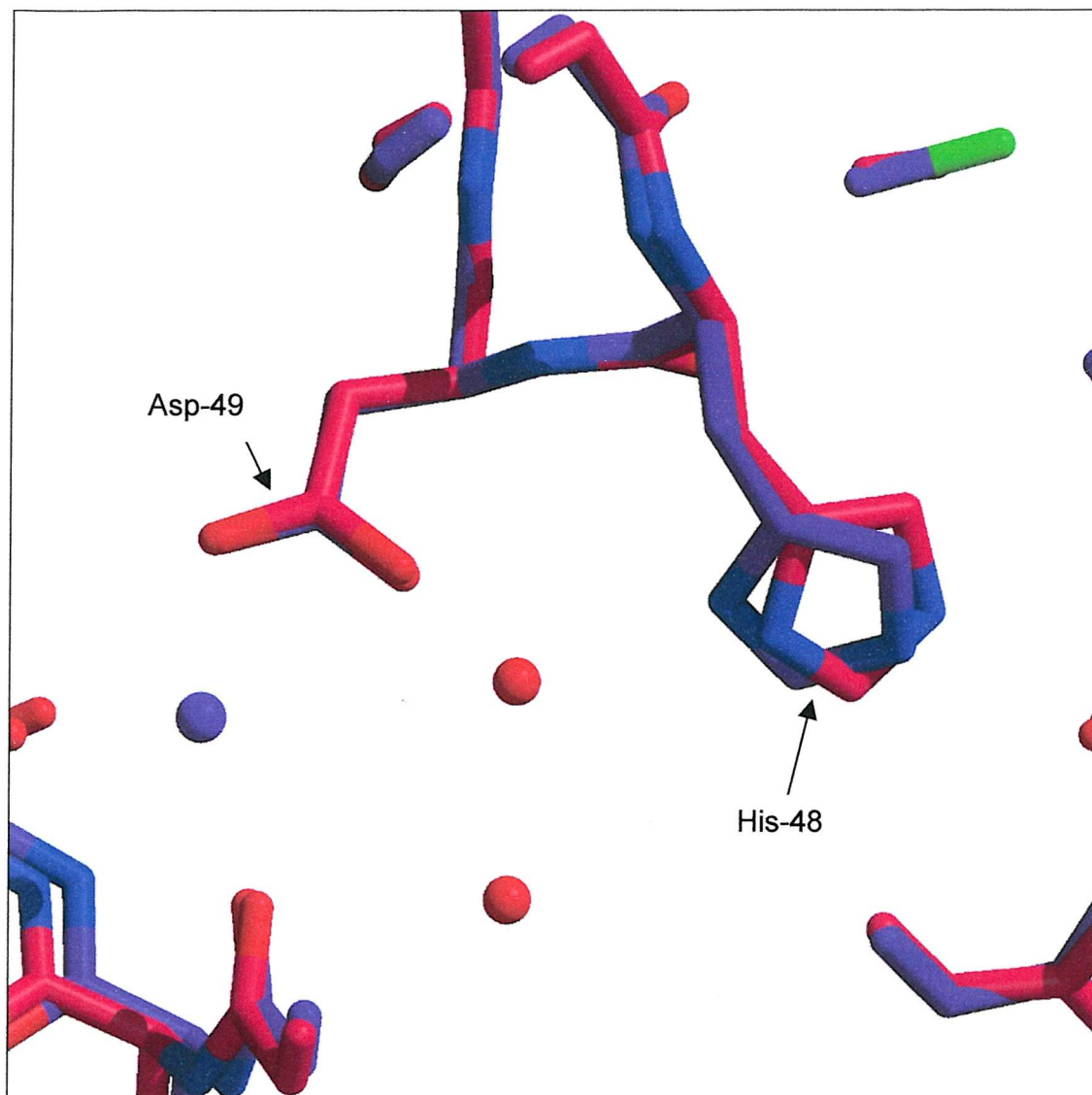
Figure 5.6 The Active Site Residues of N1A and Wild Type HnpsPLA₂.

The picture was generated using the programs Xtalview and Raster3d [131,132].

The purple and red spheres are calcium ions and water molecules respectively, from the N1A structure.

Purple - N1A hnpsPLA₂
Red - Wild type hnpsPLA₂

Figure 5.7 shows only the N1A model, and shows the active site of the enzyme in more detail. The catalytic residue His-48 can be seen with the two associated catalytic waters, adjacent to the calcium-binding residue Asp-49. All of these features have good, well-defined electron density surrounding them.

The view in figure 5.8 also shows the active site of the enzyme, but this time the catalytic dyad of His-48 and Asp-99 is shown. The two catalytic waters are also shown, and these are associated with the nitrogen on the imidazole ring of the histidine residue. In the catalytic mechanism, water-1 is H-bonded to the nitrogen atom of the His-48 residue. Water-2 is deprotonated and the proton is accepted by water-1. The deprotonated water-2 may now act as a nucleophile, and attack the sn-2 ester bond of the phospholipid. The calcium ion is required to coordinate the nucleophilic water initially, and then to help stabilise the tetrahedral intermediate [75].

Figure 5.9 shows the active site residues in relation to the hydrophobic channel, which connects the active site with the interfacial binding surface. The presence of a histidine residue at position 6 is unique to this type of sPLA$_2$ and in the N1A structure, as was found in the wild type structure; the side chain of this residue is inserted into the 'mouth' of the channel [12,71]. In the absence of substrate, the nitrogen of this histidine will be associated with a number of water molecules that lead up to the active site. These can be seen in the figure. It is thought that substrate entry into the active site channel will displace these water molecules, and result in the displacement of the imidazole ring of the His-6 from the channel [71].

The surface potential of N1A has been calculated, and is shown in figure 5.10. This highlights the global cationic charge of the enzyme, and also shows the calcium ions and water molecules required for catalysis at the active site.

194
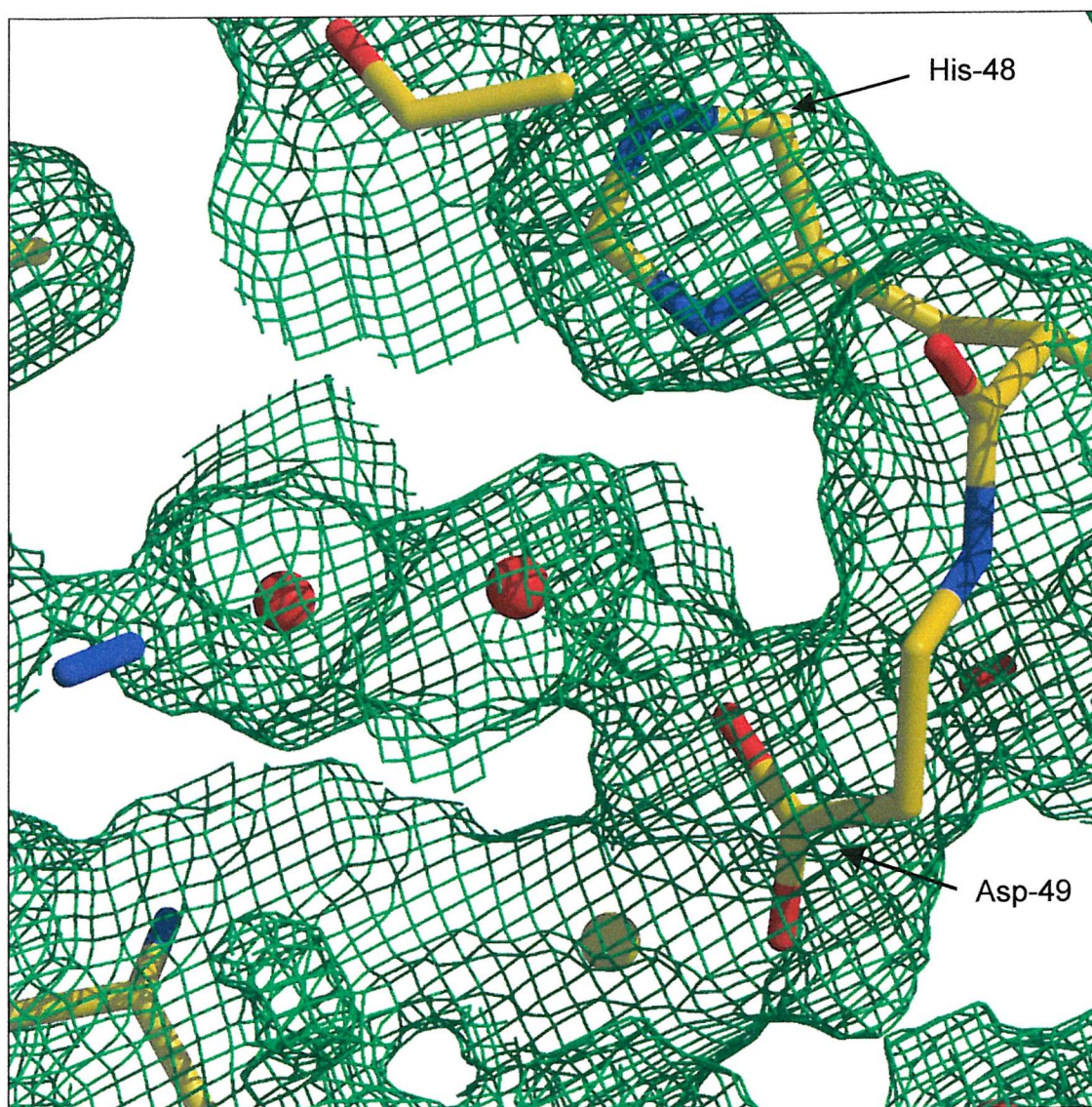
Figure 5.7 The Active Site of N1A HnpsPLA$_2$.

Xtalview and Raster3d were used to generate the picture. Electron density is shown for a 2Fo - Fc map at the 1 σ level [131,132].

Red and yellow spheres represent water molecules and calcium ions respectively.
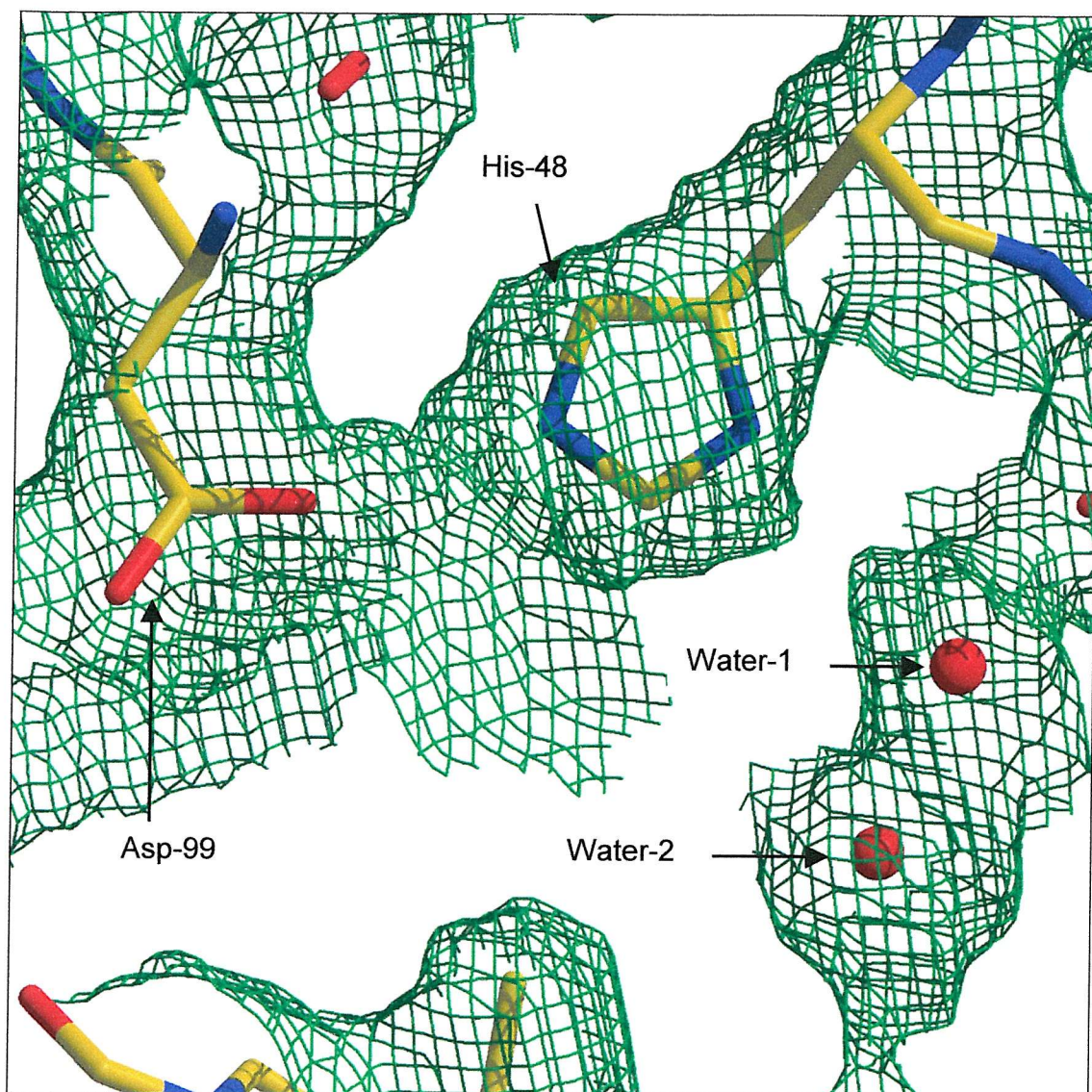
Figure 5.8 The Active Site Catalytic Dyad of N1A HnpsPLA$_2$.

Xtalview and Raster3d were used to generate the picture. Electron density is shown for a 2Fo - Fc map at the 1 σ level [131,132].

Red spheres represent water molecules.
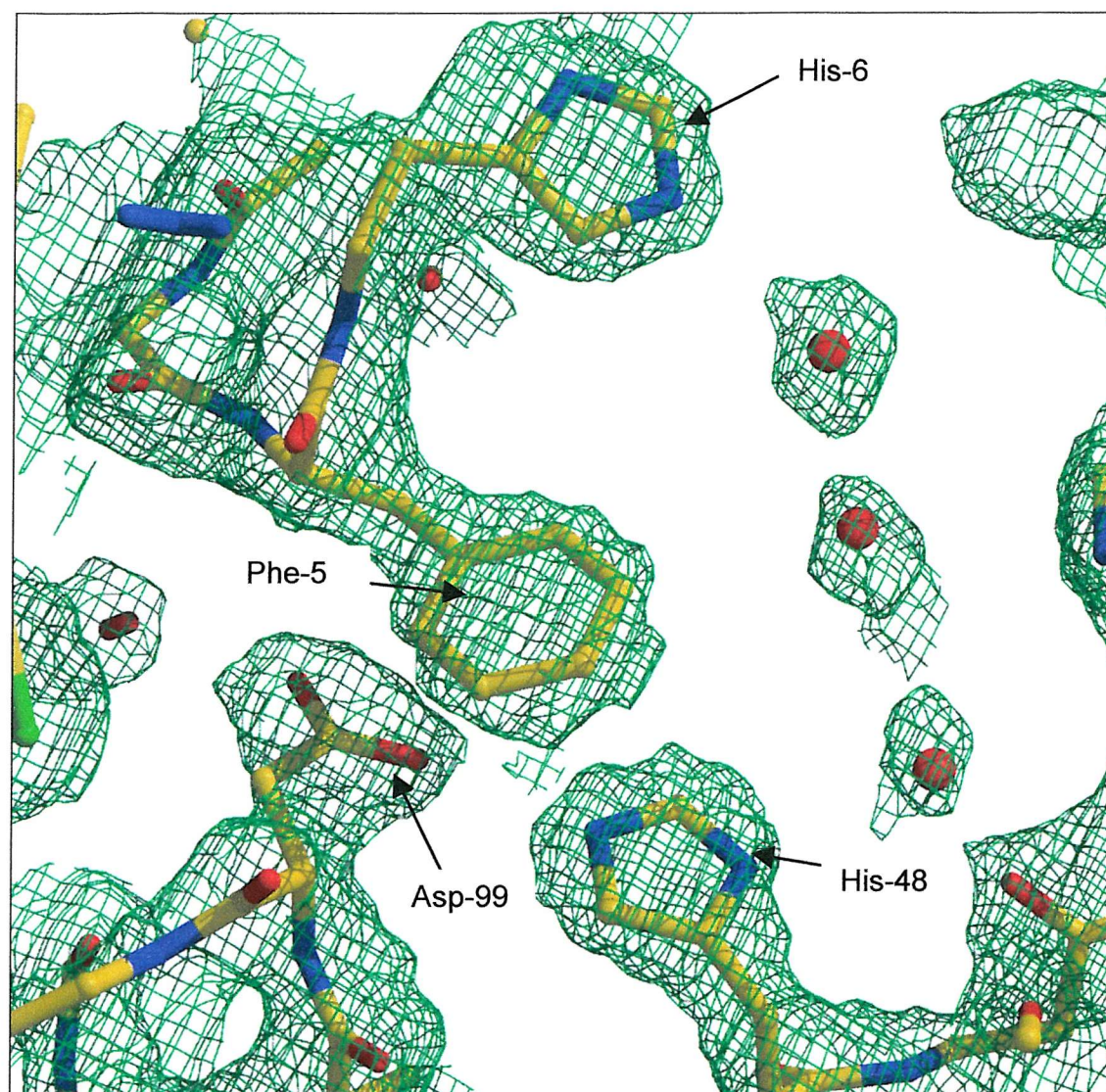
Figure 5.9 The Active Site and Hydrophobic Channel of N1A HnpsPLA$_2$.

Xtalview and Raster3d were used to generate the picture. Electron density is shown for a 2Fo - Fc map at the 1 σ level [131,132].

Red spheres represent water molecules.
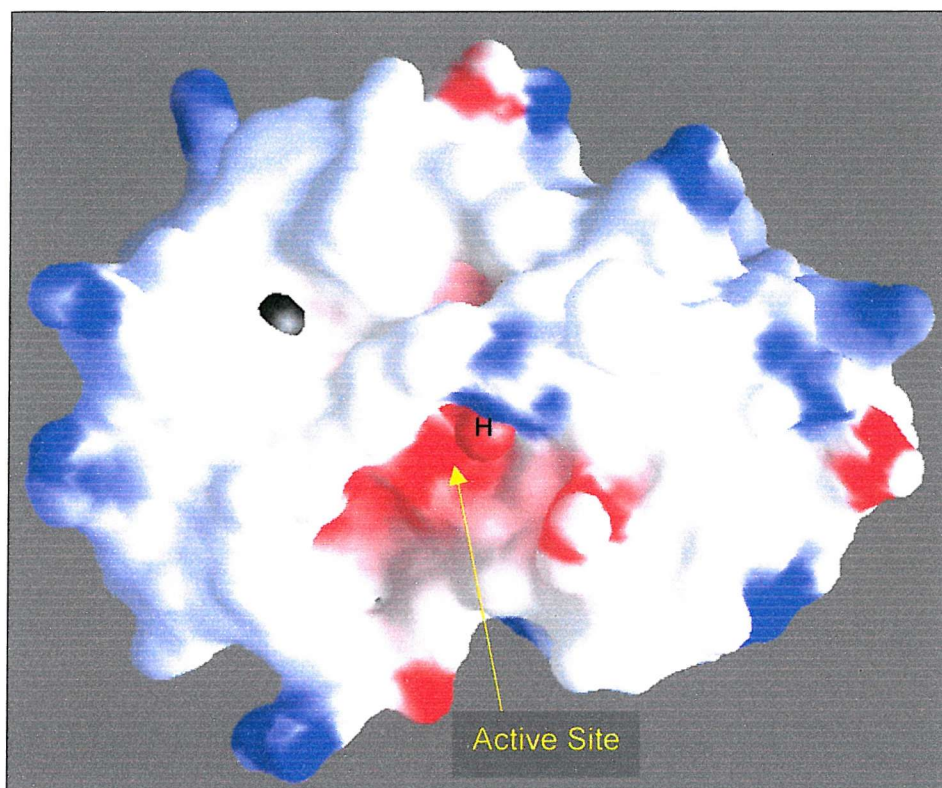
Figure 5.10 Surface Potential Diagram Showing the Distribution of Charge on the Surface of N1A HnpsPLA$_2$.

The figure was generated using the program GRASP [134].

Red spheres (H) represent water molecules, grey spheres represent calcium ions.

Red - Acidic residues

Blue - Basic residues

It is possible to see the channel leading from the interfacial binding site to the active site that contains the His-48/Asp-99 catalytic dyad along with the aforementioned calcium ion and waters. Overall, the results show that the N1A structure is identical to that of the wild type enzyme, and that the N1A mutation introduced to aid expression in *E. coli* has not caused any change in the conformation of the N-terminal. The program PROCHECK was used to calculate a Ramachandran plot for the model, and this showed that 99.1 % of residues were in permitted regions [130,135]. The data allowed two calcium ions to be included in the structure – the primary calcium, which is found in the active site and is essential for catalytic activity, and a secondary calcium ion whose function is not clearly defined. Two catalytic water molecules and 93 structural waters were also assigned density on the model.

5.4 Crystallography of H48Q HnpsPLA$_2$.

Crystals of the H48Q were grown at 4 $^{\circ}$C as the N1A (see above), except the [NaCl] was 5.3 M and the pH 7.4. A single crystal was used for data collection, which was carried out as described in section 2.7. Data collection proceeded through 180 $^{\circ}$, with an oscillation angle of 1 $^{\circ}$. A typical image is shown in figure 5.11. The crystal belonged to space group C2, as determined by the symmetry and systematic absences in the diffraction pattern. The unit cell parameters were a = 119.58, b = 34.42 and c = 73.91, with a unique β angle of 126.6 and there were two molecules in the asymmetric unit. Figure 5.12 shows the packing of molecules in a unit cell with C2 space group. The data set contains 161166 reflections (37032 unique), with an R_{merge} of 0.089 and a completeness of 83.6 % at 1.5 Å. The 2.2 Å resolution crystal structure of wild type hnpsPLA$_2$ was used as a search model [71]. The only differences in sequence between the two are the N1A and H48Q mutations.
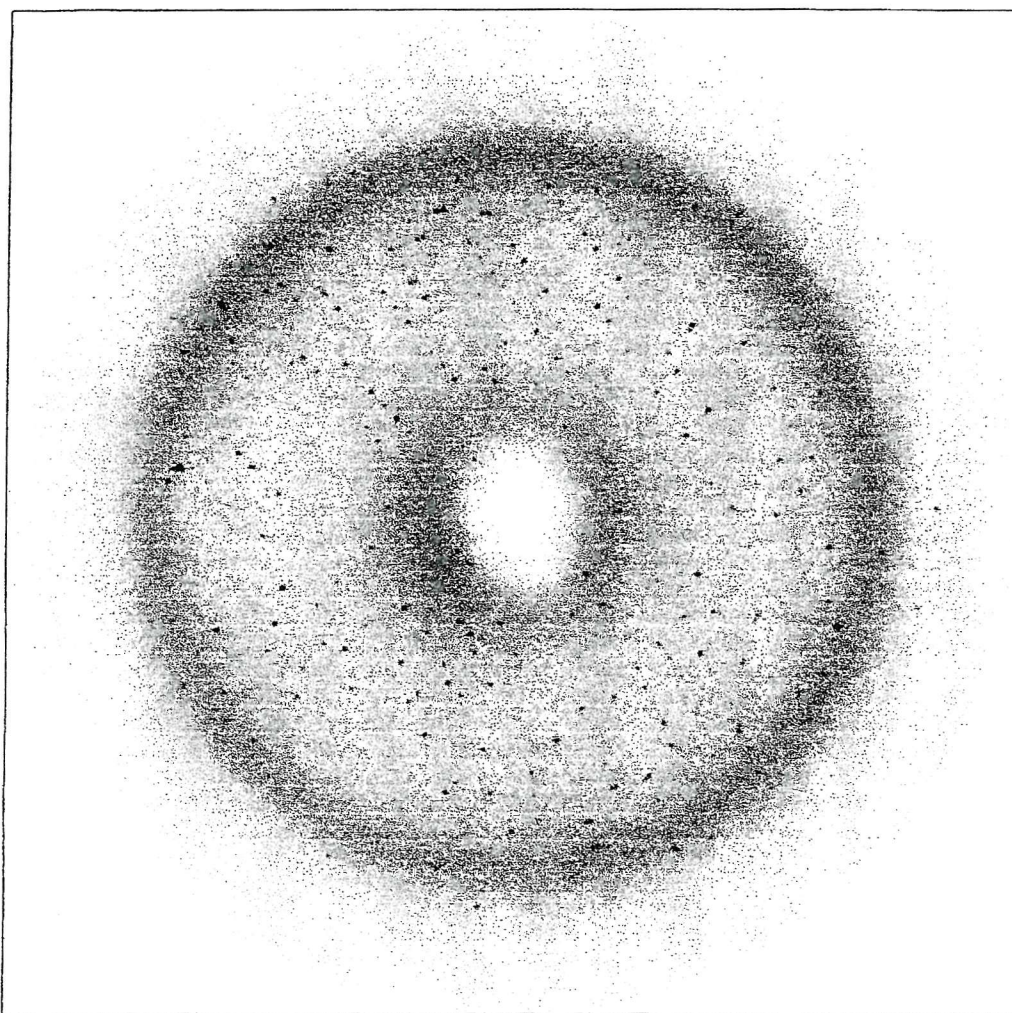
Figure 5.11 A Typical Image Measured from the Diffraction of H48Q HnpsPLA$_2$ Crystals.
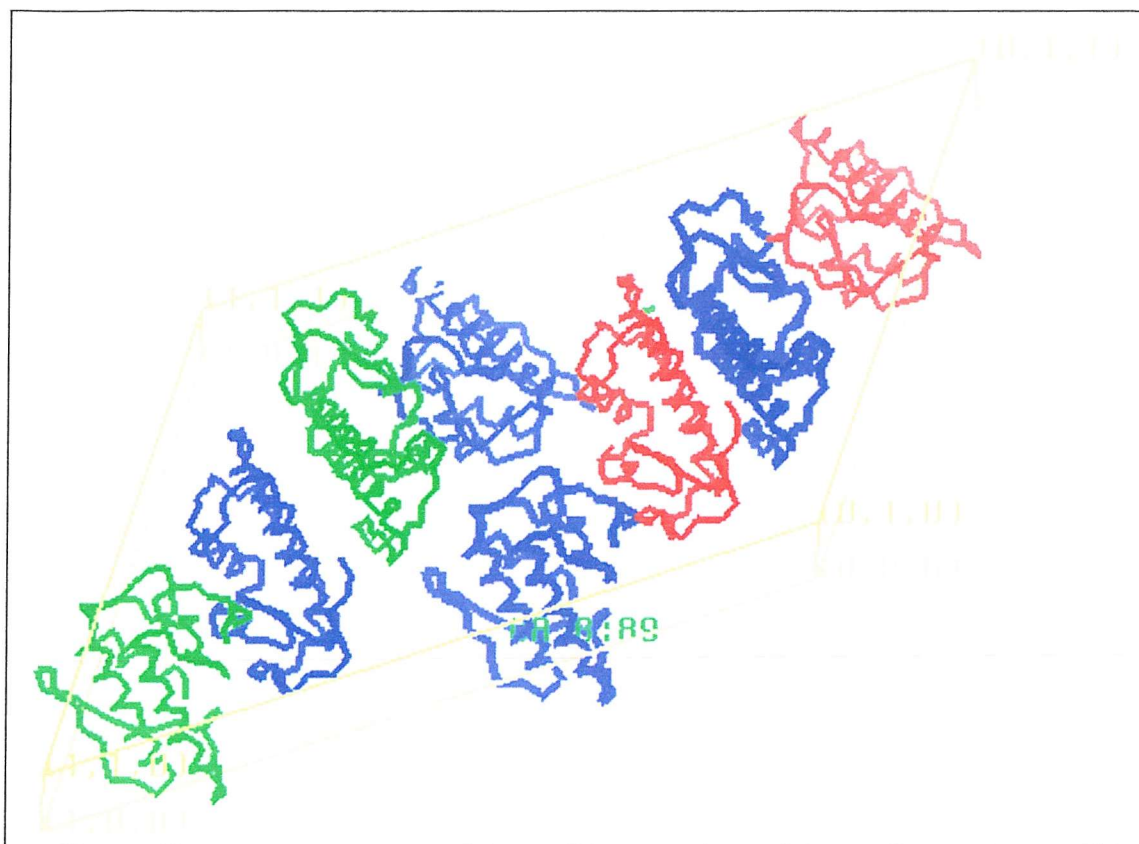
Figure 5.12 Packing Diagram Showing H48Q HnpsPLA$_2$ in the C2 Space Group.

The diagram was generated using the graphics program Quanta [129].

Molecular replacement was required to fit the H48Q data onto the model. The initial R-factor was 0.41 (R_{free} = 0.42). A summary of the crystal data and relevant parameters are shown in table 5.2.

5.4.1 The Crystal Structure of H48Q HnpsPLA$_2$.

A comparison of the C-α trace of the H48Q mutant with the N1A is shown in figure 5.13. The structures show good similarity to one another, indicating that the overall structure of the active site mutant is correct. Figure 5.14 shows the C-α backbone trace of the H48Q and the N1A superimposed onto that of the wild type, which was the original model for the structures. Some regions of the H48Q chain are slightly different to the wild type and N1A, but as the resolution of the H48Q model is much higher than for the other two structures (1.5 A compared with 2.2 Å (wild type) and 2.6 Å (N1A)), these areas may actually represent the more accurate conformation. Also, due to the fact that the crystals are from different space groups, slight differences may represent differences in contacts due to the crystal packing. The secondary structure comparison in figure 5.15 also confirms that the gross structure of the H48Q is the same as the N1A. The calcium ions present in the structures are also shown for both models, and these are shown to be in the same position in both structures.

The H48Q mutant was crystallised in order to examine the active site, to try and explain the catalytic activity shown by this mutant. Therefore, it was important to examine closely this region of the enzyme, not only to rationalise the activity seen, but also to check that the overall conformation of the residues in this area does not differ significantly from the N1A. Figure 5.16 shows a global comparison of the active site of the H48Q and N1A. Along with the residue at position 48, the calcium binding Asp-49 residue is shown. The two structures show good similarity in terms of the positioning of the residues and the bound water and calcium molecules.

Space Group	C2
Cell Parameters	a=119.58, b=34.42, c=73.91
Cell Angles	$\alpha=\gamma=90$, $\beta=126.56$
Resolution Range	15 - 1.5 Å
R-factor (R-free) - Initial	0.4149 (0.4209)
R-factor (R-free) - Final	0.2782 (0.3064)
Number of Reflections Measured	161166
Number of Unique Reflections	37032
R_{symm}	0.089
Multiplicity	2.4
Completeness (%)	83.6
Number of Protein Atoms	1861
Number of Ca^{2+} Ions	2
Number of Waters	92

Table 5.2 Summary of H48Q HnpsPLA$_2$ Crystal Data
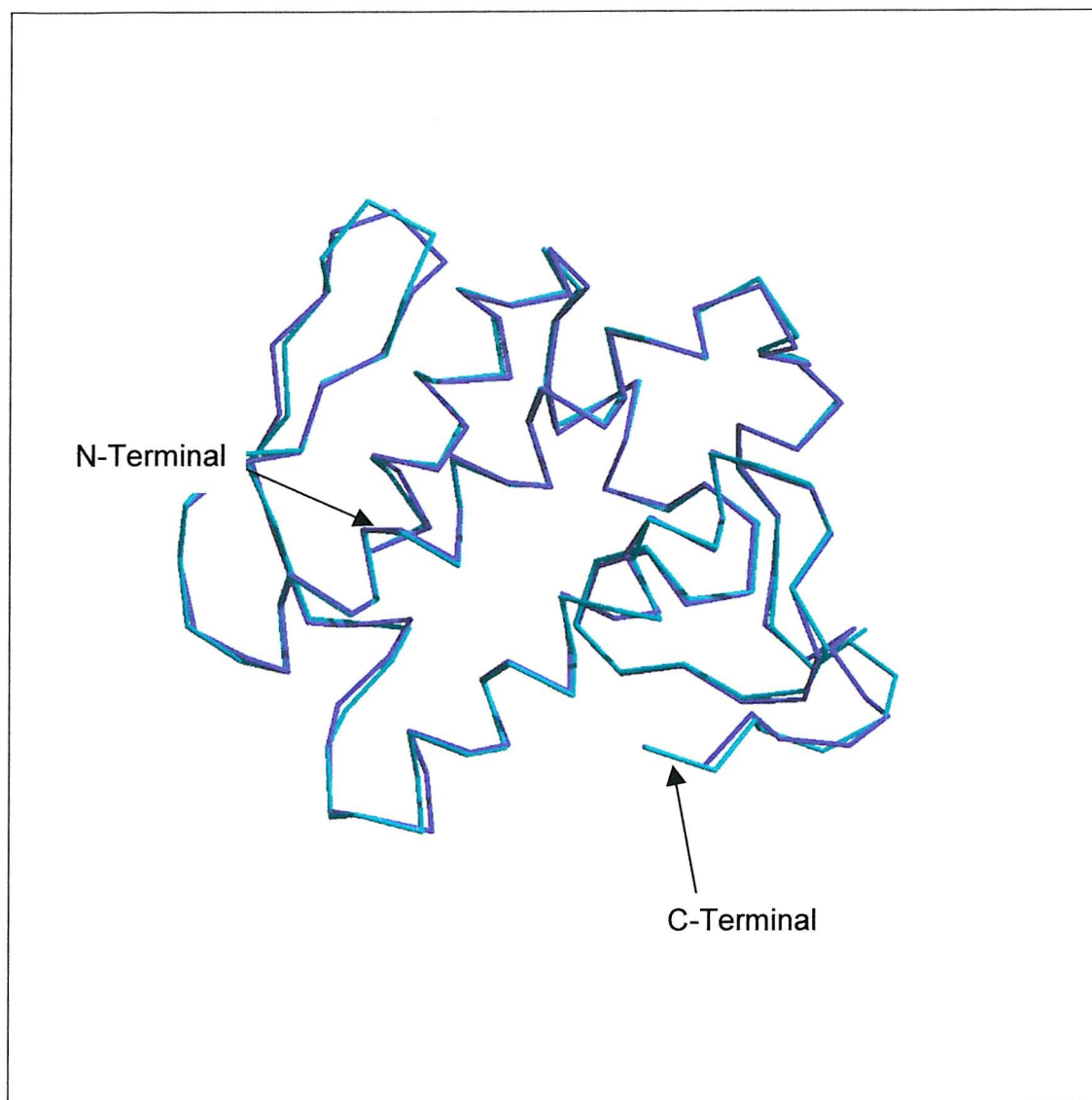
Figure 5.13 A Comparison of the C-α Trace of N1A and H48Q HnpsPLA$_2$.

The programs Xtalview and Raster3d were used to create the model [131,132].

Purple - N1A hnpsPLA$_2$

Turquoise - H48Q hnpsPLA$_2$
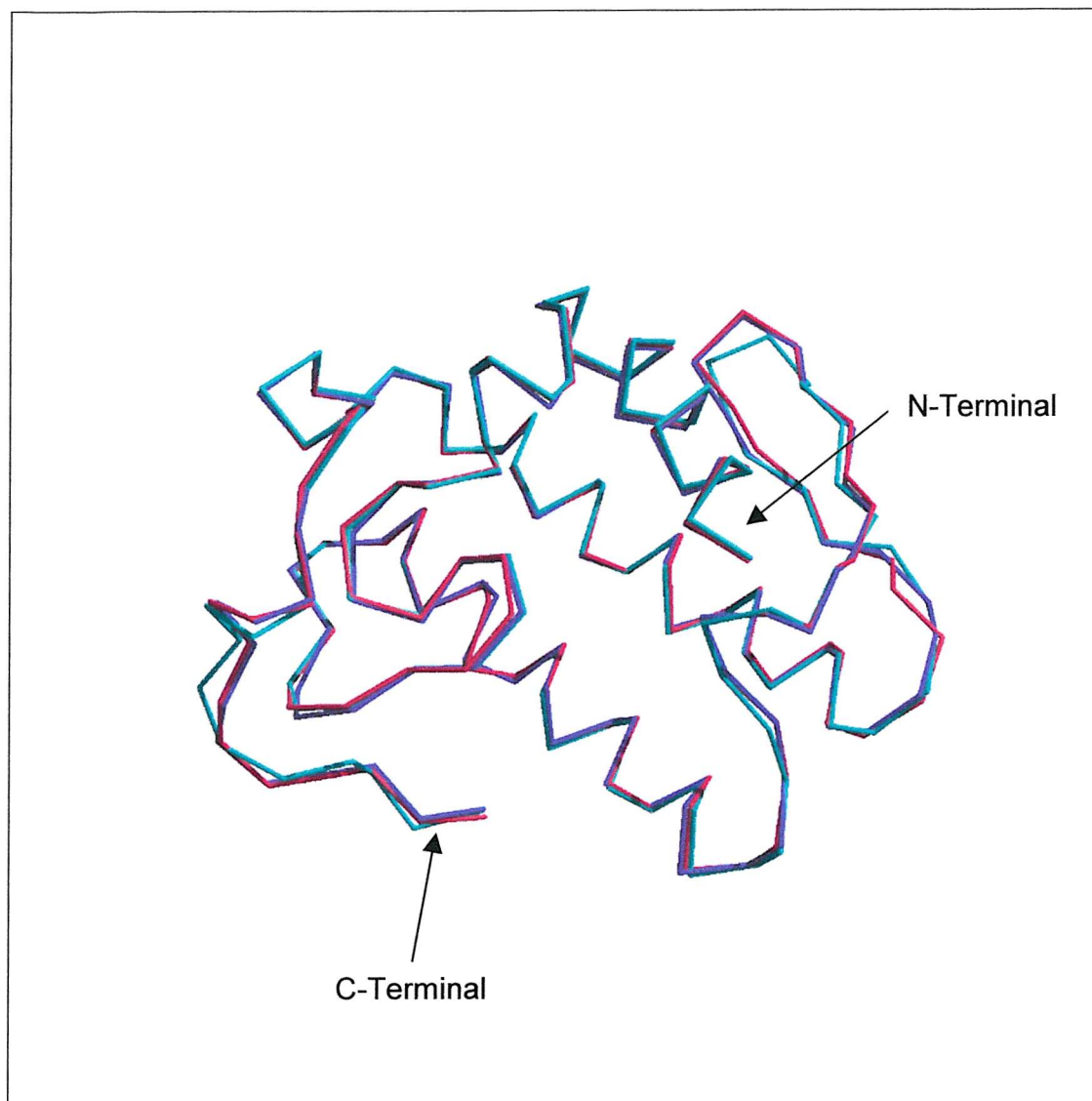
Figure 5.14 A Comparison of the C-α Trace of N1A, H48Q and Wild type HnpsPLA$_2$.

The programs Xtalview and Raster3d were used to create the model [131,132].

Purple - N1A hnpsPLA$_2$

Turquoise - H48Q hnpsPLA$_2$

Pink - Wild type hnpsPLA$_2$
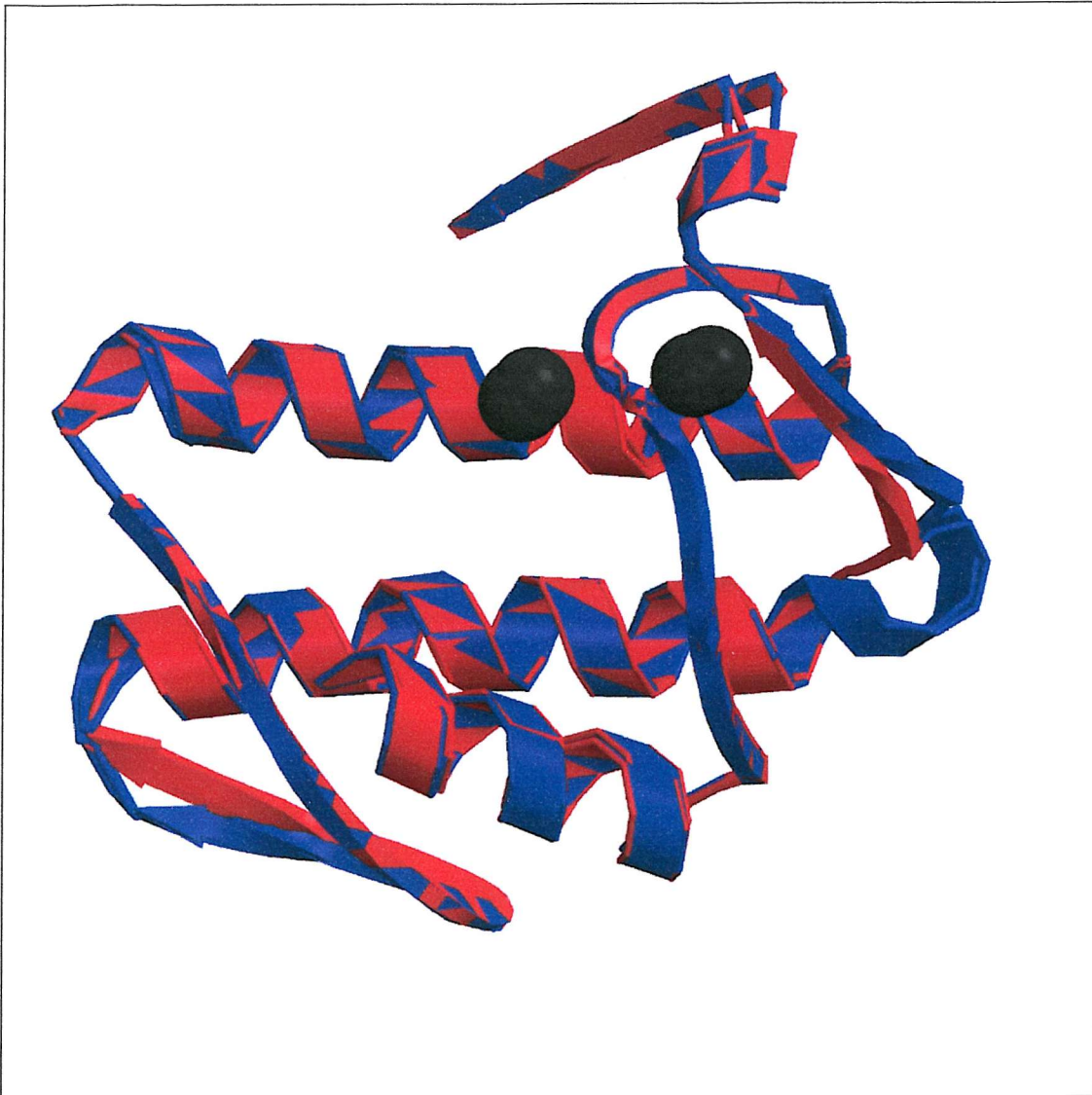
Figure 5.15 A Comparison of the Secondary Structures of N1A and H48Q HnpsPLA$_2$.

The program MOLSCRIPT was used to produce the picture [133].

The grey spheres represent the calcium ions found in the structures.

Blue - N1A hnpsPLA$_2$
Red - H48Q hnpsPLA$_2$
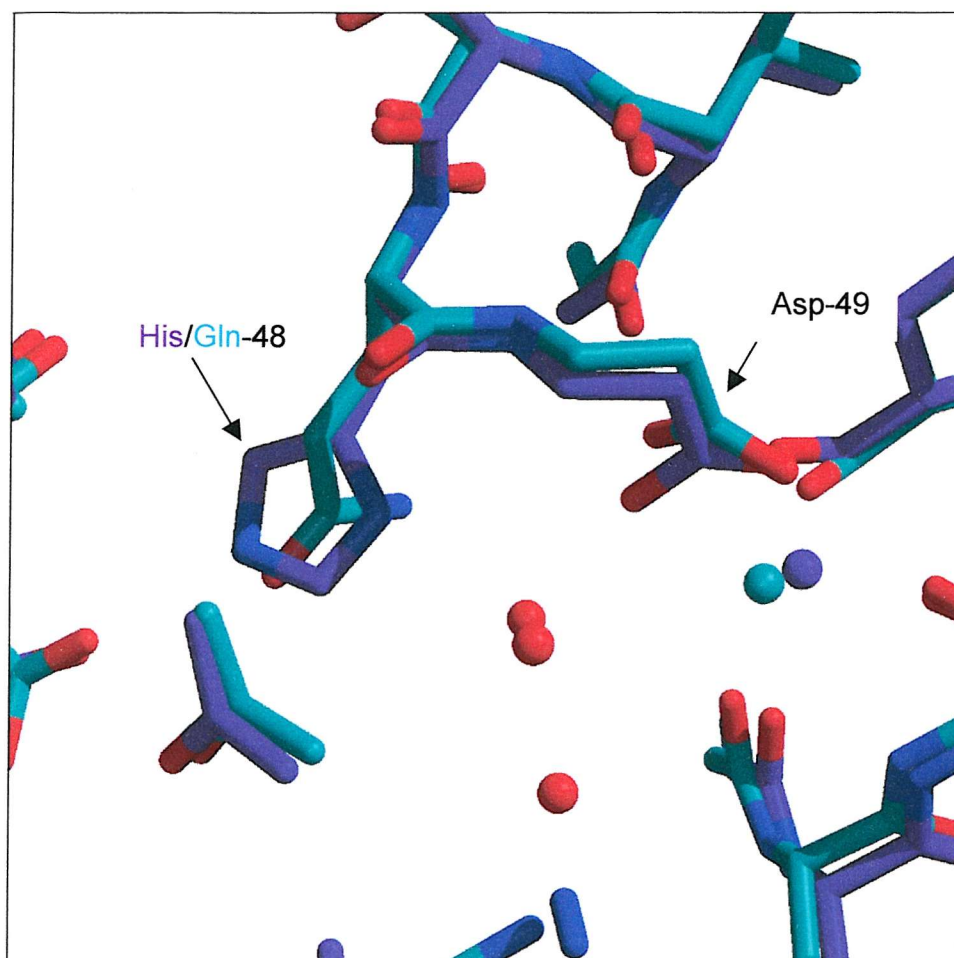
Figure 5.16 Comparison of the Active Site of N1A and H48Q HnpsPLA₂.

The picture was generated using the programs Xtalview and Raster3d [131,132].

The purple/turquoise spheres are calcium ions and the red spheres are water molecules.

Purple - N1A hnpsPLA₂
Turquoise - H48Q hnpsPLA₂

A further view of the active site is shown in figure 5.17. This shows the comparison between the N1A and the H48Q active sites, and the second residue in the catalytic dyad Asp-99 is visible. Once again, the two structures are almost totally superimposable, and the slight differences seen are likely due to the higher resolution data of the H48Q compared with the N1A.

The H48Q mutant was produced with the expectation that the resulting enzyme would be inactive, and the residual activity seen was a surprising feature of this mutant. In order to characterise the H48Q, a number of features of the enzyme were studied as reported in chapter three. One such feature was the ability of the mutant to bind calcium successfully, as this is a crucial ion for catalytic activity in fully functional hnpsPLA$_2$. The results in chapter three suggested that the H48Q mutant could coordinate calcium, and this is confirmed by the crystallographic study. Figure 5.18 shows a comparison of the calcium binding of the N1A and H48Q. Asp-49 and the carbonyl residues of the residues at positions 28, 30 and 32 coordinate the calcium ion. Importantly, the calcium binding residues are in identical positions in the structure of the H48Q and the N1A. Two water molecules are also part of the calcium-coordinating cage, but these have been omitted from the picture for clarity. The His-48 residue is adjacent to the Asp-99 residue that cordinates calcium as part of the catalytic mechanism. The substitution of this histidine with a glutamine has not, therefore, caused any change in the conformation of the residues surrounding the active site dyad, as judged from crystallographic studies, and importantly, has not impaired the calcium binding ability of the mutant. The crystal structure of the N1A and the H48Q revealed electron density for a second calcium ion in the models. This calcium is coordinated by Asn-122 and the carbonyl oxygens of residues 24, 26 and 120 (figure 5.19). The presence of a second calcium ion was reported in the published work of Scott et al, who solved the structure of hnpsPLA$_2$ isolated from synovial fluid of arthritic patients [71]. However, coordinates for this calcium ion were not included in the PDB file for this structure.

Figure 5.17 Comparison of the Active site Dyad and Calcium Binding Residue of N1A and H48Q HnpsPLA$_2$.

The picture was generated using the programs Xtalview and Raster3d [131,132].

The purple/green and red spheres are calcium ions and water molecules respectively, from the N1A structure.

Purple - N1A hnpsPLA$_2$

Turquoise - H48Q hnpsPLA$_2$

Figure 5.18 Comparison of the Primary Calcium Ion Binding of N1A and H48Q HnpsPLA₂.

The picture was generated using the programs Xtalview and Raster3d [131,132].

The purple and turquoise spheres are calcium ions.
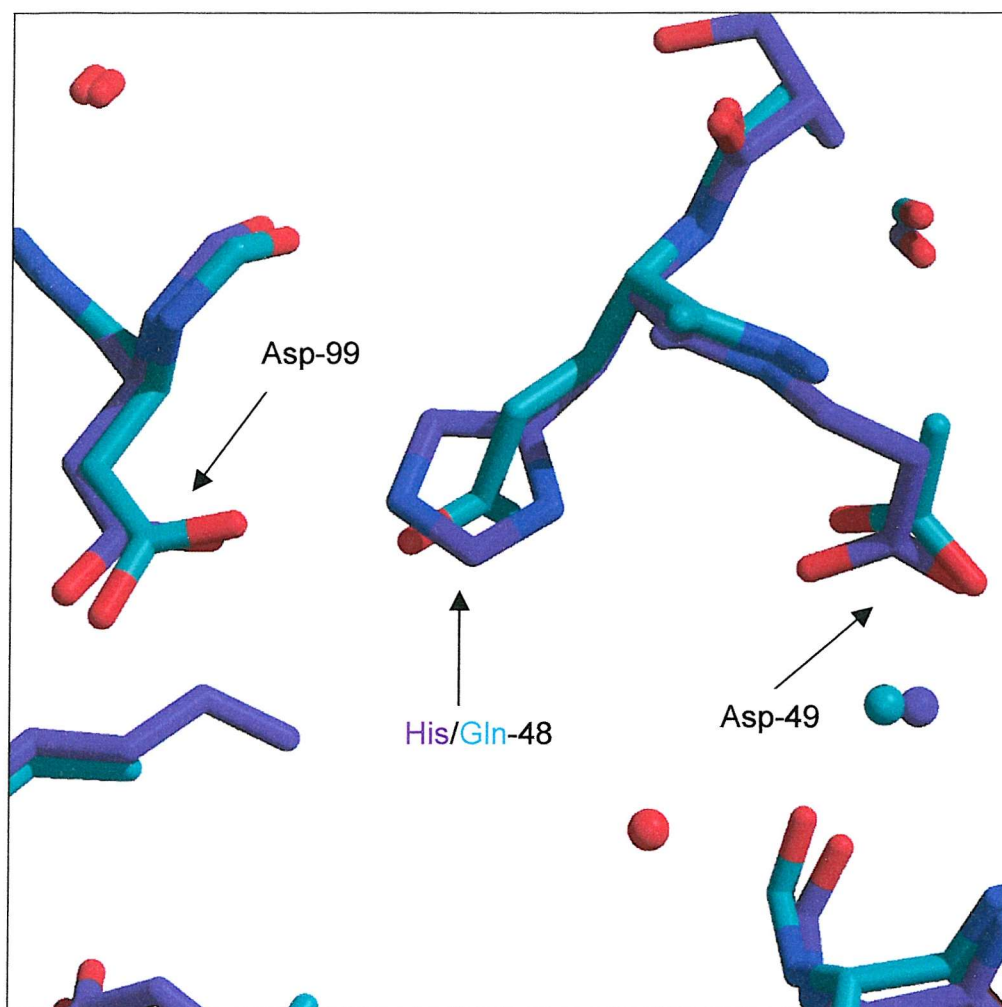
Purple - N1A hnpsPLA$_2$
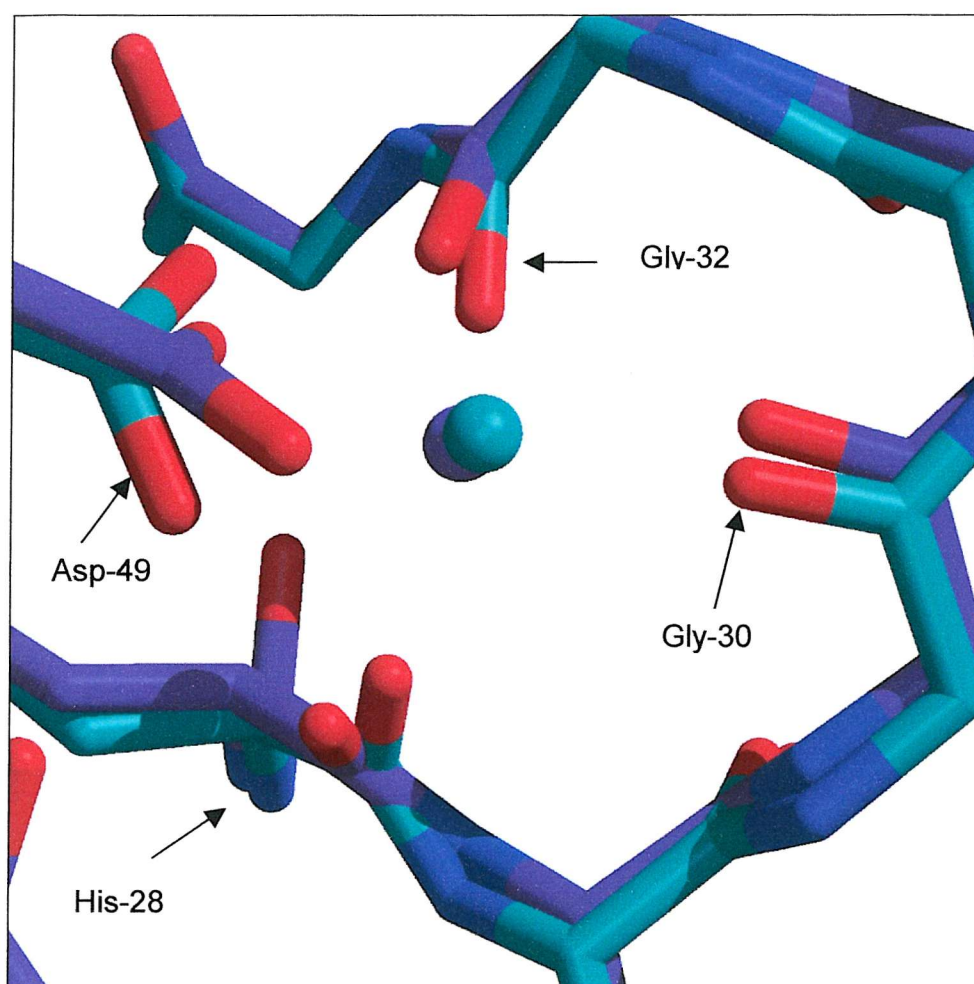Turquoise - H48Q hnpsPLA$_2$

Figure 5.19 Comparison of the Secondary Calcium Ion Binding of N1A and H48Q HnpsPLA₂.

The picture was generated using the programs Xtalview and Raster3d [131,132].

The purple and turquoise spheres are calcium ions.

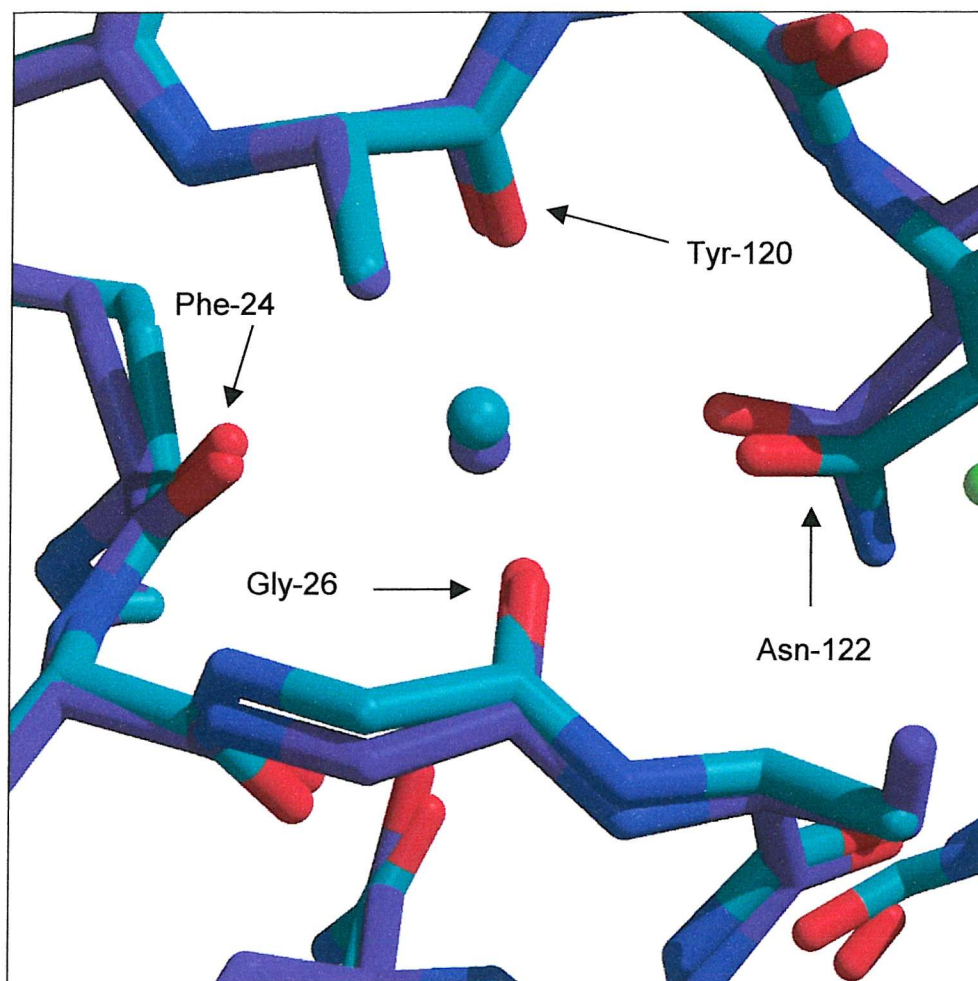Purple - N1A hnpsPLA₂
Turquoise - H48Q hnpsPLA₂

This secondary calcium ion was not thought to have a role in catalysis itself, however, it was absent in the crystal structure of the wild type enzyme when a transition state analogue was present in the active site. From this, it was inferred that the binding of calcium at this site was important in maintaining the surrounding residues in a position favourable for substrate binding. The results shown so far confirm those reported in chapter three, which suggested that the structure of the H48Q mutant was indeed the same as that of the N1A, and that substitution of the catalytic His-48 residue with a glutamine does not cause any gross structural changes.

The active site of the H48Q mutant required a detailed study, in order to try and elucidate a mechanism by which catalytic activity could still be seen, even after the His-48 residue had been mutated to a Gln. Figure 5.20 shows the glutamine residue at position 48 and the electron density surrounding it, confirming the presence of the mutation and also demonstrating that a histidine residue could not be accommodated within this density. Two water molecules are shown, which are clearly associated with the nitrogen atom of the glutamine residue, and which occupy the same space structurally as those in the N1A model. The Gln-48 residue was added into the structure by QUANTA, which placed the side chain of the residue in the conformation shown. However, it is as likely that the side chain may be orientated the alternative way to that shown, i.e. the carboxylate oxygen positioned adjacent to the water molecules.

Figure 5.21 is a view of the second member of the catalytic dyad, Asp-99, alongside Gln-48 at the active site, with the two water molecules that are part of the catalytic mechanism in the N1A. Phe-5 can also be seen at the bottom of the figure, and this is part of the hydrophobic channel that links the active site to the interfacial binding surface. The coordination of the calcium ion by Asp-49 is shown in figure 5.22 along with the His-48 residue and associated waters, all of which are situated in clearly defined density.

Figure 5.20 The Active Site Residue of H48Q HnpsPLA$_2$.

Xtalview and Raster3d were used to generate the picture. Electron density is shown for a 2Fo - Fc map at the 1 σ level [131,132]. Red spheres represent water molecules.

The picture shows the side chain of Gln-48 with the nitrogen atom oriented towards the water molecules. This is a representation only, and does reflect the absolute orientation of the side chain.

Figure 5.21 The Active Site Dyad of H48Q HnpsPLA$_2$.

Xtalview and Raster3d were used to generate the picture. Electron density is shown for a 2Fo - Fc map at the 1 σ level [131,132]. Red spheres represent water molecules.

The picture shows the side chain of Gln-48 with the nitrogen atom oriented towards the water molecules. This is a representation only, and does reflect the absolute orientation of the side chain.
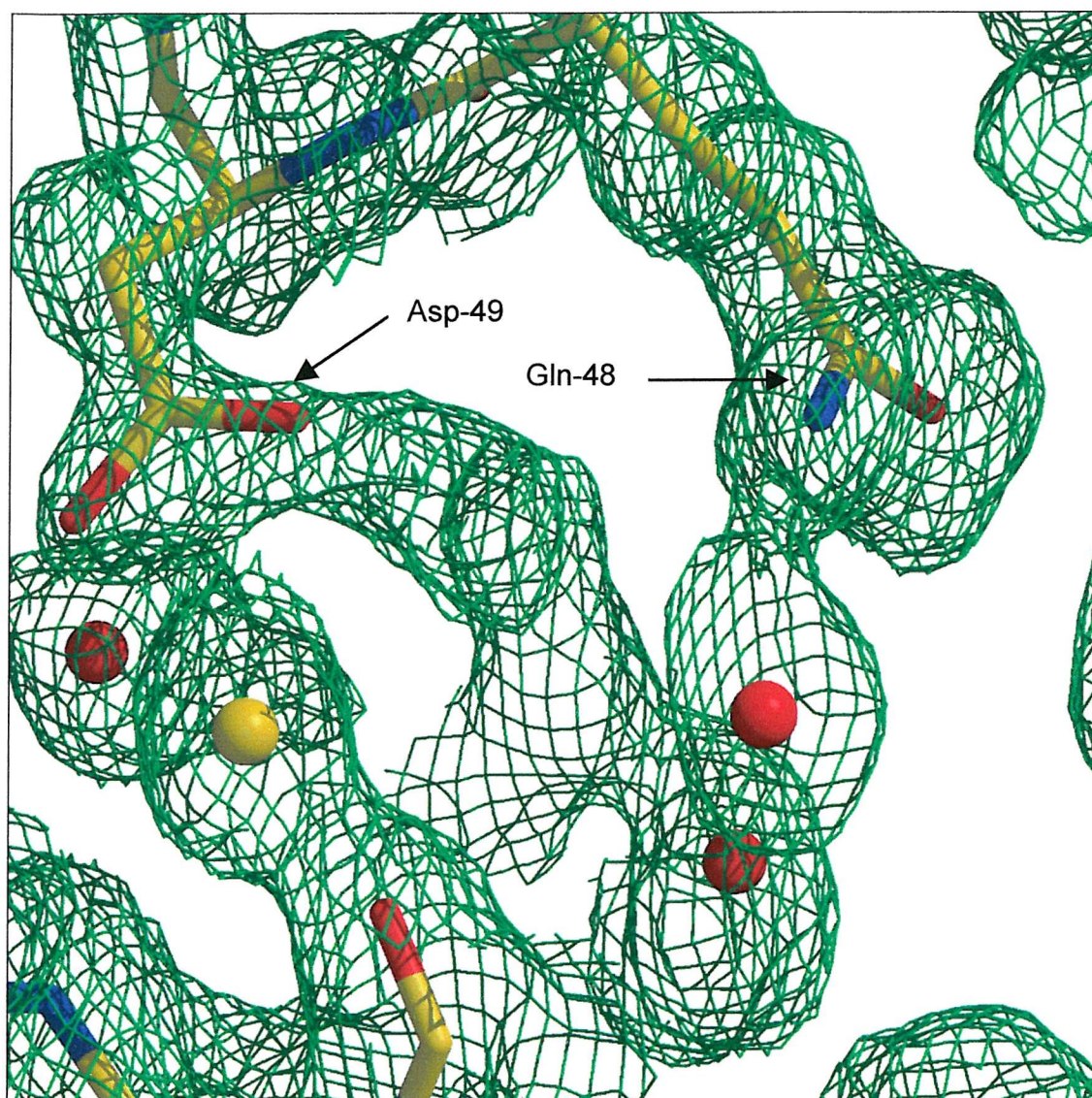
Figure 5.22 The Active Site Dyad and Calcium Binding Residue of H48Q HnpsPLA$_2$.

Xtalview and Raster3d were used to generate the picture. Electron density is shown for a 2Fo - Fc map at the 1 σ level [131,132]. Red spheres represent water molecules, yellow spheres are calcium ions.

The picture shows the side chain of Gln-48 with the nitrogen atom oriented towards the water molecules. This is a representation only, and does reflect the absolute orientation of the side chain.

Structural waters occupy the density between the calcium ion and the water molecules associated with Gln-48 but these were omitted from the figure for clarity.

The coordination of the calcium ion is clearly shown in figure 5.23. The electron density surrounding the Asp-49, Gly-30 and Gly-32 residues is well defined, confirming that this is the correct positioning of the calcium ion. The coordination of the second calcium ion is shown in figure 5.24 and, again, the association of residues 24, 26, 120 and 122 with this calcium ion is well defined.

The surface potential map of H48Q hnpsPLA$_2$ is shown in figure 5.25. This shows the distribution of charge over the surface of the enzyme, and also highlights the access to the active site. The two catalytic waters and the two calcium ions are shown as red and grey spheres respectively. The program PROCHECK confirmed that all residues were in allowed regions of the Ramachandran plot [130,135].

5.5 Discussion.

The crystal structures of N1A and H48Q hnpsPLA$_2$ have been solved. In all areas of the models, the two forms of the enzyme showed good similarity to each other and also to the wild type structure that was used as a model. In both structures, the two water molecules in the active site thought to participate in catalysis have been assigned along with the essential calcium ion, and a second calcium ion located away from the active site itself.
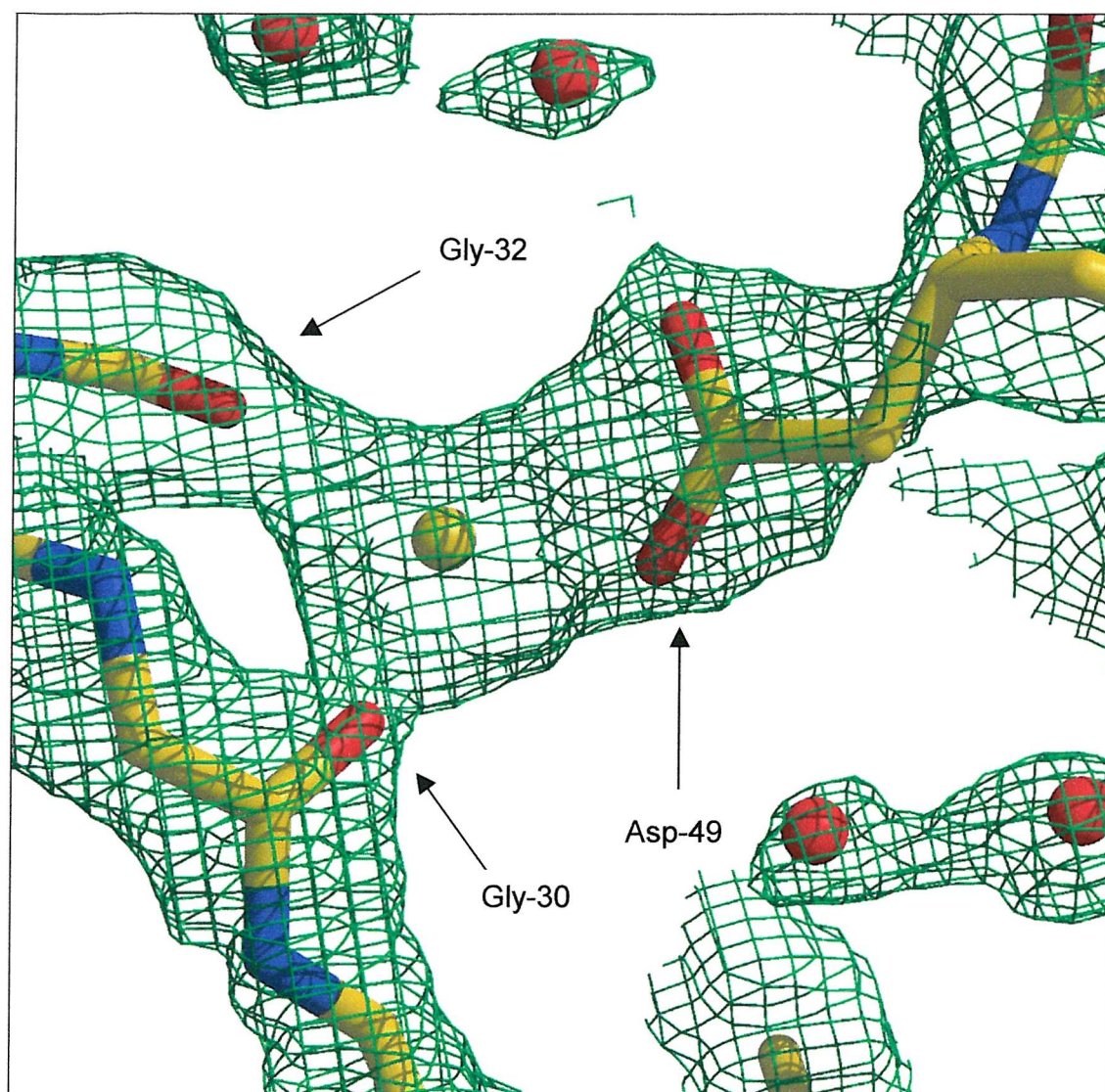
Figure 5.23 The Coordination of the Primary Calcium Ion in H48Q HnpsPLA₂.
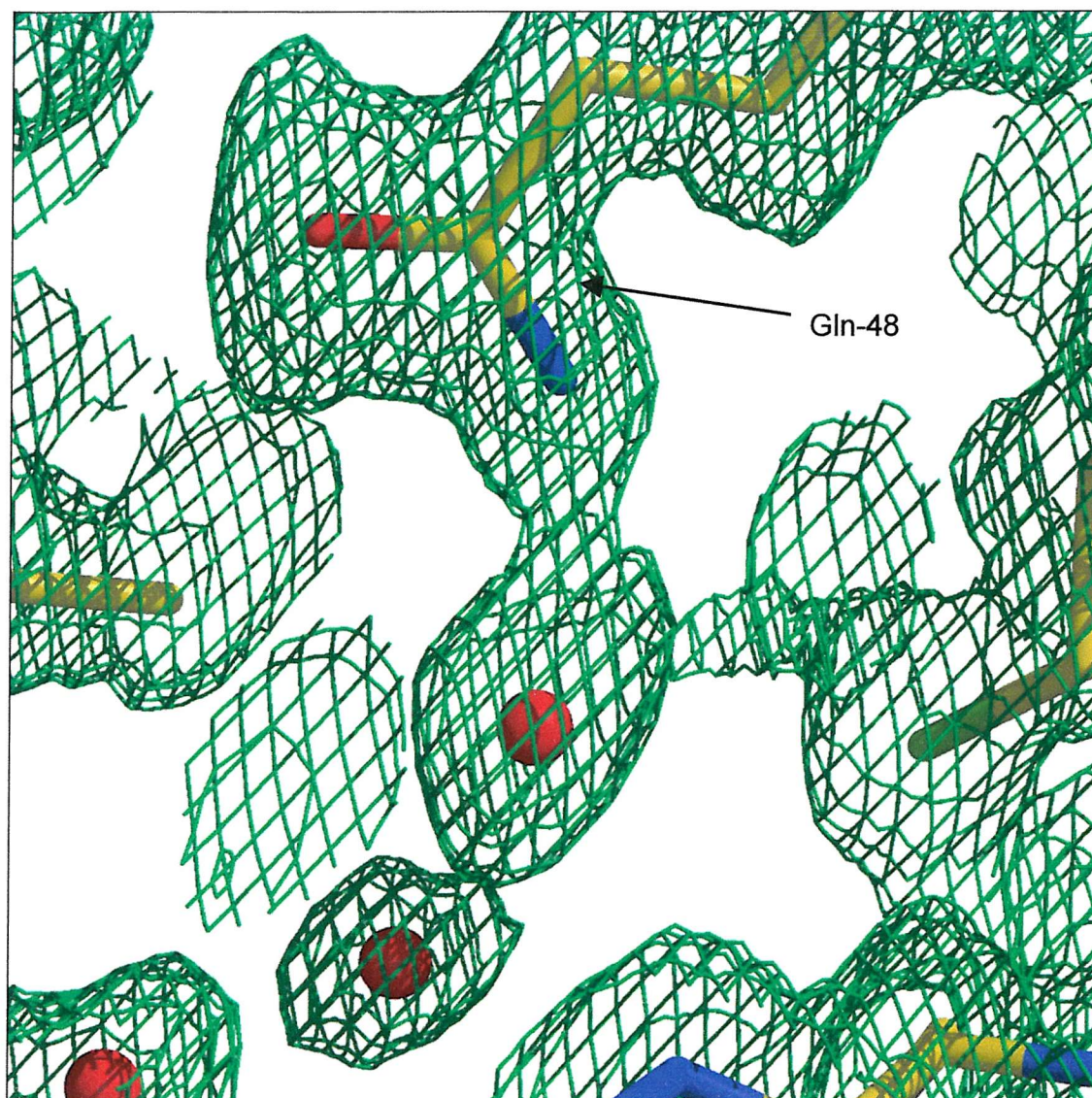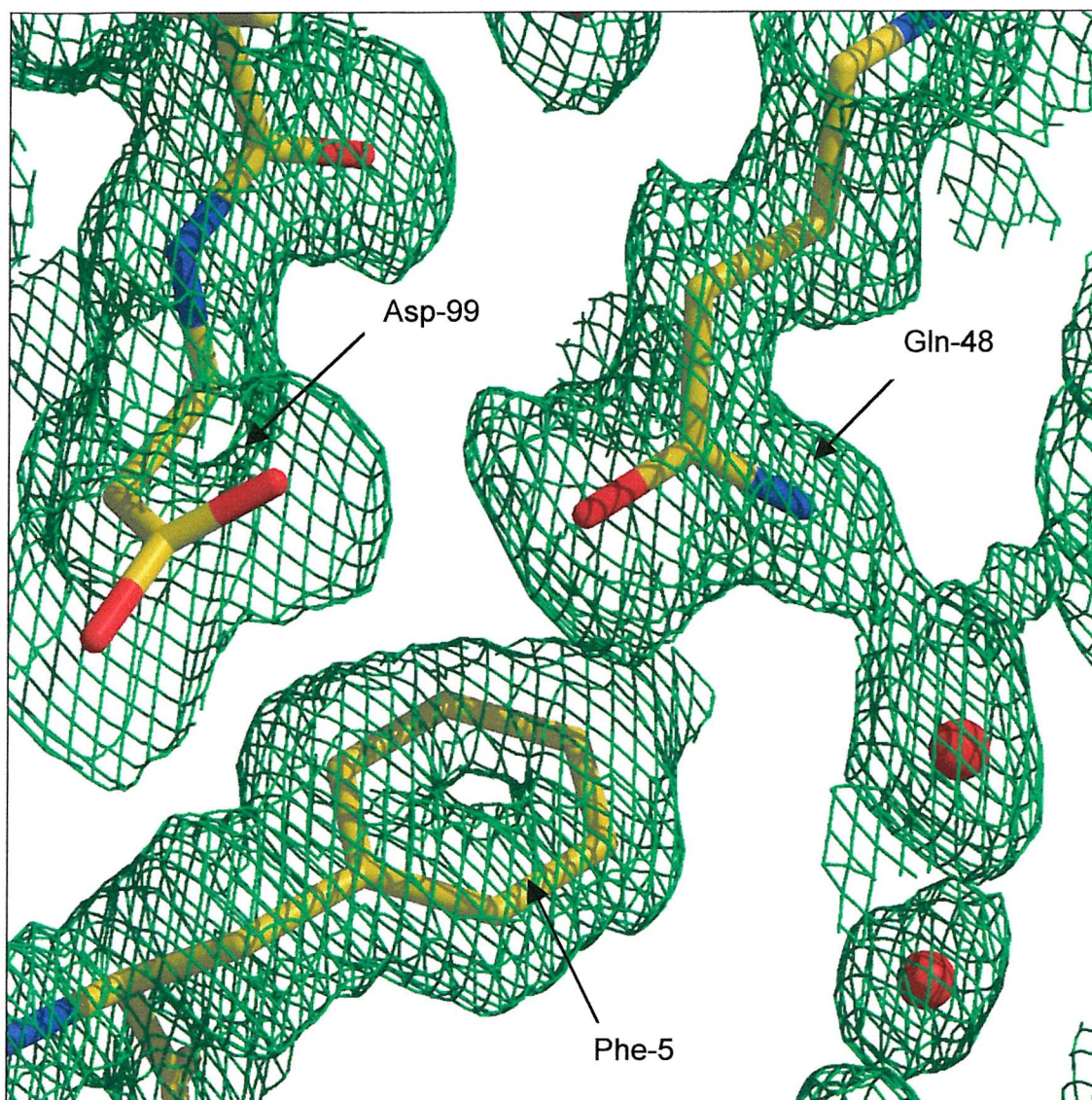
Xtalview and Raster3d were used to generate the picture. Electron density is shown for a 2Fo - Fc map at the 1 σ level [131,132].

Red spheres represent water molecules, yellow spheres are calcium ions.
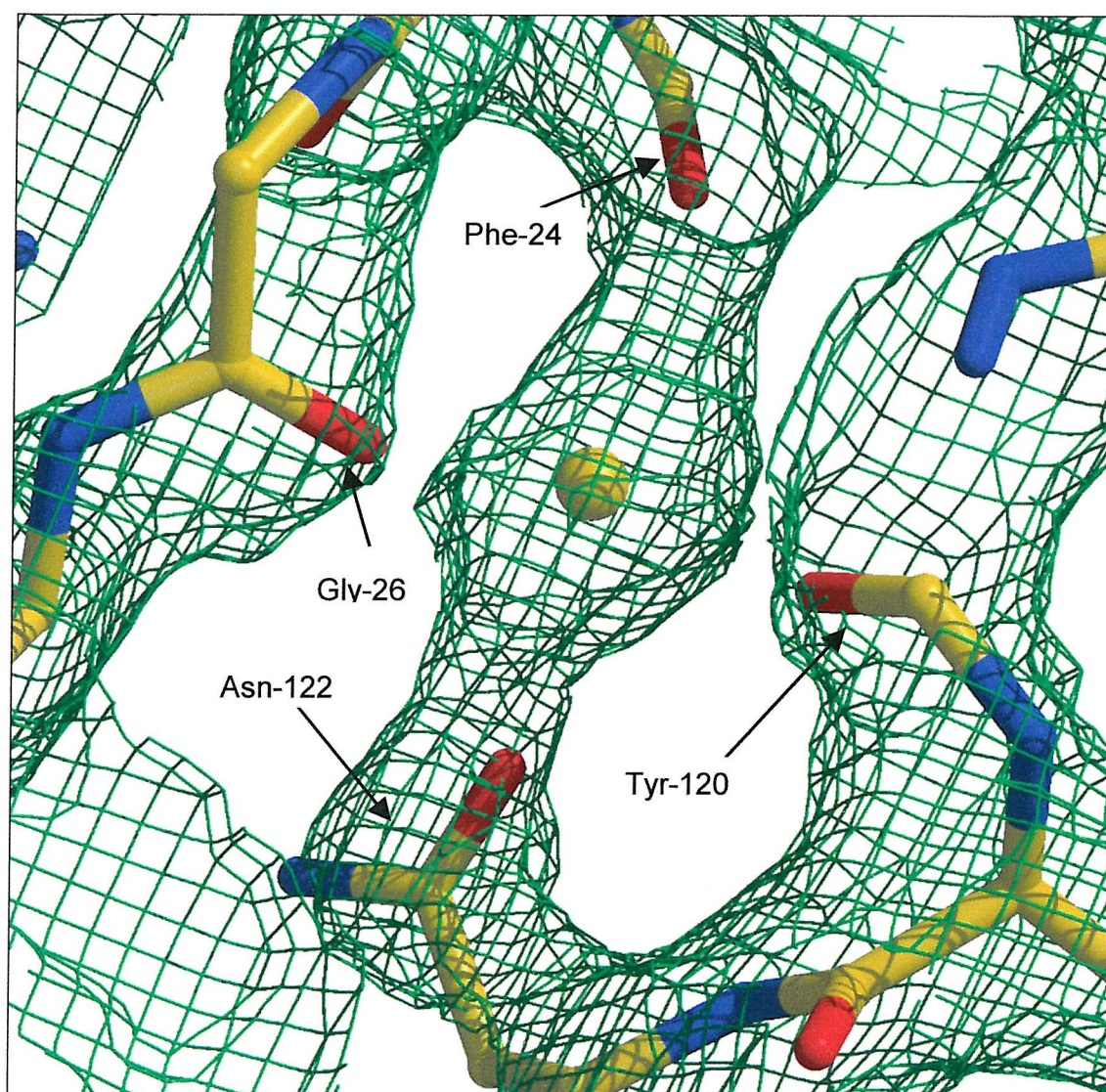
Figure 5.24 The Coordination of the Secondary Calcium Ion in H48Q HnpsPLA$_2$.

Xtalview and Raster3d were used to generate the picture. Electron density is shown for a 2Fo - Fc map at the 1 σ level [131,132].

Red and yellow spheres represent water molecules and calcium ions respectively.
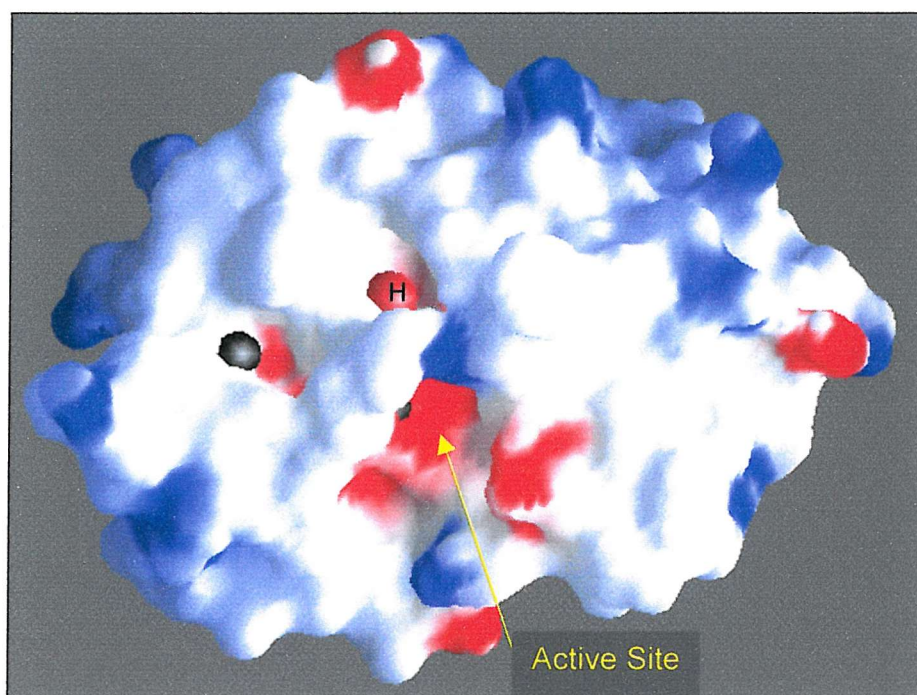
Figure 5.25 Surface Potential Diagram Showing the Distribution of Charge on the Surface of H48Q HnpsPLA$_2$.

The figure was generated using the program GRASP [134].

Red spheres (H) represent water molecules, grey spheres represent calcium ions.

Red - Acidic residues

Blue - Basic residues

The enzymes were subjected to crystallographic studies due to the remarkable ability of the H48Q mutant to show catalytic activity, albeit at a much reduced rate as compared to the N1A. With the crystal structure of the H48Q mutant solved at such high resolution, it is possible to propose how this catalytic activity is possible.

In the N1A, the Asp-99 residue functions to orient the catalytic His-48 residue by H-bonding to it. In turn, the histidine residue can H-bond to a water molecule, which will then accept a proton from a second water molecule, this generating the nucleophile that attacks the phospholipid ester bond. In the H48Q mutant, the Gln-48 residue is also shown to be associated with two water molecules.

However, it is only possible for Gln-48 to H-bond to the second water molecule, so no formal proton transfer will occur. It is proposed [76] that the rate-limiting step in the two-water mechanism lies during the decomposition of the tetrahedral intermediate and not in its formation, which is the case in the one-water mechanism [74]. Therefore, it could be argued that the significant activity seen with the H48Q is possible because no formal deprotonation of the second water occurs, and a H_3O^+ species formed from the second water molecule will be stabilised by H-bonding to the Gln-48, thus still allowing the formation of an oxyanion intermediate at a significant rate.

The calcium ion bound to Asp-49 is in an identical conformation to that in the N1A, and will therefore, presumably be able to orient the substrate molecule, and stabilise the intermediate structure as it does in the wild type enzyme. A modified two-water mechanism in which the second water molecule is not deprotonated by the His-48 residue, and hence becomes H_3O^+ has been proposed and is shown in figure 5.26 [136]. Such a mechanism should allow the significant catalytic activity seen with the H48Q mutant.

Figure 5.26 A Modified Version of the Two-water Mechanism.

C2 refers to the phospholipid molecule excluding the sn-2 fatty acyl chain, and R2 refers to the sn-2 fatty acyl chain itself. (Taken from [136] with permission).
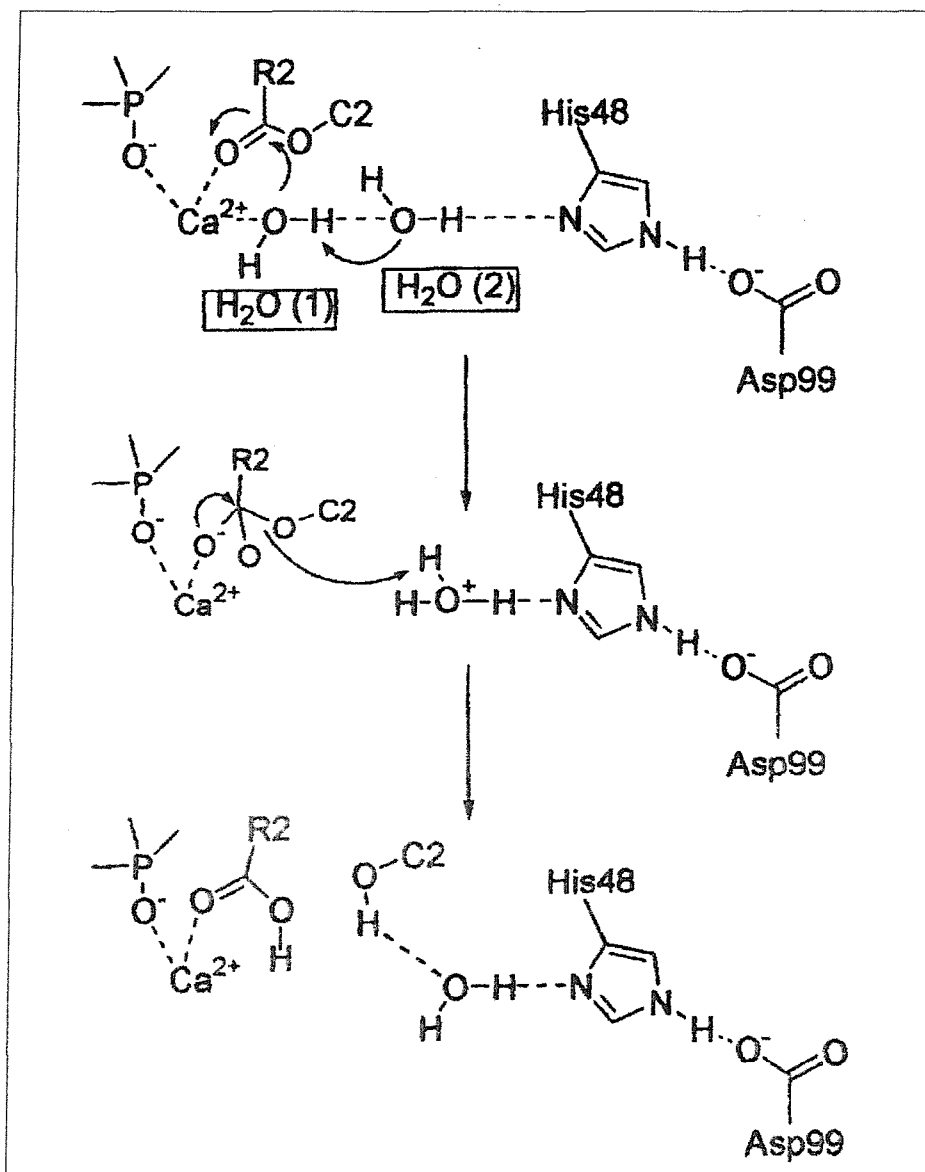
Chapter Six - General Discussion

General Discussion and Future Work

HnpsPLA$_2$ is a physiologically important enzyme, which has roles in inflammatory events and antimicrobial defence. The phospholipid hydrolysing ability of this enzyme is dependant on the interfacial binding of this enzyme to its aggregated substrate interface. In order to study this important interfacial activation, the active site mutant H48Q was produced. In both the bovine pancreatic [96] and bee venom [97] forms of the enzyme, the substitution of the equivalent catalytically crucial His residue with a Gln resulted in structurally intact and catalytically inactive mutants. Such a mutant of hnpsPLA$_2$ was desired in order that it could be employed as an interfacial binding probe in interfacial competition assays to assess the relative affinities of different sPLA$_2$s and different mutants of hnpsPLA$_2$ for their substrate interfaces.

Chapter three describes the purification and characterisation of the H48Q mutant of hnpsPLA$_2$, and of note is the significant catalytic activity that this mutant retains, even though it lacks the catalytically crucial His-48 residue. This remarkable property of the H48Q mutant has been demonstrated under a variety of conditions, and structural studies confirmed that the mutant was intact and correctly folded. A further unexpected property of this mutant was it inactivation by the alkylating agent pBPB. This reagent is commonly used to inactivate sPLA$_2$s by reacting with the active site His residue. The inhibitory effect that pBPB had on the H48Q was presumed to be exerted at the active site, as the presence of calcium in the inactivation assays protected the H48Q from inactivation. However, when the inactivated H48Q was analysed by mass spectrometry, no pBPB derivative was incorporated.

The precise mechanism by which pBPB inactivates the H48Q remains to be explained, but the transient esterification of the active site Asp-99 remains a possibility. Future work in this area will require a detailed evaluation of the conditions for mass spectrometry to prevent hydrolysis of the presumptive ester intermediate during sample preparation. Alternatively, recovery of enzyme activity should be possible by treatment of the enzyme under

conditions that would result in hydrolysis of the pBPB derivative of the enzyme. In order to ensure success it will be necessary to produce large amounts of the pBPB-modified enzyme to overcome problems associated with the low activity of H48Q.

In chapter four of this thesis the production and properties of the H48N and H48A mutants of the hnpsPLA$_2$ were described. In the case of H48A, as with the equivalent mutations in bovine pancreatic and bee venom sPLA$_2$, this mutant was not structurally intact, which resulted in no protein being available for characterisation. The H48N mutant, however, was found to be both structurally intact and relatively inactive. The use of this inactive mutant as a probe for interfacial binding was evaluated. Interfacial competition assays with this mutant have been used to assess the binding affinity of various sPLA$_2$s for DOPG and cardiolipin interfaces, and also to study the differences in binding of N1A and H48Q to DOPG presented as both SUVs and MLVs.

The inhibition of the N1A-catalysed hydrolysis of cell membranes of *M. luteus* by H48N confirmed that access of hnpsPLA$_2$ to this membrane is not related to its catalytic ability. Moreover, it supports the argument that it is the cationic charge of the enzyme that allows it to access Gram-positive bacterial cell membranes.

The experiments concerning the competitive effect of H48N on the hydrolysis of DOPG interfaces by tryptophan mutants of hnpsPLA$_2$ confirmed that the presence of a Trp residue does not greatly affect the ability of these mutants to hydrolyse DOPG. These Trp mutants show enhanced activity on DOPC, as compared to the essentially zero activity seen with the N1A. The H48N cannot be used to quantify this enhanced binding affinity, as it will not bind to DOPC interfaces itself. To overcome this, an equivalent H48N mutation could be made in a PC-binding form of the enzyme such as *Naja naja* sPLA$_2$, or alternatively a Trp residue could be inserted into the H48N mutant. Neither of these suggestions is straightforward however, and both may have consequences on the structure of the enzyme.

The H48N mutant was also used to characterise the interfacial binding of a number of charge reversal mutants of hnpsPLA$_2$. These were made in the laboratory of M. H. Gelb (Department of Chemistry, University of Washington, US) to study the contribution of electrostatic charge in interfacial binding. The competition experiments helped to confirm that the binding affinity of these mutants decreased as a function of net surface charge and not because of the contribution of one particular cluster of residues to binding. The H48N can be used in future competition assays, and will provide information on the relative affinity for anionic interfaces of future interfacial mutants of hnpsPLA$_2$.

Chapter five of this thesis reported the findings of a crystallographic study of the H48Q mutant. The structure of the N1A was also solved in order that the structure of the H48Q, which also contains the N1A mutation, could be compared to it. The N1A structure was solved at 2.6 Å, and was identical to the structure of the wild type enzyme isolated from synovial fluid. The study confirmed that the N-terminal mutation did not cause any conformational change in this part of the enzyme. The data for the H48Q mutant extended to 1.5 Å (the highest resolution of any sPLA$_2$ so far reported), and the structure showed good agreement to the N1A throughout.

At the active site, the glutamine residue at position 48 occupied the same position structurally as the histidine in the N1A, and the Asp-99 residue that makes up the catalytic dyad was also in an identical position in both structures. The key calcium binding residue, Asp-49, was also shown to be unperturbed by the mutation. Similarly, the presence of a second calcium ion coordinated in identical places in both structures confirmed that the substitution of the active site residue His-48 with a Gln, has not had any major effect on the structures, thus confirming earlier results (Chapter 3).

The residual activity shown by this mutant can be explained in part by the presence of two catalytic waters in the model, which are in identical places in both structures. There is potential for the Gln-48 residue to H-bond to the second water molecule and help generate a nucleophile from the first water molecule with which to produce the tetrahedral intermediate. The structure of

H48Q requires minor refinement before submitting the coordinates to the Brookhaven protein database in order to further reduce the R-factor and allow additional outer shell waters to be added, and this work is ongoing at present.

In terms of future crystallographic studies, it is of particular importance that the H48Q mutant is crystallised in the presence of a transition-state analogue, which would allow the interactions of the active site residues with the substrate to be more clearly defined. Given the results of the pBPB inactivation assays in chapter three, co-crystallisation of the H48Q mutant with pBPB may help clarify the manner by which the alkylating agent inactivates this active site mutant.

Chapter Seven - References

References

1) Six, D.A. and Dennis, E.A. (2000) *Biochem. Biophys. Acta* **1488** p1-19

2) Murakami, M. and Kudo, I. (2001) *Adv. Immunol.* **77** p163-193

3) Kaiser, E. (1999) *Critical Reviews in Clinical Laboratory Sciences* **36** p65-163

4) Murakami, M., Nakatani, Y., Atsumi, G., Inoue, K. and Kudo, I. (1997) *Critical Reviews in Immunology* **17** p225-283

5) Burdge, G. C., Creaney, A., Postle, A. D. and Wilton, D. C. (1995) *International J. Biochem. Cell Biol.* **27** p1027-1032

6) Huang, Z., Payette, P., Abdullah, K., Cromlish, W. A. and Kennedy, B. P. (1996) *Biochemistry* **35** p3712-3721

7) Vadas, P., Browning, J., Edelson, J. and Pruzanski, W. (1993) *Journal of Lipid Mediators* **8** p1-30

8) Laine, V.J.O., Grass, D.S. and Nevalainen, T.J. (1999) *Journal of Immunology* **162** p7402-7408

9) Fonteh, A.N., Bass, D.A., Marshall, L.A., Seeds, M., Samet, J.M. and Chilton, F.H. (1994) *Journal of Immunology* **152** p5438-5446

10) Kudo, I. And Murakami, M., Hara, S. and Inoue, K. (1993) *Biochem. Biophys. Acta* **117** p217-231

11) Yuan, C. and Tsai, M-D. (1999) *Biochem. Biophys. Acta* **1441** p215-222

12) Scott, D.L. and Sigler, P.B. (1994) *Advances in Protein Chemistry* **45** p53-88

13) Lambeau, G. and Lazdunski, M. (1999) *TiPS* **20** p162-70

14) Lambeau, G., Ancian, P., Barhanin, J. and Lazdunski, M. (1994) *Journal of Biological Chemistry* **269** p1575-1578

15) Jannsen, M.J.W., Verheij, H.M., Slotboom, A.J. and Egmond, M.R. (1999) *European Journal of Biochemistry* **261** p197-207

16) Dudler, T., Chen, W-Q., Wang, S., Schneider, T., Annand, R. R., Dempcy, R. D., Crameri, R., Gmachl. M., Suter, M. and Gelb, M. H. (1992) *Biochem. Biophys. Acta* **1165** 201-210

17) Kramer, R.M. and Sharp, J.D. (1997) *FEBS Letters* **410** p49-53

18) Perisic, O., Paterson, H. F., Mosedale, G., Lara-Gonzalez, S. and Williams, R. L. (1999) *Journal of Biological Chemistry* **247** p14979-14987

19) Sharp. J. D., Pickard, R. T., Chiou, X. G., Manetta, J. V., Kovacevic, S., Miller, J. R., Varshavsky, A. D., Roberts, E. F., Strifler, B. A., Brems, D. N. and Kramer, R. M. (1994) *Journal of Biological Chemistry* **269** p23250-23254

20) Dessen, A. (2000) *Biochem. Biophys. Acta* **1488** p40-47

21) Leslie, C. C. (1997) *Journal of Biological Chemistry* **272** p16709-16712

22) Pickard, R. T., Chiou, G., Strifler, B. A., Defelippis, M. R., Hyslop, P. A., Tebbe, A. L., Yee, Y. K., Reynolds, L. J., Dennis, E. A., Kramer, R. M. and Sharp, J. D. (1996) *Journal of Biological Chemistry* **271** p19225-19231

23) Reddy, S. T., Winstead, M. V., Tischfield, J. A. and Dennis, E. A. (1997) *Journal of Biological Chemistry* **272** p 13591-13596

24) Janssen, M. J., Vertmeulen, L., Van der Helm, A. J., Aarsman, A. J., Slotboom, M. R. and Egmond, M. R. (1999) *Biochem. Biophys. Acta* **1440** p59-72

25) Han, S. K., Kim, K. P., Koduri, R., Bittova, L., Munoz, N. M., Leff, A. R., Wilton, D. C., Gelb, M. H. and Cho, W. (1999) *Journal of Biological Chemistry* **271** p11881-11888

26) Cho, W. (2000) *Biochem. Biophys. Acta* **1488** p48-58

27) Crowl, R. M., Stoller, T. J., Connoy, R. R. and Stoner, J. (1991) *Journal of Biological Chemistry* **266** p2647-2651

28) Balboa, M. A., Balsinde, J., Jones, S. S. and Dennis, E. A. (1997) *Journal of Biological Chemistry* **272** p8576-8580

29) Tang, J., Kriz, R. W., Wolfman, N., Shaffer, M., Seehra, J. and Jones, S. S. (1997) *Journal of Biological Chemistry* **272** p8567-8575

30) Winstead, M. V., Balsinde, J. and Dennis, E. A. (2000) *Biochem. Biophys. Acta* **1488** p28-39

31) Ramanadham, S., Hsu, F. F., Bohrer, A., Ma, Z. and Turk, J. (1999) *Journal of Biological Chemistry* **274** p13915-13927

32) Balsinde, J. and Dennis, E. A. (1997) *Journal of Biological Chemistry* **272** p16069-16072

33) Tjoelker, L. W., Wilder, C., Eberhardt, C., Stafforini, D. M., Dietsch, G., Schimpf, B., Hooper, S., Letrong, H., Cousens, L. S., Zimmerman, G. A., Yamada, Y., McIntyre, T. M., Prescott, S. M. and Gray, P. W. (1995) *Nature* **374** p549-553

34) Stafforini, D. M., McIntyre, T. M., Carter, M. E. and Prescott, S. M. (1987) *Journal of Biological Chemistry* **262** p4215-4222

35) Ackermann, E. J. and Dennis, E. A. (1995) *Biochem. Biophys. Acta* **1259** p125-136

36) Miwa, M., Miyake, T., Yamanaka, T., Sugatani, J., Suzuki, Y., Sakata, S., Araki, Y. and Matsumoto, M. (1988) *Journal of Clinical Investigation* **82** p1983-1991

37) Stafforini, D. M., Numao, T., Tsodikov, A., Vaitkus, D., Fukuda, T., Watanabe, N., Fueki, N., McIntyre, T. M., Zimmerman, G. A., Makino, S. and Prescott, S. M. (1999) *Journal of Clinical Investigation* **103** p989-997

38) Hattori, M., Arai, H. and Inoue, K. (1993) *Journal of Biological Chemistry* **268** p18748-18753

39) Volwerk, J. J, Pieterson, W. A. and De Haas, G. H. (1974) *Biochemistry* **13** p1446-1454

40) Roberts, M. F., Deems, R. A., Mincey, T. C. and Dennis, E. A. (1977) *Journal of Biological Chemistry* **252** p2405-2411

41) McIntosh, J. M., Ghomashchi, F., Gelb, M. H., Dooley, D. J., Stoehr, S. J., Giordani, A. B., Malsbitt, S. R. and Olivera, B. M. (1995) *Journal of Biological Chemistry* **270** p3518-3526

42) Cupillard, L., Koumanov, K., Mattei, M., Lazdunski, M. and Lambeau, G. (1997) *Journal of Biological Chemistry* **272** p15745-15752

43) Hanasaki, K., Ono, T. and Saiga, A., Morioka, Y., Ikeda, M., Kawamoto, K., Higaskino, K. I., Nakano, K., Yamada, K. and Ishizaki, J. (1999) *Journal of Biological Chemistry* **274** p34203-34211

44) Hara, S., Kudo, I., Chang, H. W., Matsuta, K., Miyamoto, T. and Inoue, K. (1989) *J. Biochem. Tokyo* **105** p1395-1399

45) Seilhamer, J. J., Plant, S., Pruzanski, W., Schilling, J., Stefanski, E., Vadas, P. and Johnson, L. K. (1989) *J. Biochem. Tokyo* **106** p38-42

46) Kinkaid, A. R. and Wilton, D. C. (1995) *Biochemistry Journal* **308** p507-512

47) Vadas, P. and Pruzanski, W. (1993) *Circulatory Shock* **39** p160-167

48) Dua, R. and Cho, W. (1994) *Eur. J. Biochem.* **221** p481-490

49) Diccianni, M. B., Lilly-Stauderman, M., McLean, L. R., Balasubramaniam, A. and Harmony, J. A. K. (1991) *Biochemistry* **30** p9090-9097

50) Murakami, M., Kambe, T., Shimbara, S., Yamamoto, S., Kuwata, H. and Kudo, I. (1999) *Journal of Biological Chemistry* **274** p29927-29936

51) Uozumin, N., Kume, K., Nagase, T., Nakatani, N., Ishii, S., Tashino, F., Komagata, Y., Maki, K., Ikuta, K., Ouchi, Y., Miyazaki, J. and Shimizu, T. (1997) *Nature* **390** p618-622

52) Bonventre, J. V., Huang, Z. H., Taheri, M. R., O'Leary, E., Li, E., Moskowitz, M. A. and Sapitstein, A. (1997) *Nature* **390** p622-625

53) Kennedy, B. P., Payette, P., Mudgett, J., Vadas, P., Pruzanski, W., Kwan, M., Tang, C., Rancourt, D. E. and Cromlish, W. A. (1995) *Journal of Biological Chemistry* **270** p22378-22385

54) Fox, N., Song, M., Schrementi, J., Sharp, J. D., White, D. L., Snyder, D. W., Hartley, L. W., Carlson, D. G., Bach, N. J., Dillard, R. D., Draheim, S. E., Bobbitt, J. C., Fisher, L. and Mihelich, E. D. (1996) *Eur. J. Pharmacology* **308** p195-203

55) Hack, C. E., Wolbink, G-J., Schalkuijk, C., Speijer, H., Hermens, W. T. and Van den Bosch, H. (1997) *Immunology Today* **18** p111-115

56) Bratton, D. L., Fadok, V. A., Richter, D. A., Kailey, J. M., Guthrie, L. A. and Henson, P. M. (1997) *Journal of Biological Chemistry* **272** p26159-26165

57) Kemppainen, E., Hietarata, A., Puolakkainen, P., Sainio, V., Halttunen, J., Haapiainen, R., Kivilaakso, E. and Nevalainen, T. (1999) *Pancreas* **18** p21-27

58) Weiss, J., Wright, G., Bekkers, A. A., Vandenbergh, C. J. and Verheij, H. M. (1991) *Journal of Biological Chemistry* **269** p26331-26337

59) Wiese, A., Brandenburg, K., Carroll, S. F., Rietschel, E. T. and Seydel, U. (1997) *Biochemistry* **36** p10311-10319

60) Buckland, A. G., Heeley, E. L. and Wilton, D. C. (2000) *Biochem. Biophys. Acta* **1484** p195-206

61) Weinrauch, Y., Elsbach, P., Madsen, L. M., Foreman, A. and Weiss, J. (1996) *Journal of Clinical Investigation* **97** p250-257

62) Weinrauch, Y., Abad, C., Liang, N. S., Lowry, S. F. and Weiss, J. (1998) *Journal of Clinical Investigation* **102** p633-638

63) Buckland, A. G. and Wilton, D. C. (2000) *Biochem. Biophys. Acta* **1488** p71-82

64) Peters, A. R., Dekker, N., Van den Berg, L., Boelens, R., Kaptein, R., Slotboom, A.J. and De Haas, G. H. (1992) *Biochemistry* **31** p10024-10030

65) Di Marco, S., Marki, F., Hofstetter, H., Schmitz, A., Van Oostrum, J. and Grutterm, M. G. (1992) *Journal of Biochemistry* **112** p350-354

66) Snitko, Y., Koduri, R. S., Han, S. K., Othman, R., Baker, S. F., Molini, B. J., Wilton, D. C., Gelb, M. H. and Cho, W. (1997) *Biochemistry* **36** p14325-14333

67) Koduri, R. S., Baker, S. F., Snitko, Y., Han, S. K., Cho, W., Wilton, D. C. and Gelb, M. H. (1998) *Journal of Biological Chemistry* **273** p32142-32153

68) Ghomashchi, F., Lin, Y., Hixon, M. S., Yu, B., Annand, R., Jain, M. and Gelb, M. H. (1998) *Biochemistry* **37** p6697-6710

69) Lin, Y., Nielson, R., Murray, D., Mailer, C., Hubbel, W. L., Robinson, B. H. and Gelb, M. H. (1998) *Science* **279** p1925-1929

70) Wery, J.P., Schweitz, R. W., Clawson, D. K., Bobbitt, J. L., Dow, E. R., Gamboa, G., Goodson, T., Hermann, M. R. B., Kramer, R. M. and McClure, D. B. (1991) *Nature* **352** p79-82

71) Scott, D. L., White, S. P., Browning, J. L., Rosa, J. J., Gelb, M. H. and Sigler, P. B. (1991) *Science* **254** p1007-1010

72) Dijkstra, B. W., Kalk, K. H., Hol, W. G. J. and Drenth, J. (1981) *Journal of Molecular Biology* **147** p97-123

73) Zhu, H., Dupureur, C. M., Zhang, X., Tsai, M-D. (1995) *Biochemistry* **34** p15307-15314

74) Verheij, H. M., Volwerk, J. J., Jansen, E. H. J. M., Puyk, W. C., Dijkstra, B. W., Drenth, J. and De Haas, G. H. (1980) *Biochemistry* **19** p743-750

75) Rogers, J., Yu, B. Z., Serves, S. V., Tsivgoulis, G. M., Sotivopoulos, D. N., Ionnou, P. V. and Jain, M. K. (1996) *Biochemistry* **35** p9375-9385

76) Berg, O. G., Gelb, M. H., Tsai, M-D. and Jain, M. K. (2001) *Chemical Reviews* (in press)

77) Jain, M. K., Gelb, M. H., Rogers, J. and Berg, O. G. (1995) *Methods in Enzymology* **249** p567-620

78) Jain, M. K. and Berg, O. G. (1989) *Biochem. Biophys. Acta* **1002** p127-156

79) Kunkel, T. A. (1985) *PNAS USA* **82** p488-492

80) Higuchi, R., Krummel, B. and Saiki, R. K. (1988) *Nucleic Acids Res.* **16** p7351-7367

81) Cohen, S. N., Chang, A. C. Y. and Hsu, L. (1972) *PNAS USA* **69** p2110-2114

82) Dower, W. J., Miller, J. F. and Ragsdale, C. W. (1988) *Nucleic Acids Res.* **16** p6127-6145

83) Bhat, K. M., Sumner, I. G., Perry, B. N., Collins, M. E., Pickersgill, R. W. and Goodenough, P. W. (1991) *Biochemical and Biophysical Res. Commun.* **176** p371-377

84) Van Scharrenberg, J. M., De Haas, G. H. and Slotboom, A. J. (1980) *Hoppe-Seylers Z. Physiol. Chem.* **361** p571-576

85) Wilton, D. C. (1990) *Biochemical J.* **266** p435-439

86) Radvanyi, F., Jordan, L., Russo-Marie, F. and Bon, C. (1989) *Anal. Biochem.* **177** p103-109

87) Bligh, E. G. and Dyer, W. J. (1959) *Canadian Journal of Biochemistry and Physiology* **37** p911-918

234

88) Smith, P. K., Krohn, R. I., Hermanson, G. T., Mallia, A. K., Gartner, F. H., Provenzano, M. D., Fijimoto, E. K., Goeke, N. M., Olsen, B. J., and Klenk, D. C. (1984) *Anal. Biochem.* **150** p76-85

89) Bradford, M. M. (1976) *Anal. Biochem.* **72** p248-254

90) Perkins, S. J. (1986) *European Journal of Biochem.* **157** p169-180

91) Laemmli, U. K. (1970) *Nature* **227** p680-685

92) Lee, B. I., Yoon, E. T. and Choo, W. H. (1996) *Biochemistry* **35** p4231-4245

93) Othman, R., Baker, S. F., Worrall, A. F. and Wilton, D. C. (1996) *Biochem. Biophys. Acta* **1303** p92-102

94) Baker, S. F., Othman, R. and Wilton, D. C. (1998) *Biochemistry* **37** p13203-13211

95) Gelb, M. H., Cho, W., Wilton, D. C. (1999) *Current Opinion in Structural Biology* **9** p428-432

96) Li, Y. and Tsai, M. D. (1993) *J. Am. Chem. Soc.* **115** p8523-8526

97) Annand, R. R., Kontoyianni, M., Penzotti, J. E., Dudler, T., Lybrand, T. P. and Gelb, M. H. (1996) *Biochemistry* **35** p4591-4601

98) Baker, S. F. (1998) *PhD Thesis*

99) *Biochemistry* **Vol. 4** (2000) Stryer, L.

100) *Spectrophotometry and Spectrofluorimetry* (2000) ed. Gore, M. G.

101) Buckland, A. G. and Wilton, D. C. (1998) *Biochem. Biophys. Acta* **1391** p367-376

102) Yu, B-Z., Rogers, J., Nicol, G. R., Theopold, K. H., Seshadri, K., Vishweshwara, S. and Jain, M. H. (1998) *Biochemistry* **37** p12576-12587

103) *Liposomes-A Practical Approach.* ed. New, R. R. C. (1990)

104) Patriarca, P., Beckerdite, S., Pettis, P. and Elsbach, P. (1972) *Biochem. Biophys. Acta* **280** p45-56

105) Foreman-Wykert, A. K., Weiss, J. and Elsbach, P. (2000) *Infection and Immunity* **68** p1259-1264

106) Zhao, H., Tang, L., Wang, X., Zhou, Y. and Lin, Z. (1998) *Toxicon* **36** p875-876

107) Raynal, P. and Pollard, H. B. (1994) *Biochem. Biophys. Acta* **1197** p63-93

108) Buckland, A. G. and Wilton, D. C. (1998) *Biochemistry J.* **329** p369-372

109) Koumanov, K., Wolf, C. and Bereziat, G. (1997) *Biochemistry J.* **326** p227-233

110) Huber, R., Romisch, J. and Paques, E. P. (1990) *EMBO. J.* **9** p3867-3874

111) Liemann, S. and Huber, R. (1997) *Cellular and Molecular Life Sciences* **53** p516-521

112) Davidson, F. F., Dennis, E. A., Powell, M. and Glenney, J. R. (1990) *Journal of Biological Chemistry* **265** p5602-5609

113) Buckland, A. G., Kinkaid, A. R. and Wilton, D. C. (1998) *Biochem. Biophys. Acta* **1390** p65-72

114) Yau, W. M., Wimley, W. C., Gawrisch, K. and White, S. H. (1998) *Biochemistry* **37** p14713-14718

115) Hirs, C. H. W., Timasheff, S. N. and Wyckoff, H. (eds.) (1986) *Methods Enzymology* **114**

116) Hampel, A., Labanauskas, M., Connors, P.G., Kirkegard, L., Rajbhandary, U., L., Sigler, P.B. and Bock, R.M. (1968) *Science* **162** p1384-1387

117) Strauss, M. G., Westbrook, E. M., Naday, I., Coleman, T. A., Westbrook, M. L., Travis, D. J., Sweet, R. M., Pflugrath, J. W., Stanton, M. (1990) *Nuclear Instruments and Methods in Physics Research* **297** p275-295

118) Ealick, S. E. and Walter, R. L. (1993) *Current Opinion in Structural Biology* **3** p725-736

119) Wonacott, A. J. (1997) *The Rotation Method in Crystallography* North Holland Publishers, Amsterdam

120) Henry, N. F. M. and Lonsdale, K. (eds.) (1969) *International Tables for X-ray Crystallography* Reidel,NE/Kluwer Acacdemic Publishers, Masachusetts

121) Leslie, A. G. W. (1994) *MOSFLM User Guide*

122) Collaborative Computational Computer Project Number 4 (1994) *Acta. Crstallography* **D50** p760-763

123) Rossman, M. G. and Blow, D. M. (1962) *Acta. Crstallography* **15** p24-29

124) Vagin, A. and Teplyakov, A. (1997) *Journal of Applied Crystallography* **30** p1022-1025

125) Hendrickson, W. A. (1985) *Methods in Enzymology* **115** p252-270

126) Brunger, A. T., Kuriyan, J. and Karplus, M. (1987) *Science* **235** p458-460

127) Brunger, A. T., Karplus, M. and Petsko, G. A. (1989) *Acta. Crystallography* **A45** p50-61

128) Brunger, A. T., Adams, P. D., Clore, G. M., Delano, W. L., Gros, P., Grosse-Kuntsleve, R. W., Jiang, J-S., Kuszewski, J., Nilges, M., Pannu, N. S., Read, R. J., Rice, L. M., Simonson, T. and Warren, G. L. (1998) *Acta. Crystallographica* **D54** p905-921

129) QUANTA 96, *X-Ray Structure Analysis Users' Reference* (1996) Molecular Simulations, San Diego

130) Laskowski, R. A., MacArthur, M. W., Moss, D. S. and Thornton, J. M. (1993) *Journal of Applied Crystallography* **26** p283

131) McRee, D. (1992) The Scripps Research Institute

132) Merritt, E. A. and Bacon, D. J. (1997) *Methods in Enzymology* **277** p505-524

133) Kraulis, J. (1991) *Journal of Applied Crystallography* **24** p946-950

134) Nicholls, A., Sharp, K. and Honig, B. (1991) *PROTEINS: Structure, Function and Genetics* **11** p281

135) Kleywegt, G. J. and Jones, T. A. (1996) *Structure* **4** p1395-1400

136) Schurer, G., Lanig, H. and Clark, T. (2000) *Journal of Physical Chemistry* **104** p1349-1361